Cranfield UNIVERSITY

DEFENCE COLLEGE OF MANAGEMENT AND TECHNOLOGY

BALLISTIC IMPACT ON COMPOSITE ARMOUR

By: Paul Bourke

Supervisor: Professor I Horsfall

Submitted for the award of PhD
Spring 2007

Cranfield University
Defence College of Management and Technology
Shrivenham
Wiltshire
SN6 8LA

© Cranfield University, 2007. All rights reserved. No part of this publication may be reproduced without the written permission of the copyright holder.

BEST COPY
AVAILABLE
Variable print
quality

ABSTRACT

Armoured vehicles in current military service are requiring ever more protection to enable them to carry out their mission in a safe, effective manner. This requirement is driving vehicle weight up to such an extent that the logistics of vehicle transport is becoming increasingly difficult. Composite materials are an important material group whose high specific properties can enable structures to be manufactured for a far lower weight than might otherwise be possible. Composite materials in an armoured vehicle will require structural performance as well as ballistic performance.

The mechanical and ballistic performance of thick armour and structural composites has been investigated against deformable and armour-piercing ammunitions, over a range of impact velocities. Testing has indicated that heavy/coarse reinforcement weaves perform well against deformable ammunition and light/fine weaves well against armour piercing ammunition. The effect of individual mechanical properties on ballistic performance has been investigated as has the damage morphology of impacted materials. High tensile strength combined with low fracture toughness has been identified as an important requirement.

Failure mechanisms have been identified from sections of ballistic impacts and through the use of mechanical test data the energy absorbed by each mechanism has been calculated. An energy audit has been carried out of all materials tested and a modelling procedure developed based on mechanical characteristics, damage morphology and failure mechanisms. This model has been tested against literature results and found to give very satisfactory performance.

ACKNOWLEDGEMENTS

There are many people to thank for their help and support throughout this project, particular thanks is due to the following:

Ajay Kapadia of VT Halmatic for his help in organising the provision of the materials for this project. VT Halmatic, AGY Europe and Reichold for supplying the materials and manufacturing the test panels.

Professor Horsfall for his help and direction as well as allowing me to find my own direction. Steve Champion, Celia Watson, Dave Miller, Jim Harber and Caroline McKenna for their help with trials work, friendly conversation and generally putting up with me at the Bashforth Laboratories.

Miles Tawell for his invaluable assistance in proof-reading the document, Aimee Lister, Stuart Gilby, Mike Gibson, John Renyolds and Leon Rosario for their sense of humour which kept me sane during my incarceration in the Heavyside labs. My many other friends who have had to put up with my absence and complaining, you know who you are and I am deeply grateful.

And finally Avril and Martin my parents for their support and encouragement, without which I would have never had the opportunity to pursue an interest in engineering, science and technology which has lead to this document.

CONTENTS

Chapter 5 – Rear surface penetration mechanisms

Chapter 6 - General Discussion

LIST OF IMAGES

Chapter 2 – Literature Review

Chapter 3 – Ballistic testing

Chapter 4 – Front face penetration mechanisms

Chapter 5 – Rear face penetration mechanisms

Chapter 6 – General Discussion

LIST OF FIGURES

List of Tables

Chapter 7 – Summary and Conclusions

List of Graphs

Chapter 5 – Rear surface penetration mechanisms

Chapter 6 – General discussion

LIST OF EQUATIONS

Chapter 4 – Front surface penetration mechanisms

Chapter 5 – Rear surface penetration mechanisms

Chapter 6 – General discussion

LIST OF SYMBOLS

a	Crack length (mm)
a_0	Pre-Crack length (mm)
B	Mode I Sample width
d	Beam Depth (mm)
t	Thickness
H_F	Depth of waist from front face
H_R	Depth of waist from rear face
M	Mass (Kg)
v	Velocity (ms^{-1})
A	Contact area between projectile and armour (mm^2)
A_x	Cross-sectional area of specimen (mm^2)
C	Compliance
D_F	Diameter of damage on front face
D_R	Diameter of damage on rear face
D_w	Diameter of damage at waist
D_l	Deflection of lower surface of beam (mm)
D	Flexural rigidity (J)
d	Indentation Diameter (mm)
d	Cone base diameter (mm)
d2	Equivalent tangent ogive cone base diameter (mm)
E	Youngs Modulus (Pa)
F	Force
F_a	Surface force on annulus (N)
F_I	Indentation force (N)
Fy	Yield force (N)
r	Chordal Radius
h	Depth of paraboloid (mm)
H	Load block Height (mm)
J	Energy Joules
K	Fracture toughness
L	Length / Span (mm)
l_1	Width of loadblock (mm)
l_2	Load hole x-axis location (mm)
l_3	Load hole y-axis location (mm)
m	Slope of tangent to initial straight-line portion of σ/ε curve
m	Mass (Kg)
P	Indentation Pressure (Pa)
P_o	Yield Pressure (Pa)
R	Reaction force perpendicular to projectile surface (N)
U_b	Bending energy (J)
U_t	Tensile energy (J)
w	Beam Width (mm)
y	*y* co-ordinate
y_{off}	Centre of rotation *y* offset (mm)
x	*x* co-ordinate
x_{off}	Centre of rotation *x* offset (mm)

x	Annulus radius (mm) / x-axis displacement (mm)
MIP	Mean Indentation Pressure (Pa)
ds	Width of annulus on surface of indentation (mm)
ds	Annulus width (mm)
ms	Time (ms)
α	Cone Semi-angle (Degrees)
μ	Coefficient of friction between indenter and material
τ	Shear stress (Pa)
σ	Stress (Pa)
ε	Strain (%)
δ_z	Through thickness displacement
δ	Displacement (mm)
Δ	y-axis intercept
Q	Large displacement correction
ν	Poissons ratio
ω	Depth of deformation (m)
α	Radius of bending zone (m)
r	Radius of curvature (mm)
L	Base length of ogive
β	Angle between secant and x-axis centreline
α_c	Angle between radial lines from centre of rotation to either end of chord
d	Diameter of base of paraboloid (mm)

NOMENCLATURE

AAAV	Advanced Amphibious Armoured Vehicle
ACAV-P	Advanced Composite Armoured Vehicle Programme
AFV	Armoured Fighting Vehicle
AP(I)	Armour Piercing (Incendiary)
AP	Armour Piercing
APFSDS	Armour Piercing Fin Stabilised Discarding Sabot
ASTM	American Society for Testing of Materials
CAV	Composite Armoured Vehicle
CAV-ATD	Composite Armoured Vehicle Advanced Technology Demonstrator
CBT	Corrected Beam Theory
CVR(T)	Combat Vehicle Reconnaissance (Tracked)
DCB	Double Cantilever Beam
DCMT	Defence College of Management and Technology (former RMCS)
ECM	Experimental Compliance Method
EFP	Explosively Formed Projectile
ESIS	European Structural Integrity Society
FE	Finite Element
FRP	Fibre Reinforced Plastics
FSP	Fragment Simulating Projectile
GFRP	Glass Fibre Reinforced Plastic
IED	Improvised Explosive Device
IFV	Infantry Fighting Vehicle
IFW	Instrumented Falling Weight
ISO	International Standards Organisation
KED	Kinetic Energy Density
MBT	Main Battle Tank
MIP	Mean Indentation Pressure
PTFE	Poly-Tetra-Fluro-Ethylene
RPG	Commonly known as Rocket Propelled Grenade, actual acronym is of Russian designation
RTM	Resin Transfer Moulding
RHA	Rolled Homogeneous Armour
SAER	Small Arms Experimental Range
TC4	Technical Committee 4 (of the European Structural Integrity Society)
UD	Uni-Directional
UTS	Ultimate Tensile Strength
VE	Vinylester

CHAPTER 1:

INTRODUCTION

This chapter will introduce the body of work covered by this thesis. It will cover the motivation for the project as well as an introduction to the problem to be tackled. A summary of intended objectives will be made along with the intended methods of achieving them.

1.1 Introduction

Fibre Reinforced Plastics (FRP's) are amongst the most important group of engineering materials to have been developed in the last century. As understanding of the behaviour of these materials, a product of the aerospace industry[1] improves usage has widened from high cost, high performance applications to a far wider field of applications.

The main use of these materials has been in structural applications[2] where high specific strength and stiffness has allowed designs and constructions not possible with existing materials. The suitability of composites for other applications is a constant area of development. The ability of components made from these materials to be built such that mechanical properties are optimised in certain desired ways has allowed a huge scope of applications. The disadvantage of this material diversity however is that research into material behaviour has had to be application specific, thus making general observations or 'rules of thumb' difficult. When compared to our knowledge of metals or plastics composites materials are still an embryonic technology.

1.2 Use of composites in Military applications

The specific strength of composite materials has allowed far lighter structures to be built than would be otherwise possible.

In a military environment there is a great need to reduce the weight of armoured vehicles. At present to provide adequate protection vehicles have become almost impossible to transport due to their size and weight.

Since their inception FRP's have been considered as armour materials, initially as personal protection and later as installed protection on aircraft. Development has continued to the present day to the extent that composite materials are used to compliment existing armour systems[3]. There is even consideration to using these materials to produce an entirely composite armoured vehicle, to this end very costly demonstrator programmes have been carried out to verify this concept[3].

The main barrier to the use of composite materials as a solution to the vehicle weight problem is there is very little understanding of the way in which mechanical properties translate to ballistic performance. Additionally a vehicle which makes significant use of

composite materials is likely to require both structural and armour functions to be performed by the same components.

The behaviour of these materials subject to ballistic impact and the process of optimising for ideal performance is not well understood due to the specialised nature of the application.

1.3 Objectives

The objectives of this research project are:

- To evaluate the mechanisms which govern the defeat of a projectile by composite armour.
- To investigate the influence of standard mechanical properties on armour performance.
- To attempt to model the contribution of mechanical properties to the arrest (or otherwise) of a projectile.
- To propose a 'recipe' for a satisfactory composite armour system suitable for protecting light – medium weight vehicles against the types of threat likely to be encountered in the modern battlefield. The weight of the proposed solution is as important as the level of protection.

This will be achieved by ballistic testing using the Small Arms Experimental Range (SAER) range facility at Cranfield Universities Shrivenham campus. Mechanical properties will be investigated with standard techniques modified where applicable for the size and type of material being tested. Where no standard test exists a suitable method will be developed.

CHAPTER 2:

REVIEW OF THE PROBLEM AND CURRENT SOLUTIONS

This chapter will review the current literature, technology relating to composite armours, and armoured fighting vehicles (AFV's).

A review of AFV types and their requirements will be first undertaken so as to establish limits to the area of interest. An analysis of the sort of threats in current and future war fighting scenarios will then be made to establish what sort of threat an armour will have to face.

2.1 Armoured Fighting Vehicles – The concept of protected mobility

The idea of taking a mobile weapon which protects its crew and allows them to fight to the battlefield can be traced through the history of warfare in the forms of siege weapons (such as protected battering rams or wall-scaling towers).

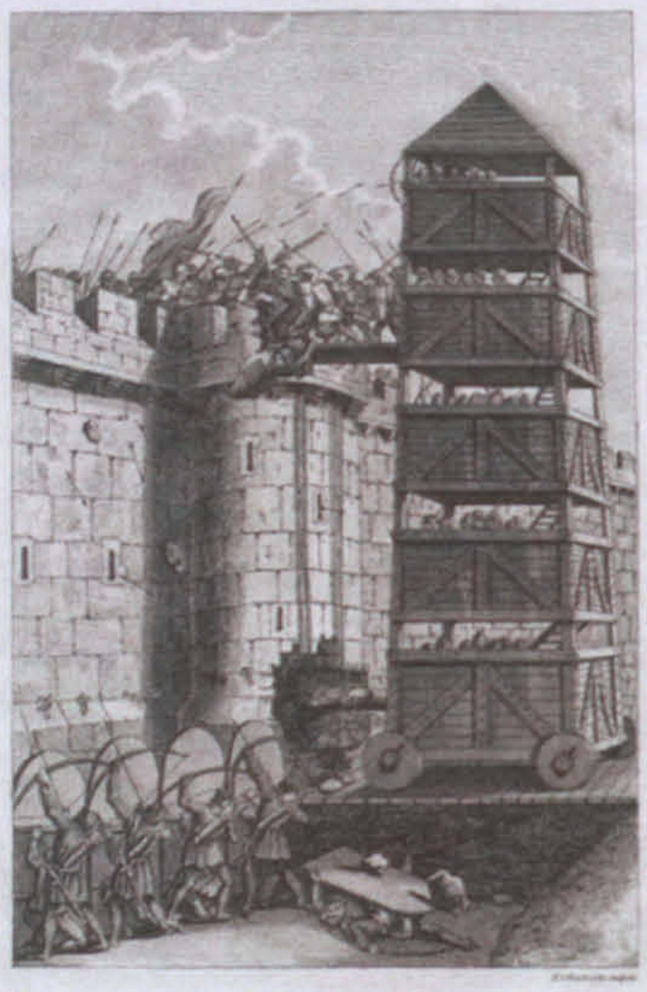

Fig. 1. Fig. 2. A Moveable Tower.

Image 2.1: Protected siege machines (RH image[4])

It wasn't until work by Leonardo DaVinci[5] that the concept of a powered vehicle capable of mobility in a hostile environment with the ability to be used aggressively emerged. It has taken however until the last century for such a vehicle to begin to develop as an effective war fighting weapon. In the most basic sense an Armoured Fighting Vehicle (AFV) is one that enables a strategic mission to be carried out whilst protecting its crew from hostile attack.

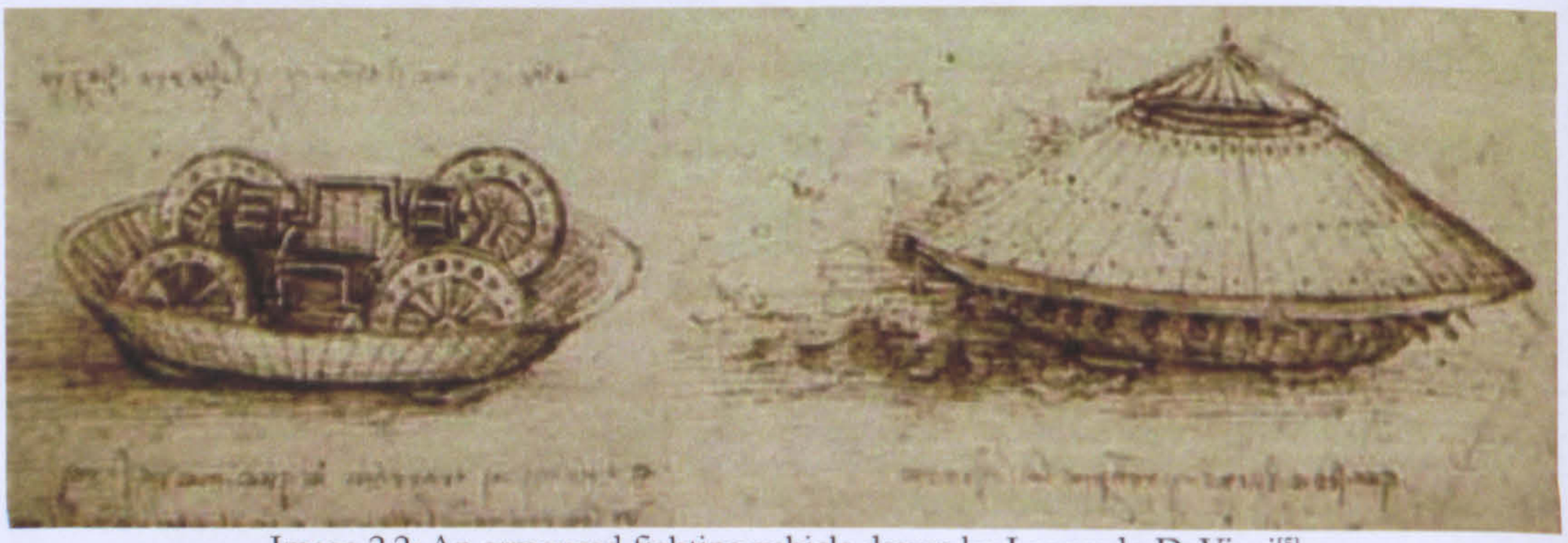

Image 2.2: An armoured fighting vehicle drawn by Leonardo DaVinci[5]

The armouring of combat vehicles has always been a practical necessity, however a compromise is required between protection, weight and mobility to suit the vehicles intended role. As a result there will always be a drive for lighter armours with higher protection capabilities.

2.2 Types of AFV

The term 'AFV' covers a range of vehicles ranging in size from small, wheeled troop carriers through to Main Battle Tanks (MBT's). The scope of this work concentrates on wheeled and light tracked vehicles ranging from 4x4 troop carriers (such as the 'Snatch' Landrover or Humvee (HMMWV)) through to more aggressive tracked Infantry Fighting Vehicles (IFV's) (such as the Warrior or M113).

The reason for this focus is due to the difference in threats expected throughout the size range of vehicles and the differing armour technology required to protect against small arms threats compared to that required for heavy munitions.

Image 2.3: 'Snatch' armoured Landrover (c Prof I Horsfall) (L) and Warrior IFV (R)

2.3 Requirements of an AFV in modern warfare

Whilst there is a wide diversity in types of vehicle which require armour protection, there are a number of constant requirements for vehicles of the size being considered.

These vehicles are operated as part of a modern, fast moving military force where mobility and speed are essential. The vehicles must also be capable of quick deployment, often by air transport. As a result of this size and weight are critical considerations, the vehicles need to be as small and light as possible whilst at the same time providing high

levels of protection and an adequate payload capacity – requirements which often conflict with one another.

The problem with the current generation of armoured vehicles is that their design is based on Cold War era military thinking. To make these vehicles suitable for service in current theatres of operations AFV's must have additional appliqué armour installed to increase protection, especially against mines and IED's (Improvised Explosive Devices). Failure to do so will result in unacceptable losses of vehicles and crew.

2.4 Composite materials

Composite materials are a class of engineering materials which are manufactured from discreet components, usually a continuous phase and a discontinuous reinforcement. The most popular form of these materials is as a fibre re-enforced plastic (FRP), typically a thermoset resin with a stiff fibrous reinforcement. The principle behind this combination of materials is that the high strength and stiffness reinforcement material can be supported and bonded together within a tough matrix resulting in a material stronger and tougher than either of its components and more importantly a material with very high specific properties (strength and stiffness to weight ratio)[6].

2.5 Relevance of composite materials technology to AFV design

As the protection requirements have increased so has the size of the protected vehicle, this is often for purely mechanical reasons to carry the weight of armour required.

The increased need for tactical mobility is highlighted by recent conflicts in, Iraq and Afganistan. The current logistics of transporting armoured vehicles is complicated and expensive, shipping is the easiest but is slow and road transportation equipment is also required. Air transport is the only solution to the need for rapid deployment.

There are three current heavy lift aircraft which can be used to transport AFV's, the Lockheed-Martin C130-J 'Hercules' has been the stalwart of air transport for decades, the future Airbus A400M which is currently entering production [7] and the heavy lift Boeing C-17.

Based on current vehicle weights (for an IFV) of around 20 tonne, the C130J (payload = 21,687kg[8]) can lift one vehicle, the A400M (payload = 37,000kg [9]) will be able to carry two vehicles and the massive C-17 (payload = 72,575kg [10]) three. As well as this the additional armour required to make these vehicles fit for purpose requires transportation.

Any further increases in the required armour will make the transport of vehicles suitable for combat duties impossible by air. This means that a military force will either be inadequately protected or will not be deployable at any speed faster than cargo ship and to nowhere without a friendly port.

The only proposed solution to this problem with current vehicle construction technology is known as the "Fly Light, Fight Heavy" approach. This is based on the idea of using a relatively large and heavy vehicle stripped down to an air portable 'Fly Light' size and weight for quick deployment which can later be up armoured to 'Fight Heavy' and go anywhere you may send a tank[11].

This can be achieved in a number of ways.

Size constraints:

- Kneeling suspension
- Removable stores
- Removable external armour

Weight constraints:

- Drain fluids / minimal fluids i.e. fuel
- No / Minimal ammunition or weapons removed
- Lighter / less durable components (such as tracks or wheels)
- Removable or reduced armour

The justification of this approach is that it is very rare that a vehicle will be fighting the minute it comes off an aircraft therefore there will (hopefully) be time to fit the armour. If this is not the case and immediate use is required the vehicles can be used in fly light configuration for rapid deployment and military presence on the ground, with the acknowledgement that casualties may be inevitable.

The following table categorises the protection a fly light fight heavy vehicle must have in both the fly light and the fight heavy roles, Armour Piercing (AP) ammunition, Fragment Simulating Projectiles (FSP's) and Explosively Formed Projectiles (EFP's) are dealt with later.

Fly Light Protection Levels

Threat	max Elevation	Azimuth	Protection
20mm FSP	90°	360°	10m
7.62mm AP	60°	360°	0m
14.5mm AP	30°	***±60°***	***500m***
20mm KE	0°	***±30°***	***1000m***
RPG CE	***No***	***No***	***No***
Blast Mines	Belly	N/A	***Partial***
EFP Mines	Belly	N/A	***No***

Fight Heavy Protection Levels

Threat	max Elevation	Azimuth	Protection
20mm FSP	90°	360°	10m
7.62mm AP	60°	360°	0m
14.5mm AP	30°	360°	100m
40mm KE	0°	±30°	1000m
RPG CE	0°	±90°	Yes
Blast Mines	Belly	N/A	Yes
EFP Mines	Belly	N/A	Yes

Table 2.1: Fly Light, Fight Heavy protection levels, (reduced levels for fly light are in bold) [12]

Failure to achieve the logistical integrity of this approach will simply result in what critics refer to as "Fly Light, Die Early".

Whilst this compromised approach may be the only option with current vehicle technology, increased use of advanced materials and construction techniques could allow heavily armoured vehicles within an air portable weight, thus solving the problem.

Whilst there is still much scepticism regarding the use of composite materials it would seem that they are one of the options that cannot be ignored when the armour design for future vehicles is considered.

Composite vehicles have been experimented with in the past and results indicate that higher than current levels of protection can be achieved for a considerably lower weight than that possible using current aluminium technology. Whilst cost has been an issue with these vehicles, the cost of a hull is relatively minor in comparison to the systems installed in some of these vehicles. Cheng [13] lists low weight, high strength tailor-ability and damage tolerance as major reasons for the selection of composites for protection systems and vehicle hulls.

Edwards[14] commented that the parallel needs for mobility, transportability and protection make a composite solution for armour protection quite desirable. Similarly James [15] explains that the "Army's manouverist doctrine demands greater strategic and tactical mobility" something which can only be achieved with vehicles of a practical weight.

It is the author's opinion that the only way to achieve the desired future protection levels and remain within air-transportable weight is through the major use of composites in the design and construction of these vehicles.

2.6 Current use of composite materials in armour systems

The biggest single use of composite materials at present is in the up-armouring of conventional metallic vehicles. This extra protection usually takes the form of a 'spall liner' which is fitted to the inside of the vehicle main armour[3], [16]. These spall liners are designed to protect the vehicle crew in the event of the main metallic armour being defeated (which has become more likely as weapons technology evolves). The liners not only add a small amount of ballistic protection but more importantly they heavily mitigate the behind armour effects should the main armour be perforated[3]. This is done by stopping projectile fragments and containing any material separated from the back of the armour due to the impact. This is a common problem with conventional metallic armours (especially aluminium), even when not penetrated deeply. Often significant spall can be caused by concentrated blast loading.

The cause of this spall is an impact generated compressive stress wave which passes through the armour at the speed of sound (in the struck material). When this wave strikes the rear face of the material it is reflected as a tensile stress wave. This tensile wave can exceed the tensile strength of the material causing a disc shaped fracture which results in a large 'scab' of material being separated from the back of the armour. This scab poses significant danger to whatever is behind the armour as illustrated by the following image.

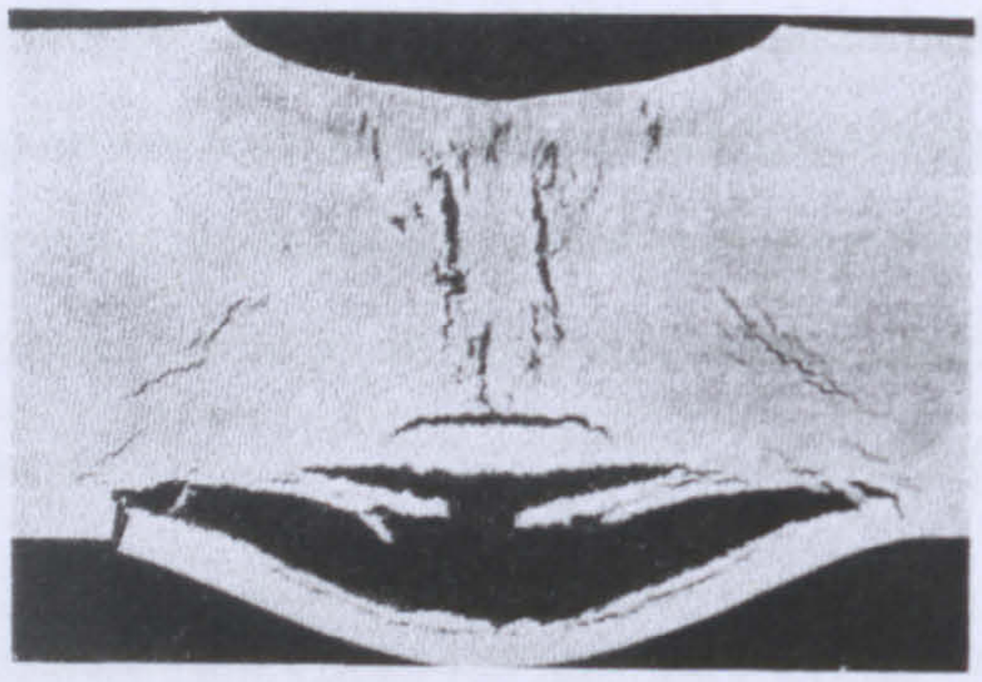

Image 2.4: Spall on rear surface of an aluminium armour[17]

As well as material knocked off the rear of the armour a perforating projectile will cause a wide spray of material fragments resulting from the projectile and displaced armour material creating a significant behind armour danger to equipment and individuals alike.

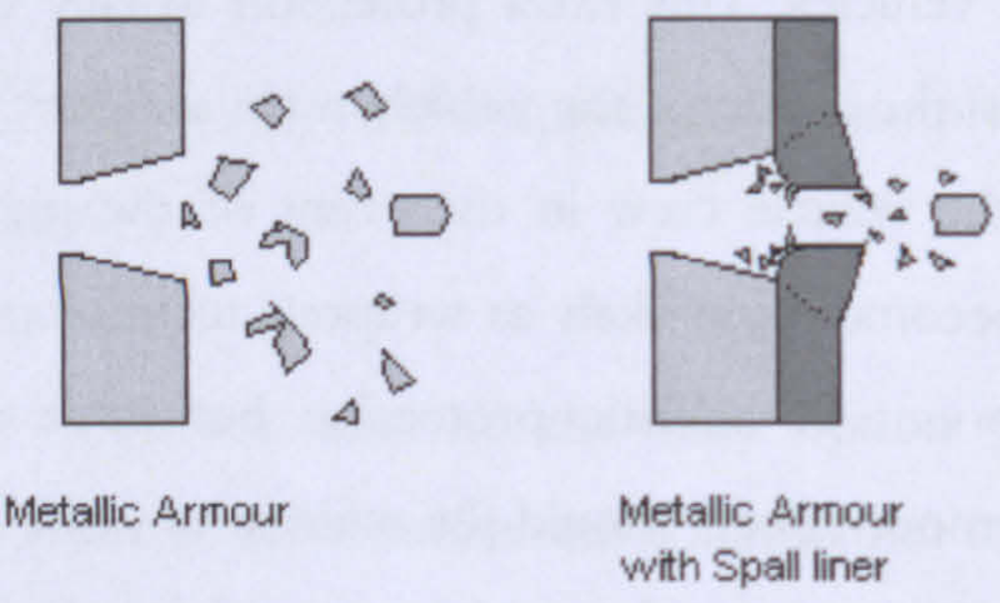

Fig 2.1: Effect of spall liner

Spall liners are able to contain these fragments as they are usually quite large and slow moving and as a result the cone of danger behind the armour is greatly limited[3]. These liners are especially useful when it comes to mitigating the effects of shape charge jets

Image 2.5: A Kevlar spall liner in an M113 APC vehicle

Another form of additional protection where composite based armours have seen use has been in the form of external appliqué panels. These panels are usually a glass fibre backing designed to work with a ceramic front face such as Alumina or Silicon Carbide and can provide quite a significant armour upgrade for relatively low weight cost. An example of this system can be seen applied to a CVR(T) vehicle in the following image.

Image 2.6: Ceramic appliqué panels on a CVRT vehicle (Photo Courtesy of Lt Col A Roxburgh)

2.7 Composite vehicles to solve the Fly light, Fight heavy problem?

As previously stated there is an increasing need for light, air portable vehicles with high levels of protection. The increasing understanding and use (and thus decreasing cost) of composite materials allows their significant inclusion in the design of a vehicle which supplies high protection for minimum weight. To achieve this, composites will have to be used for both structural and vehicle armour requirements. By using composite armour the need for an additional spall liner is removed immediately saving a significant amount of weight.

There are a small number of development programmes which are taking or have taken place which have made use of significant amounts of composites and have pushed composite armour technology forward. These following case studies used only to illustrate the current level of technology and use of all composite armour systems.

2.8 Existing Vehicle programmes

2.8.1 CAV-100

Image 2.7: CAV 100 Vehicles

This vehicle project involved adding a light composite armoured body a Landrover chassis. The intended use of the vehicle was for urban peace keeping duties and for protection of aid personnel near combat zones. The vehicle was designed to protect against small arms threats, fragments, mine blast and can be seen in extensive use by UK armed forces in current theatres of operations as well as in service with a number of police forces.

The armour developed for this vehicle is known by its manufacturer (NP Aerospace) as 'CAMAC'. This system of composites can incorporate a range of reinforcement including S-2 Glass, E-Glass, Aramid and Polyethylene fibres. The composite 'pod' which makes up the rear portion of the vehicle is unique to this vehicle and is a main reason for its success. It is made from press-cured, formed components (a relatively expensive procedure) which are adhesively bonded together. The crew compartment is closed with a separate bulkhead / floor assembly constructed in the same fashion.

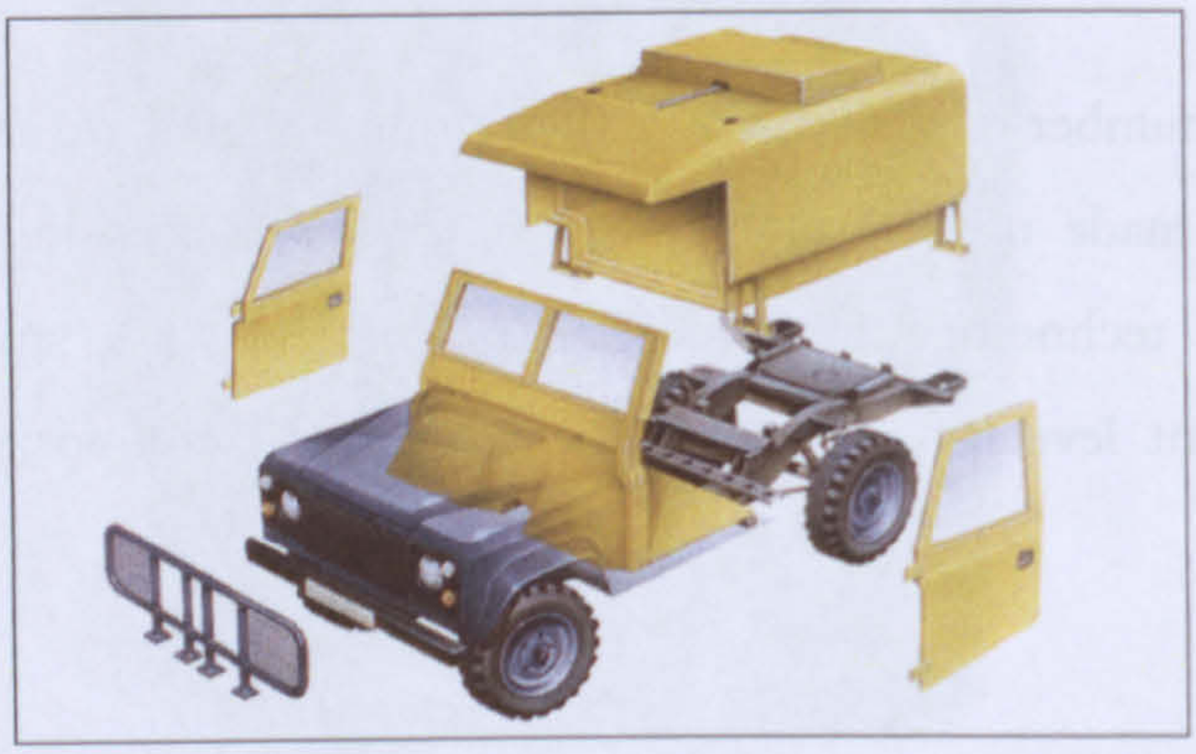

Img 2.8: CAV 100 Construction – Pale components are composite

This is a successful and versatile vehicle which has proved very tough in in-service conditions the composite components have proved easy to maintain, and has been able to achieve a good serviceability record.

Initial critics of the durability of this kind of armour have been silenced by the fact that the original vehicles manufactured in the 1980's for use in Northern Ireland have been refurbished and are now in service in Iraq. The composite body required only cosmetic attention whilst the vehicle chassis and mechanical components were found to be entirely worn out and have been replaced completely. Having been used in numerous theatres of operations NP describe the CAV 100 as thus: "Battle proven in the former Yugoslavia, the CAV100 offers ballistic protection levels up to CEN Level B6[18] coupled with a payload of over half a tonne, within the original Land Rover design weight of 3,500 Kg."[19]

Image 2.9: Successful crew protection after mine detonation

These ageing vehicles are currently being used in service in Afghanistan and Iraq however they are proving to be inadequate for the threats they are being exposed to. British forces are being regularly exposed to heavy small arms fire, and more serious threats such as RPG attacks, EFP's and large IED's to which these vehicles offer only scant protection.

2.8.2 ACAV-P

Image 2.10: ACAVP Demonstrator Vehicle

ACAVP (Advanced Composite Armoured Vehicle Platform) was unveiled by Vickers Defence Systems in April 2000. It is a tracked AFV of approximately 22 tonnes, of which 6 tonnes is a hull constructed entirely from plastic / E-Glass composites[20], the first of its kind and is one of the heaviest single RTM (Resin Transfer Moulding) components ever manufactured.

This vehicle has been tested extensively and despite suffering from subsystem failures in trials the composite hull has performed successfully and been unaffected by a number of fuel and hydraulic leaks. Testing has also proved that a by-product of the composite construction is reduced internal and external noise levels due to the higher natural damping of the composite material compared to steel and aluminium. This is important due to EU noise and vibration exposure legislation limiting the time in which a crew can operate a vehicle in non-war situations[21].

The ACAVP is guarded against 14.5mm armour-piercing (AP) attack through 360° and has protection against 30mm AP attack over frontal areas. It has to be remembered this vehicle type is a light IFV rather than a heavy tank, and that a 30mm threat is a dangerous projectile to defeat.

2.8.3 CAV-ATD

Image 211: CAV – ADT Demonstrator Vehicle

The CAV-ATD (Composite Armoured Vehicle – Advanced Technology Demonstrator) is the result of a successful programme of research into composite vehicles which first resulted in a experimental version of the M2 IFV in 1989. This initial vehicle had a hull of S2-Glass fibres in a Polyester resin and weighed 27% less than a equivalent aluminium hull[3] . The CAV-ATD programme aimed to further demonstrate the feasibility of both a composite structure and a composite armour solution for a air transportable vehicle of around 20 tonnes. It was aimed at achieving a weight at least 33 percent less than an equivalent aluminium vehicle with the same level of protection[22]. Additionally the demonstration of manufacturability, reparability, was required along with integration of signature management (stealth) technologies. All this was required at a cost not greater than 1.4 times that of an aluminium vehicle[23].

This vehicle was successful in its aim of reduced weight being approximately 35% lighter than an equivalent conventional vehicle. The cost target however was not met; the CAV-ATD hull cost was approximately 1.9 times the cost of an aluminium vehicle[24]. In the years between this projects completion and present day aluminium prices have risen considerably, having more than doubled in Summer 2006 since Autumn 1992, peaking at nearly three times the price in early 2006[25]. Co-incidentally increasing use of composite materials has resulted in reinforcement materials price falling, matrix materials being an oil product have seen some volatility but nowhere near as drastic as the increase seen in aluminium prices. As a result the difference in cost of the same composite hull will be far less in today's economic terms.

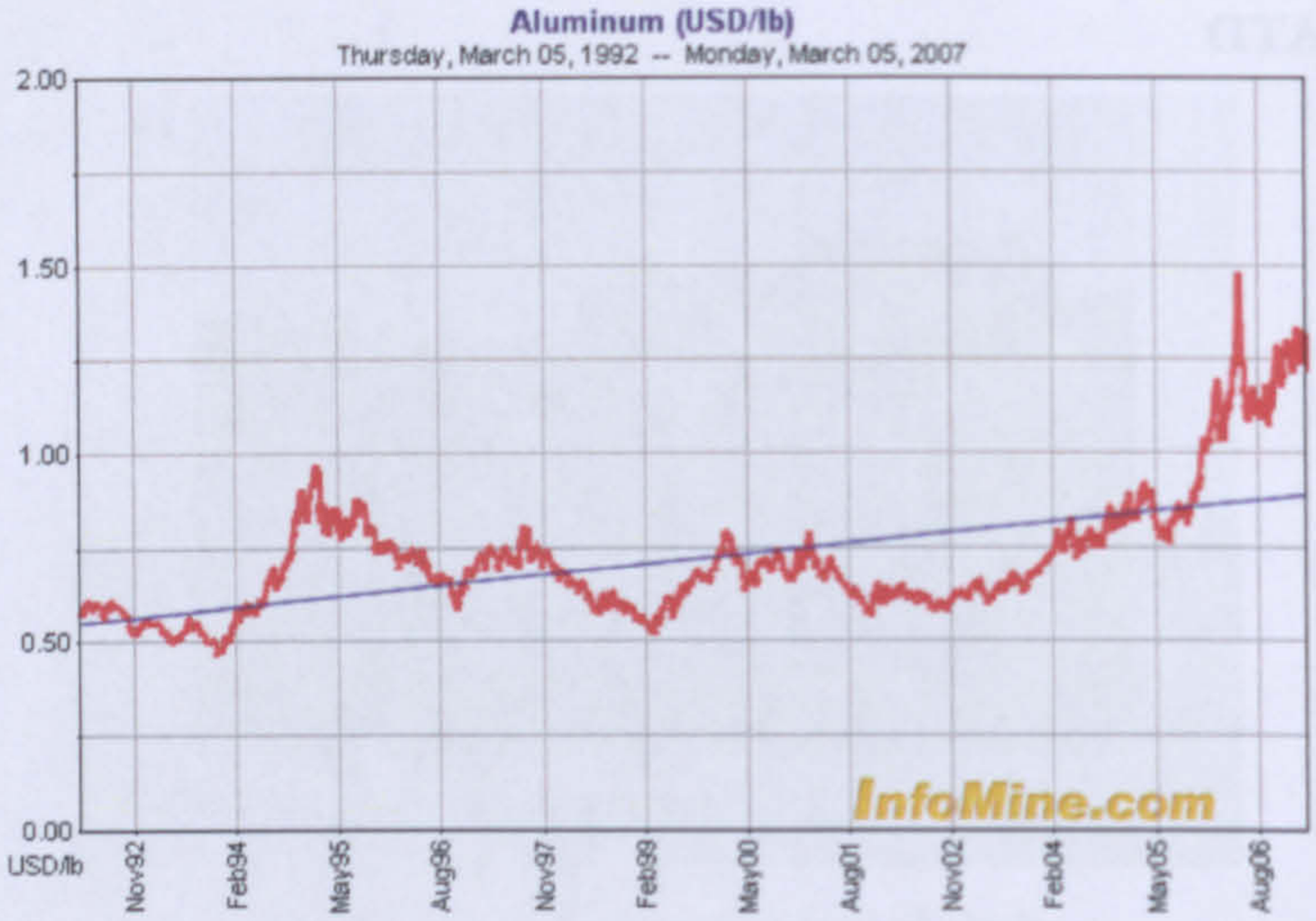

Graph 2.1: Aluminium prices $/lb between 1992 and 2006 [25]

2.9 Practicalities and limitations of composite armour systems

One of the biggest limitations of the use of composite materials is initial and whole life cost of their use; this is especially the case when ceramics are used in the stopping of higher energy threats. These costs are however falling and the increased use of composite and ceramic materials can only bring costs down further. Processing cost is also an issue, especially so with certain types of press-cured composites. The use of materials more suited to large scale manufacture of complex shapes through the use of an industrial grade (as opposed to aerospace grade) process (such as Resin Transfer Moulding (RTM) and vacuum bag consolidation) is a desirable goal. As previously mentioned the current high price of Aluminium means the price difference between conventional and composite vehicles is falling.

There is also concern regarding the in service durability of composite components. Whilst it has been proven through the ACAV-P and CAV-100 programme that durability is achievable, testing is required to prove that composites can last in other applications. Leading from this, the ease of repair of these materials is an issue which must be considered. NP Aerospace (CAV-100) found that a repair system suitable for use in the field produced more than satisfactory results[26] additionally work by authors including Edwards [14] and Hosur et al [28] has shown that armour composites can be repaired in such a way that provides adequate physical strength and ballistic performance in the repaired material. It is worth noting however these results may be very heavily system specific

2.10 Future directions

It can be anticipated that the application of composite technology to vehicles will become of great importance, especially so if improvements can be made regarding cost in comparison to conventional vehicle manufacture.

The use so far of composites in lighter vehicles such as the CAV Landrover has involved a separate, non-structural 'pod' or bolt on panels mounted on a conventional existing chassis. Despite the flexibility of vehicle use that this may offer, this method is quite inefficient in terms of the resultant design. Should a similar vehicle be solely constructed from a composite material a notable weight and thus performance gain (or increased armour capacity) would be seen with an added reduction of external joints, ballistic gaps and other such weaknesses. The design could also be optimised for a specific task rather than using a universal chassis which by design will always be a compromise.

Cost savings can be achieved through adaptation of industrial processes (such as those found in the ship-building industry). For example if a resin which cures at room temperature could be used it would eliminate the need for autoclave processing, if a commercial vacuum bag and resin infusion process was used (such as that used in ship building and other large scale projects) then large structures could be made in one process saving much time spent assembling and fabricating a conventional metallic hull.

The specifics of current armour development are hard to come by due to their often classified status however there are a few vehicle programmes which plan to make significant use of composite materials. Examples of these programmes are the US marine AAAV and the UK 'FRES' programme.

2.11 Threats and protection

There is a great diversity in ammunition types, each with its own unique characteristics., despite this they can be grouped into classes with similar levels of performance. The STANAG standard 4569 [29] is a widely used threat classification system employed in the development of armour materials and will be regularly referred to in this project. It groups a number of common ammunitions into five categories ranging from small calibre rifle ammunition up to heavy anti-tank ammunition.

The following tables list the previously mentioned standard threats and their general characteristics.

	5.56 x 45mm NATO	7.62 x 51mm NATO	7.62 x 39mm Steel core	7.62 x 54mm Dragonuv
Type	Ball	Ball	AP	AP
STANAG Level	I	I	II	III
Bullet Diameter (mm)	5.66	7.82	7.82	7.87
Bullet Weight (g)	4	9.65	9.65	10.04
Muzzle Velocity (ms^{-1})	924	848	710	870
STANAG protection velocity (ms^{-1})	900	833	695	854
Muzzle Energy (J)	1708	3470	2432	3800
Impact Energy (J)	1620	3348	2331	3661
	14.5 x 114mm Soviet HMG	**25 x 137mm APDS-T**		**RPG-7**
Type	AP - Steel	AP - Tungsten		Shapecharge
STANAG Level	IV	V		N/A
Bullet Diameter (mm)	14.5	25		N/A
Bullet Weight (g)	63.44	150		
Muzzle Velocity (ms^{-1})	1000	1335	**Jet velocity**	8-10,000
STANAG protection velocity (ms^{-1})	911	1258		
Muzzle Energy (J)	31720	133667		
Impact Energy (J)	26325	118692		

Table 2.2: Ammunition information STANAG Level I-V [11] [27] [30]

An important threat not considered in this standard (but included in the table) is shaped charge attack from weapons such as the RPG-7. Whilst there are a great variety of weapons capable of similar threats few are more prevalent than the RPG-7, a cheap and rugged anti-armour weapon of choice amongst dissident organisations particularly in Middle Eastern theatres of operations. For comparison a RPG-7 shape charge jet has more than three times the energy density of a 120mm APFSDS* longrod penetrator (though only around 3% of the total energy)[15]As such the chances of this threat perforating the armour on anything but the heaviest of vehicles is high. This makes the rear surface behaviour and behind armour effects of a perforated armour of great importance.

The most common baseline threat which light AFV's are required to protect against is the STANAG level II ammunition introduced above. This soviet designed ammunition is manufactured worldwide and can be used in any 7.62x39mm chambered weapons such as the ubiquitous Kalashnikov AK-47 Assault Rifle.

* Armour Piercing Fin Stabilised Discarding Sabot

The design of this projectile is very much conventional; a boat-tail shaped copper gilded steel jacket contains a very high hardness (900Hv) armour piercing steel core surrounded by lead-antimony guilding metal. AP(I) (Incendiary rounds) are also common and contain an incendiary charge behind the core at the back of the bullet. Upon striking a surface this core exits through the front of the bullet jacket and concentrates a great deal of energy over a small area without deforming thus achieving penetration through the target. As the core is the main penetrator we can essentially ignore the jacket and gilding from any analysis.

Image 2.12: 7.62x39 AP STANAG level II ammunition. L-R Complete round, Bullet, Core

2.12 Defining the danger of a threat

Whilst there are many different types of projectile there are only a small number of parameters which are required to describe just how dangerous a particular threat is.

2.12.2 Kinetic Energy Density

Any moving body will posses kinetic energy. A light and very fast projectile can carry the same as a heavy and slow projectile. What determines the ease at which a projectile can be stopped is the area over which this kinetic energy is spread i.e. the energy applied to the armour per unit area – the *Kinetic Energy Density (KED).*

Following from this a pointed, hard cored round which will not deform and spread out on impact (thus increasing the area over which impact energy is applied) will be more

dangerous than a soft, deformable 'ball' round. In order of performance, lead cored rounds deform the most followed by steel cored rounds, armour piercing rounds have a hardened steel core embedded within the bullet, it is this which penetrates the armour.

The harder these rounds are the less they will be eroded by the impact event (assuming the tip is not shattered) and therefore the longer they will keep their point. By having a pointed nose the impact energy is concentrated over an exceptionally small area.

Iremonger[31] comments that "A composite cannot absorb sufficient energy if it is spread over too small a area i.e. if the kinetic energy density of the impact is too high".

2.12.3 Hardness

Hardness is very important in determining whether a projectile defeats an armour or not, a projectile which is significantly harder than a armour will penetrate very easily, the analogy of 'Like a knife (hard) through butter (soft)' being surprisingly appropriate.

Should however, the target be significantly harder than the projectile the projectile will be eroded and broken up on the surface rather than penetrate the target.

Fibre-reinforced plastic composites are on their own not hard at all, as such penetration is almost inevitable. When used as an armour system, composites are often used in conjunction with a very hard sintered ceramic face.

2.12.4 Hit velocity / dynamic effects

Ballistic impacts impart very high loading rates on a target material, it is entirely possible for the projectile to pass through an armour before it has had time to deflect in the same way as it might when hit by a large but slow object. Often basic material properties at high rates are different to those measured at quasi-static rates.

Shock wave transmission is also an issue worthy of consideration. The reflection of a compressive wave as a tensile wave from the rear surface of an metallic armour is responsible for spallation by exceeding tensile strength which is a characteristic of this material.

In composite systems it has been suggested that shockwaves are transmitted along reinforcement fibres and reflected from fibre ends[32]. It is proposed that upon convergence at the impact site these reflected stress waves promote fibre failure though there is limited evidence to back up this theory.

2.13 Theory of impact and indentation of composite armours

2.11.1 Overview

The development and understanding of composite armour technology can be approached from a number of different angles. Computer based finite element (FE) testing is very popular as it avoids expensive practical testing however tends to be very application specific. The modelling of composite materials is a very complex problem and is still a developing field. Wang and Chou[33] comment that "The process of penetration and perforation of composite materials is extremely complex involving not only the in-homogeneity and anisotropy of the material but also complicated dynamic and thermal effects, finite displacement and rotation with inelastic strain, fracture and tearing" as such generating a complete model which works over a range of impact conditions, for different projectiles, and different armour systems (i.e. fibre/matrix changes) is a challenge which numerous authors have attempted to match with varying degrees of success[34,35], thus far there is no complete solution.

Another approach is through practical testing of mechanical and ballistic performance combined with careful observation.

2.11.2 General armour theory and practice

In an ideal world an armour will defeat a projectile by being so hard and tough that a projectile is entirely defeated on the armours surface. This however is an unlikely scenario and it is inevitable that the projectile will penetrate (break the surface) of an armour (this is especially the case with a soft composite material).

Should penetration be so deep that the projectile travels through the armour and breaches the rear surface it is referred to as complete penetration, or perforation. There are a number of variations on the definition of perforation as shown in the following diagram. This work is focused on composite materials which have reduced spall

characteristics relative to metals. As a result of this the 'Navy' ballistic limit definition is used throughout this report, or in words: 'Perforation is when the projectile or a fragment of projectile exits the rear face of the armour material'

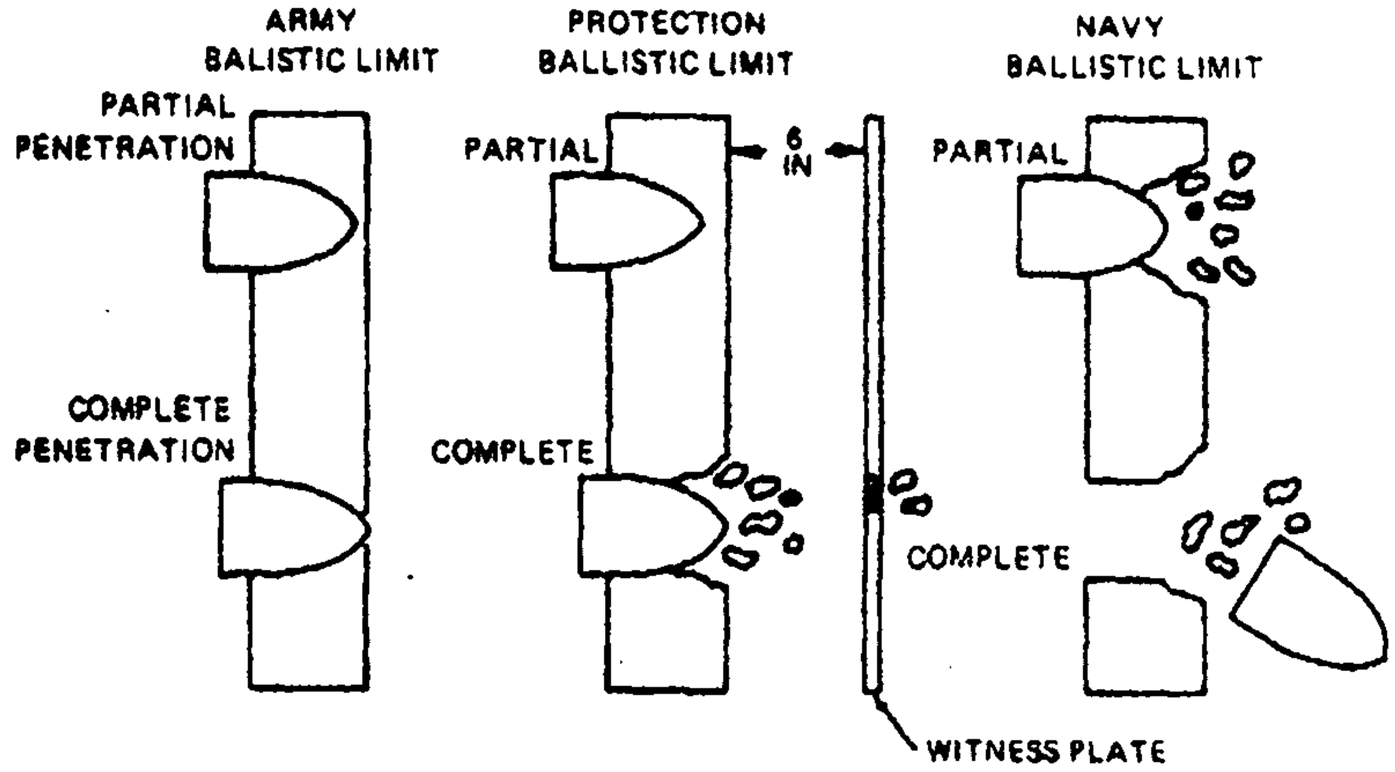

Fig 2.2: Definition of perforation[36]

After defining what is meant by penetration it is also important to define the limiting point at which a projectile succeeds in perforating an armour. This is known as the 'ballistic limit' and is dependent on the armour being used, the application / arrangement of its use and the projectile which is striking it.

Blackman and Goldsmith[36] cite the following definition for ballistic limit velocity :

"Ballistic limit – The average of two striking velocities one of which is the highest velocity giving a partial penetration and the other of which is the lowest velocity giving a complete penetration...."[36]

2.12.2 Ballistic impact on composites

In defeating a projectile the damage suffered by a composite armour can be analysed by dividing attention to two distinct areas, the front face and rear face of the armour with an un-defined transition between the two. This approach is based on the observation that the mechanisms responsible for visible damage on either face tend to be particular to that face i.e. a mode of failure seen at the rear may not be encountered on the front.

On the front face; indentation resistance, compressive strength and shear strength contribute to the initial slowing of the projectile. After penetrating through the

composite material a distance the impact energy begins to be absorbed by the propagation of delamination damage, matrix cracking[37] and the displacement of large areas of composite (due the reduced stiffness caused by delamination). This mechanism is controlled by the fracture toughness of the composite (how much energy can be absorbed by damage growth) and the tensile strength of the fibres as the rear surface of the composite bulges and attempts to 'catch' the projectile.

There is some debate in the literature as to the contribution of these two types of defeat mechanism to the overall ballistic performance of a composite armour. Delamination damage is generally the most visible mechanism however plugging and shearing stages consume a lot of energy. There is some suggestion that delamination should be encouraged (via a weak fibre/matrix bond) to allow a more compliant laminate [38].

The geometry of the projectile is often shown to be significant in the literature [38,39,40,41,42]. As a result it is expected that the impact of a pointed projectile (i.e. a bullet) will cause little in the way of plugging therefore the total contribution of plugging / shearing energy to the total failure energy will be small.

Also of debate are the conditions which lead to the transition between one mechanism and another. There has been a body of analytical work done in the field of impact on metallic plates by the likes of Awerbuch [42][43] and Goldsmith & Finnegan [44] which considered the first stage in terms of inertia and compressive forces applied to the target in the deceleration of the projectile, the second stage (a shear plug failure through the material thickness) being initiated by the formation of a shear plug of material. It is possible that a similar mechanism occurs in composite materials, where material displaced by the initial impact and penetration causes other failures.

Observations by Gellert et al[45] and Mascianica[46] have also suggested that a bi-linear trend exists in a plot of perforation energy vs target thickness, (see graph 2.2), a trend which holds true for a range of projectile geometries.

This transition in rate of energy absorption is the point at which a target material can be no longer defined as 'thin' and at which damage geometry changes, this is backed up by

the difference in damage architecture observed in post impact sectioning. This observation suggests that bulk effects due to a larger thickness target material contribute to increased energy absorption in penetrating impact.

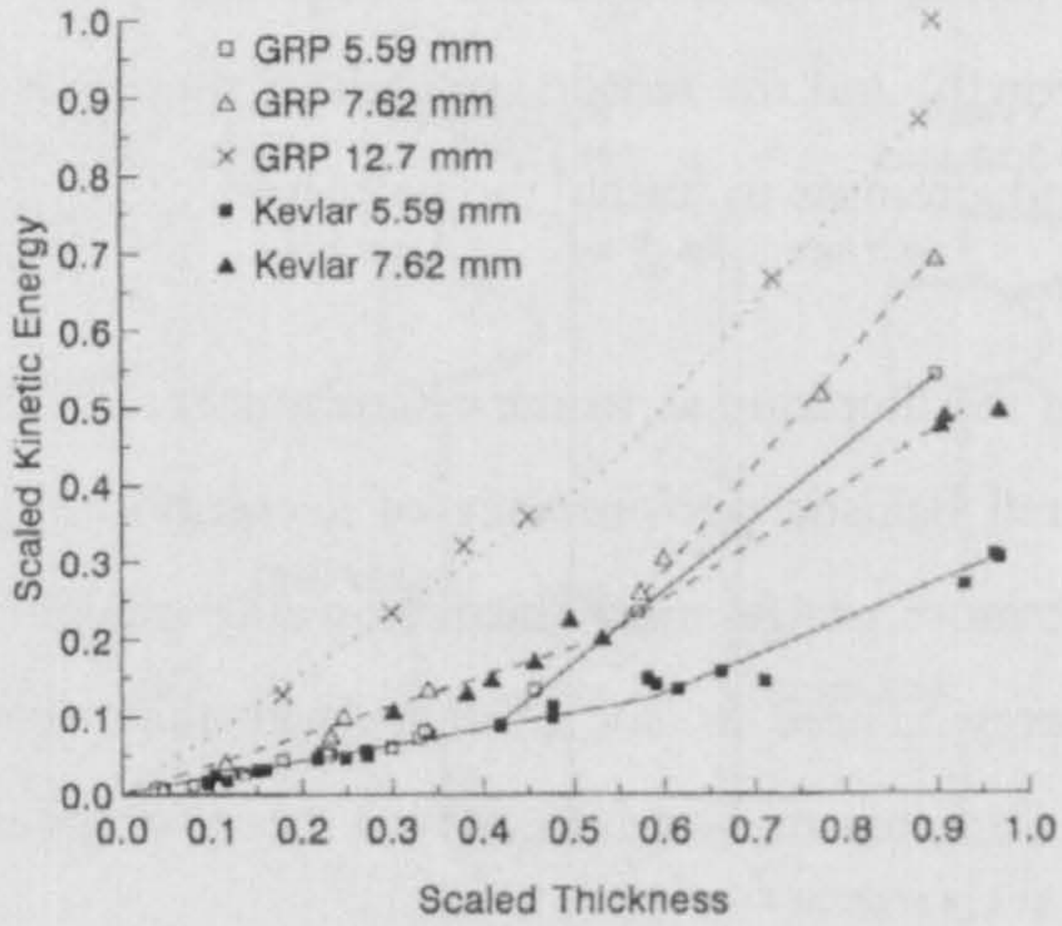

Graph 2.2: Bi-Liniear perforation energy/thickness trend seen by Gellert et al [45]

These observations are backed up by similar work carried out by Roylance and Wang [47] who studied the penetration mechanics of thick fabric panels. Plotting energy absorption versus time also gave a bi-linear relationship. This suggests that a longer impact event time afforded by a thicker panel allows a greater amount of energy absorption within the reinforcement fibres compared to the short event seen by a thin / grossly overmatched panel.

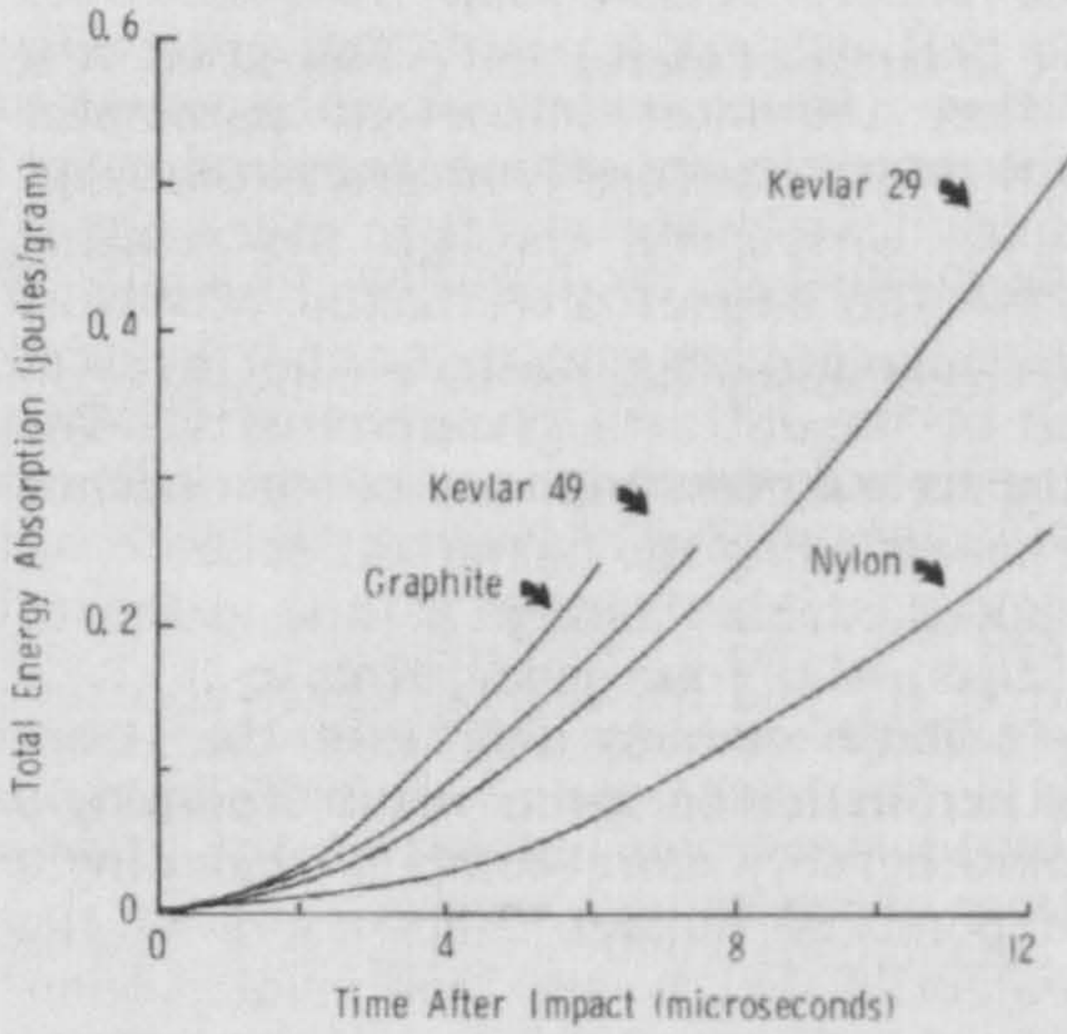

Graph 2.3: Bi-Liniear perforation energy/time trend seen by Roylance and Wang [47]

In thick materials the front and rear surface damage mechanisms manifest themselves as visible cones growing from each surface to form a non-symmetric 'hourglass' pattern through the thickness of the material. Damage is caused by the initial compressive loading on the material front face, this creates a radial pressure as a result of displaced material which causes motion at the nearest free surface (the front face) and as a result material damage. As penetration continues material is motivated by the projectile towards the rear face, delaminating and deforming as it does so.

Geometric analysis of this shape allowed Gellert et al[45] to conclude that the damage geometry after an impact is largely independent of striker nose geometry with the exception of the amount visible on the rear face, this was shown to increase with blunting point geometry. 'Thin' materials however were shown not to develop the upper region of the hourglass shape instead exhibit a simple cone expanding shaped damage pattern.

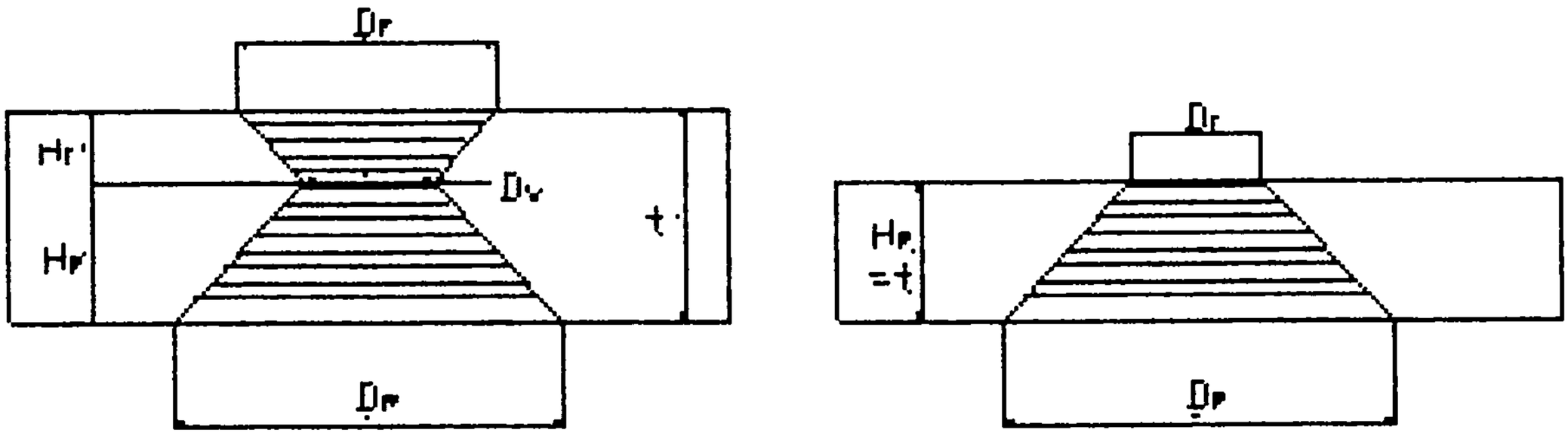

Fig 2.3: Gellert damage geometry for a) thin and b) thick targets [45]

The definition of the problem of increasing ballistic protection within tight weight restraints has been highlighted, the threats defined and the use of composites as an armour material introduced. The following chapters will evaluate a range of engineering composites which may be suitable for ballistic and structural requirements. Initially ballistic testing to evaluate ballistic performance will be carried out followed by mechanical testing to establish a relationship between mechanical properties and ballistic performance. If the findings of Gellert [45] are mirrored an attempt will be made to link damage geometry to ballistic energy absorption via physical damage mechanisms i.e. delamination and fibre failure.

CHAPTER 3:

EXPERIMENTAL INVESTIGATIONS;

BALLISTIC TESTING

This chapter will cover the ballistic testing (and related experimental) undertaken during this project. Each experiment will be detailed in terms of aim, methodology results and observations.

The majority of these tests have been carried out on materials initially supplied by VT Halmatic Ltd.

3.1 Overall Aims of ballistic testing

The overall aims of the ballistic testing carried out in this chapter are to:

1. Assess the effect of weave weight on the ballistic performance of thick engineering composites
2. Assess the effect of thickness on the ballistic performance of thick engineering composites
3. Evaluate the failure mechanisms and damage geometry of the failed material
4. Attempt to investigate the findings of Gelert et al [45],[46] with regards penetration energy
5. Evaluate the ballistic performance in terms of V_{50} against both soft ball and hard armour piercing ammunition.

3.2 Experimental facilities

The experimental facilities of the Engineering Systems Department of Cranfield Universities Shrivenham campus (DCMT) were utilised for this work. Ballistic testing was undertaken in an instrumented small arms range facility.

3.3 Ballistic testing of GFRP material

3.3.1 Aims:

- To define V_{50} velocities for GFRP materials against STANAG 4569[27] level I and II threats. In accordance with MIL-STD-662F [48]

- To visually evaluate the response of the panels to impact.

- To test more than one thickness of armour against STANAG level II for analysis similar to that carried out by Gellert [45].

3.3.2 Experimental

The first round of ballistic testing was carried out on a range of S2 glass reinforced GFRP panels of varying thickness, matrix material and reinforcement weave.

A V_{50} determination will be carried out in accordance with the standard practice for determining a V_{50} velocity set out by with MIL-STD-662E [48]. A V_{50} investigation provides a figure for ballistic limit velocity. Defined; a V_{50} is the speed (within a 40ms^{-1} bracket) at

which 50% of 6 individual impacts do not perforate and 50% perforate. This allows a statistically valid figure to be recorded and avoids anomalous results from influencing the final value.

Perforation is defined by the 'Navy' standard as discussed previously (Figure 2.2). This was decided upon because of the fact that spall from a composite armour is less dangerous than that from a metallic armour[35]. If the projectile does not leave the rear surface of the armour (i.e. it can have broke the rear surface) it is not classed as a perforation.

Projectile velocity will be recorded by an optical chronograph apparatus which derives speed from a time measurement started and ended by a projectile breaking two sets of light beams. The equipment is calibrated regularly with sophisticated electronic timers leaving the greatest source of error being due to the positioning of the screens relative to one another. All possible sources of error taken into account, the system used is accurate to within 1%.

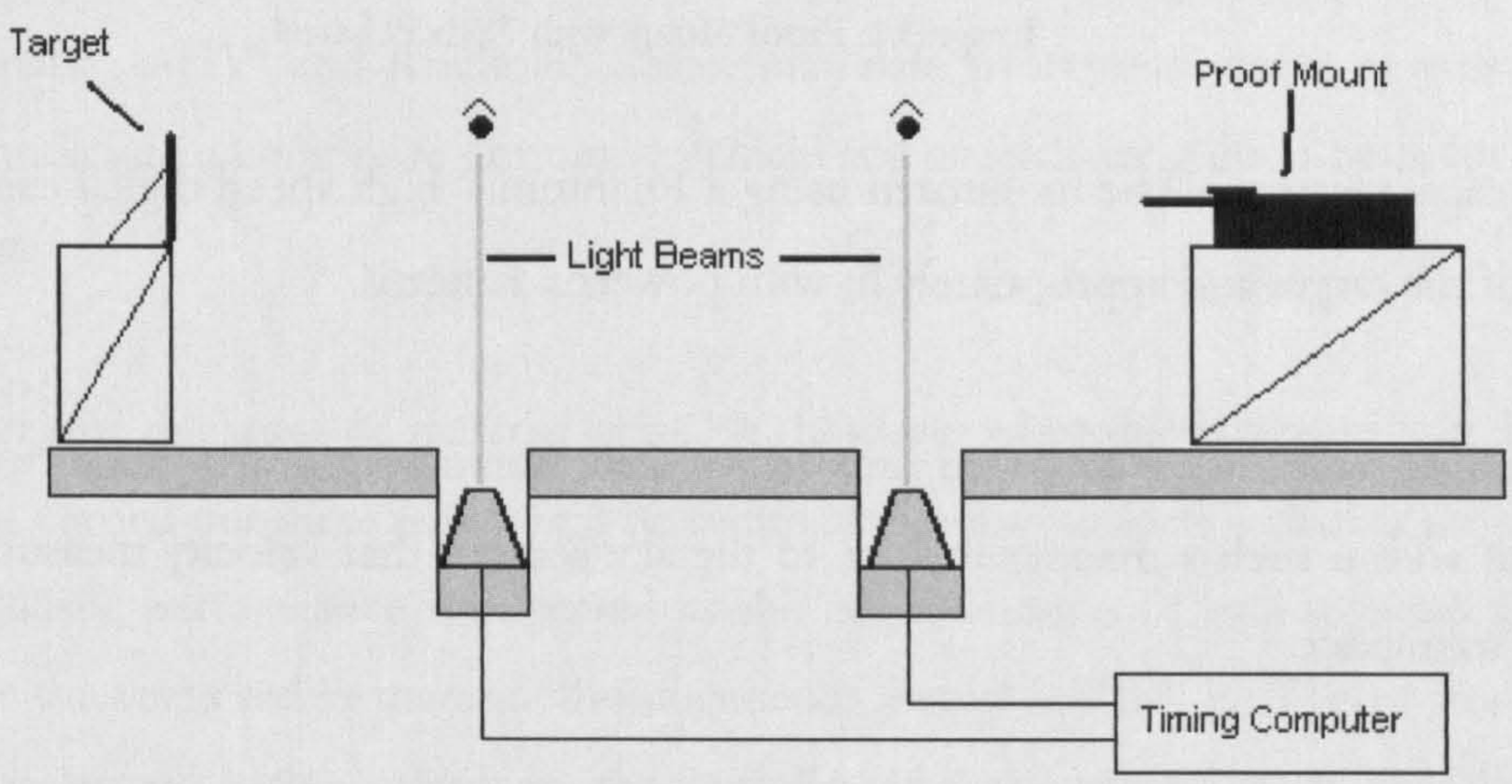

Figure 3.1: Sky Screen Schematic

Projectile velocity will be varied by removing the bullet from the case and adjusting the amount of propellant charge. There is both an upper and lower limit on the amount of charge variation which can be performed; too little charge and the bullet may not leave the barrel or will fly very poorly. Too much and it will not be possible to fit the bullet into the case securely due to sheer volume of propellant.

The projectiles are fired from 7.62mm rifle barrels chambered for the respective ammunitions used and fitted to a universal proof mount. This apparatus is capable of mounting many different weapon barrels and firing them accurately for test purposes. The ammunition is remotely fired by a solenoid activated from a secure firing room.

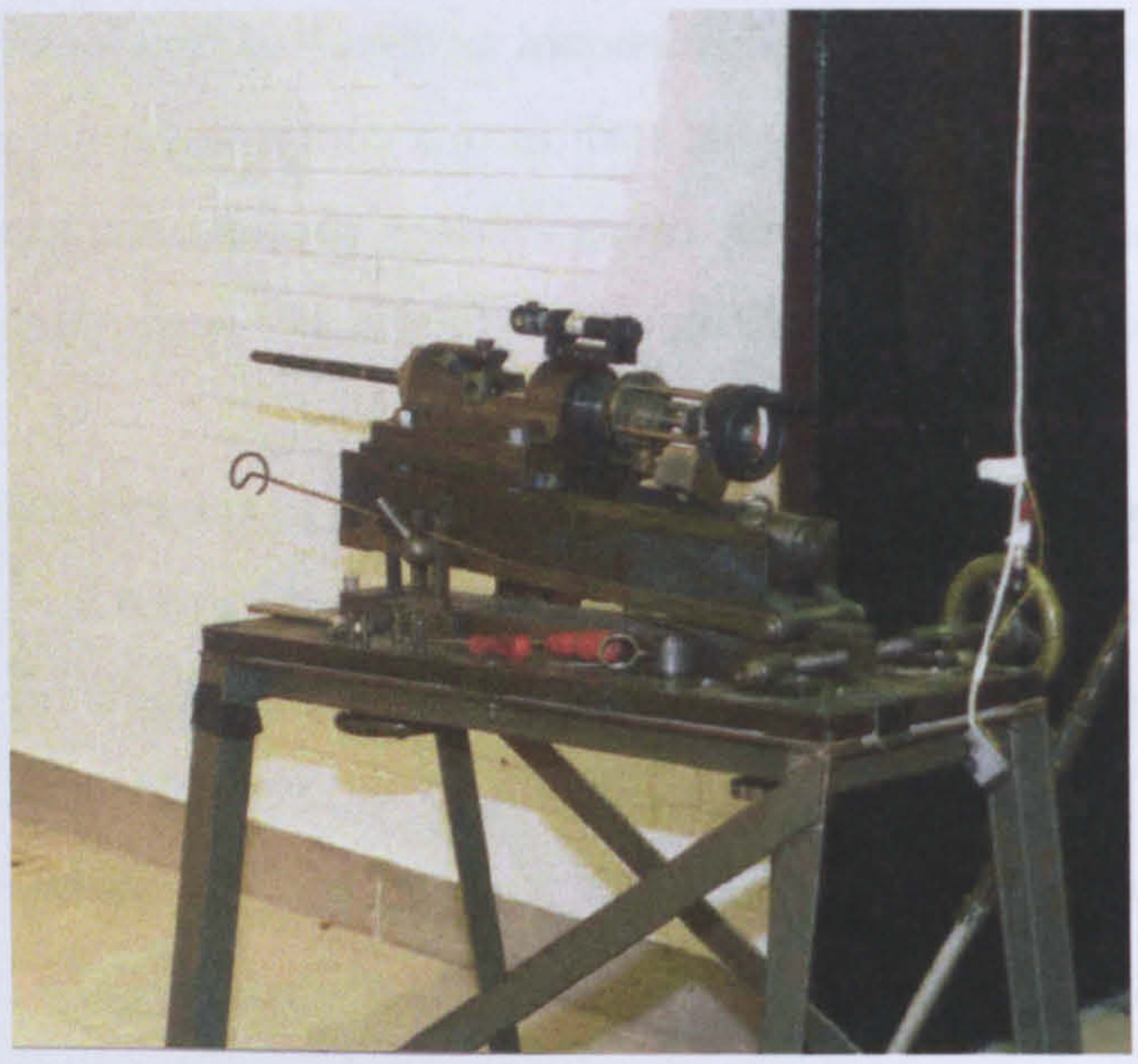

Image 3.1: Proof Mount with 7.62x39 barrel

The impact event will be monitored using a Phantom 7 high speed digital camera set to one side of the target and appropriately lit with powerful lanterns.

The target panels were mounted on a heavy steel frame 10m down range from the weapon mount and in such a manner relative to the sky screens that velocity measurement is made prior to impact.

The target was securely clamped to the frame with the provision for additional paper witness screens for checking for spall / perforation and for ensuring the bullet was straight in flight prior to impact, an important check for low velocity rounds).

Image 3.2: Target arrangement with front and rear witness screens

3.3.3 Material available for testing

The majority of the experimental work in this project will be carried out on a set of thick structural composite materials which have been supplied for investigation by a collaboration of VT Halmatic[a], AGY[b] and Reichold[c]. These materials are representative of what can be used to manufacture a composite armoured vehicle and as such are a good basis for detailed investigation.

There is only one thickness of material available, however to enable testing at a higher areal density to be carried out these panels will be clamped together to form a thicker target. Some effect on ballistic performance is expected as the target consists of two separate panels to make up the thickness rather than one homogeneous material. Work by Tekyeh-Marouf and Bagheri [49] on layered beams subject to impact indicated that a layered target absorbed more energy than a target of single equivalent thickness. Careful examination of the tested materials will be required to determine if the layered construction of the target has affected the ballistic performance.

---

a VT Halmatic Ltd, Portsmouth, UK

b Advanced Glass Yarns, Aiken, S-Carolina (EU; Lyon, France)

c Reichhold UK Ltd, Mitcham, UK

3.3.3.1 Reinforcement material

The reinforcement material used in these panels is an Magnesium Aluminosilicate glass [50] fibre known as S2 glass and is manufactured by the AGY group. These fibres are woven into different pattern fabrics which are then laid one on another to the required design.

The reinforcements used are of three different weave weights, 830gsm with 1000tex size fibres (a coarse and heavy weave), 300gsm with 66tex fibres (a fine weave) and 190gsm with 66text warp and 33 tex weft fibres (a fine and light weave).

1. Heavy – 830gsm Plain weave 1000 tex
2. Medium – 300gsm Plain weave 66 tex
3. Light – 190gsm Plain weave 66/33 tex

3.3.3.2 Matrix material

The S2 Glass reinforced panels were used with two different matrix materials; Vinylester (x3 panels) and Phenolic (x1 panel).

The Vinylester matrix resin was supplied by Reichold and was selected by the panel manufacturers for its toughness, environmental resistance and high mechanical strength. This is a common commercial matrix resin which chemically is part of the epoxy family of plastics. This resin is well suited to structural applications due to its relatively high strength and toughness and is widely used in the manufacture of large scale Resin Transfer Moulding (RTM) components due to its room temperature cure cycle.

The Phenolic materials were supplied through AGY, Phenolic was chosen for comparison as it is a common matrix used in ballistic composites, Phenolic resins require a heated press-tool for consolidation and cure.

3.3.3.3 Manufacture

The Vinylester panels have been manufactured by an industrial grade hand lay-up and RTM process. The Phenolic panels have been manufactured by a hot press curing technique. The resultant test materials are as follows:

1. S2 Glass, Heavy 830gsm cloth, Phenolic Matrix
2. S2 Glass, Heavy 830gsm cloth, Vinyl Ester Matrix
3. S2 Glass, Medium 300gsm cloth, Vinyl Ester Matrix
4. S2 Glass, Light 190gsm cloth, Vinyl Ester Matrix

The construction and properties of the raw Vinylester panels available for testing are summarised in the following table:

Reinforcement	830gsm S2	830gsm S2	300gsm S2	300gsm S2	190gsm S2	190gsm S2
Weave	2000 tex	2000 tex	66 tex	66 tex	66/33 tex	66/33 tex
Weave Weight (gsm)	830	830	300	300	190	190
T (mm) [Cured panel]	22	22	23	23	21	21
Plies	30	32	90	90	100	100
Volume Fraction (%)	47.9	51.1	47.4	47.4	36.6	36.6

Table 3.1: Target material details

3.3.3.4 Target material quality assessment

3.3.3.4.1 830gsm – Heavy weave Phenolic

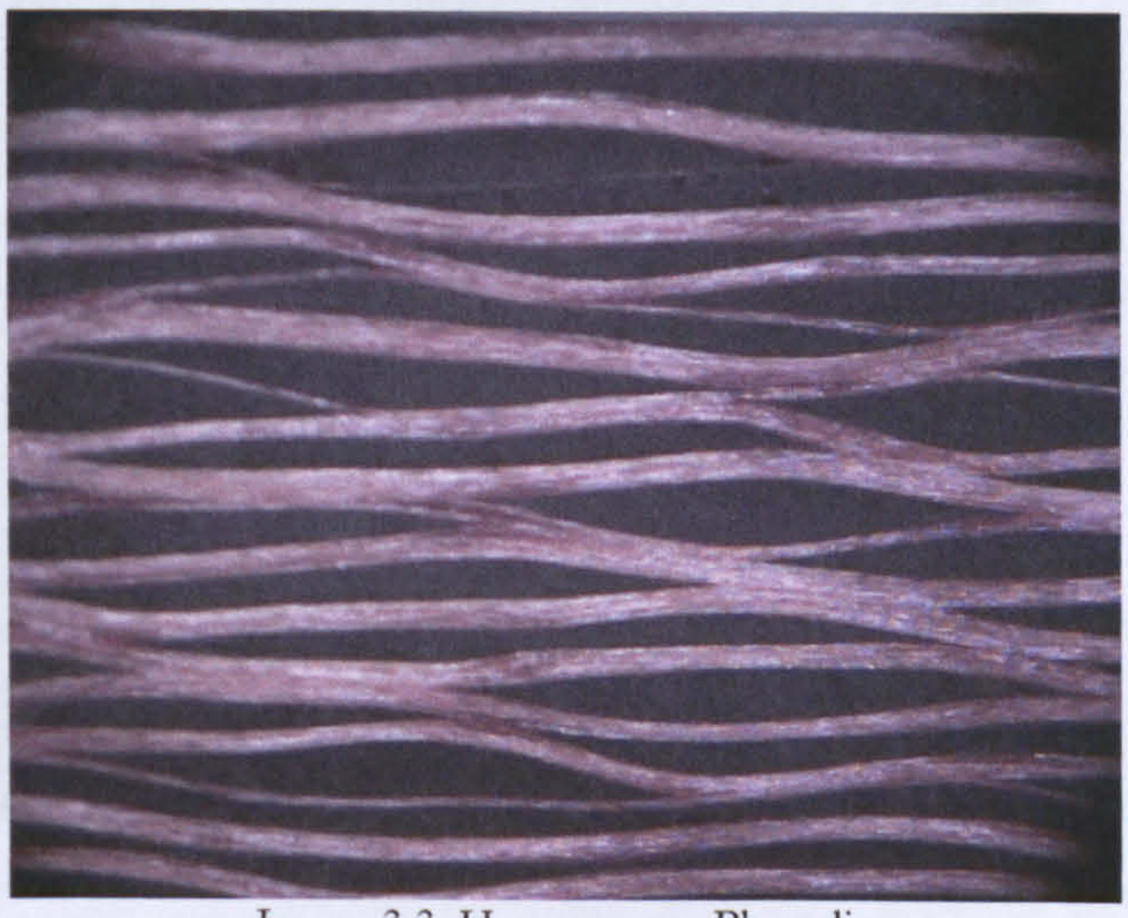

Image 3.3: Heavy weave Phenolic

This is a coarse laminate – many resin rich areas, despite press curing some air bubbles along lamina. Non-straightness of the weft fibres is very apparent. Variation through thickness of lamina density i.e. some areas lamina are closer packed, than others.

3.3.3.4.2 830gsm – Heavy weave Vinylester

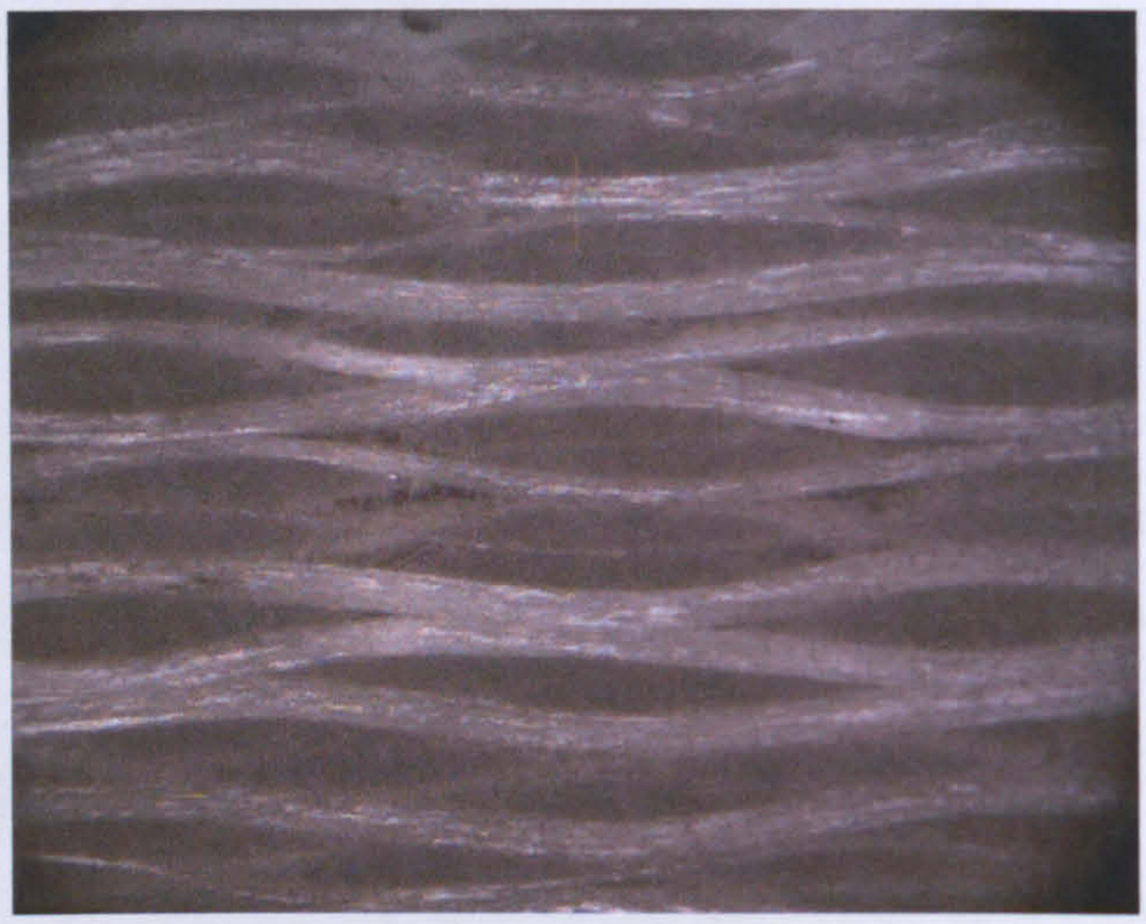

Image 3.4: Heavy weave VE

This is a coarse laminate – many resin rich areas, despite vacuum bag curing some air bubbles along lamina. Only slightly poorer laminate than the press cured Phenolic. Non-straightness of the warp fibres is very apparent. Variation through thickness of lamina density i.e. some areas laminas are closer packed, this is more apparent than in the Phenolic panel.

3.3.3.4.3 300gsm – Medium weave Vinylester

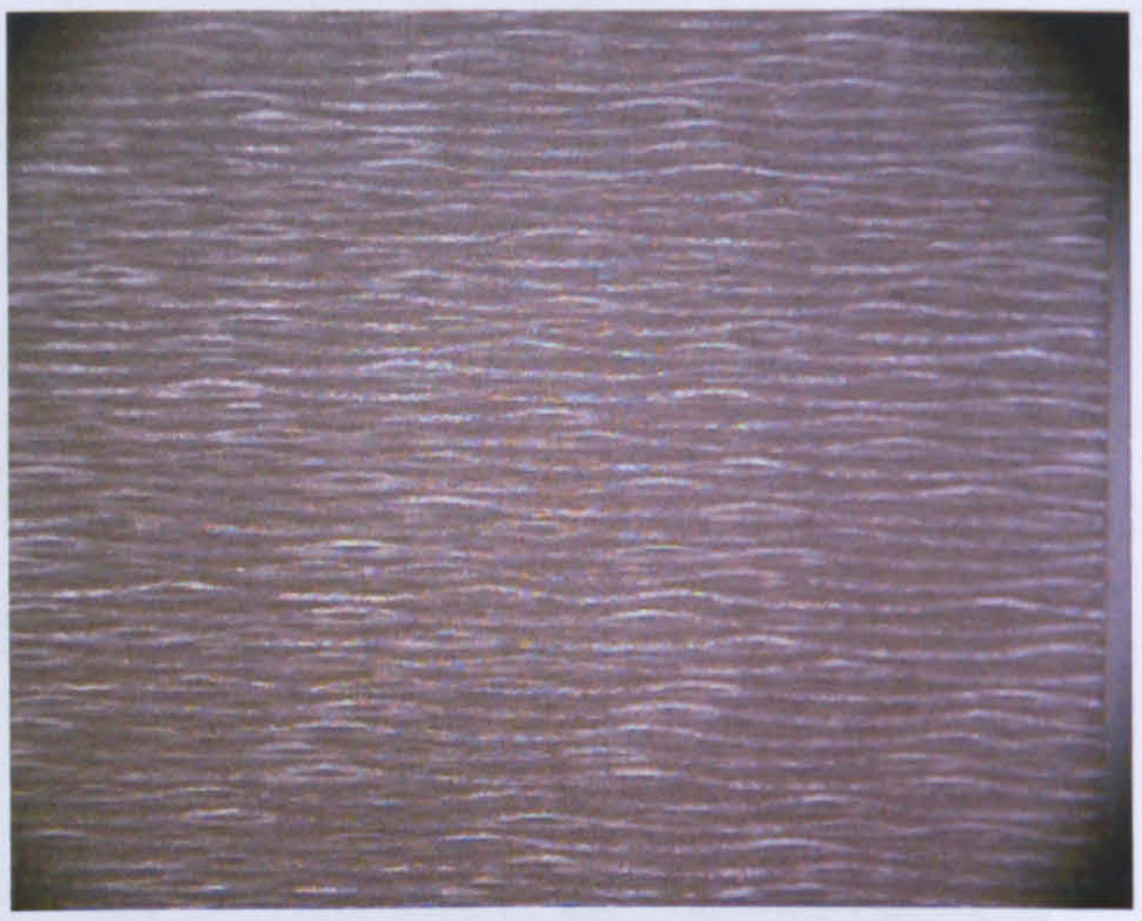

Image 3.5: Medium weave VE

This is a very densely packed laminate, numerous very fine air bubbles are present – estimated as being a similar volume of trapped air to the 830gsm VE material.

3.3.3.4.4 190gsm – Light weave Vinylester

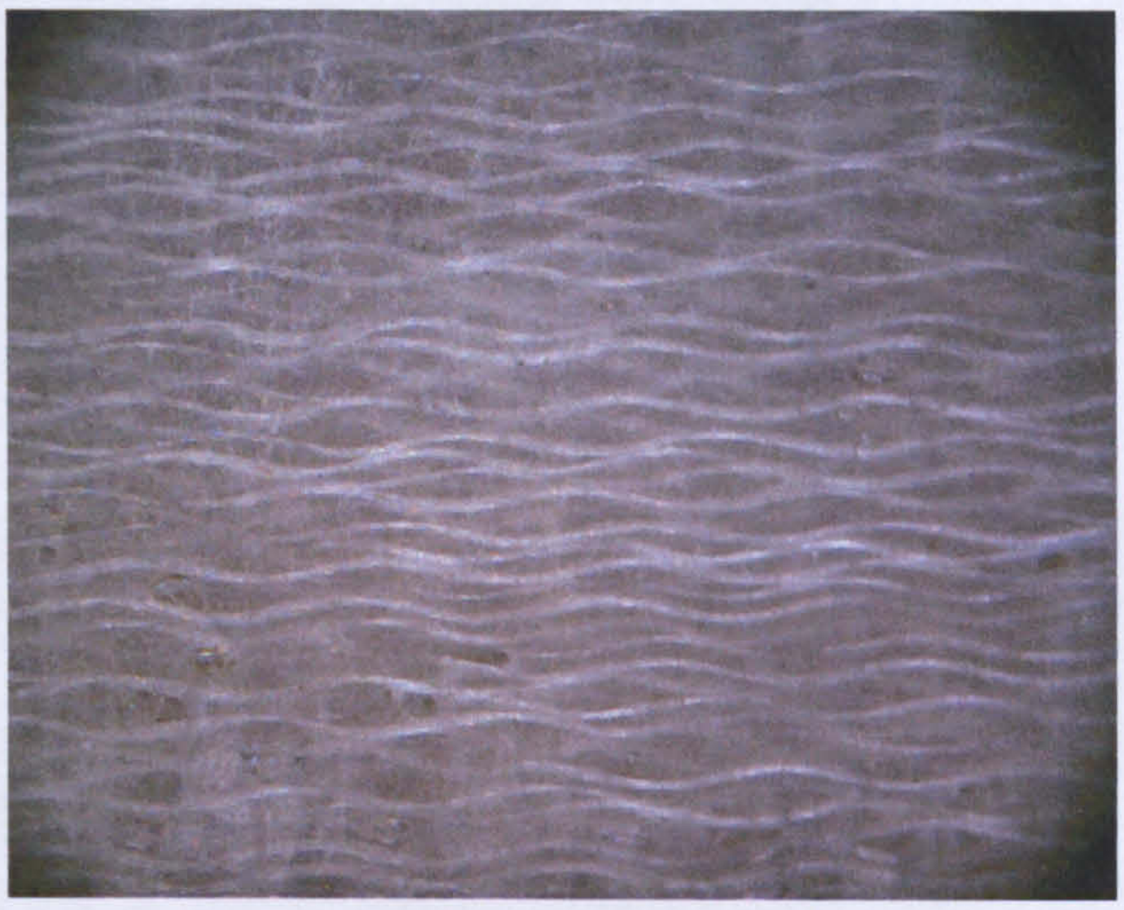

Image 3.6: Light weave VE

This is a very densely packed laminate however there is a very large number of air bubbles present between plies. These bubbles appear to be quite large. The lamina density appears to vary somewhat through thickness, however this could be a visual effect due to the cut edge of the material examined being at a slight angle to the fabric orientation. The reinforcement weave is light but quite open compared to the other weaves.

It can be seen from the above set of images under the same low magnification that the heavy weave materials are relatively free from voids, also visible is the 'wavyness' of the fibres due to the weave. Presence of voids is not visible to the eye in the medium weave material, the straightness of the weave however is apparent. The final picture shows the finest weave, the size and amount of air bubbles is clearly visible as is the apparent irregularity of the weave.

3.3.4 Threats

The panels were tested against:

1. 7.62mm calibre ball ammunition (7.62 x 51 Ball) as per STANAG 4569 level I
2. 7.62mm calibre armour piercing rounds (7.62x39 AP) as per STANAG 4569 level II

Image 3.7: Ammunition: Left – Right 7.62x51 Ball (FMJ), 7.62x39 AP (Steel Core), 7.62 bullet, 7.62 AP core

3.3.5 Results

3.3.5.1 Ball Ammunition (STANAG level I)

Six shots with three perforations and three successful stops within a 40ms^{-1} velocity bracket were recorded and averaged for V_{50} (as per MIL-STD-662F [48]) and are tabulated below. Results are plotted in the form of V_{50} against areal density (the weight of the armour per unit of surface area) as this is the most suitable method for comparing material performance, the closer to the *y*-axis a material is the lighter it is, the further from the *x*-axis, the better its ballistic performance. Results closest to the top left corner of the chart are the best performers (in terms of weight and ballistic performance alone).

Material	**Heavy Phen**	**Heavy VE**	**Medium VE**	**Light VE**
Areal Density (kgm^{-2})	40.6	34.4	39.5	34.6
Thickness (mm)	21	21	23	21
V_{50} Speeds (ms^{-1})				
#1 (perf)	773	665	662	439
#2 (perf)	778	665	650	424
#3 (perf)	788	654	637	442
#4 (stop)	753	634	639	416
#5 (stop)	767	648	649	418
#6 (stop)	777	642	635	434
V_{50} (ms^{-1})	773	651	645	429

Table 3.2: Ballistic testing results vs Ball Ammunition

The diameter of the observed damage was recorded in the following table and averaged over the V_{50} shots.

Material	Thickness (mm)	Areal Density (kgm^{-2})	V_{50} (ms^{-1})	Damage	
				Front (mm)	Rear (mm)
Heavy weave Phenolic	21	40.6	773	36	150
Heavy weave VE	21	34.4	651	51	252
Medium weave VE	23	39.5	645	75	192
Light weave VE	21	34.6	430	28	103

Table 3.3: Damage assessments vs Ball Ammunition

Image 3.8: Successful stops, front surface: CW from Top Left; Heavy Phenolic, Heavy VE, Light VE, Medium VE

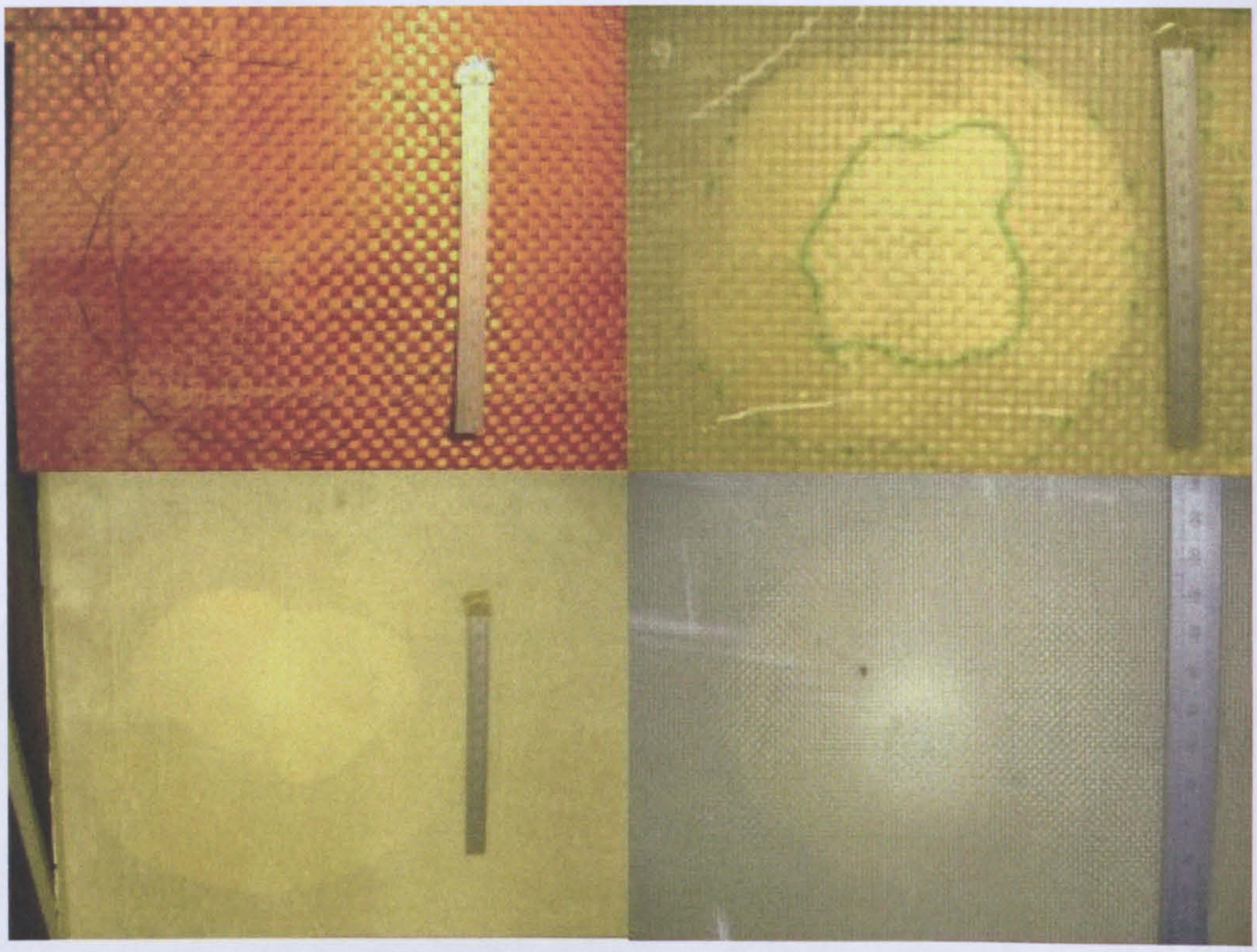

Image 3.9: Successful stops, rear surface: CW from Top Left; Heavy Phenolic, Heavy VE, Light VE, Medium VE

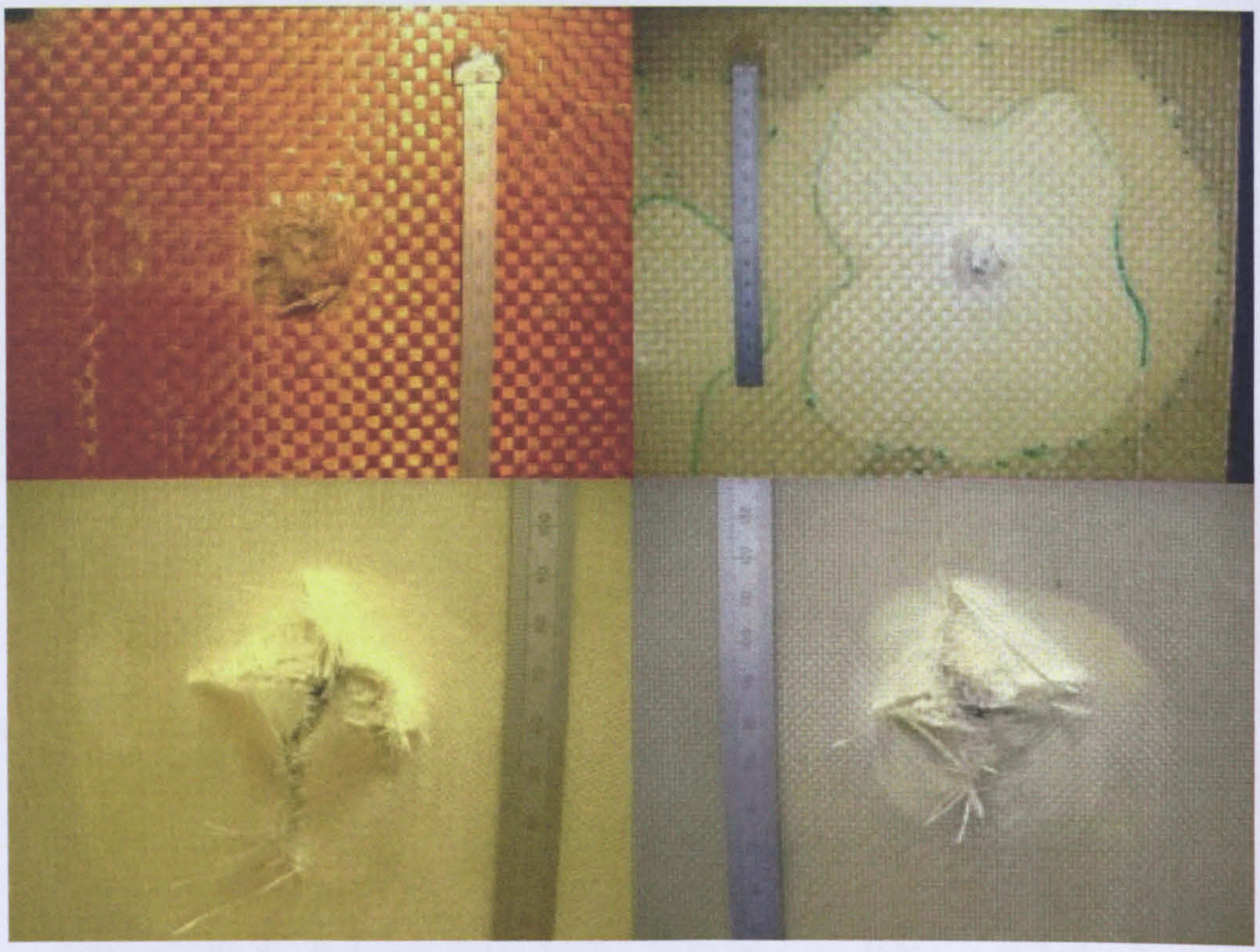

Image 3.10: Perforations, rear surface: CW from Top Left; Heavy Phenolic, Heavy VE, Light VE, Medium VE

3.3.5.2 AP Ammunition (STANAG level II)

As against Ball ammunition in section **3.3.5.1** the six shots V_{50} are tabulated below. Graph 3.1 plots V_{50} against areal density for the same reasons as previously discussed.

Material	Heavy Phen	Heavy VE	Medium VE	Light VE
Areal Density (kgm^{-2})	41.9	33.9	38.9	34.7
Thickness (mm)	21	21	23	21
V_{50} Speeds (ms^{-1})				
#1 (perf)	450	411	425	372
#2 (perf)	440	425	433	384
#3 (perf)	445	392	440	384
#4 (stop)	421	362	413	356
#5 (stop)	436	409	420	360
#6 (stop)	427	363	413	356
V_{50} (ms^{-1})	436	394	424	362

Table 3.4: Ballistic testing results; Thin targets vs AP Ammunition

Material	Heavy Phen	Heavy VE	Medium VE	Light VE
Areal Density (kgm^{-2})	84.3	73.9	78.6	67.7
Thickness (mm)	40	40	44	41
V_{50} Speeds (ms^{-1})				
#1 (perf)	686	638	696	632
#2 (perf)	693	636	687	621
#3 (perf)	684	629	686	623
#4 (stop)	685	610	660	610
#5 (stop)	675	623	688	624
#6 (stop)	676	622	680	603
V_{50} (ms^{-1})	683	626	683	619

Table 3.5: Ballistic testing results; Thick targets vs AP Ammunition

As in the previous section the diameter of the observed damage was recorded and averaged over the V_{50} shots to produce the following table.

Material	Thickness (mm)	Areal Density (kgm^{-2})	V_{50} (ms^{-1})	Damage diameter (mm) Front	Rear
Heavy weave Phenolic	21	41.9	436	48	130
	40	84.3	683	-	-
Heavy weave VE	21	33.9	394	50	111
	40	73.9	626	56	96
Medium weave VE	23	38.9	424	64	119
	44	78.6	683	57	132
Light weave VE	21	34.7	362	33	77
	41	67.7	619	45	75

Table 3.6: Damage assessment vs AP Ammunition

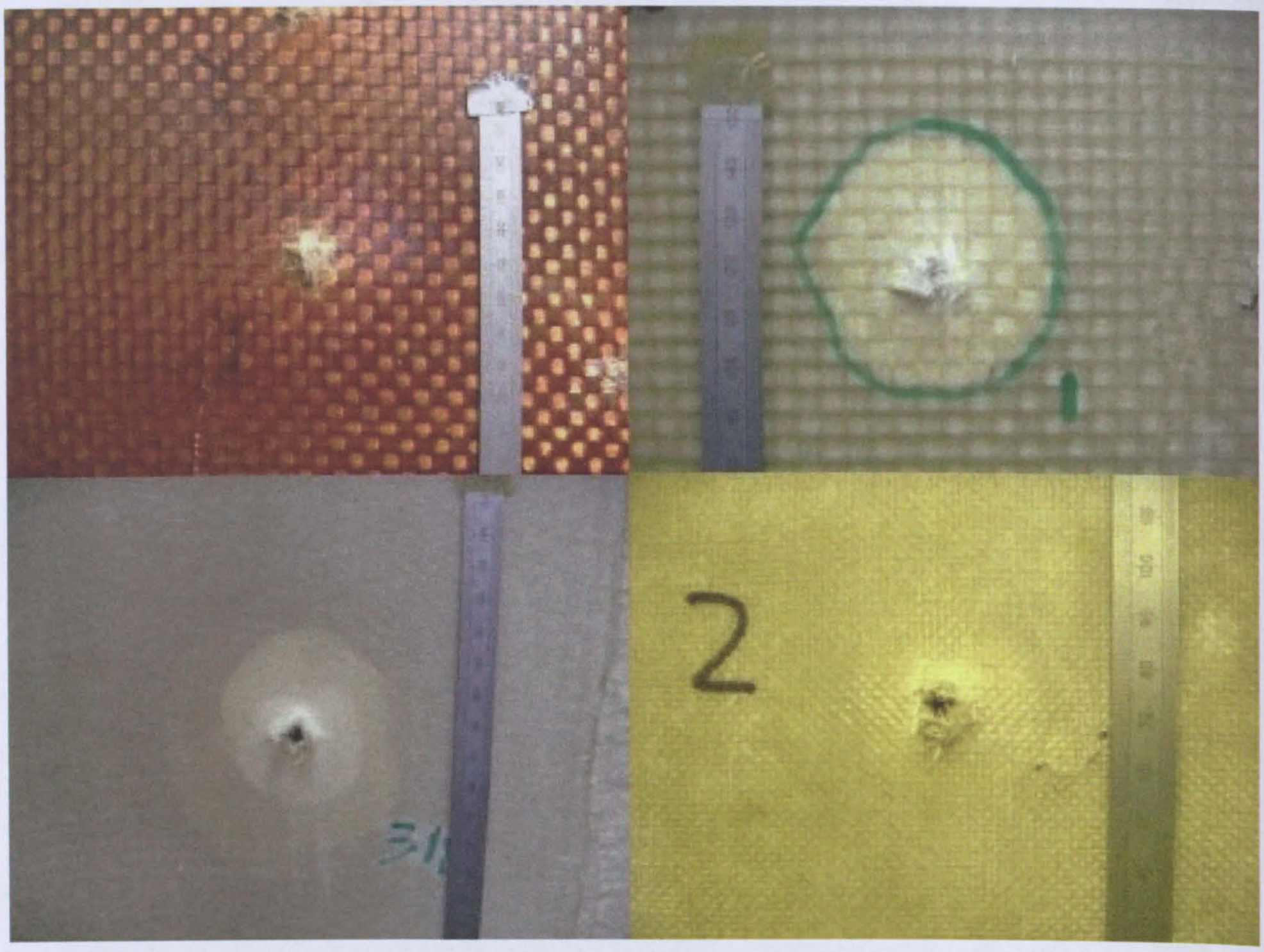

Image 3.11: Successful stops, front surface: CW from Top Left; Heavy Phenolic, Heavy VE, Light VE, Medium VE

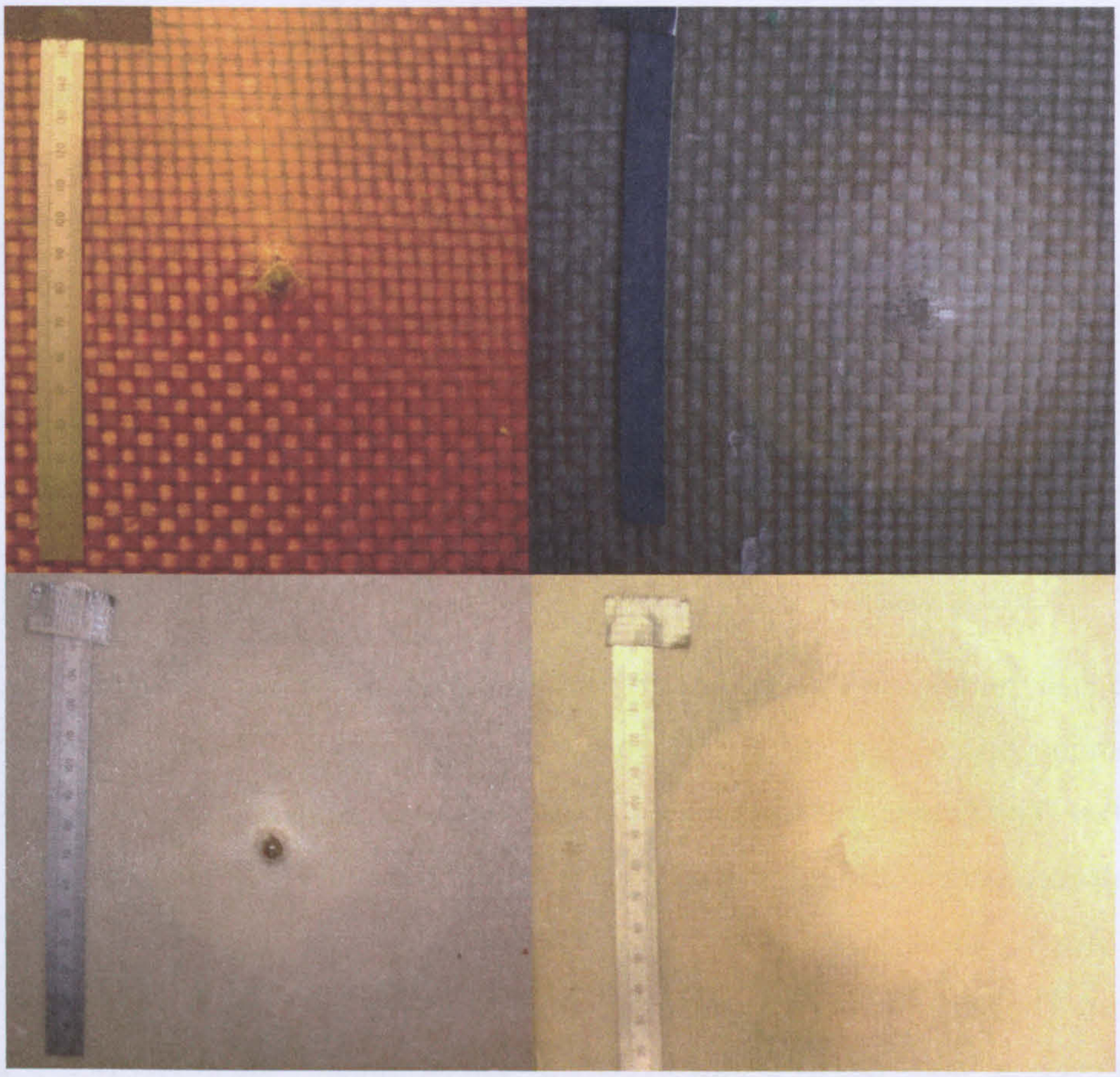

Image 3.12: Successful stops, rear surface: CW from Top Left; Heavy Phenolic, Heavy VE, Light VE, Medium VE

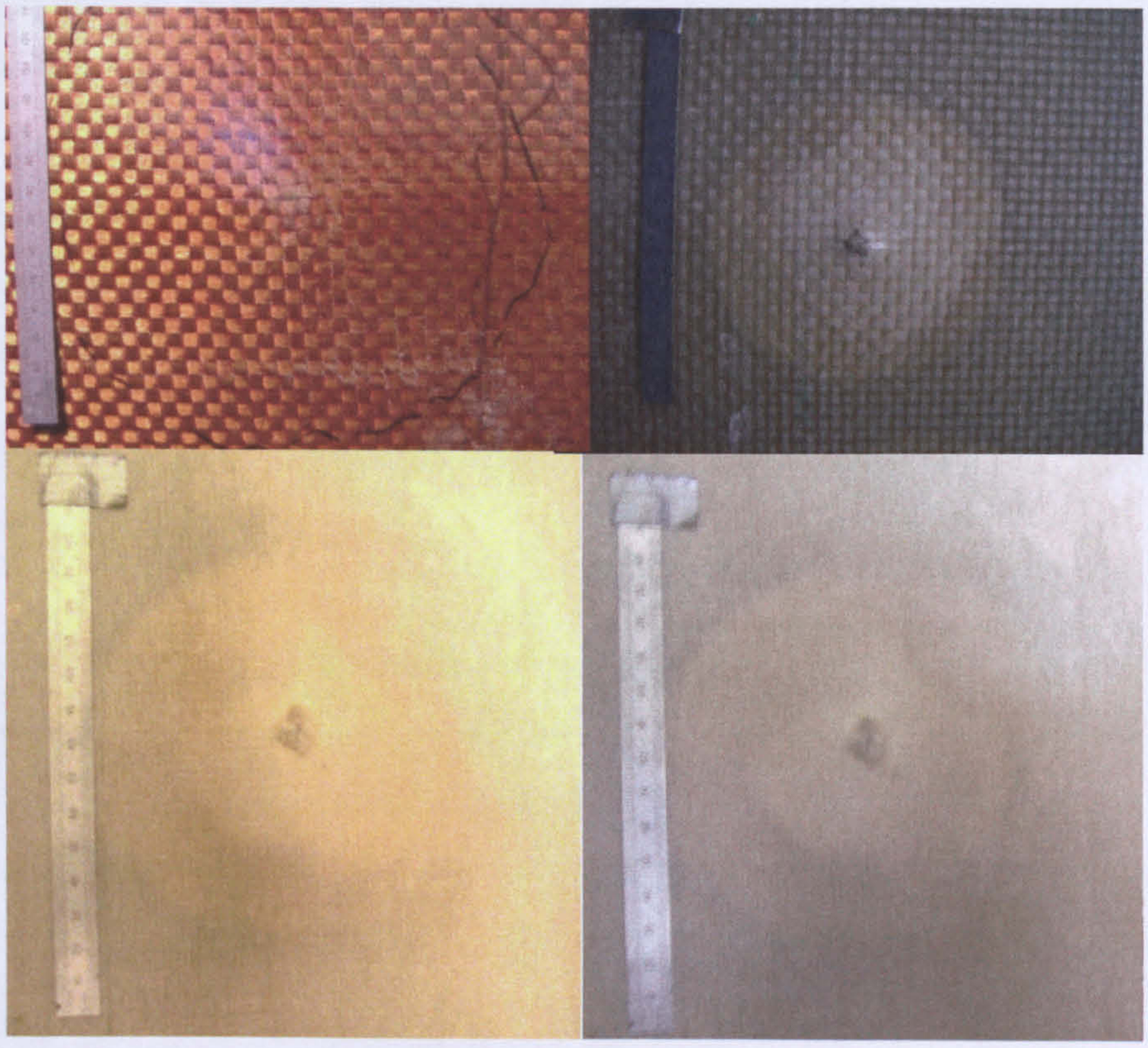

Image 3.13: Perforations, rear surface: CW from Top Left; Heavy Phenolic, Heavy VE, Light VE, Medium VE

3.3.6 Observations of damage

The following observations are made on the basis of visible evidence and are very much limited to delaminations near the material surface. Due to the lack of contrast between damaged and un-damaged material it not possible to make complete observations of the damage to the Phenolic targets.

It was noticed that whilst AP rounds perforated the panels at much lower velocities than the ball rounds the delamination caused was much less, the relationship between visible damage and ballistic performance will be discussed in Chapter 6.

The ball round stops in the heavy weave panels (both Phenolic and VE) caused large delamination areas, in some cases these were in excess of 250mm in diameter on the rear surface The lighter weaves suffered smaller areas of damage for a stop. The medium VE reinforced panels suffered damage that was approximately $^{2}/_{3}$ of the size of the size seen in the heavy panels, however the velocities required to stop a round were also considerably lower. The light weave VE panels suffered an even smaller degree of damage during a stop however the stop velocity is little over ½ of that stopped by the heavier weave panels.

The damage caused by ball rounds perforating panels seemed to be very dependent on the reinforcement architecture. The heavy weave reinforcing cloth was torn out in a bundle fashion shedding matrix material from the fibres. The medium weave VE material acted in a brittle manner and tore in the 0° and 90° directions with far more damage. The light weave panel failed in a similar fashion to the medium panel however the damage area and torn material was much smaller, no doubt as a result of the lower velocity of the impacts.

3.3.7 Discussion and Summary

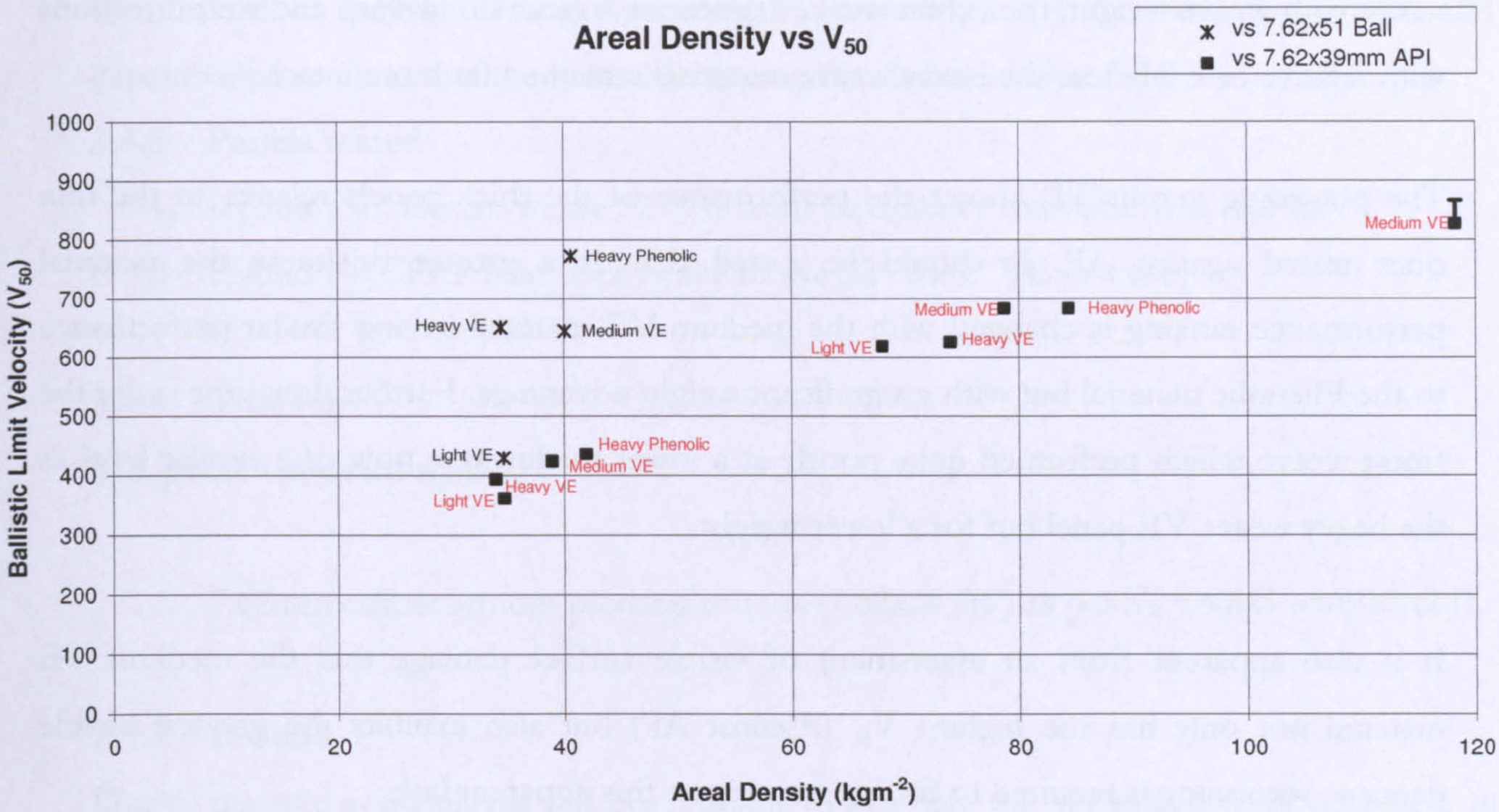

Graph 3.1: Ballistic Testing Summary

It can be see from the above chart where the materials shot fall in relation to each other. The better the material is (on both accounts of V_{50} and areal density) the closer it will be to the top left hand corner of the chart, the closer to the bottom right a material is the less mass efficient and the poorer its ballistic performance. The spread in performance between the materials tested against ball ammunition is far greater than that between those tested against AP ammunition (against ball the poorest panel is approximately half the performance of the best whilst against AP the poorest panel has more than two thirds of the best panels performance). This suggests that there are material properties which significantly affect ballistic performance against deformable ammunition but are less important against rigid, non deformable AP projectiles.

It can be seen in both single thickness cases (ball and AP) that whilst the heavy weave Phenolic panel has the highest V_{50} it is also has the greatest areal density. The heavy weave VE panel however is considerably lighter, it does however have a poorer ballistic performance. Against ball ammunition the heavy and medium VE panels have similar performance (though the lighter weave of the two has a higher areal density) however, against AP ammunition the medium weave material performs appreciably better.

It is apparent that against ball ammunition the failure pattern of the rear face of the target varies with weave weight, the lighter weaves appearing to tear along warp and weft directions with relative ease whereas the heavy weave materials remained far more intact.

The preceding graph (3.1) shows the performance of the thick panels relative to the thin ones tested against AP. It should be noted that at a greater thickness the material performance ranking is changed with the medium VE material having similar performance to the Phenolic material but with a significant weight advantage. Further down the order the finest weave which performed quite poorly at a lower thickness is now of a similar level as the heavy weave VE panel but for a lower weight.

It is also apparent from an assessment of visible surface damage that the medium VE material not only has the highest V_{50} (Against AP) but also exhibits the greatest visible damage, sectioning is required to further investigate this apparent link.

To estimate the errors likely to be present when using only 2 data points to create a ballistic performance trend a very thick panel of medium weave material was tested. The panel exceeded the capabilities of the ammunition being used (no rounds could be made to perforate). This prevented a rough bracket of the V_{50} velocity being made, instead it was proved that V_{50} was considerably in excess of the recorded velocity, this velocity can then be used as a rough 'minimum' data point.

The V_{50} value for the thickest medium weave panel (Shown in Graph 3.1) is not a valid V_{50} due to no shots being able to perforate the amour, the V_{50} is hence somewhat higher than the plotted value (hence error bars) however at the STANAG level II velocity of 695 ms^{-1} it is apparent that the error relative to a best fit line through the results for other areal densities is small. This suggests a fairly linear increase in ballistic limit velocity with increasing areal density.

3.4 Ballistic testing of hybrid materials

3.4.1 Aims

As a result of previous ballistic testing, combinations of panel materials were assembled as targets and tested to try and optimise front and rear faces. Materials were selected on the basis of observations and performance in previous testing. Whilst hybridisation of metallic armours is not a new idea there is little literature relating to composites[38].

3.4.2 Experimental

This round of ballistic testing was carried out with exactly the same equipment and experimental setup as that used in earlier testing detailed in section **3.3.2**

3.4.3 Panels tested

1. Hybrid 1 – Medium weave S2/VE front face, heavy weave S2/VE rear face
2. Hybrid 2 – CFRP front face heavy weave S2 Glass/ VE rear face

3.4.4 Threats

The panel was tested against:

1. 7.62mm calibre armour piercing rounds (7.62x39 AP) as per STANAG 4569 level II.

3.4.5 Results

Due to material availability it was not possible to ascertain full V_{50} values, however based on the results it was possible to estimate the region in which the value might fall. The following graph (Graph 3.2) plots the performance of the hybrid materials along with the results against STANAG level II ammunition from previous GFRP testing (Sections **3.3**) for comparison.

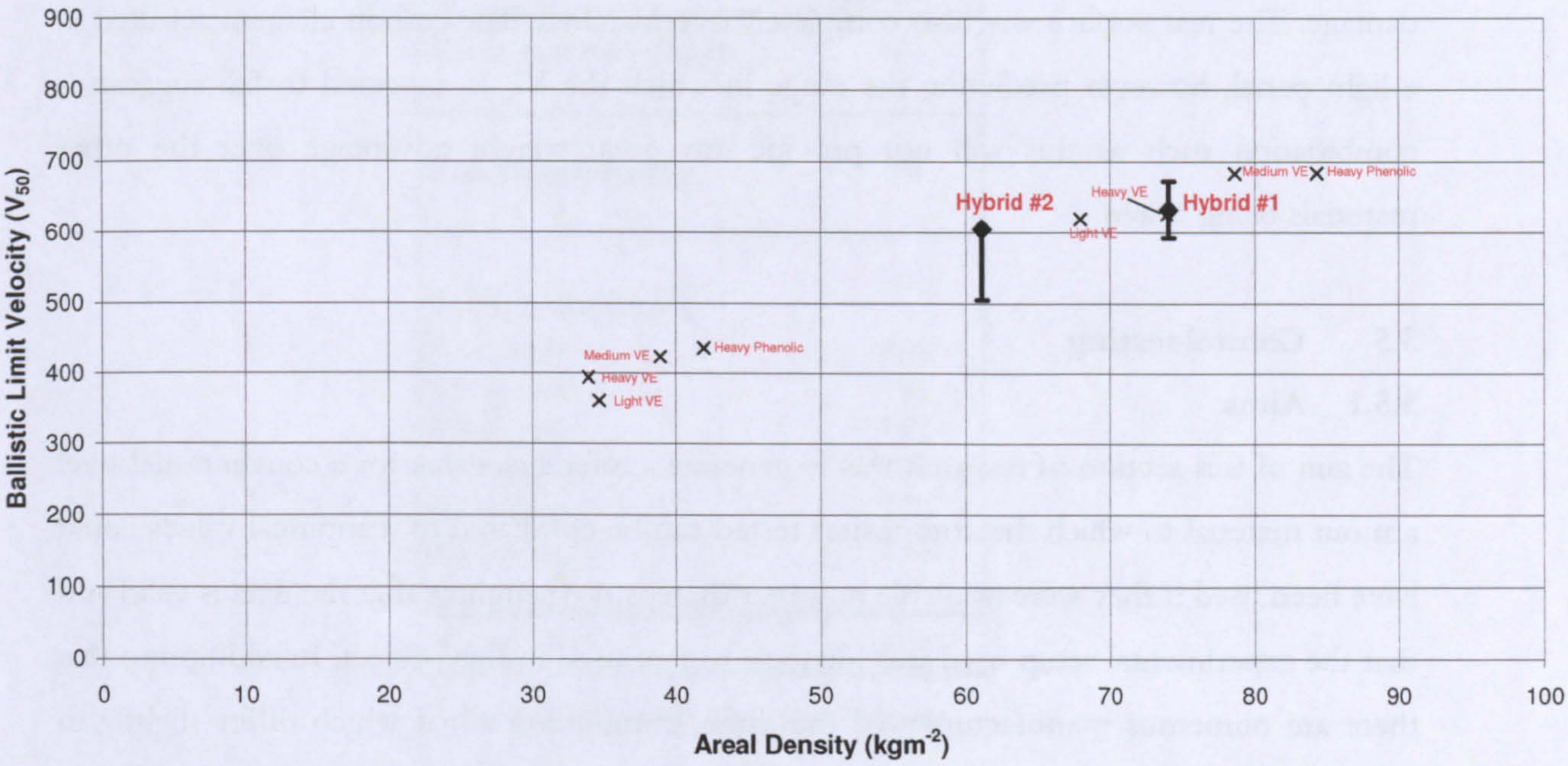

Graph 3.2: Ballistic testing of hybrid materials (GFRP testing included for comparison, error bars indicate V_{50} spread)

3.4.6 Discussion and summary

The theory was that the medium weave material on the front face would slow down the round sufficiently that, by the time that the material damage reached the coarse weave rear face the energy density would be such that the rear face could begin to delaminate and catch the projectile. The intention was that this material would have a higher V_{50} than both the double thickness medium and thick materials on their own.

The material was approximately the same areal density as the heavy weave VE material and around 5 kgm^{-2} lighter than the medium weave VE material.

The performance was however not as good as expected, the material achieved a stop at a velocity only a little higher than the equivalent all heavy weave target and 50ms^{-1} slower than the equivalent all medium weave target.

It was noted that the small material coupon tested was too small and delaminations in the rear material ran out to the edge of the coupon, this is anticipated to have had a small but negative effect on performance.

The second hybrid panel performed very poorly, the carbon front surface appearing to absorb little energy, damage was limited to a neatly punched hole with little delamination damage. The rear surface was also completely overmatched. The carbon element resulted in a light panel, however predicting the range in which the V_{50} is expected to fall suggests a combination such as this will not provide any great weight advantage over the other materials being tested.

3.5 Control testing

3.5.1 Aims

The aim of this section of research was to generate a reference value for a conventional steel armour material to which the composites tested can be compared to. Empirical values could have been used if they were available however there is no guarantee that the data is valid and that the experimental setup used was identical to that used in this project. In addition to this there are numerous manufacturers of the same ammunition all of which differ slightly in performance. By using the same test ammunition being used for all trials within this here a good reference value can be made.

3.5.2 Experimental

This round of ballistic testing was carried out with exactly the same equipment and experimental setup as that used in earlier testing detailed in section **3.3.2**

3.5.3 Panels tested

A sheet of 12mm thick RHA (Rolled Homogeneous Armour) steel was taken from the standard stock held at DCMT.

3.5.4 Threats

The panel was tested against:

1. 7.62mm calibre armour piercing rounds (7.62x39 AP) as per STANAG 4569 level II.

3.5.5 Results

The material tested was a standard RHA steel, however it took more shots than expected to achieve the V_{50}. The results are plotted below in Graph 3.3, included as a point of reference are the V_{50}'s recorded for three different areal densities of medium weave S2/VE material tested in sections **3.3** of this project.

Material	**12mm RHA**
Areal Density (kgm^{-2})	99
Thickness (mm)	12
V_{50} Speeds (ms^{-1}) **#1 (perf)** **#2 (perf)** **#3 (perf)** **#4 (stop)** **#5 (stop)** **#6 (stop)**	 800 791 762 777 770 768
V_{50} (ms^{-1})	778

Table 3.7: V_{50} shots for reference target

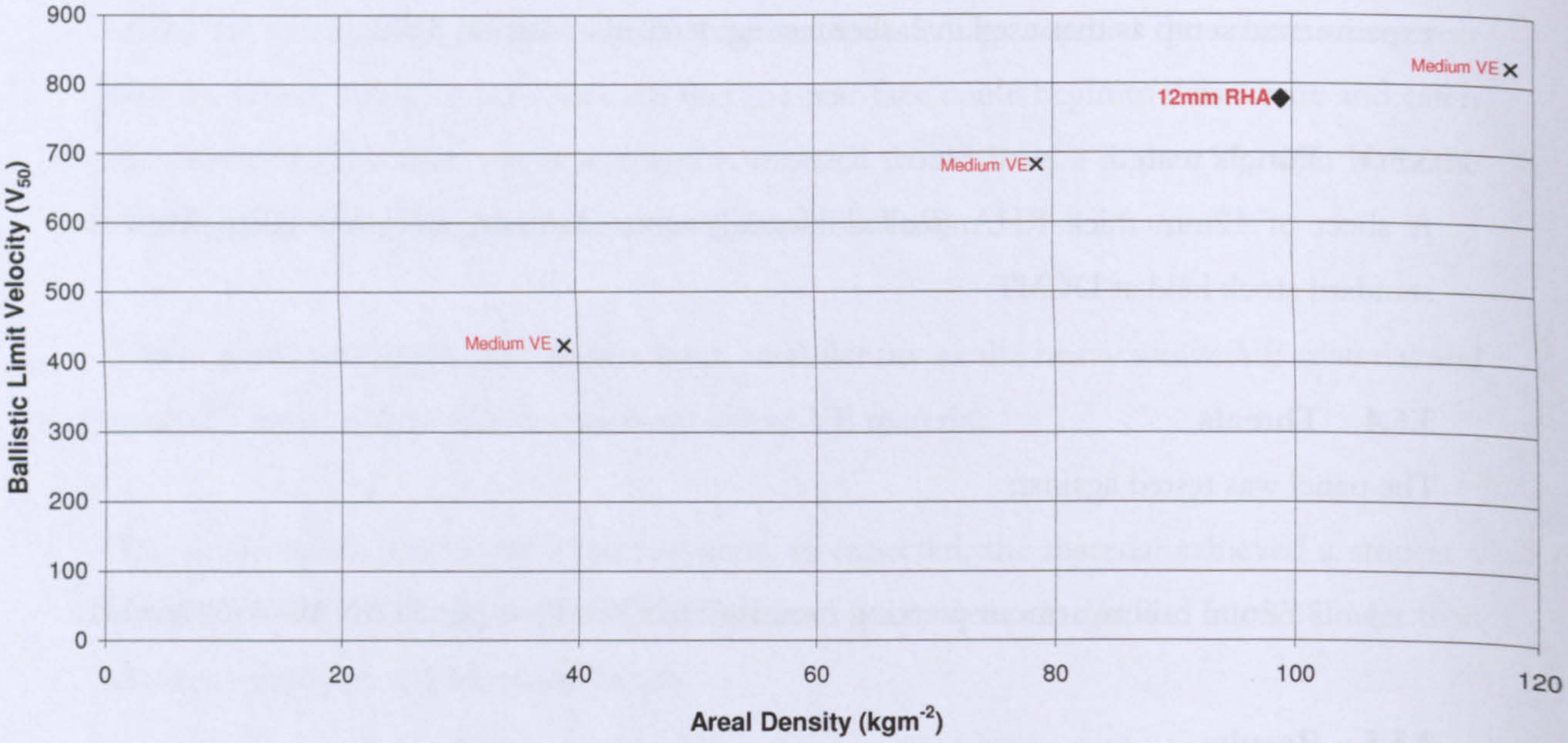

Graph 3.3: Control testing against AP ammunition (Medium weave GRFP testing points included for reference)

3.5.6 Discussion and summary

This testing gave the expected results with the V_{50} of the steel target being over that for STANAG level II. More importantly it has provided a reference value to compare the performance of the composite armours tested against. This is important not only for this work but for all follow up work as this data point provides a benchmark, especially important if different ammunitions (from different origins) are being used.

Plotting the results of this test against the medium weave VE data suggests that the steel panel is of comparable specific performance by the fact that is appears to lie in line with the composite data. This is not however representative of a steel armour system as there would be a requirement for a significant spall liner to catch the behind armour debris as a result of the armour being perforated. This will increase the weight of the system considerably making the all-composite systems a far more desirable solution.

3.6 Sectioning of Ballistic Impacts

3.6.1 Aims

The aim of this section of the investigation is to allow observation and comparison of the damage inflicted upon the composite armours being tested by ballistic impact. By sectioning ballistic impacts where the armour has stopped a projectile and also where it has failed should allow a qualitative evaluation of the material response to impact and hopefully lead to the identification of failure mechanisms and comparison with observations from mechanical testing.

3.6.2 Experimental

The impacts to be sectioned were selected from the shots used to calculate the V_{50} of the test material. A section was taken from an impact where the armour just failed and the projectile perforated and one in which the armour just succeeded and the projectile was stopped. By using such selection criteria the resultant sections will be from a velocity very close to the materials ballistic limit.

The panels were sectioned by a water cooled abrasive saw (for smaller targets) or by a water-jet cutting machine (this was undertaken by commercial contractors able to deal with large targets). These techniques allowed clean cutting of the composite without hiding or disturbing internal damage and also kept the majority of remaining bullet fragments in place. Where required X-ray analysis of the target materials will be carried out to identify any uncertain projectile locations.

All panels subjected to ballistic testing at STANAG levels I and II have been sectioned.

3.6.3 Results

3.6.3.1 Against Ball ammunition (STANAG level I)

Sectioning of the impacts showed the following damage architecture (Note; shot direction is from top, down in all images i.e. front face is near top of page):

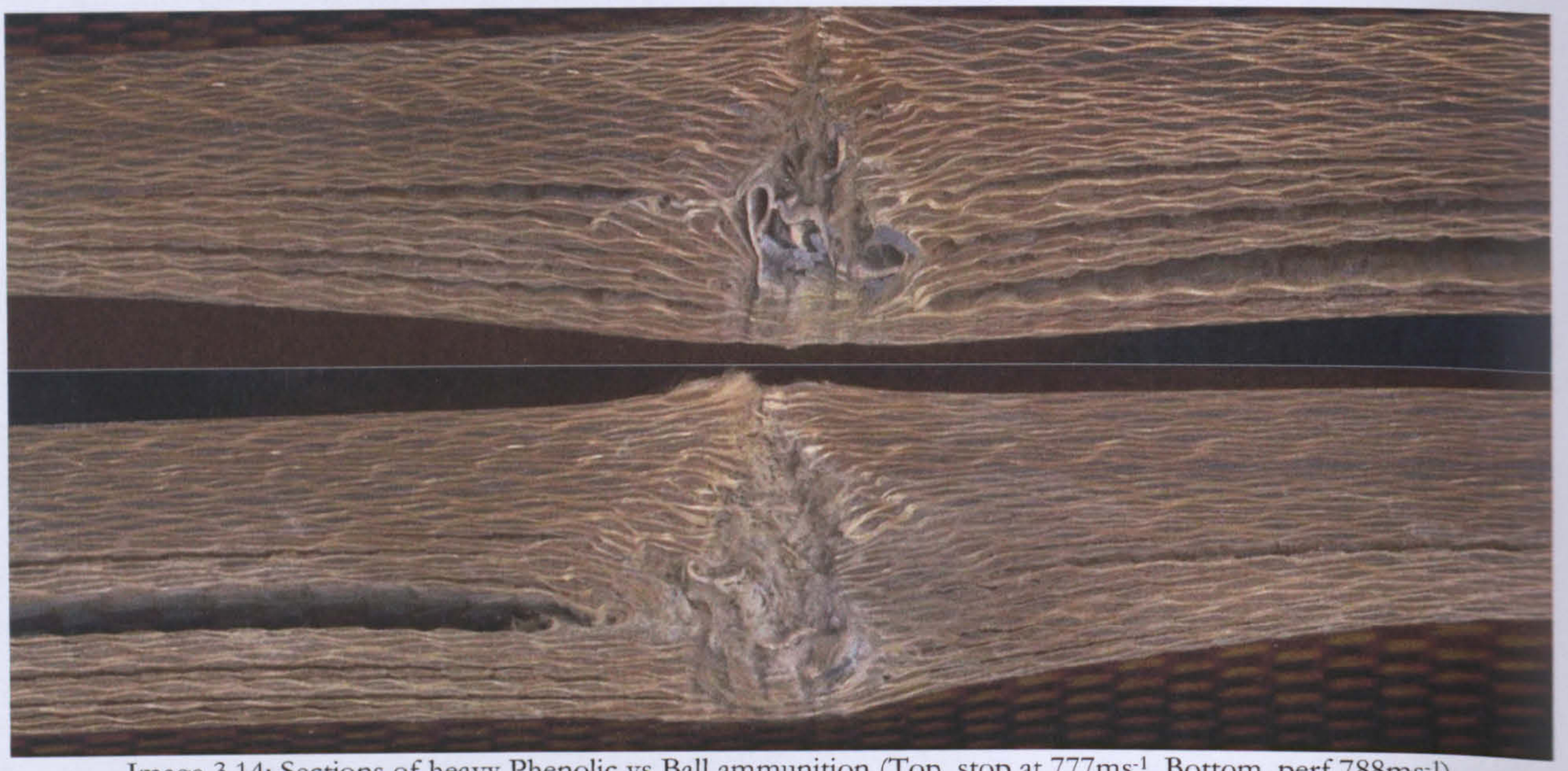

Image 3.14: Sections of heavy Phenolic vs Ball ammunition (Top, stop at 777ms^{-1}, Bottom, perf 788ms^{-1})

The impacting bullet has in both cases penetrated before beginning to break up, it is obvious at the point of breakup a great deal of damage is caused to the material and an internal cavity is formed. This cavity appears to be caused by the lead core of the bullet spreading outwards along the plane of the laminate and onwards through the material. The final failure of the perforated material is not directly in line with the bullet path but is rather a tensile failure of the material being displaced in front of the bullet cavity. There is far greater amounts of delamination in the panel which has stopped the bullet, though the pattern of damage does not appear to be symmetric either side of the bullet path.

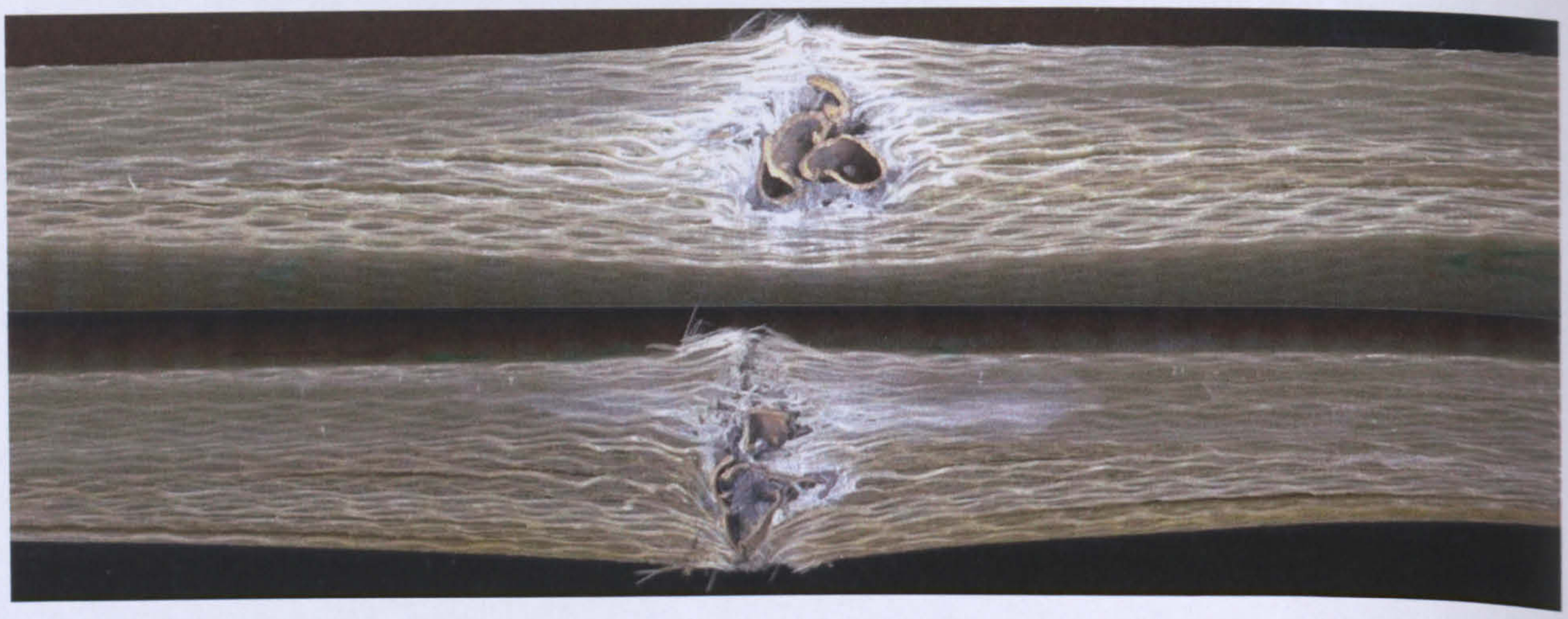

Image 3.15: Sections of heavy VE vs Ball ammunition (Top, stop at 620ms^{-1}, bottom, perf 665ms^{-1})

Sectioning of this material also showed the internal cavity caused by the breaking up of the impacting bullet, the cavity grows in size (with respect to thickness) at a slower rate than that observed in the equivalent Phenolic material (i.e. at a shallower angle), this may be due to the greater initial indentation resistance of the Phenolic material over the VE causing more deformation of the projectile.

The difference in shape of this cavity between the successful stops and perforated panels appears to be that in the perforated panel the base of this cavity has failed allowing the bullet remains to complete perforation. The successful armours back face has delaminated and deformed in such a way as to catch the bullet, this deformation and delamination damage is less visible in the failed panel.

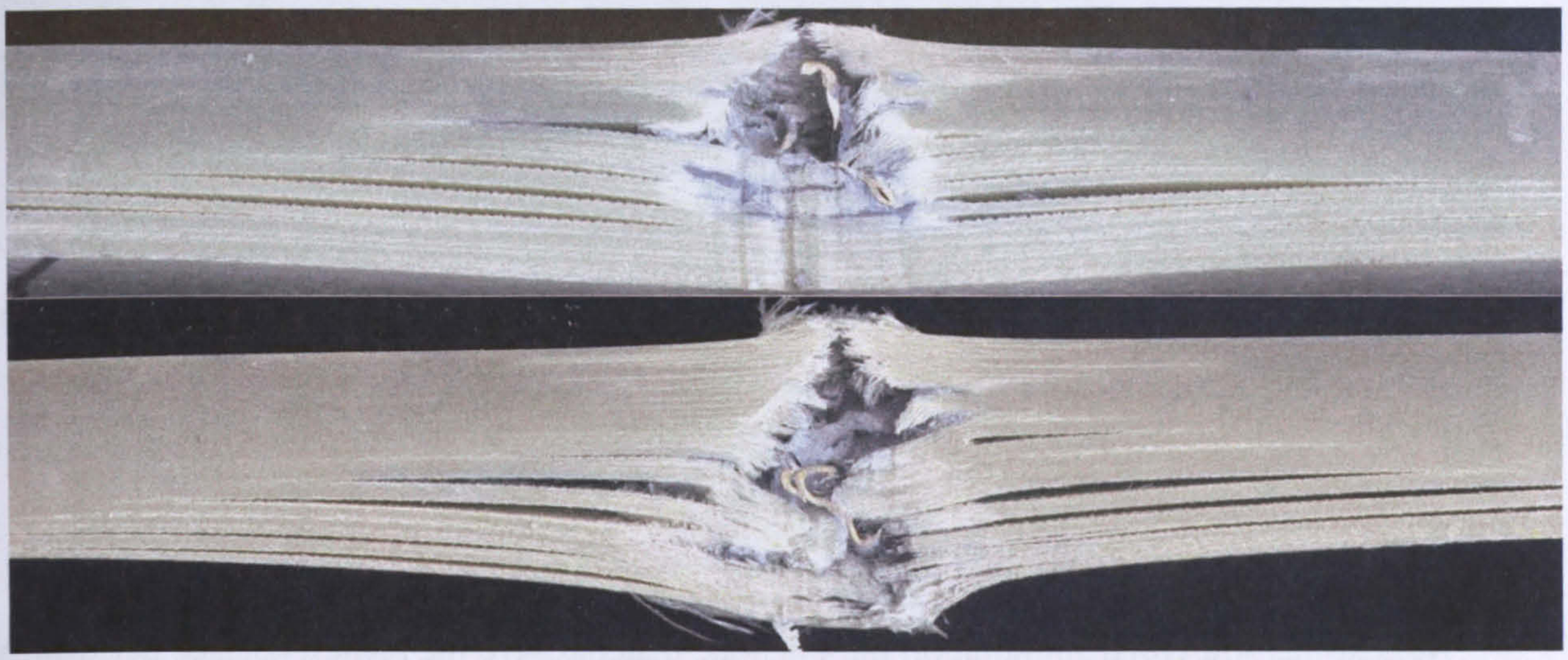

Image 3.16: Sections of medium VE vs Ball ammunition (Top, stop at 622ms^{-1}, bottom, perf 625ms^{-1})

The most noticeable thing about these panels compared to the heavy weave materials sectioned previously is the larger number of visible delaminations. As well as this the cavity caused by bullet breakup appears larger. The rear face of both materials has failed by delaminating such that there are thick layers of material infront of the bullet path. The successful material appears to have two of these thick layers infront of the bullet cavity which have torn to one edge of the cavity (tensile failure) before what remains of the lead bullet core is stopped. The failed material shows the same failure of plys with the exception that the failures have progressed through the back face of the material. The failure path is very jagged and irregular indicating the material is being torn apart rather than cut through.

There is also significant bending deformation of the delaminated plys, this suggests the tensile failure of the lamina on the rear face is due to bending loading.

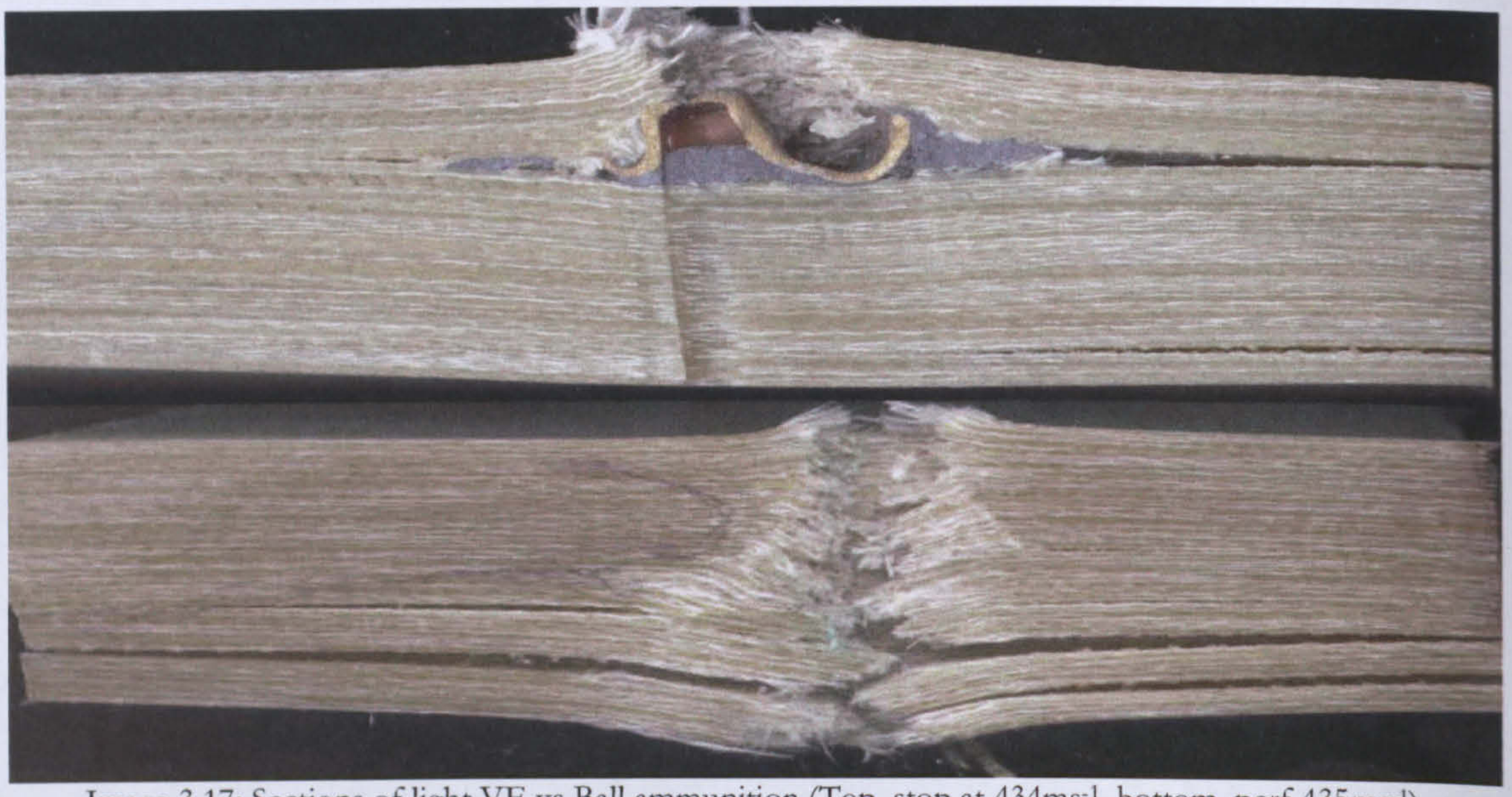

Image 3.17: Sections of light VE vs Ball ammunition (Top, stop at 434ms^{-1}, bottom, perf 435ms^{-1})

This light weave material has a far lower V_{50} than the other materials tested, as a result of this the bullet jacket is far more intact and as can be seen from the sections is only just starting to form the damage cavity visible in the other panels tested. The lead core of the bullet has spread out in-between lamina. In the successful panel there is visible plastic deformation throughout the material thickness and some rear surface delamination.

Against this soft cored ammunition the Phenolic material gave the highest ballistic performance, however this was at the cost of the highest weight. The heavy and medium weight reinforcement Vinylester panels performed at a similar level, however the heavy weave reinforced panel was significantly lighter. The remaining Vinylester panel (Light weave) whilst lighter performed very poorly. STANAG level I is to stop this round at 833 ms^{-1}, the best performance at the thickness tested was the Phenolic at 773ms^{-s}. The worse was the light weave VE at 429ms^{-1}.

Sectioning of these materials revealed that the break-up of the bullet caused a large internal cavity which was worse for the lighter weave materials. In all cases the material ahead of this cavity delaminated and deformed. Failure of each body of delaminated material appears to be due to tensile failure / tearing of the material caused by the distributed load from broken bullet material rather than a shearing / indentation failure. This is further indicated by the observation that failure of these bodies of material is often not along the bullet path but

rather at one edge. The difference between a successful stop and a perforation of the panel seems to be that successful panels have far more delamination damage and permanent deformation.

3.6.3.2 Against AP ammunition (STANAG level II)

The resulting AP impacts were sectioned in the same manner as the targets tested against ball ammunition, the resulting sections and some discussion follow.

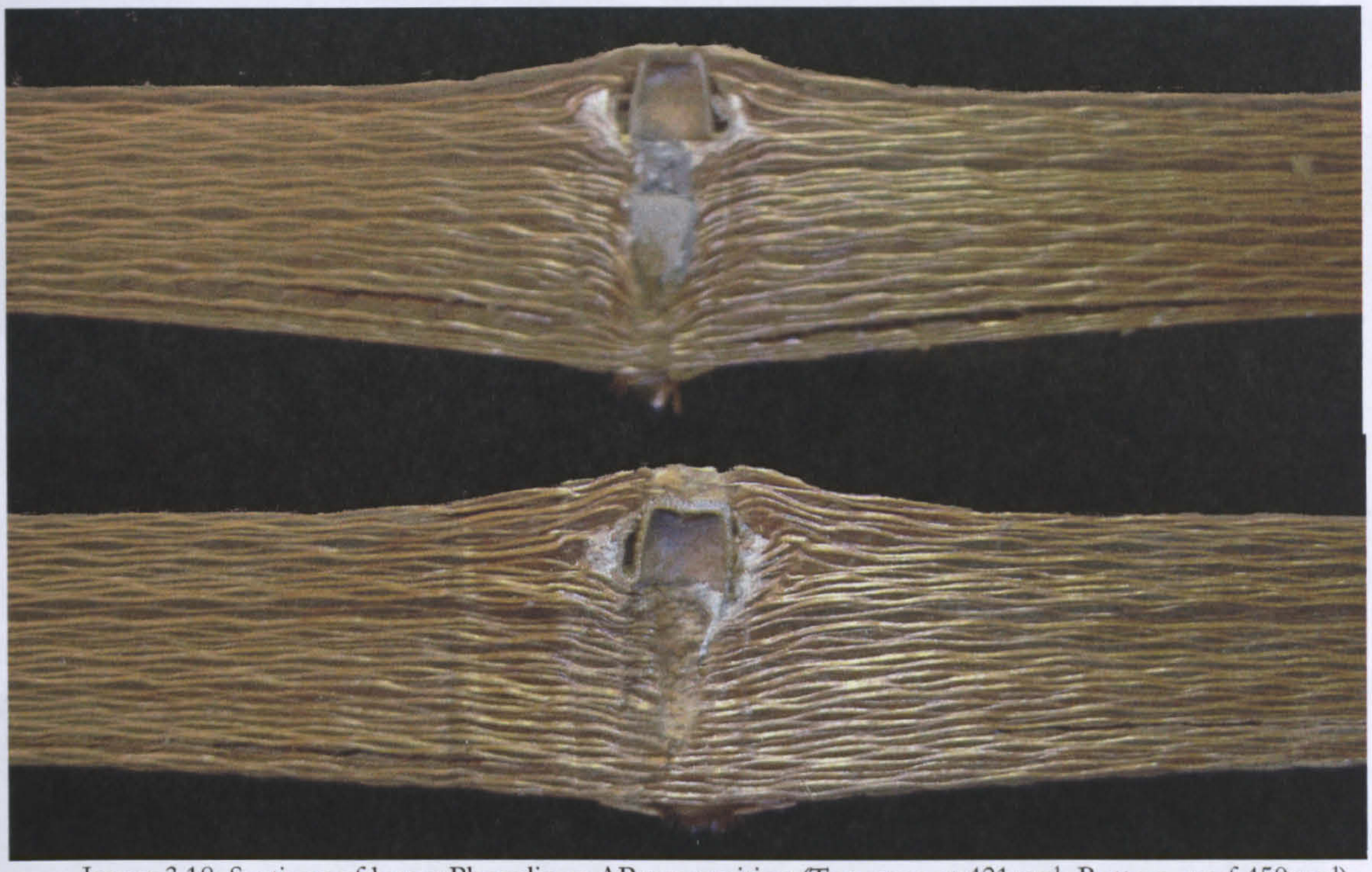

Image 3.18: Sections of heavy Phenolic vs AP ammunition (Top, stop at 421ms^{-1}, Bottom, perf 450ms^{-1})

It is clear in the sections that the successful stop has more delamination and deflection (especially local to the arrested core) than the perforated panel. Whilst there are delaminations present in the perforated panel they are smaller, fewer in number and not opened to the same extent as those in the successful panel. Peeling back of the jacket can be clearly seen causing up-thrust on the front surface.

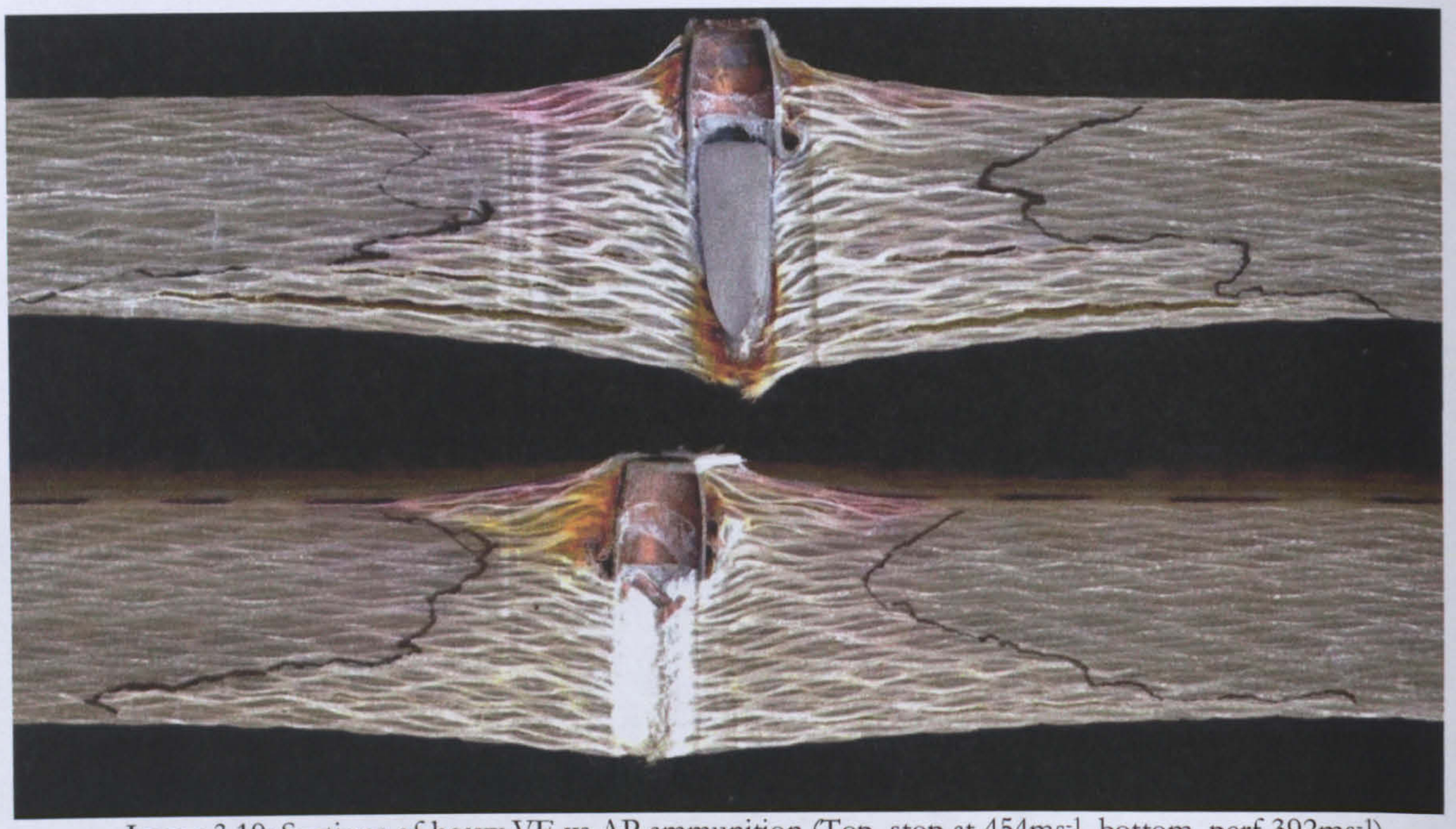

Image 3.19: Sections of heavy VE vs AP ammunition (Top, stop at 454ms^{-1}, bottom, perf 392ms^{-1})

The sections show that relatively little delamination has taken place, though there is more visible for the successful stop. The difference in deformation in the damage zone between the stop and the perforation is significant, the perforated panel shows relatively little plastic deformation on anything but the front face (caused by the peeling of the jacket and its subsequent up-thrust).

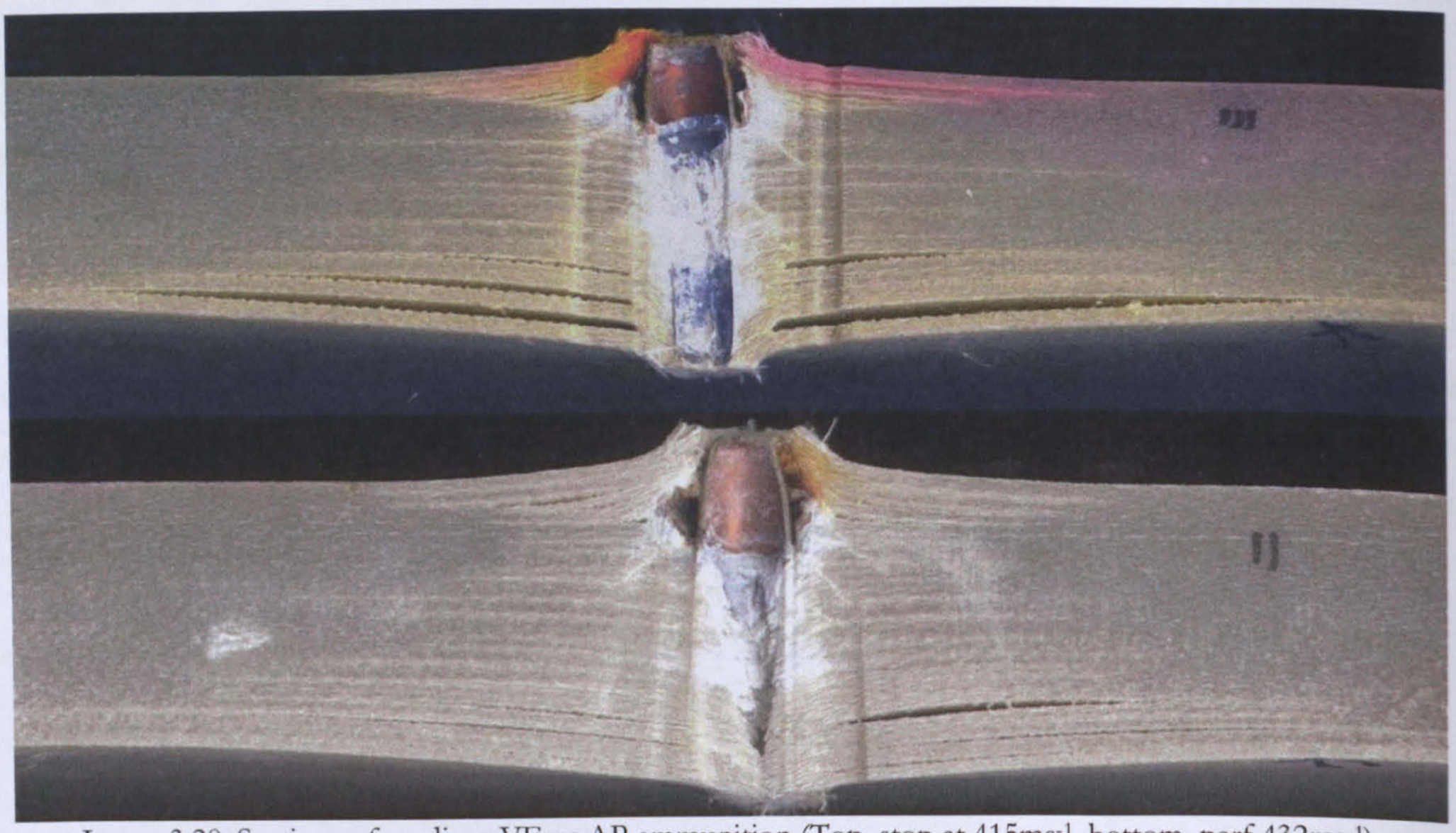

Image 3.20: Sections of medium VE vs AP ammunition (Top, stop at 415ms^{-1}, bottom, perf 432ms^{-1})

This material shows significant amounts of delamination damage, especially so for the successful stop which has more of and larger delaminations. The waisted 'hourglass' shape discussed earlier

is visible. It is also noticeable that the 'waist' occurs sooner in the successful stop than it does when the panel is perforated.

Another feature visible in this material which wasn't seen in the heavy weave material is the presence of 45° shear planes extending radially out from the bullet path and downwards towards the rear face. These features appear to be caused by the radial flow of material away from the bullet path and have been observed in indentation and compression testing. There is plastic deformation of laminates visible close to the bullet path but not to the same degree as that seen in the coarse weave material. This deformation is more visible in the successful stop section than it is in the perforated panel.

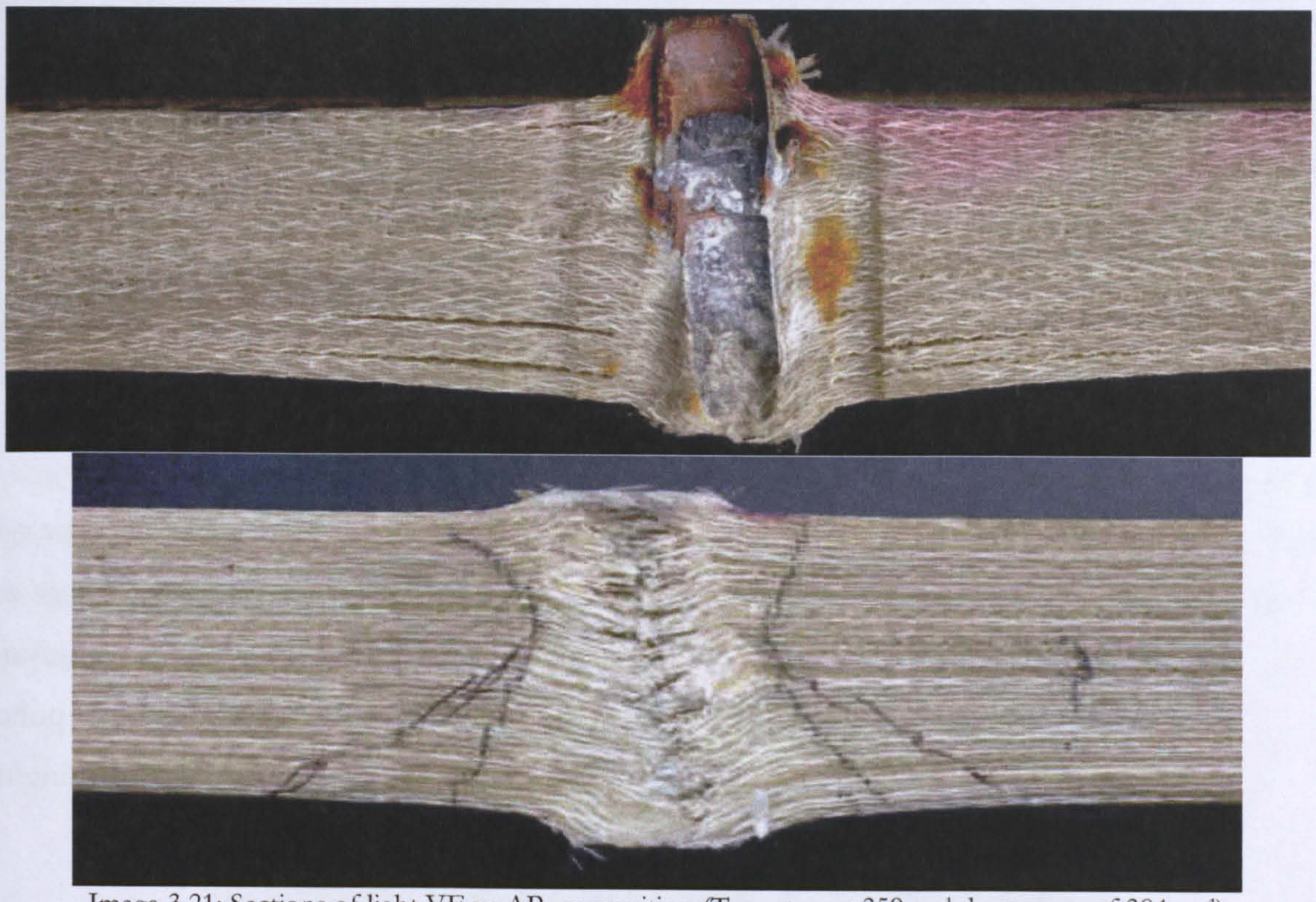

Image 3.21: Sections of light VE vs AP ammunition (Top, stop at 359ms^{-1}, bottom, perf 384ms^{-1})

Once again the perforated panel shows negligible signs of delamination (a few cracks are present but are barely visible to the eye). The successful stop however shows some visible delamination. (core was lost during sectioning however the impression left is visible. Note the presence of lead on the surface of the impression) The size and amount of these delaminations are small compared to other materials tested.

3.6.3.3 Thick panels against AP ammunition (STANAG level II)

The sections of these thicker targets showed the following architecture:

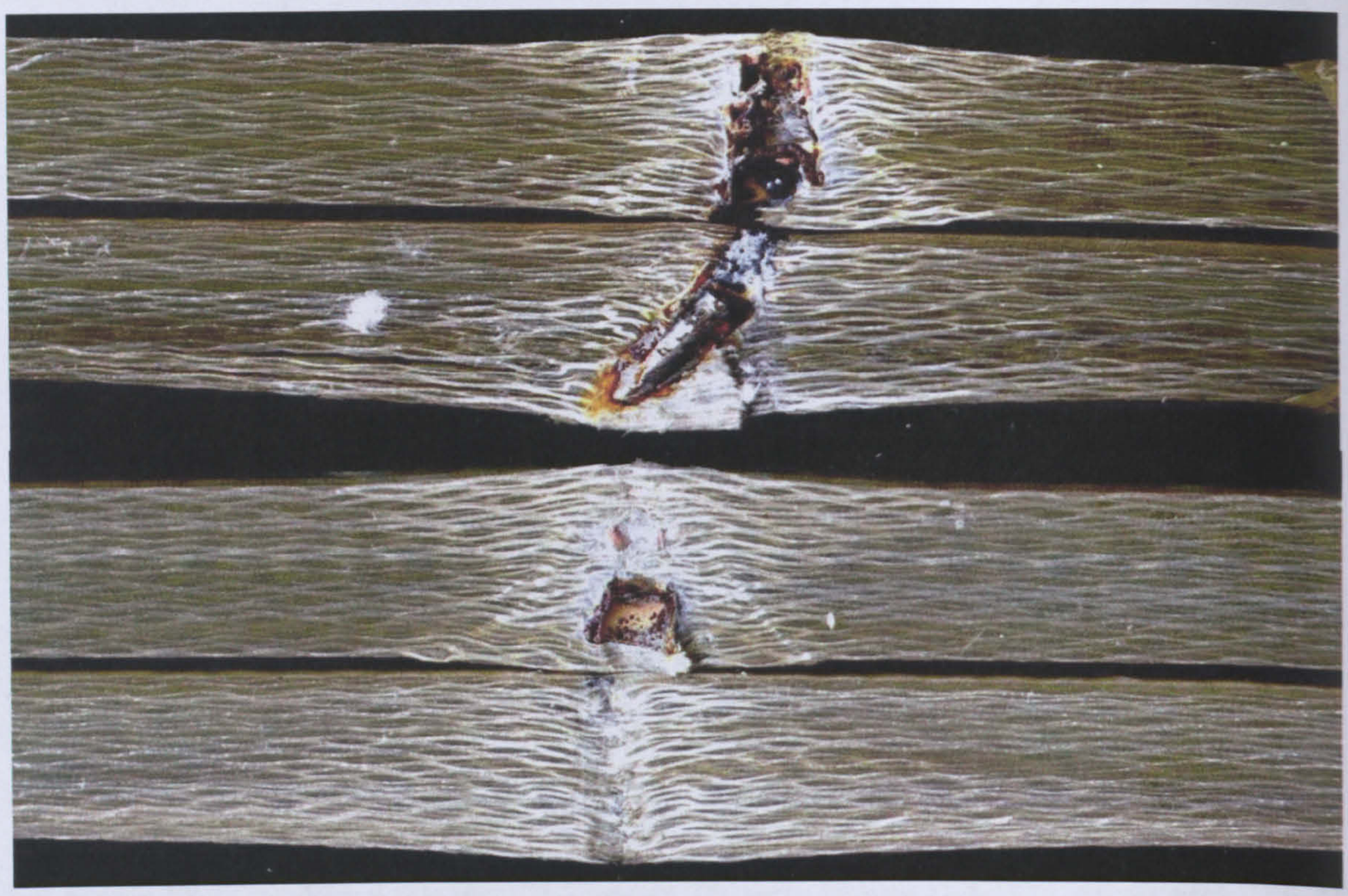

Image 3.22: Sections of heavy VE vs AP ammunition (Top, stop at 623ms^{-1}, bottom, perf 636ms^{-1})

The most striking feature of this section is the yaw of the arrested projectile, this yaw is less apparent in the section of perforated material. The successful stop shows delamination damage offset towards the direction of the projectile yaw, whilst delaminations are present in the perforation section they are less obvious and not opened up. The perforation is very clean and has been punched through the material. The hourglass damage pattern is repeated in the backing panel suggesting that the target behaved like two separate panels rather than a solid thickness.

Image 3.23: Sections of medium VE vs AP ammunition (Top, stop at 660ms^{-1}, bottom, perf 696ms^{-1})

A clear difference in the pattern of delamintion damage between the successful stops and perforated panels was observed in the sections of the medium weave VE (note final perforation is not on the surface of the section due to yaw but is actually deeper within panel – exit tuft is visible in lower image). The successful panel has larger delaminations in both, size and number as well as greater amounts of permanent plastic deformation. The 45° shear planes noted in the single thickness sections are also visible here and appear to be greater in number and start closer to the struck surface in the successful panel.

Image 3.24: Yaw in medium weave panel

As previously mentioned significant amounts of yaw in bullet path was observed within the material. As a result of this the sections illustrated have not cut the bullet path entirely. The section above (Image 3.24) follows the bullet path closer than other sections presented and indicates the amount of yaw experienced.

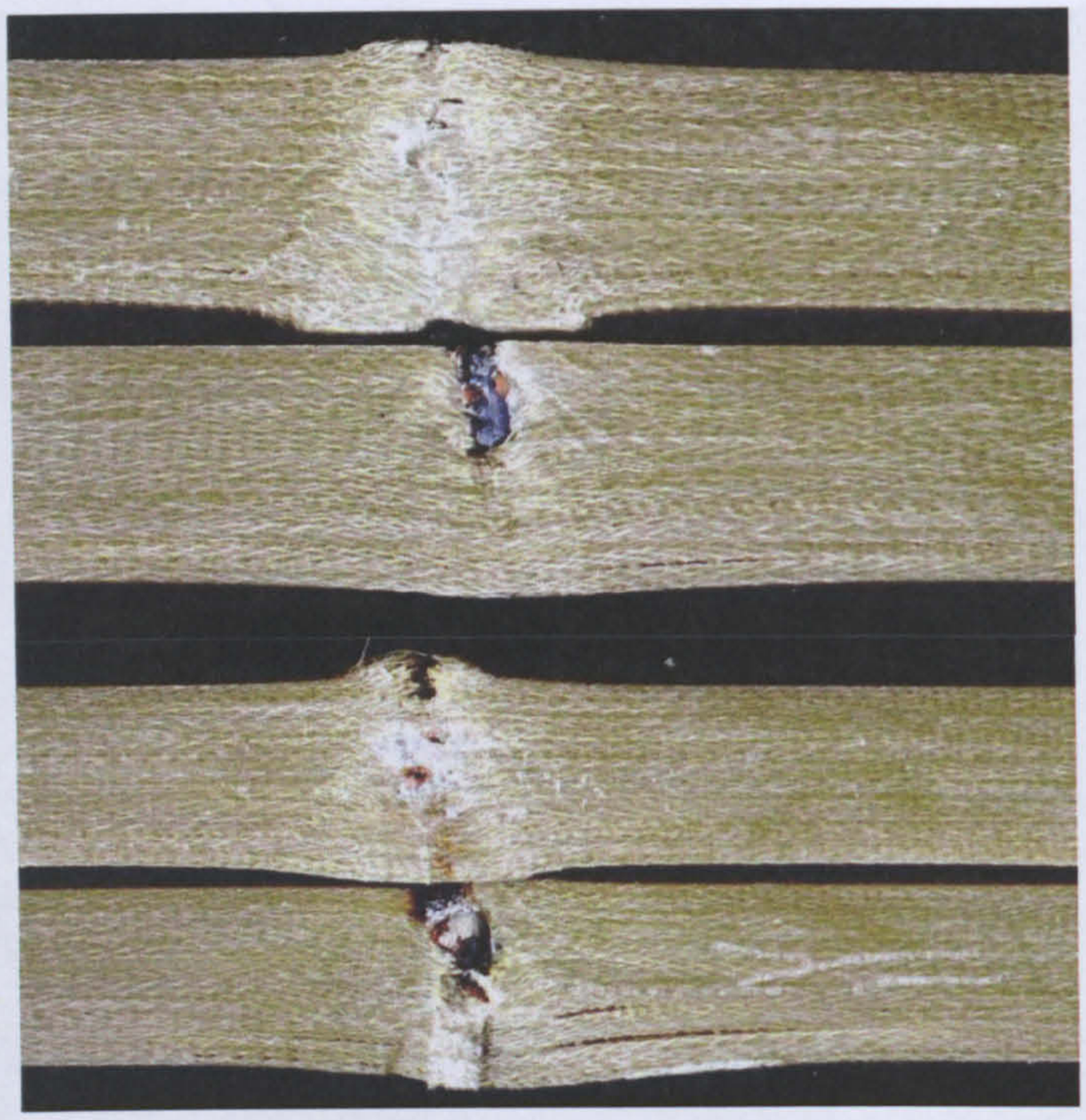

Image 3.25: Sections of light VE vs AP ammunition (Top, stop at 603ms^{-1}, bottom, perf 623ms^{-1})

The lightest weave VE material performed better than expected (expectations based on results of single thickness testing). The amount of delamination in both successful stops and perforated panels is visibly less than other materials tested. There is also a visible amount of permanent deformation of the rear surface material, more so for the successful panel. The perforated panel shows more evidence of damage in the front face of the material, 45° shear planes are also apparent.

Also tested was an exceptionally thick medium weave VE target constructed from three layers of material. It was not possible to achieve perforation of this material due to ammunition limitations. The method used to increase projectile velocity caused a corresponding decrease in accuracy.

Image 3.26: X-Ray of rear lamination of treble thickness target (bullet debris visible in white)

The above X-Ray shows the rear layer of the target and shows the significant yaw has taken place for the upper impact despite the laminations being tightly clamped together. The impact close to the edge of the panel however has travelled quite straight and as a result was selected for sectioning. The X-Ray also shows that despite this yaw and high impact velocity the core of the AP bullet is not fractured or broken up.

Image 3.27: Sections of treble thickness, medium weave Vinylester panel

There appears to be delamination damage throughout the material, though these are larger towards the rear face they have not opened significantly compared to those seen in equivalent sections from successful thinner amounts targets. It is interesting to note that the bullet jacket material has penetrated through to the middle layer of material before the core is fully free of it,

as well as this, it appears that the front surface damage is low due to jacket material being forced so far into the composite. It appears that the angled shear features are worse for the part of the impact path where the core is not free of the jacket.

An interesting observation for the first shot (which yawed within the panel) was that two of the three constituent layers had a PTFE insert at mid-plane (for construction of Mode I samples with a pre-crack tested in Chapter 5), this effectively acted as a large, pre-existing delamination within the material which was away from the influence of the clamps used to hold the target in place.

The most significant yawing of the previous double thickness panels tested was also observed in material furthest away from the influence of clamps. This suggests that the presence of internal interfaces which are free to move relative to one another encourages yawing behaviour of a penetrating projectile.

3.6.3.4 Sectioning of Hybrid targets

Sectioning of the impacted material yielded the following:

Image 3.28: Sections of Hybrid panel #1 (medium VE front face, heavy VE rear vs AP ammunition (stop at $632ms^{-1}$, perf at $638ms^{-2}$)

Both panels show similar front surface damage in the medium weight material relative to each other and relative to testing of the medium weight material on its own. It also appears that the two different materials have remained 'together' whereas previous testing seems to show the panels having moved away from each other due to insufficient clamping pressure. There is also a small amount of yaw compared to the double thickness panels seen previously (Section **3.6.3.3**), this is possibly due to the same reason.

Once again the failed panel shows far less delamination than the panel which has just stopped the bullet core (it is noticeable how little the core has been damaged due to its passing through the soft composite material). The over all appearance of the front panel appears to be almost identical for both successful and perforated panels.

It was not possible to get a good section of an impact in this material, the following image (Image 3.29) is made up from sections of two different impacts, it was not possible to section a successful stop. There was also a degree of yaw in projectile path observed in this material, the exit in the rear material is behind the visible plane.

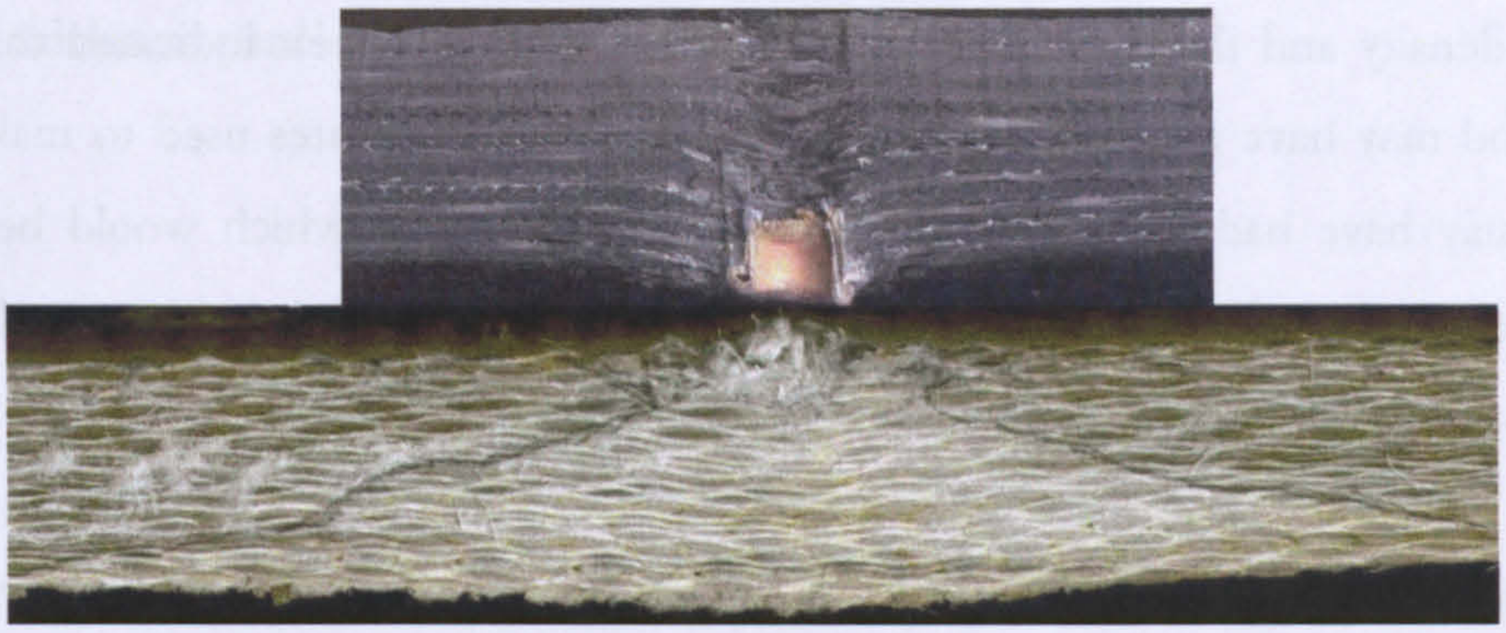

Img 3.29: Sections of Hybrid panel #2 (CFRP front face, heavy Vinylester rear)

The damage visible in the GFRP rear section is concurrent with than seen in a 'thin' panel as defined by Gelert [45] (see section **2.13**) which is of interest and indicates minimal contribution of the front surface to slowing the projectile or deforming such that a distributed load is applied to the backing material. There is some delamination damage (not clear in image 3.29) however it is not to any large extent.

In general there is little visible damage in the carbon panel. The visible damage is limited to local fragmentation of fibres with only small amounts of delamination. Little plastic deformation of

fibres is present towards the front face as laminates have fractured as opposed to bending, however there is some deformation in delaminated layers towards the back face. On the front face the first lamina has torn away along a fibre axis (Uni-Directional (UD) laminates) however this delamination is very narrow and constrained to the surface ply only.

3.7 Overall summary of ballistic testing

The ballistic trials carried out and recorded in this chapter have concluded the following:

Against ball ammunition (STANAG Level I) the material with the highest V_{50} (see Graph 3.1 & Table 3.2) was the heavy weave Phenolic matrix material (V_{50} = 767ms^{-1}). Below this the heavy and medium weave Vinylester materials have similar V_{50}'s (V_{50} = 651ms^{-1} and 645ms^{-1}), however the heavy weave material is more than 10kgm^{-2} lighter. The worst material (by far) was the lightest reinforcement weave Vinylester material (V_{50} = 430ms^{-1}) which for an equivalent areal density to the heavy weave material performed far poorer.

Two main areal densities of material were tested against armour piercing ammunition (STANAG Level II). This was achieved by layering available material to achieve the desired areal density and thickness. Sectioning of the impacted panels indicated that the clamping method may have allowed some movement between the plates used to make up the target this may have had the effect of increasing V_{50} over that which would be achieved by a homogeneous target of the same areal density. The interface between panels also appeared to cause yawing of the bullet path within the material.

Against AP ammunition (STANAG Level II) the best material of the lower areal density group tested (see Graph 3.1) was again the heavy weave reinforced Phenolic material (V_{50}= 436ms^{-1}), however the medium weave Vinylester material was only slightly poorer performing (V_{50} = 424ms^{-1}) but weighed roughly 10kgm^{-2} lighter. The heavy reinforced Vinylester material had an even lower areal density however this had a V_{50} less than 400 ms^{-1}(V_{50} = 394ms^{-1}). The lightest weave material tested was slightly heavier than the heavy weave material and also had a much lower V_{50} (V_{50} = 362ms^{-1}).

Testing of the higher areal density material group (Graph 3.1b) shows that for the first time the heavy weave Phenolic matrix material is not the best performer, the medium weave Vinylester panel has the same V_{50} but has a significantly lower areal density (V_{50} = 683ms^{-1}).

The remaining materials (heavy weave and light weave Vinylester) both have similar ballistic performance (V_{50} = 626ms^{-1} and 619ms^{-1} respectively) however the light weight weave panel provides this protection for a far lower areal density than the heavy weave material.

One further areal density of material was tested, this testing was limited to the medium weave Vinylester material and due to tight material constraints only two shots were possible. Neither of these shots could be made to penetrate however the material performance hinted at a V_{50} around 850ms^{-1}. The data for the medium weave material only suggests a relationship between ballistic limit velocity and areal density at least up to 850ms^{-1} against STANAG II ammunition.

Layered targets made of a combination of materials were trialled in an attempt to achieve a more optimised solution however, results were not as good as anticipated. This is possibly due to the fact that the targets used were too small which allowed delaminations to run to the material edge. Additionally the size of the targets meant that the front and back plies were far better constrained by the clamping arrangement than the large double thickness panels tested earlier. It is believed that this did not allow the interface effects noted in these large double thickness panels to occur.

CHAPTER 4:

EXPERIMENTAL INVESTIGATIONS; FRONT FACE PENETRATION MECHANISMS

This chapter will cover the mechanical testing work undertaken to evaluate the material failure mechanisms which take place during the initial phases of ballistic impact, against a composite armour.

Testing is carried out on materials supplied by VT Halmatic for ballistic testing and described at the beginning of Chapter 3

4.1 Overview

The initial stages of any impact have an important influence on the following impact and penetration event. Conventional armours attempt to resist penetration by being very hard [45] and as a result resist, as well as damage the projectile as it breaks the armour surface and begins penetrating. It is not possible to achieve this through the use of composite materials without the use of ceramic front facings as composite materials are limited in hardness by their soft polymeric matrices.

Conventional laboratory equipment will be used to evaluate the front surface performance of a range of composite armour materials from initial impact through to deep penetration of front surface material. The difference between 'front' and 'rear' surfaces is defined in Chapter 2.

4.2 Indentation and front surface properties

In principle the comparison of quasi-static and low speed dynamic testing to ballistic data is likely to be affected by a range of dynamic effects, however there is precedent in the literature for such trials. Wang and Chou[33] compared ballistic tests with quasi-static tests of a bullet profile mounted in a conventional tension/compression machine and found that despite observing some small differences in material response energy dissipation was very similar. This allowed the quasi-static data to characterise the dynamic impact properties of the materials being tested.

The initial breaking of a free surface and subsequent penetration will be very much dependent on the projectile geometry, also fragments / soft, lead cored ball rounds will deform significantly thus reducing the energy density applied to the armour surface impeding penetration. Some fragments and armour piercing projectiles are by their nature very hard and non-deformable, as a result of this deform very little allowing their kinetic energy to be applied to the armour over a very small area (due to the undamaged pointed / sharp nature of the projectile) thus achieving a very high kinetic energy density (defined below).

$$KED = \frac{mv^2}{2A}$$

Where:

m = Mass (Kg)

v = Velocity (ms^{-1})

A = Contact area between projectile and armour (mm^2)

Equation 4.1: Kinetic Energy Density

Composite materials are however very 'soft' in comparison to metallic armours hence penetration is almost inevitable for anything but very low KED's. Little is understood about the way in which a structural composite armour reacts when it is struck and penetrated by a hard projectile. It is proposed that the indentation resistance of the composites in question can be assessed using existing experimental equipment and techniques.

The indentation of ductile solids by a conical indenter was first dealt with by Ludwick in 1908 for the hardness testing of soft metals[52]. Ludwick defined hardness as the mean pressure between an indenter and the test material over the surface area of the indentation.

This is not however the true pressure between the indenter and the surface of the indentation. Meyer [53] later proposed for spherical indenters that assuming no friction the true pressure is given by the ratio of the load to the projected area of the indentation. The Meyer proposal was later found to be applicable for both conical and pyramidal indenters. This 'Meyer hardness' is described as follows:

Taking an annulus on the surface of the indentation (diameter = d) with a radius of *dx* and a width of *ds* the area of which is given by:

$$A_a = 2\pi x dx$$

Where:

x = annulus radius (mm)

ds = width of annulus on surface of indentation

Equation 4.2: Projected area

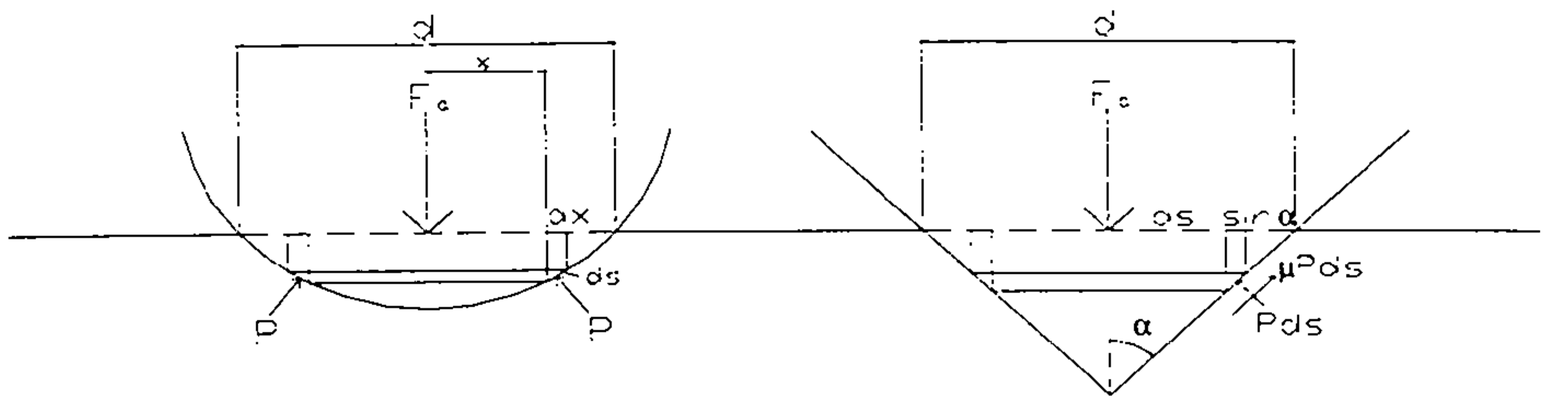

Figure 4.1: Projected area of indentation

Concurrently the force applied to this surface is given by:

$$F_a = P\,2\pi x ds$$

Where:

F_a = Surface force on annulus

P = Indentation Pressure

x = Annulus radius

ds = Annulus width

Equation 4.3: Force applied to indentation surface

By symmetry the horizontal component of the indentation pressure force must equal zero, thus summing across the entire area of the indentation the vertical force will be equal to Equation 4.3. Rearranging for Equation 4.4 gives a term describing how the mean surface pressure between the indenter and the indentation is a function of the projected area of the indentation. This analysis assumes that the effects of friction are zero.

$$F_I = \int_0^a (P2\pi x)dx = P\pi r^2$$

Where:

F_I = Indentation force

P = Indentation Pressure

r = Chordal Radius

d = Indentation Diameter

x = Annulus radius

Equation 4.4: Expression for indentation force

Thus:

$$MIP = \frac{F_I}{\pi r^2} = \frac{4F_I}{\pi d^2}$$

Where

MIP = Mean Indentation Pressure

F_I = Indentation force

r = Chordal radius

d = Indentaion diameter

Equation: 4.5: Expression for Mean Indentation Pressure

Experiments show that for conical indenters the mean indention pressure is practically independent of load though not of cone angle. Work by Bishop Hill and Mott[54] is illustrated in Graph 4.1 found that the indention pressure rises sharply for narrow cone angles. Hankins[55] suggested that this effect may be due to friction forces governing the indentation event at narrow angles where at wide angles the event is dominated by the yield strength of the material. As a result it was suggested that steps to reduce the friction would yield better results. The dotted trend in Graph 4.1 shows that this is to a certain extent true.

Hankins'[55] work showed that by lubricating the indenter the tendency for the mean indentation pressure curve to rise sharply for low values of α can be largely negated (though not entirely removed). This is due to the fact that whilst at large values of α yield strength effects are large relative to friction at small values of α the reverse is true[56]. Atkins et al[57] suggested that the effect of friction was negligible for large angle indenters as there was in all probability very little slip between the indenter and the specimen. The effects of friction however, are likely to be more important for smaller indenter angles. Atkins [57] cites work by Hadow and Johnson which suggests that this requires further consideration.

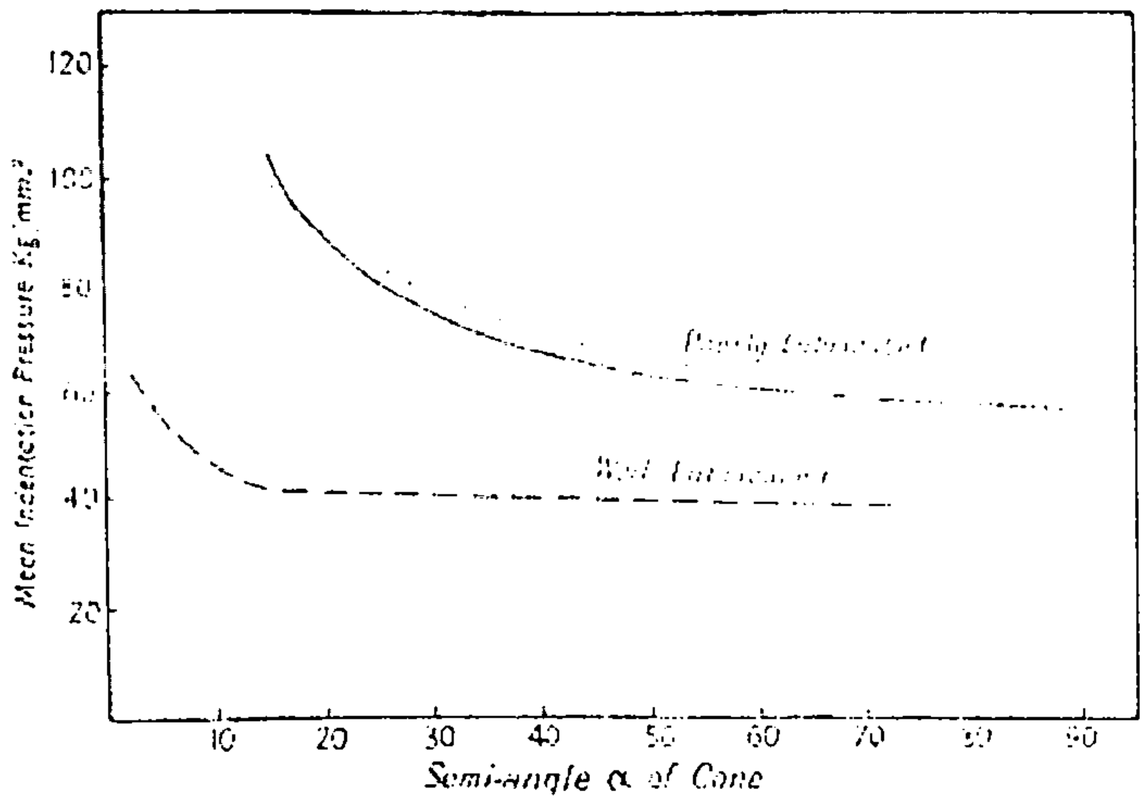

Graph 4.1: Indentation Pressure vs Cone semi-angle[52]

Hankins[55] also assumes that there is an intrinsic yield pressure (P_o) which is a material property and thus independent of indenter shape and proposed that the indentation force is better given by:

$$F_I = \frac{P_o(1+\mu\cot\alpha)\pi d^2}{4}$$

Where:

F_I = Indentation force

P_o = Yield Pressure

α = Cone Semi-angle

d = Indentation Diameter

μ = Coefficient of friction between indenter and material

Equation 4.6: Hankins indentation force in terms of Yield pressure

Re-arranging Equation 4.5 for indentation force and substituting into Equation 4.6 gives an expression for the indentation pressure in terms of indentation load and the yield strength of the material.

$$P = P_o(1+\mu\cot\alpha)$$

Where:

P = Indentation Pressure

P_o = Yield Pressure

α = Cone Semi-angle

μ = Coefficient of friction between indenter and material

Equation 4.7: Indentation pressure in terms of load and material yield strength

Thus by measuring the diameter of the indention the mean indention pressure can be found from Equation 4.5. Using this value in Equation 4.7 gives a yield pressure (P_o) for each value of α, this can then be evaluated over a range of cone angles.

Work by Horsfall[56] has applied this theory for conical indenters to the indentation of polymers. The resulting testing was successful in showing trends which follow those observed by Bishop et al[54], and which predict yield strength with acceptable accuracy. Composite materials (specifically fibre reinforced composites) however present a problem, unlike simple polymers and metals they do not possess an isotropic structure. Instead structures can range from a simple polymer filled with many random 'short' fibres to ordered anisotropic woven fabrics set within a polymeric matrix. Despite this there is good reason to attempt to apply this theory to composite materials.

The through thickness resistance of a composite material will vary from lamina to lamina and between one lamina and the next. Each individual laminate will resist penetration differently depending on the position of the indenter to the reinforcement fibres. This is especially the case with woven fabrics where the indenter could alternately be trying to penetrate overlapping warp and weft bundles or a pocket between warp and weft fibres.

It is believed that a deep penetration into the material will give the best results. Bishop et al[54] suggested that for a ductile metallic material 'deep penetration' consisted of a "penetration equal to four or five times the diameter of the punch". This is a sensible proviso as by careful selection of indenter dimensions a general material behaviour can be observed from a composite laminate. Bishop, et al [54] however used small conical punches which were fully submerged into their metallic sample material with great force, not a practical approach for strong engineering composite materials with large internal structures (i.e. fibre bundles), hence a different definition of 'deep' is required.

Pointed indenters are only half of the indentation problem, flat nosed projectiles (i.e. fragments) are known to penetrate materials by a different mechanism than that previously discussed. The energy density applied to the material surface is often too low (due to a large contact area) to allow much ductile flow of material away from the projectile. Instead the force applied to the material surface causes a shear failure of the material directly below the

projectile circumference thus forming a discommuted 'shear plug' which is forced through the remaining material. This is an especially dangerous form of failure as upon perforation not only is there projectile related debris loose behind the armour but there is also the shear plug material.

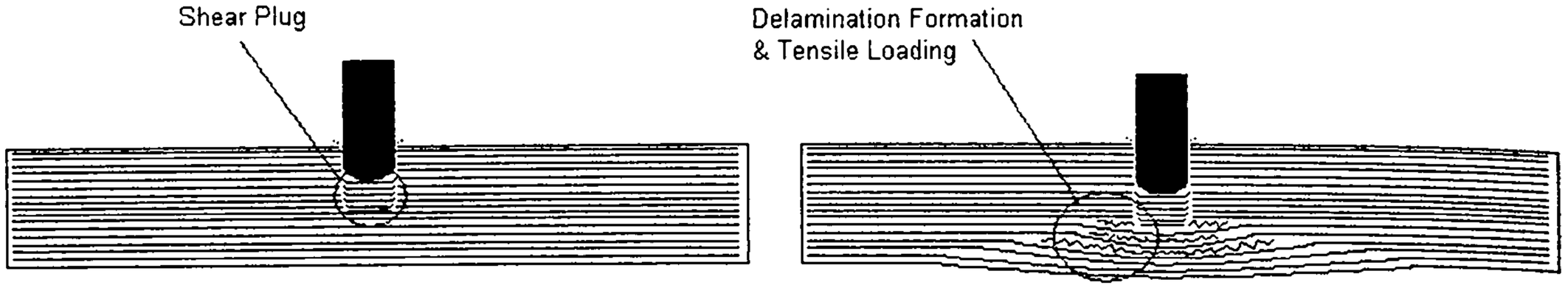

Figure 4.2: Shear plug formation

The ductile flow analysis discussed previously becomes unworkable for flat nosed projectiles. Additionally it is not the projectile as such which is leading the penetration through the material but rather the plug. It is unknown what geometry this plug assumes and if it can be dealt with by established analysis methods.

The previous failures discussed all assume immediate penetration of the material, impact by large soft fragments or similar will not immediately penetrate the material due to the low energy density of the impact. In these cases the compressive strength of the material is important for the resisting of the impact loading. Penetration of the material from this kind of impact is likely to be due to failure of the composite by another mechanism i.e. shear failure at the edge of the loaded area. The shear stress (τ) can be calculated using standard formula:

$$\tau = \frac{F}{A}$$

Where:

τ = Shear stress (Pa)

F = Force (N)

A = Area over which force is applied (mm^2)

Equation 4.8: Shear stress

When a circular projectile is being considered the equation simply becomes:

$$\tau = \frac{F}{(\pi \times r^2)}$$

Where:

τ = Shear stress (Pa)

F = Force (N)

r = Radius of projectile (mm)

Equation 4.9: Shear stress for circular projectile / punch

4.3 Mechanical testing

The aim of the work detailed in this chapter is to evaluate the mechanical properties of a range of structural composites for use as armour materials. The work is to concentrate on the initial phases of impact as a projectile strikes an armour and as it begins to penetrate.

Both quasi-static and dynamic testing will be carried out to evaluate armour performance the results are to be compared to ballistic testing carried out later in this report.

4.4 Experimental facilities

Facilities belonging to the Engineering Systems Department of Cranfield university were used for this trials work. A large 250kN Zwick 1484 tension/compression machine and a Roasand IFW drop tower facility, standard Vickers hardness testing machines as well as customised equipment were all employed to undertake investigations into the front surface performance of composite armour materials

4.5 Material available for testing

The experimental work will be carried out on the same thick, structural composite panels supplied for ballistic investigation by a collaboration of VT Halmatic, AGY and Reichold. These materials are representative of what could be used to manufacture a composite armoured vehicle and as such are a good basis for detailed investigation.

4.6 Compression testing

4.6.1 Aims

The compressive strength of the materials being tested is believed to be important to the way composites reacts to impact. The aim of these trials is to evaluate this strength to allow comparative material evaluation of the performance of the materials tested against ballistic impact.

4.6.2 Experimental

The materials to be tested were cut into square specimens, 14mm x 14mm in size and of the same full thickness as the ballistic panels they were cut from. Samples were then mounted between two thick steel anvils in to a Zwick 1484 Compression / Tension testing machine and loaded at a crosshead speed of 1mm/min.

As the samples were available it was decided to test the materials in two orientations as described in Figure 4.3:

1. Loaded perpendicular to laminate direction
2. Loaded parallel to laminate direction

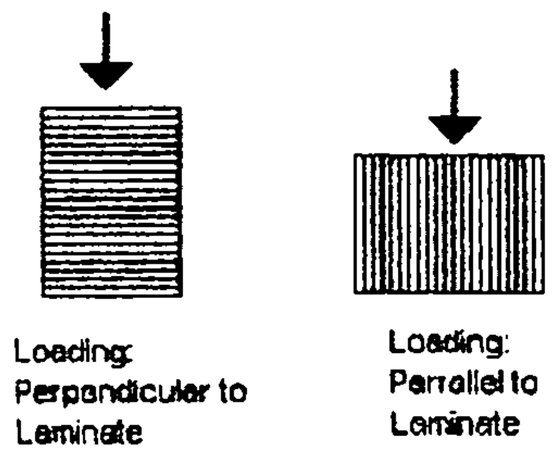

Figure 4.3: Laminate orientation

Compressive testing of these materials required a far smaller sample than expected due to the strength of the material. The machine being used for this testing was fitted with a 250kN capacity load cell, and at the current time is the biggest machine available with force / time logging capabilities.

A high speed (Phantom 7) camera (and associated lighting equipment) was used to film the failure event.

4.6.3 Panels tested

Examples of the four main materials investigated throughout this project were tested:

1. Heavy weave S2 Glass / Phenolic
2. Heavy weave S2 Glass / Vinylester
3. Medium weave S2 Glass / Vinylester
4. Light weave S2 Glass / Vinylester

4.6.4 Results

All samples loaded parallel to the laminate failed in a similar manner however the heavy weave Phenolic failed at an unexpectedly low stress. The equivalent VE material failed suddenly such that the test machine stopped the test, no other materials experienced such a load drop-off to stop the test hence the large amount of post yield data.

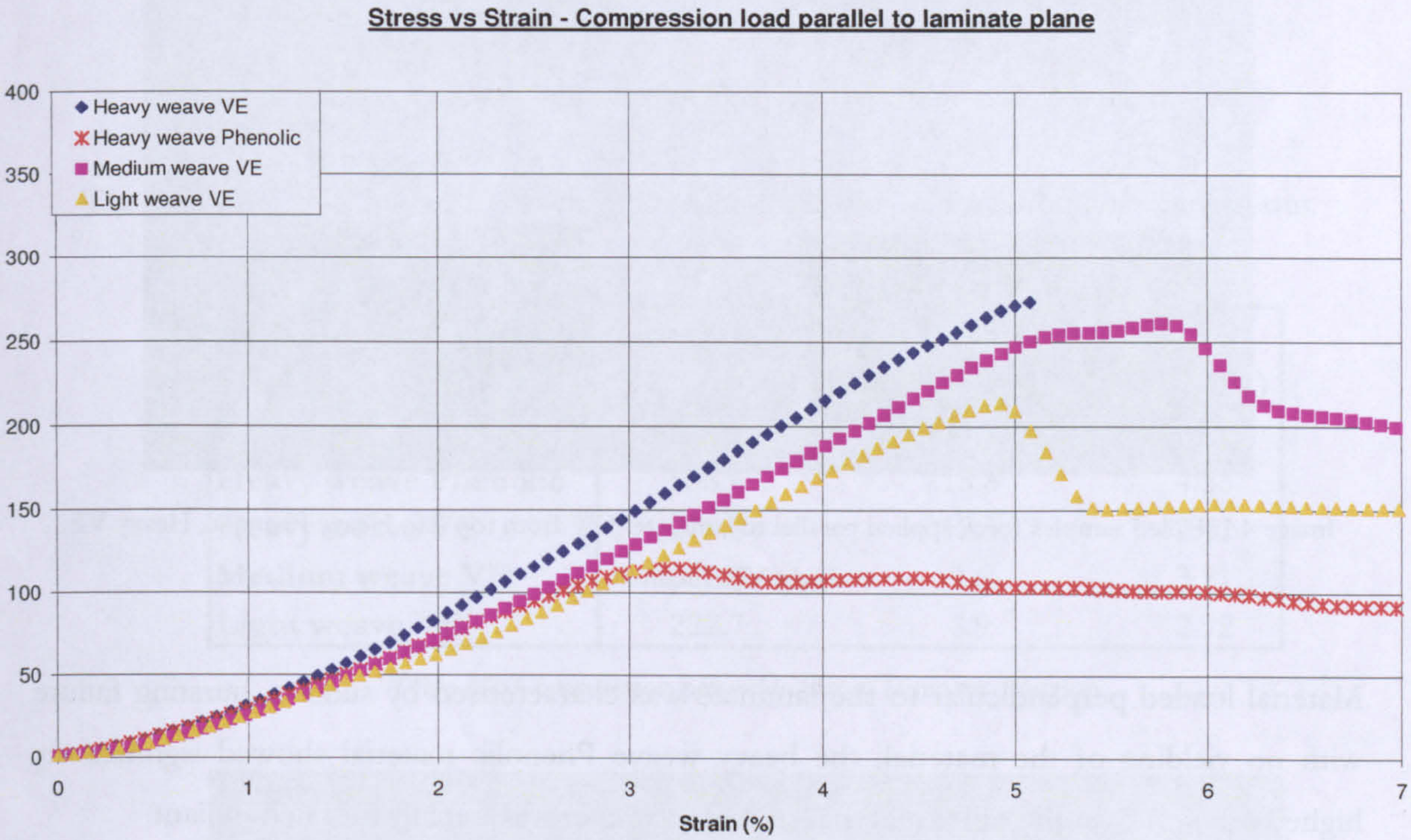

Graph 4.2: Stress/Strain curves, force applied parallel to laminate

The following table shows the averaged results from the compression tests carried out

Material	Averaged results		
	UCS (MPa)	Failure strain (%)	E (GPa)
Heavy weave Phenolic	114.8	3.2	39.3
Heavy weave VE	273.0	5.1	63.1
Medium weave VE	260.8	5.8	56.4
Light weave VE	213.6	4.9	53.1

Table 4.1: Compression (force applied parallel to laminate)

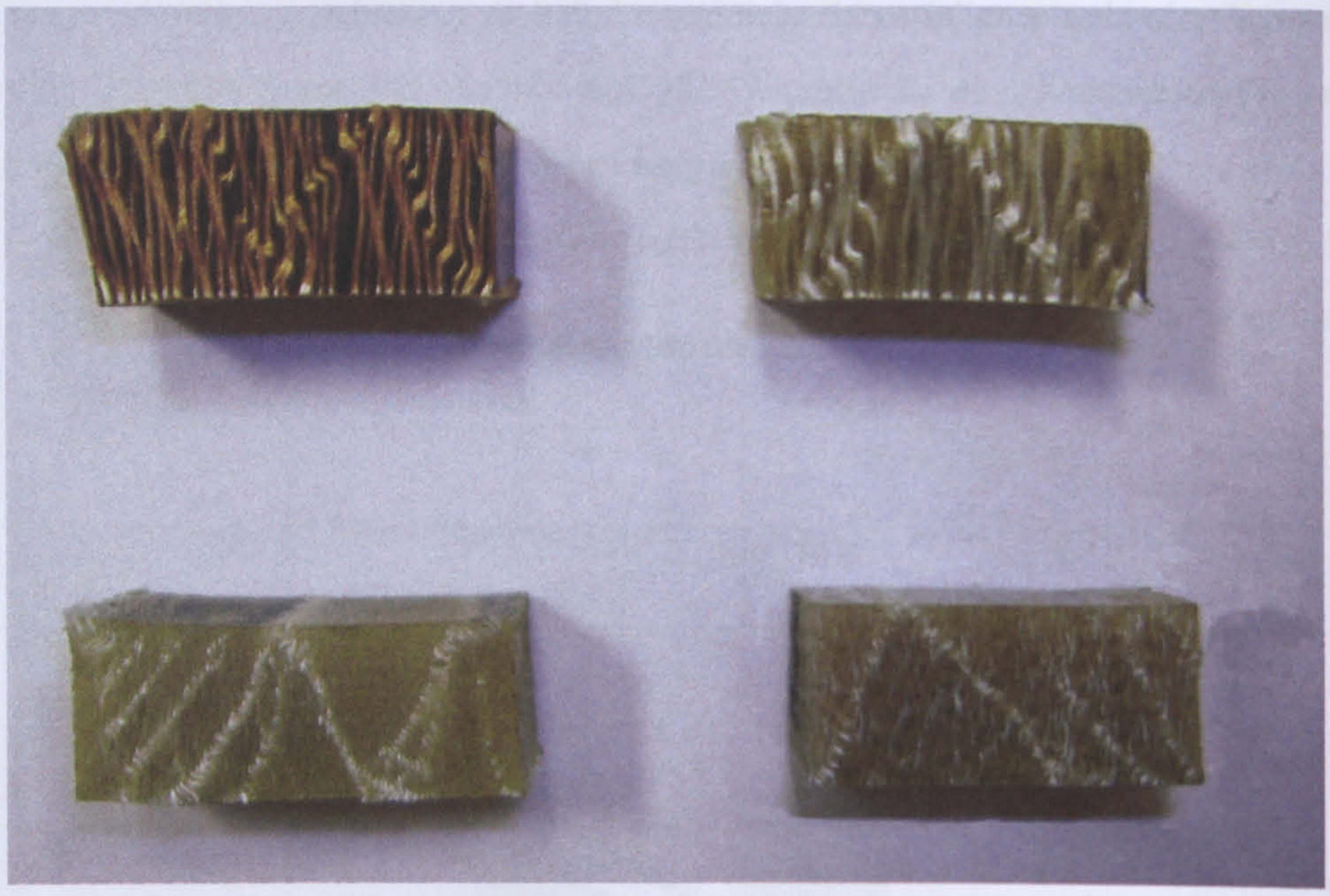

Image 4.1: Failed samples force applied parallel to laminate (CW from top left, Heavy Phenolic, Heavy VE, Light VE. Medium VE.

Material loaded perpendicular to the laminate was characterised by sudden, bursting failure with no yielding of the material, the heavy weave Phenolic material showed significantly higher strength than the other materials tested, however was initially more compliant

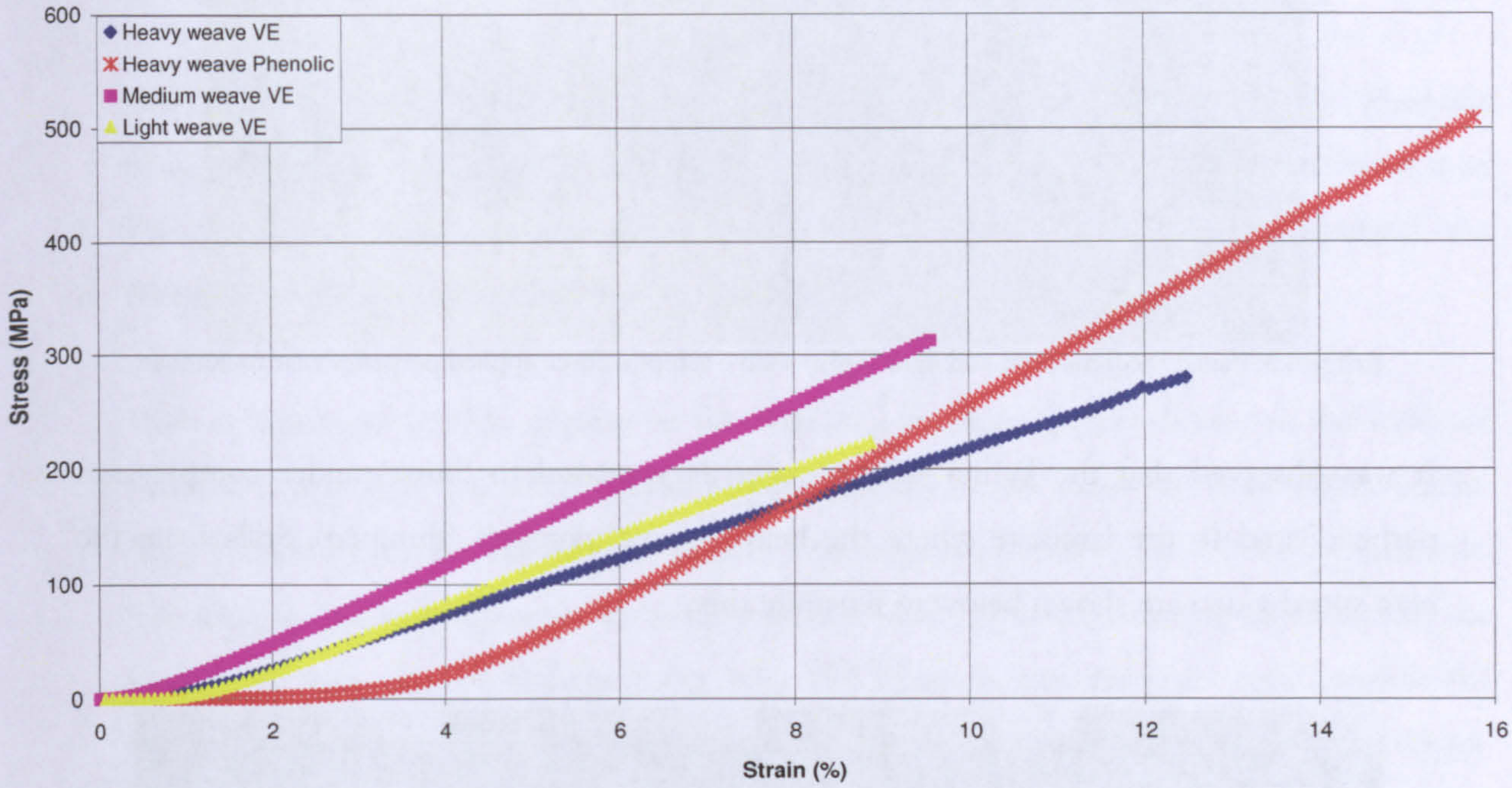

Graph 4.3: Stress/Strain curves, force applied perpendicular to laminate

The following table shows the averaged results from the compression tests carried out

Material	Averaged results UCS (MPa)	Failure strain (%)	E (GPa)
Heavy weave Phenolic	508.6	15.8	4.33
Heavy weave VE	279.8	12.5	2.41
Medium weave VE	312.6	9.6	3.51
Light weave VE	222.7	8.9	2.92

Table 4.2: Compression perpendicular to laminate direction

Image 4.2: Failed heavy weave samples force applied perpendicular to laminate (L – Phenolic, R – VE)

Image 4.3: Failed medium (left) and light (right) weave samples force applied perpendicular to laminate

It was observed that the lighter weave materials appeared to 'burst' under compression perpendicular to the laminate where the heavy weave materials 'slumped'. Stills from the high speed video are shown below to illustrate this:

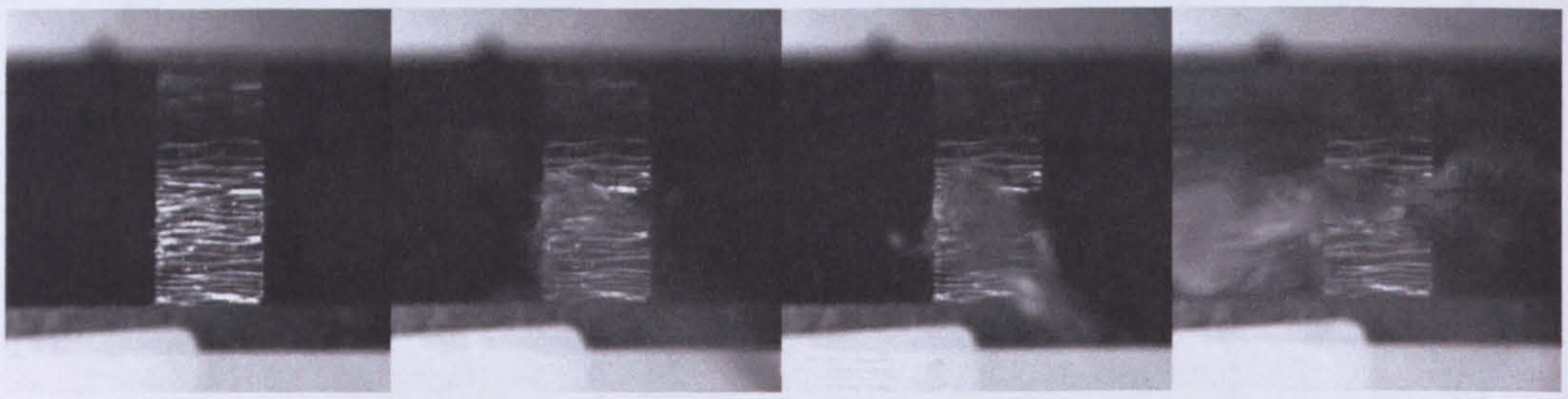

Image 4.4: Failing heavy weave material

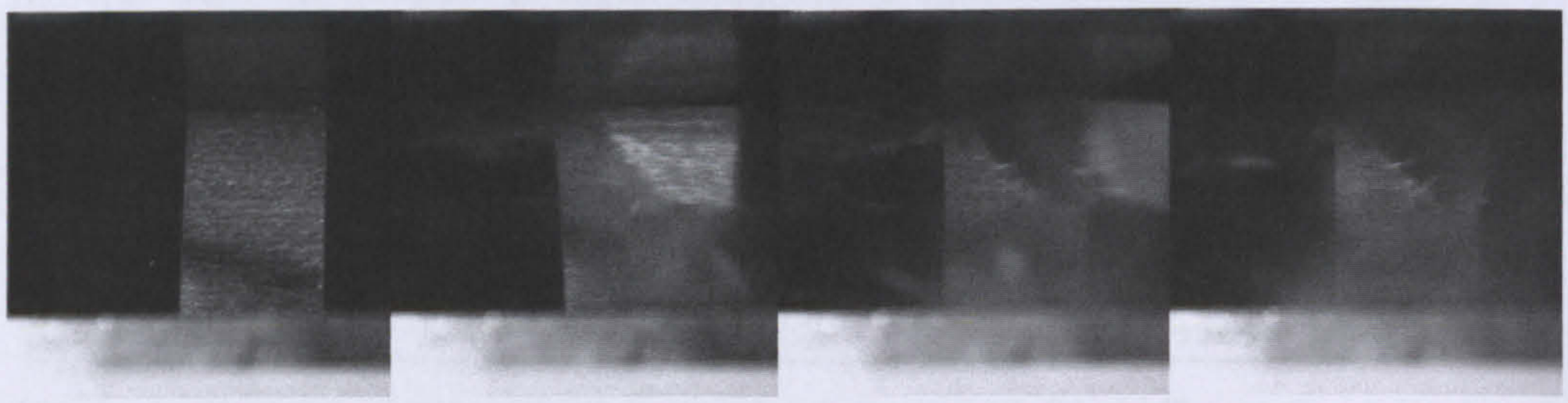

Image 4.5: Failing light weave material

4.6.5 Discussion

It is apparent from these tests that the compressive strength parallel to laminate direction is of a similar order for the Vinylester materials tested, however the press-cured Phenolic panel is significantly weaker. This indicates that the Vinylester based materials have a higher resistance to radial flow of material from the path of an indenter penetrating through the laminate, pushing material out from its path. The Vinylester materials exhibit a force peak whilst the Phenolic material merely yields. The Vinylester materials all fail at similar strain

levels however the Phenolic material failed far sooner, at little over half this strain value and at a far lower force

The medium weave Vinylester material appears to be initially stiffer than the Phenolic material but fails at a lower stress level. This failure takes place at slightly higher strain than the light weave Vinylester and slightly less than the heavy weave Vinylester material, the Phenolic has by far the highest strain to failure.

With compressive loading applied to the face of a laminate (perpendicular to the laminate plane) it is apparent that whilst the initial performance of the Vinylester materials is similar, the Phenolic is far more compliant. There is a wide spread in failure loads between materials. The samples loaded perpendicular to the laminate plane all failed suddenly (as shown by the high speed film captures Images 4.4 & 4.5). The Phenolic material burst from roughly the middle of the specimen whilst the Vinylester materials all failed at one end of the specimen. The Vinylester specimens all show signs (especially in the medium weave material) of shear failure, this is less evident in the heavy weave material presumably due to the coarseness of the reinforcement architecture restricting damage growth by this means.

As a result of the extremely high loads required to successfully fail these samples it was decided not to perform a dynamic series of these tests however, there is evidence in the literature that this material property is rate sensitive [58].

4.7 Indentation testing

The initial impact of a projectile (especially a hard, armour piercing one) against a soft composite is an important event to understand. As a result a range of testing has been carried out using various indenters and indentation techniques to evaluate the performance of the composites being tested during initial stages of impact.

The tests carried out are as follows:

1. Quasi-Static non-penetrating indentation of a free surface
2. Dynamic penetration of a pointed ogival penetrator at various energies
3. Dynamic penetration of a flat, cylindrical penetrator at various energies
4. Quasi-Static ductile hole growth with steel cones of various semi-angles

Quasi-static indentation of the free surface was done using a technique very similar to the Brinel hardness test for metals. The aim of this is to determine the 'hardness' of the laminate and hence their ability to resist initial penetration by soft impactors with distributed load. An example of this could be a large, soft cored bullet or fragment.

Dynamic penetration was carried out with two main sub-types of experiment. The first was designed as a high rate, penetrating impact by a pointed projectile. This is likely to pass through the target by causing material to move radially away from the penetrator in a ductile fashion. The second sub-type was a flat cylinder designed to cause a 'plugging' failure by shearing a plug of material ahead of the impact face and forcing the plug through the remaining material.

4.7.1 Quasi-Static, non-penetrating

4.7.1.1 Aims

The aim of this testing is to evaluate the surface 'hardness' of the materials being tested. This measure of initial indentation resistance to a large, blunt indenter is believed to be of use explaining ballistic performance against large fragments.

4.7.1.2 Experimental

A very simple programme of experimental research was carried out. Indentations were made on the surface of each specimen with a 10mm hardened steel ball forced into the specimen with a force of 750kg. The diameter of this indentation was then measured with a travelling microscope with a resolution of 0.2mm in the same manner that a Brinel test would be carried out on a metallic specimen. The values for indentation size were then averaged and compared.

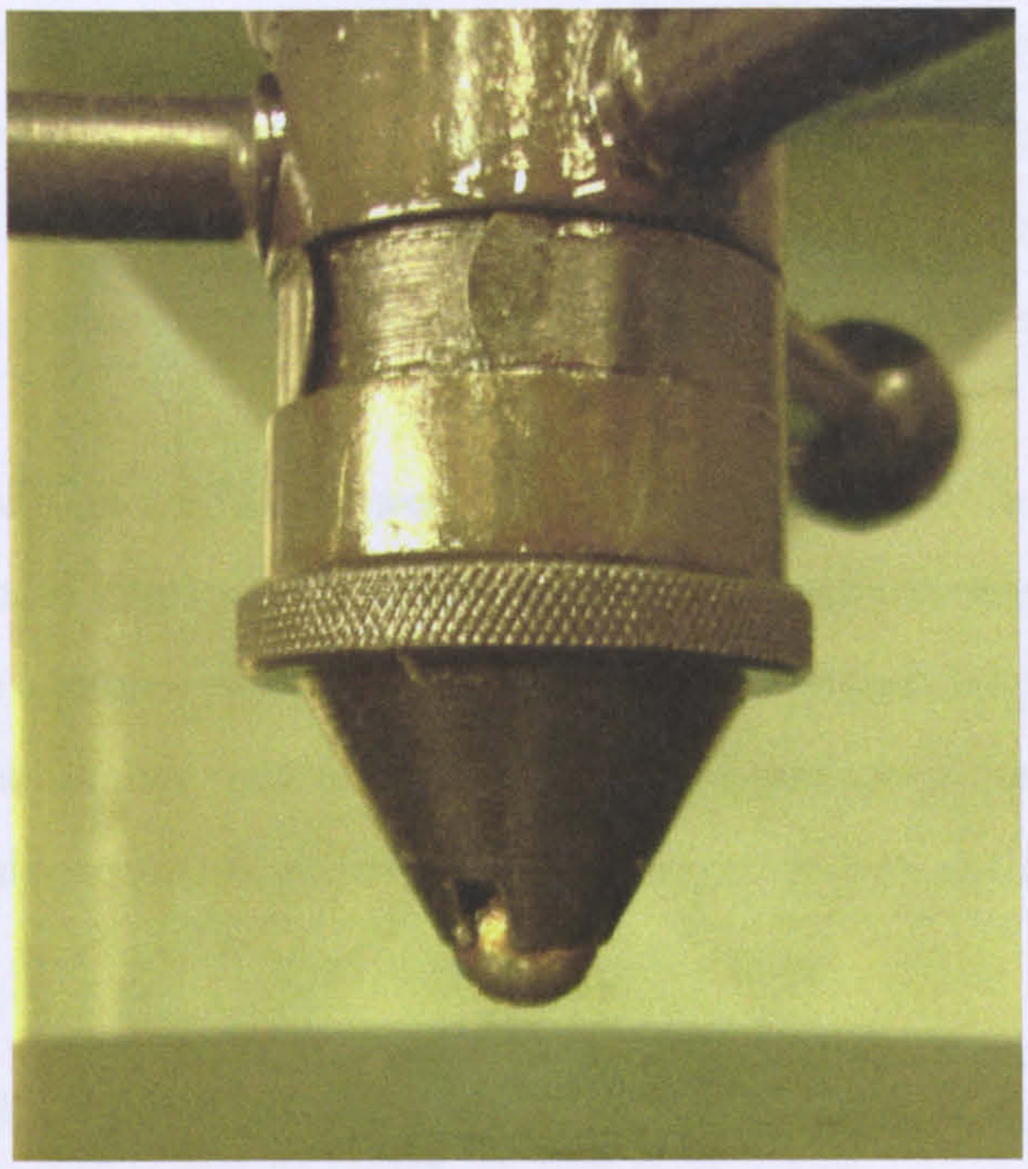

Image 4.6: Brinel Indenter

4.7.1.3 Panels tested

Samples from all 4 GFRP materials subjected being evaluated are to be tested:

1. Heavy weave S2 Glass / Phenolic
2. Heavy weave S2 Glass / Vinylester
3. Medium weave S2 Glass / Vinylester
4. Light weave S2 Glass / Vinylester

4.7.1.4 Test equipment

A standard Brinel metals hardness testing machine with a 10mm indenter ball and an optical microscope were employed for this testing, no other specialist equipment was used.

4.7.1.5 Results

The individual indentations and the calculated mean values are shown in Table 4.3

Material	Ave indentation Diameter (mm)
Heavy Phenolic	3.00
Heavy VE	4.67
Medium VE	3.50
Light VE	3.67

Table 4.3: Indentation diameter as a result of Brinel 10mm ball test

4.7.1.6 Discussion and summary

This trial consisted of simple non penetrating surface 'hardness' assessment of the composite. The aim of this is to evaluate the resistance of the materials being tested to a relatively blunt indentation.

It is interesting to note how superior the press-cured Phenolic panel appears compared to the equivalent Vinylester material which is by far the 'softest' of the materials tested. This may be due to the coarseness of the weave meaning that readings are unduly influenced by the presence of a fibre bundle directly below the indentation, however numerous indentations were made and averaged to attempt to avoid this problem.

4.7.2 Quasi-Static, Penetrating

4.7.2.1 Aims

The aim of the following trials is to evaluate the response of FRP materials to penetrating impact. Very little is understood about the way in which a soft, composite armour reacts when it is penetrated by a hard projectile.

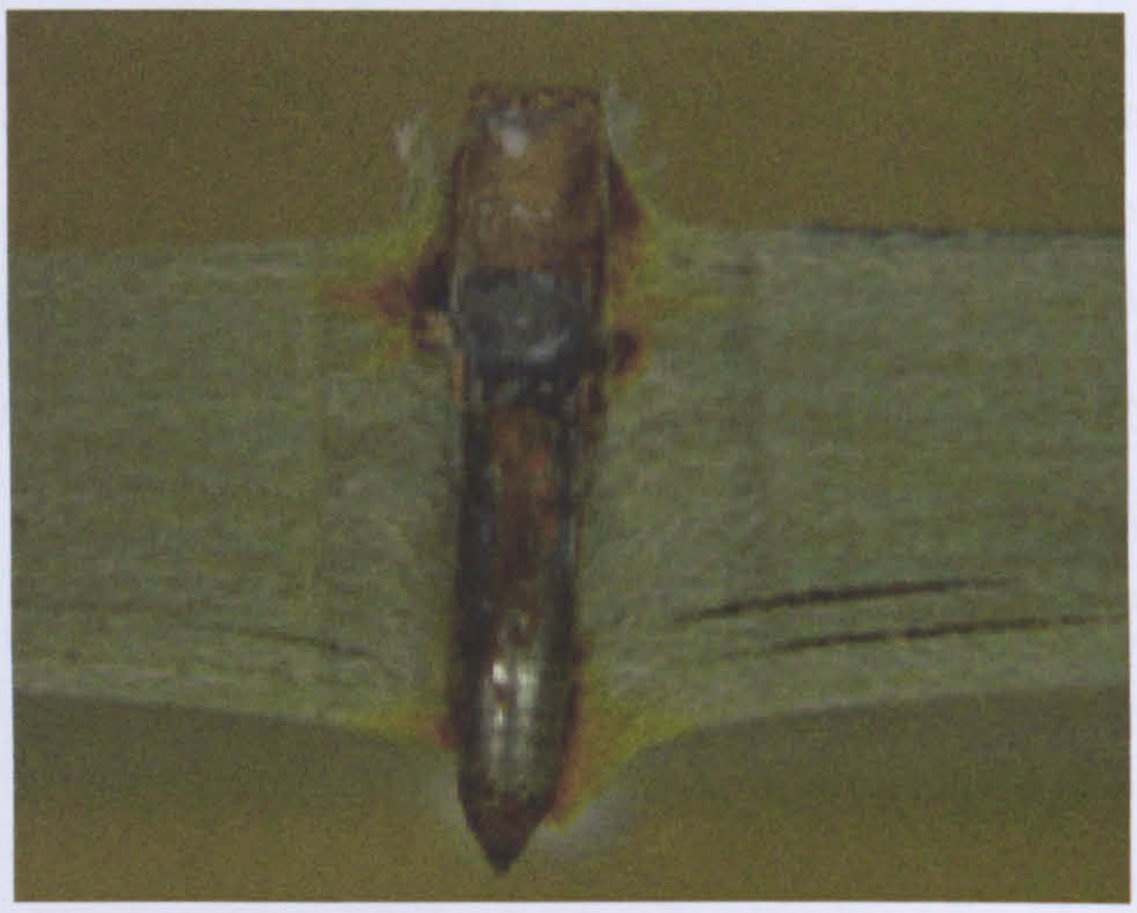

Image 4.7: Bullet embedded in armour showing plastic deformation through thickness from front face

The above image shows a bullet which has struck a composite, the core has exited through the front of the round and lead the penetration. Plastic deformation is evident and betrayed by deformation of the reinforcement fibres. The bullet jacket is embedded in the hole left on the front face. On the rear face the presence of delaminations betray a rear surface mechanism, the point at which an composite armour stops absorbing impact energy by plastic deformation and starts delaminating is not fully understood and will be discussed in later chapters.

4.7.2.2 Experimental

As discussed in section **4.2** of this report the use of conical indenters has been successfully used by Horsfall[56] to evaluate the indentation resistance of polymers. The same techniques shall be used here with some minor differences discussed below.

With large metallic indenters, full submersion into the test material is not practical. Instead of defining 'deep' by the depth of penetration (which is sure to vary with cone angle) this testing will instead be concerned with indentations which have fully penetrated at least two laminates. The reason for this choice is to minimise any effect of laminate in-homogeneity i.e. should an indenter encounter a resin rich pocket in one lamina.

When fine cone angles such as those planned are used there is a risk of damaging the indenter, this is especially the case if dynamic indentations are performed in the future. To avoid this complication a pilot hole shall be drilled in the material to be tested. This starter hole should be as small as practically possible, for the purposes of this work a 1mm diameter hole was drilled in the test material with a high speed rotary drill. This step may not be possible when dealing with dense, press cured or similar composites.

The indenters were manufactured out of EN24 steel with 90°, 60°, 45° and 30° angles (α being 45°,30°,22.5° and 15° respectively), finer cone angles were not manufactured for fear of the indenters becoming too fragile. A standard Vickers machine set up to apply 100kgs of force was used to press the indenters into the composite. The surface of the indentation samples was painted white to ease identification of the edge of the indentation.

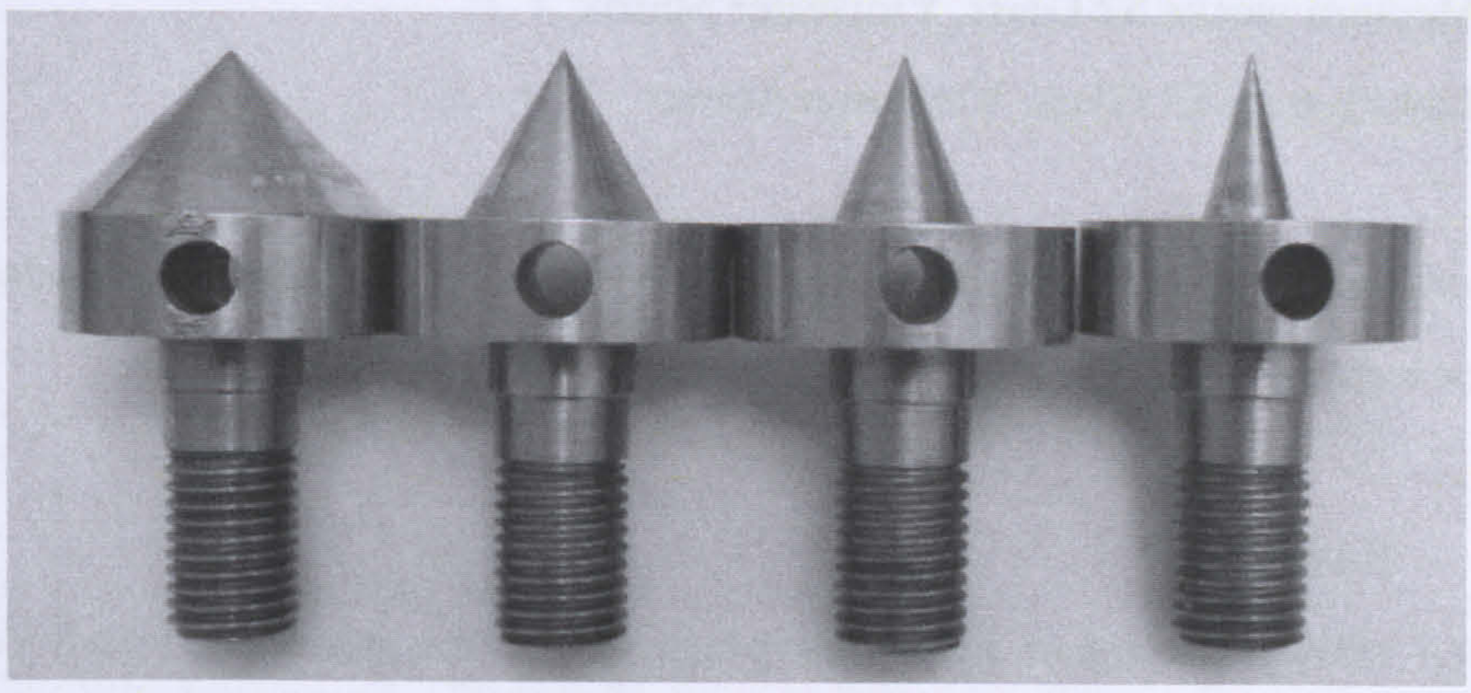

Image 4.8: Indenters L-R 90°,60°,45°,30°

Concurrent with the theory discussed in section **4.2** indentations were carried out with both dry and lubricated indenters.

To perform the indentation a load will have to be applied then removed and the diameter of the indention observed. This observation can be made using the standard Vickers machine ocular, the numbers on the ocular instrument being the dimension measured in 0.001mm. If the indentations prove too large to be measured by the Vickers ocular then a travelling microscope with a resolution of 0.01mm was available for use. Repeated indentations will be carried out till the surface diameter of the indentation fails to increase. Lubricant will be applied after each indentation, for those tests where lubrication is used. To prevent contamination of the indention surface with a 'wet' lubricant which may effect the material behaviour a dry PTFE spray will be used.

After a plot of mean indentation pressure versus cone semi angle has been plotted from equation ***4.6*** a curve fitting exercise will be performed through the use of equation ***4.7***. Values of P_o and μ will be iteratively varied so that the resultant curve of calculated indentation pressure matches the mean indention pressure results. This will then provide a value of friction and more importantly yield strength for the material tested.

4.7.2.3 Panels Tested

The standard materials available for testing in this project are to be evaluated here and are listed as follows:

1. Heavy weave S2 Glass, Vinylester Matrix
2. Medium weave S2 Glass, Vinylester Matrix
3. Light weave S2 Glass, Vinylester Matrix

It was not possible to drill pilot holes in the Heavy weave Phenolic matrix material therefore it was not tested.

4.7.2.4 Results

Graph 4.4 shows the mean indention pressure for the materials tested calculated from indentation diameter using equation ***4.6*** and plotted against cone angle. The curves (especially the non-lubricated curves) appear to be flattening out at a far lower rate with respect to angle than that seen in the literature.

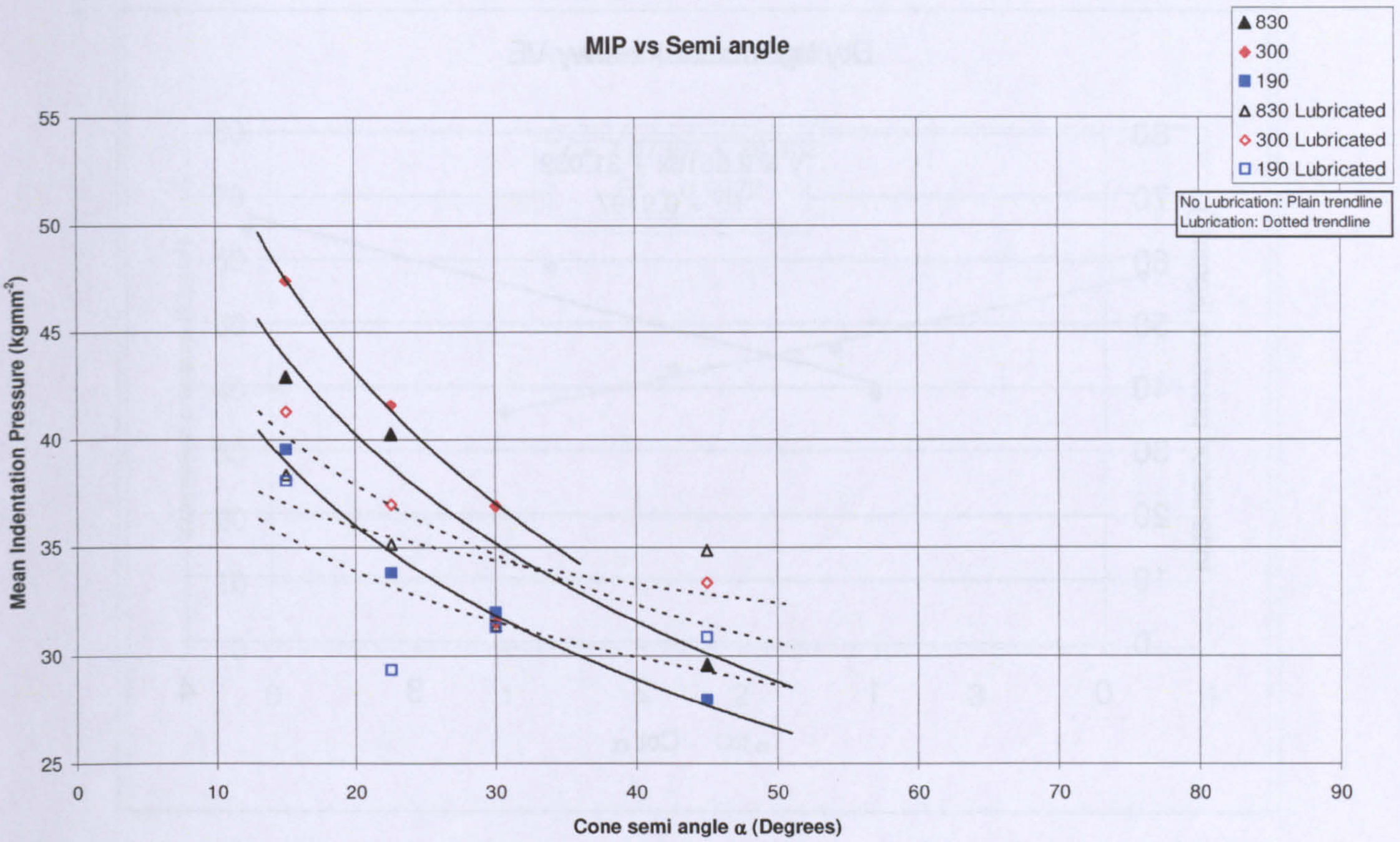

Graph 4.4: Mean Indentation pressure vs Cone angle, all materials, with and without lubrication

Through the use of equation ***4.7*** to fit a curve to the experimental plots has yielded values of yield stress and indentation friction for all tests. Indentation pressure was plotted against cot α. As equation ***4.7*** can be arranged into the standard form for a straight line ($y=mx+c$), the intercept (P_o)and gradient ($P_o\mu$) can be recorded to give yield strength and coefficient of friction. This approach is shown in the following graphs and tables:

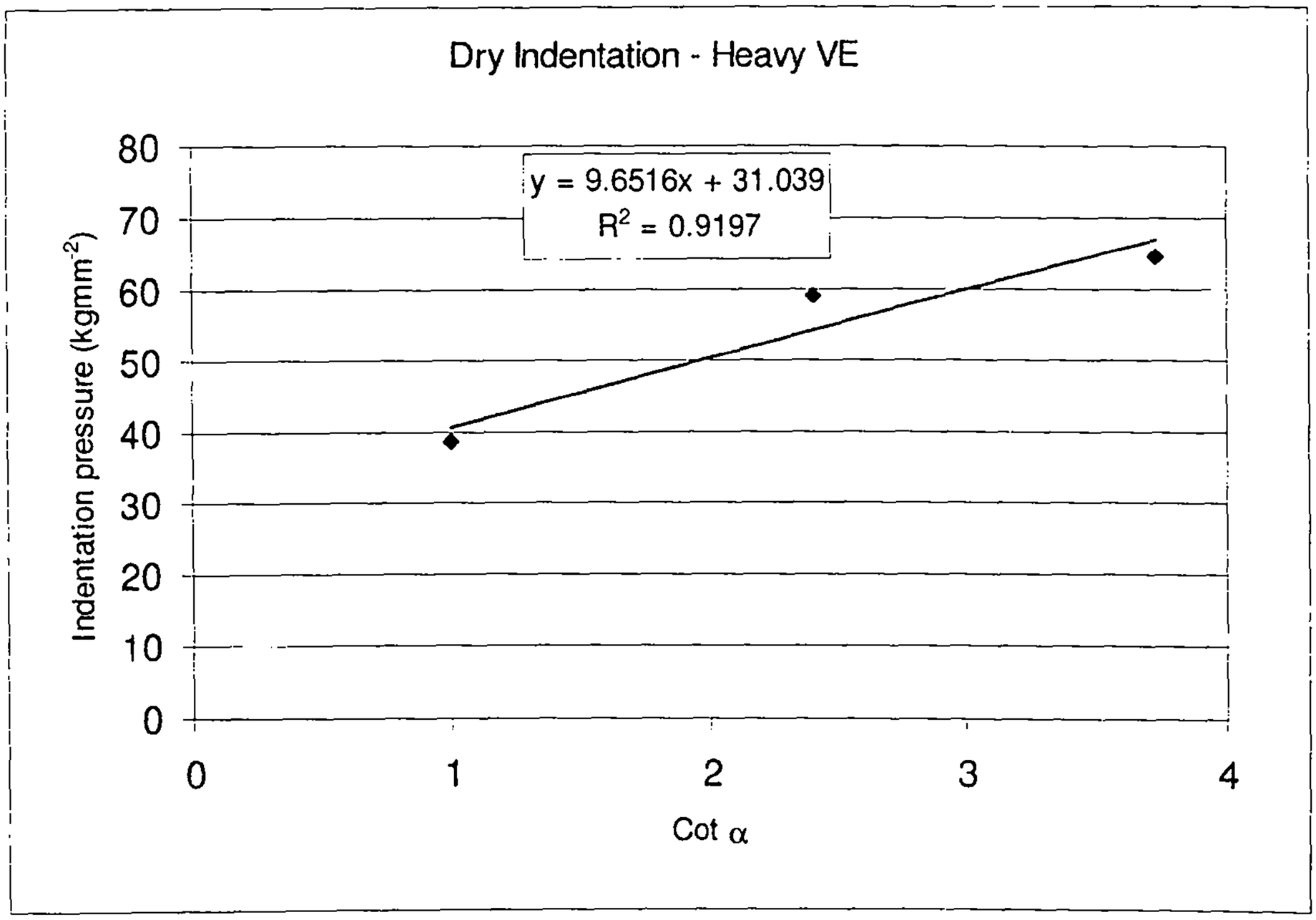

Graph 4.5: Equation fit to measured indentation pressure data for heavy weave VE dry indentation

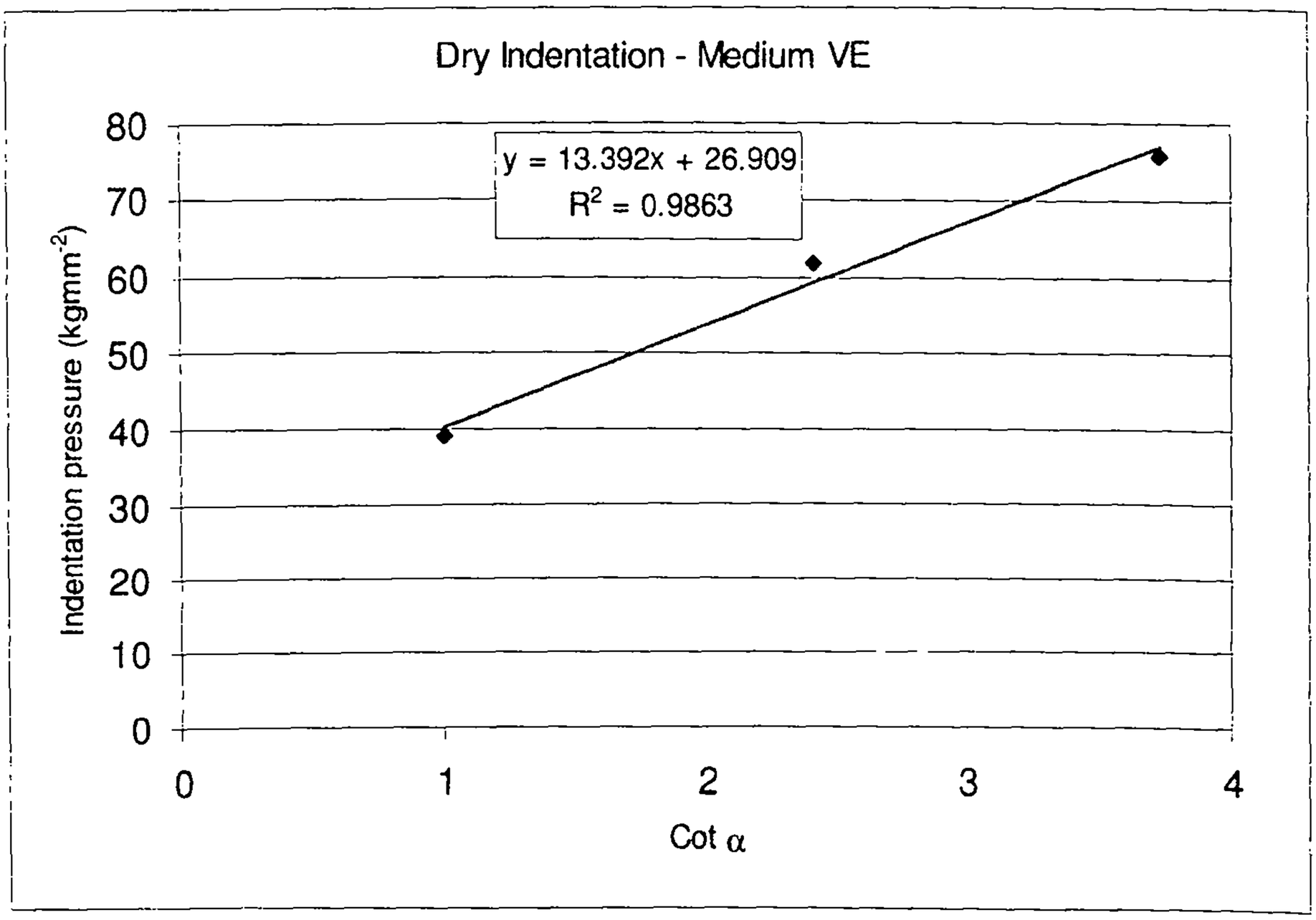

Graph 4.6: Equation fit to measured indentation pressure data for heavy weave VE lubricated indentation

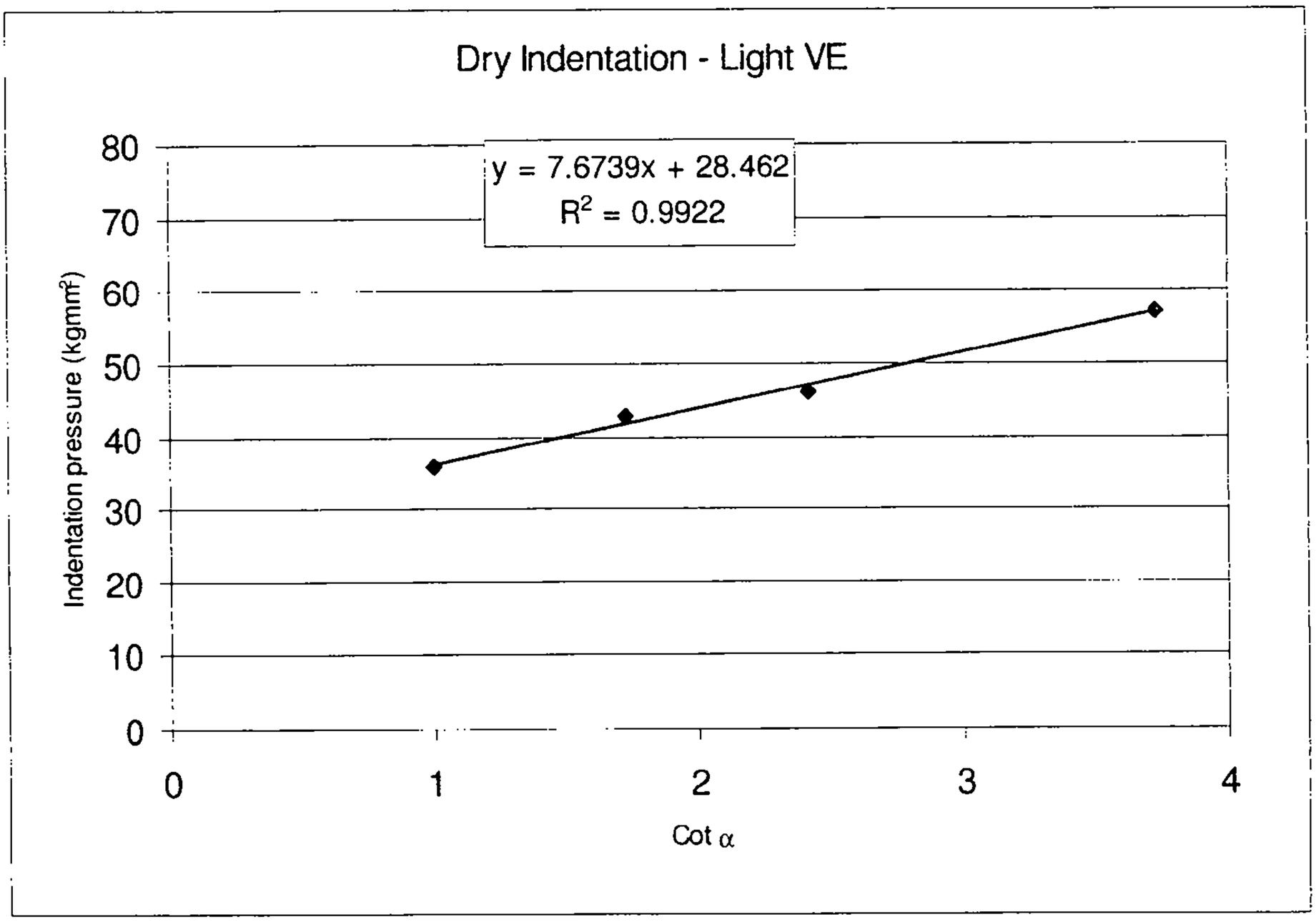

Graph 4.7: Equation fit to measured indentation pressure data for medium weave VE dry indentation

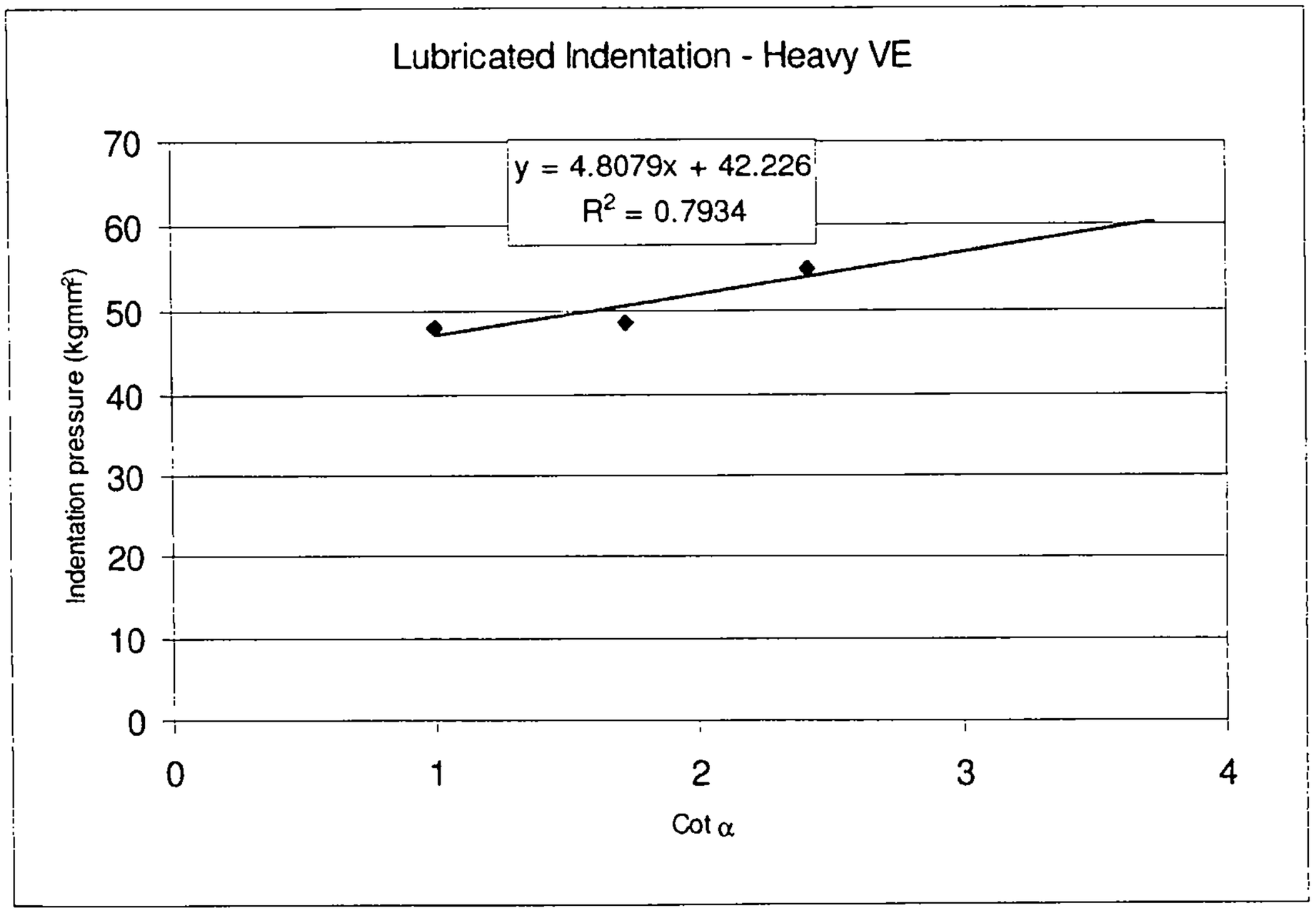

Graph 4.8: Equation fit to measured indentation pressure data for medium weave VE lubricated indentation

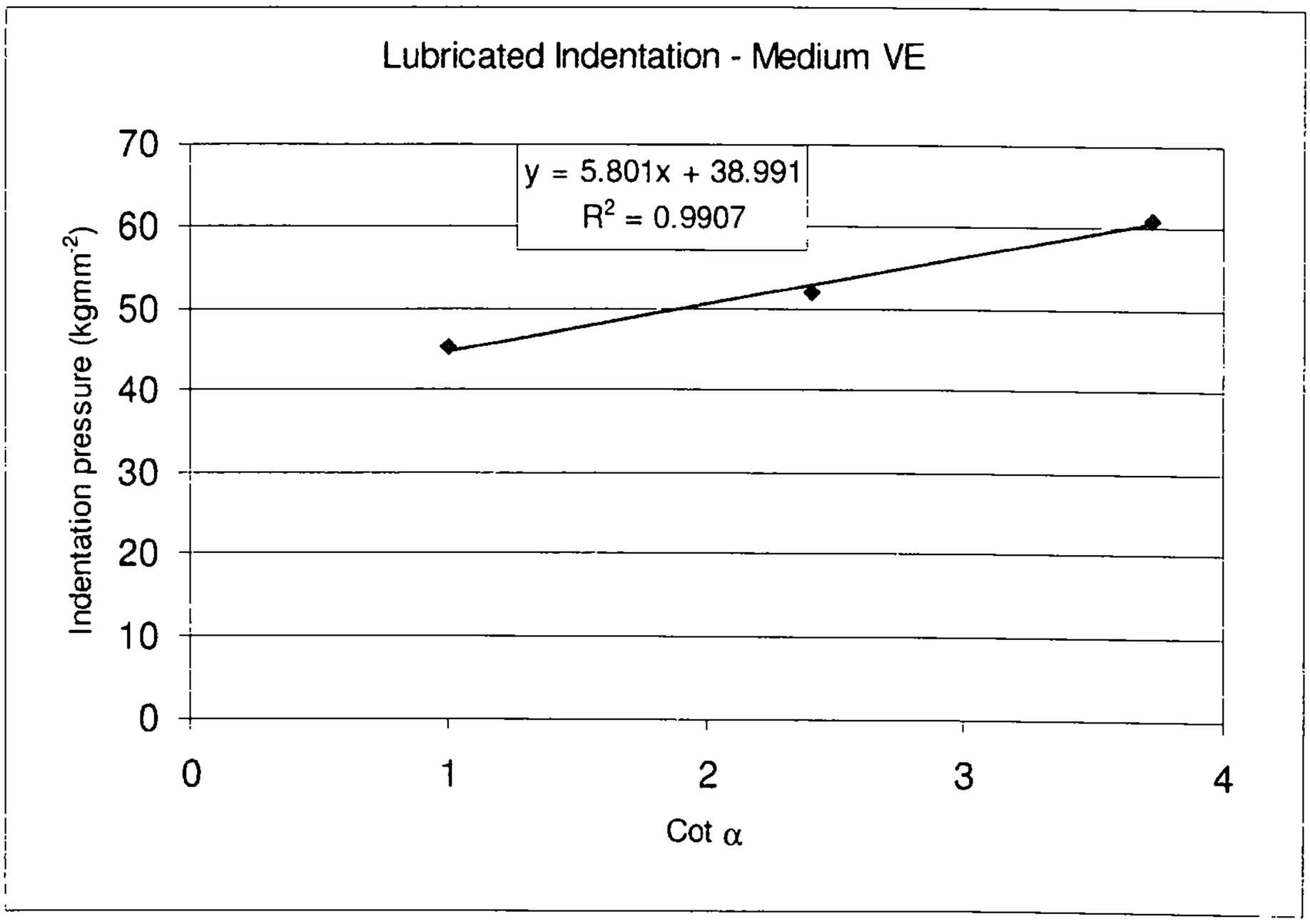

Graph 4.9: Equation fit to measured indentation pressure data for light weave VE lubricated indentation

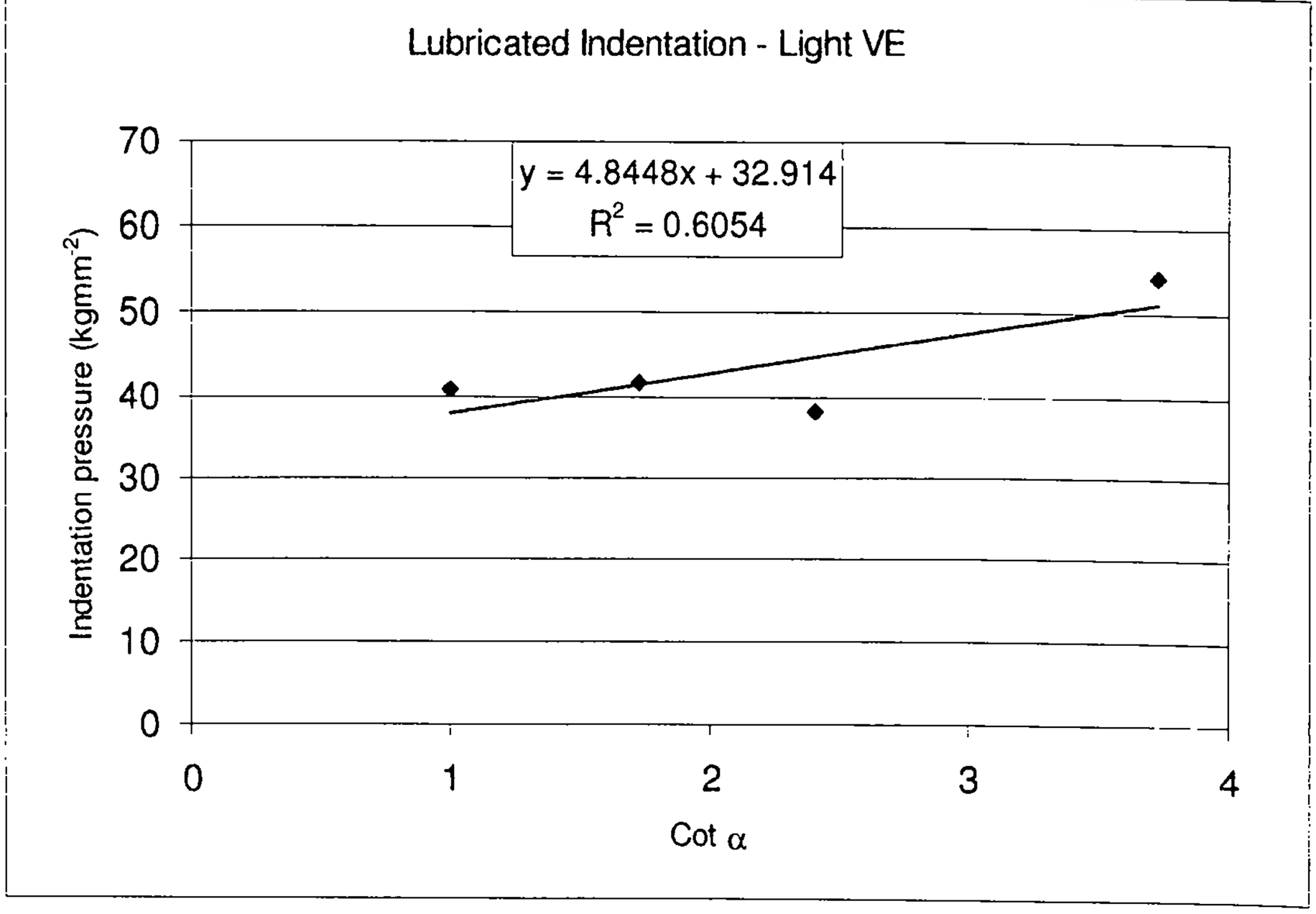

Graph 4.10: Equation fit to measured indentation pressure data for light weave VE lubricated indentation

	Results of curve Fit	
	μ	Po (MPa)
Heavy VE Dry	0.31	304.5
Heavy VE PTFE	0.11	414.2
Medium VE Dry	0.5	263.9
Medium VE PTFE	0.15	382.5
Light VE Dry	0.27	271.2
Light VE PTFE	0.08	322.8

Table 4.4: Yield strength (P_o) and friction values from curve fit

4.7.2.5 Summary

The trends seen in the literature for the indentation of metals with conical indenters are also seen in the composite materials tested though it appears the effect of low values of α on indentation pressure are more pronounced, values of α less than 20° (40° full cone angle) should be avoided.

Graph 4.4 plots the mean indention pressure for the materials tested calculated from indentation diameter using equation ***4.6*** plotted against cone angle. Results for lubricated and dry indentions are shown. The un-lubricated curves (full lines) slow less sign of fully levelling out by 90° cone angle than the lubricated trends. The relationship between lubricated and un-lubricated curves is similar to that in Graph 4.1. However the curves appear to be levelling out at a far lower rate with respect to α than behaviour observed in metals.

The application of lubrication to the indenter, whilst not making as big a difference to the mean indentation pressure curve as the literature indicates it does for metals, does make a large difference in the values of derived yield strength (shown in Table 4.4).

The use of equation ***4.7*** has allowed values for yield strength to be obtained as per table 4.4, comparing these to the compressive yield strengths found in section **4.6** and summarised in the following table (table 4.5) show very good agreement between the values of yield

strength for loading parallel to the laminate and un-lubricated indentations. The yield strength values perpendicular to the laminate also show good agreement with the exception of the medium weave material. Using lubricated indentations over-estimates measured yield strength values significantly in all cases. This method has also generated indentation coefficients of friction for the composites which will be of use when discussing ballistic indentation later in this report.

Material	Yield strength (MPa)			
	Parallel	Perp	Indentation Dry	Indentation Lubricated
Heavy weave Phenolic	114.8	508.6	N/A	N/A
Heavy weave VE	273.4	279.8	304.5	414.2
Medium weave VE	252.9	312.6	263.9	382.5
Light weave VE	213.6	222.7	271.2	322.8

Table 4.5: Yield strength (P_o) values from compression and indentation testing

4.7.3 Dynamic penetration

4.7.3.1 Aims

This experimental work was carried out with the aim of applying the same theories as used in quasi-static indentation to equivalent dynamic events. As well as this the testing will evaluate the stand alone performance of the composites when subjected to penetrating impact by the very threat that is experienced in ballistic testing. A flat indenter/punch geometry is also to be tested as this type of impact / penetration is of the type associated with high velocity fragments.

4.7.3.2 Experimental

The dynamic apparatus (Rosand IFW 5) consists of an instrumented falling weight (25kg) housed in a tower (which also contains winch apparatus and guide rails) to which the indenter is attached. Load measurements are taken with a piezoelectric load cell attached close to the indenter. Data logging is triggered by an optical gate array as the falling weight approaches the target, this array is also responsible for velocity measurement.

A 7.62x39 AP core was used as an indenter, this allowed indention of a pointed indenter with the ogival end as well as the indentation of a flat indenter achieved by reversing the core in a holder.

Image 4.9: Core in droptower holder with loadcell (left) Rosand IFV Droptower (right)

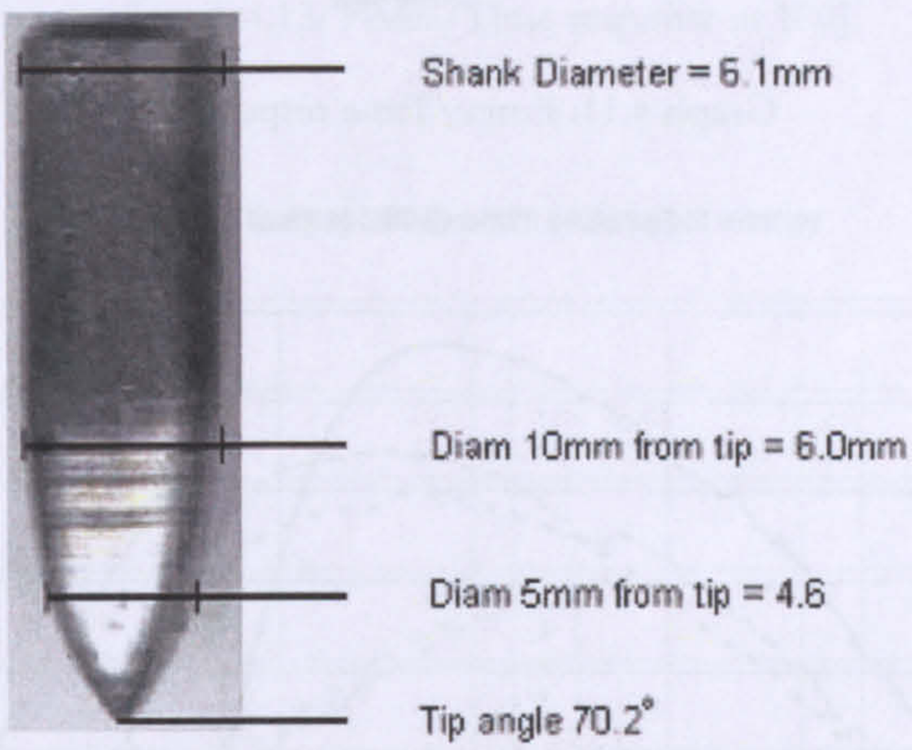

Image 4.10: Indenter details

4.7.3.3 Panels tested

Samples from all 4 GFRP materials due to be subjected to ballistic testing are to be tested:

1. Heavy weave S2 Glass, Phenolic Matrix
2. Heavy weave S2 Glass, Vinylester Matrix
3. Medium weave S2 Glass, Vinylester Matrix
4. Light weave S2 Glass, Vinylester Matrix

4.7.3.4 Results – Ogival indenter

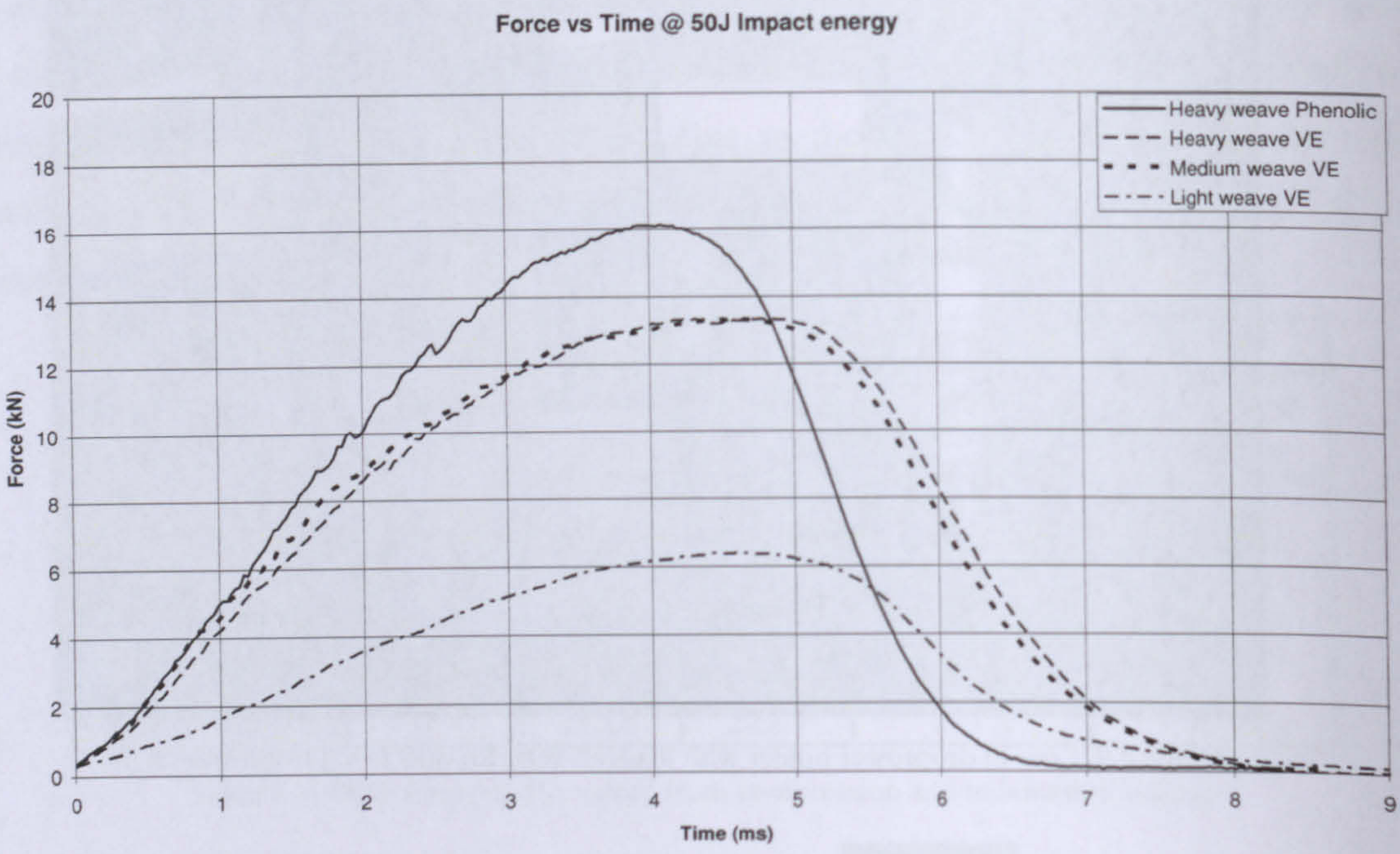

Graph 4.11: Force/Time response at 50J

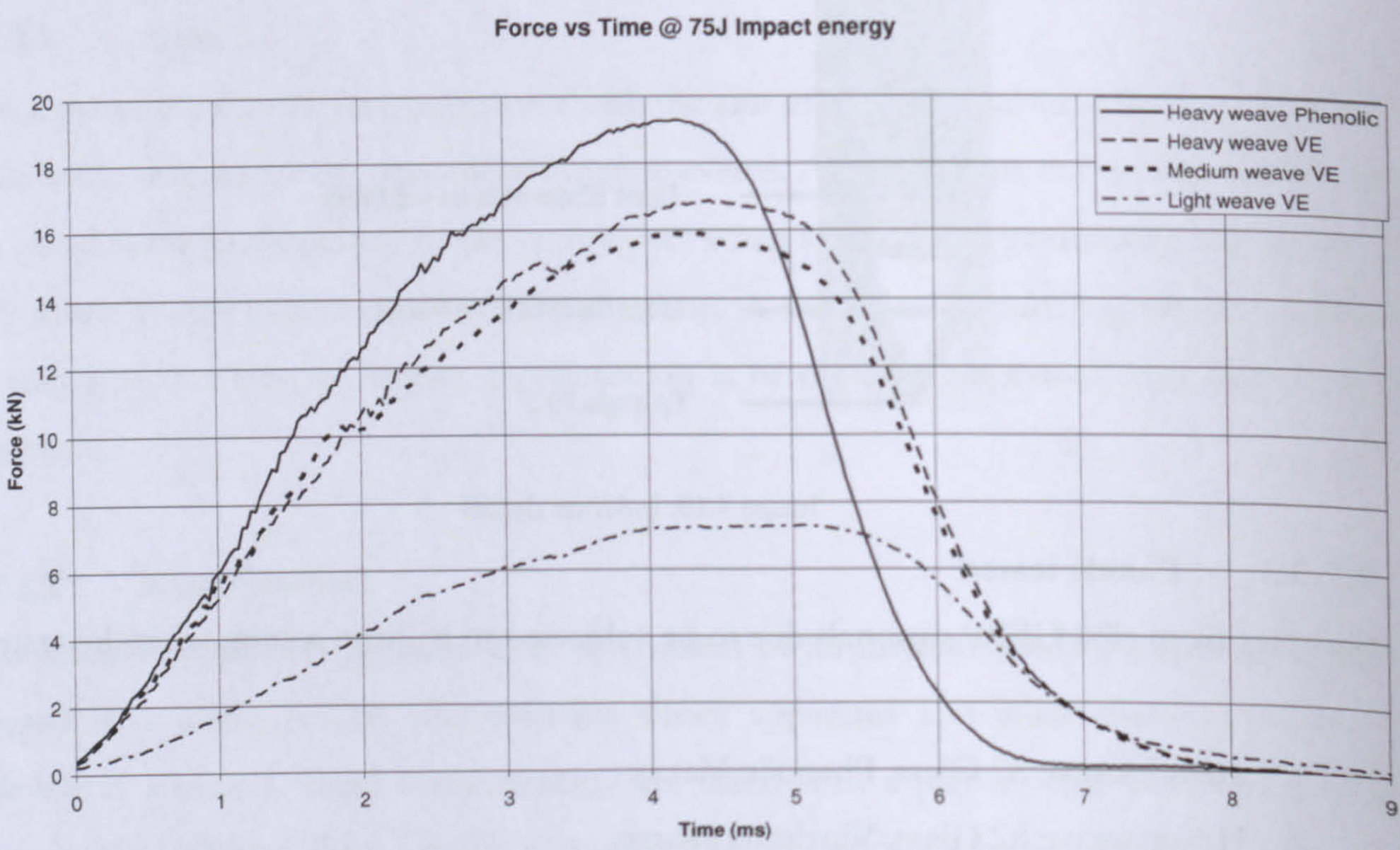

Graph 4.12: Force/Time response at 75J

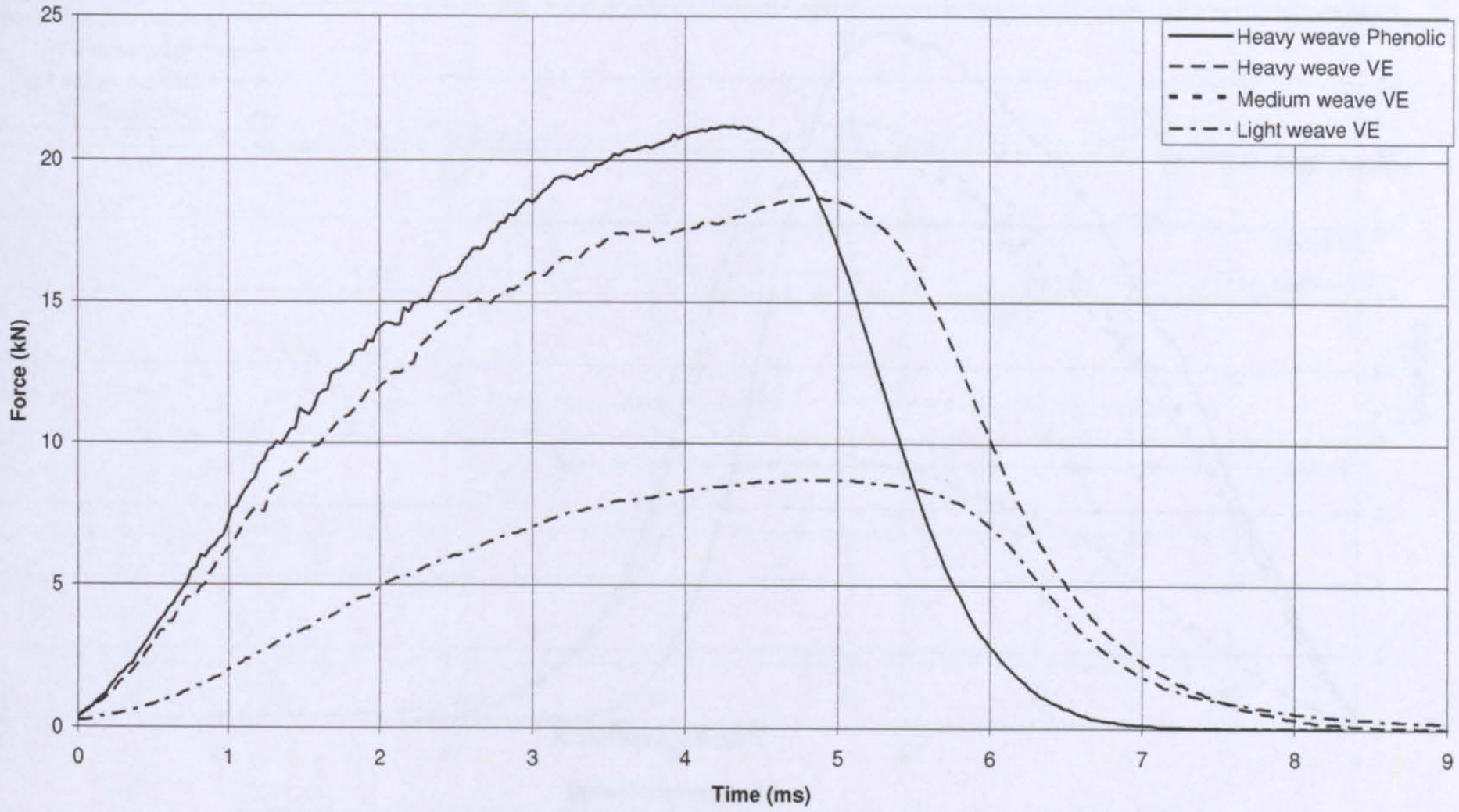

Graph 4.13: Force/Time response at 100J

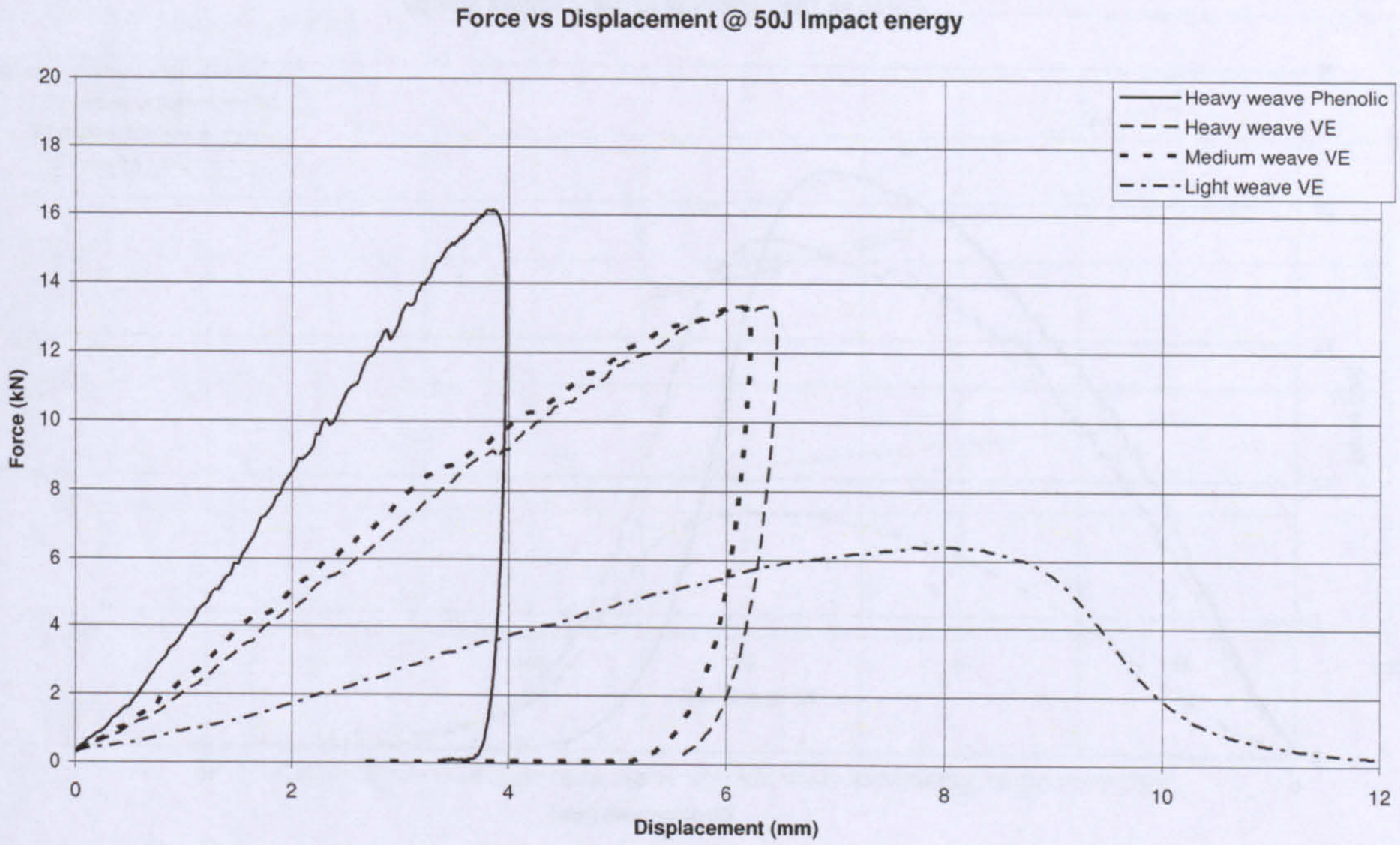

Graph 4.14: Force/Displacement response at 50J

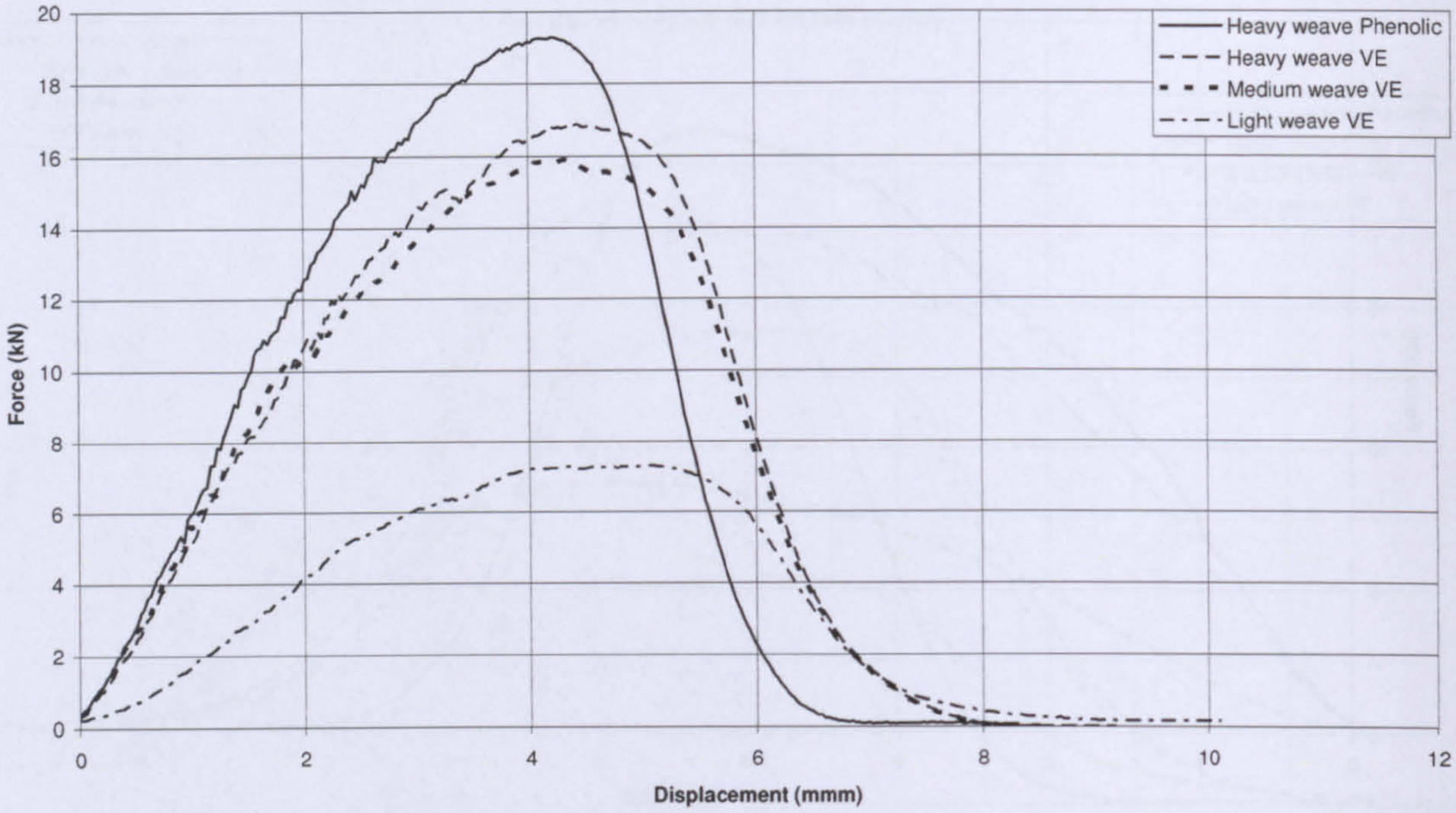

Graph 4.15: Force/Displacement response at 75J

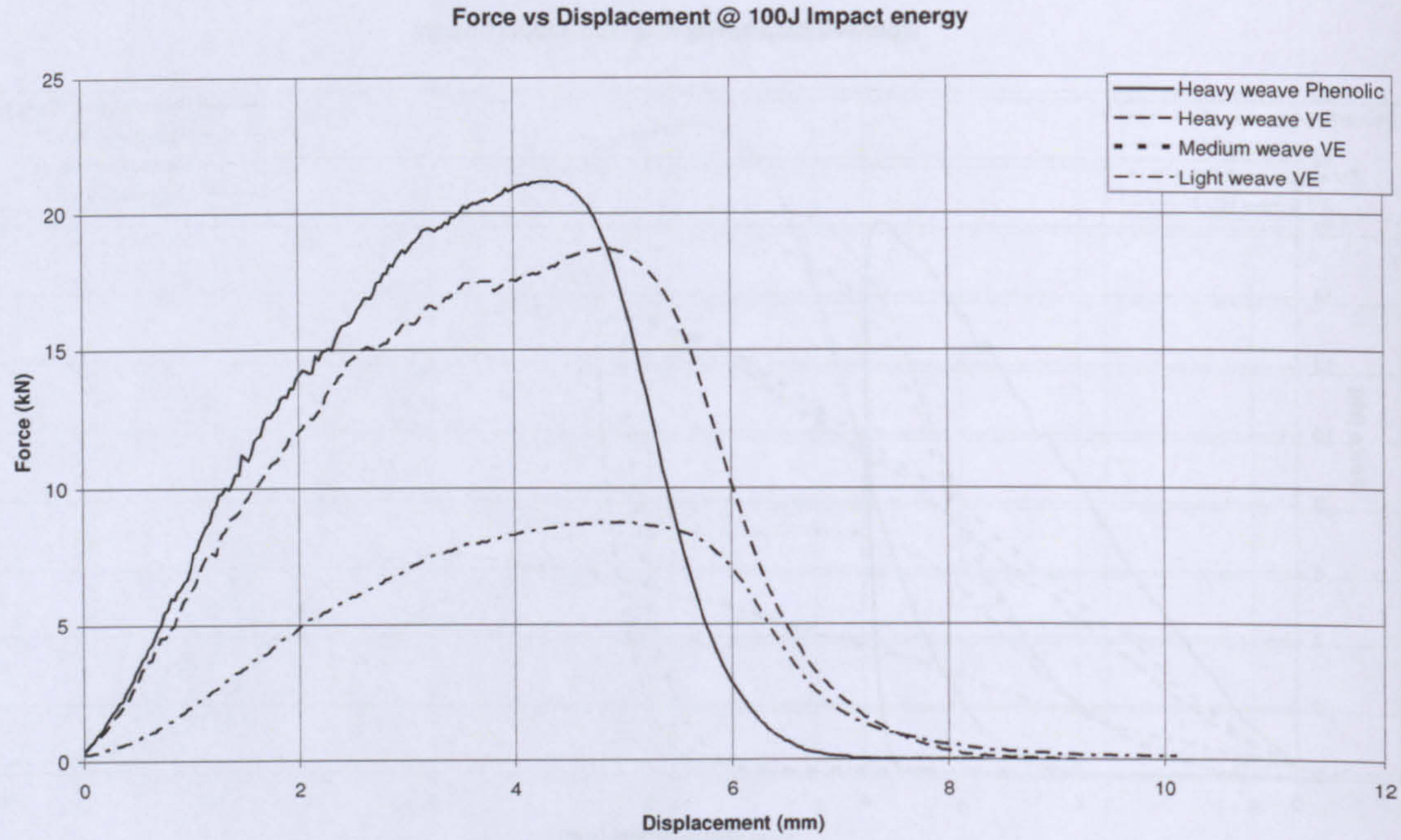

Graph 4.16: Force/Displacement response at 100J

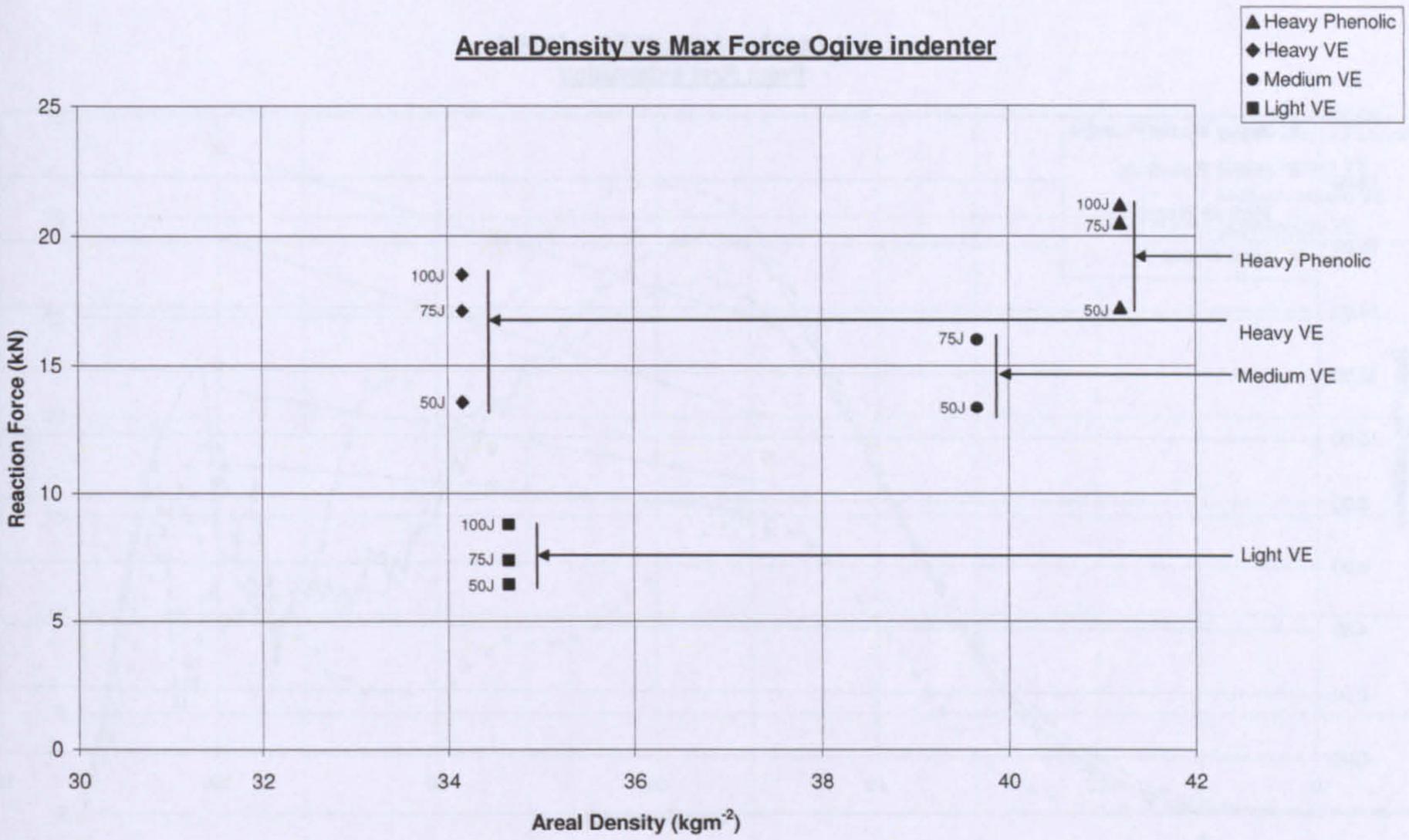

Graph 4.17: Average max force for 3 impact energies vs material areal density

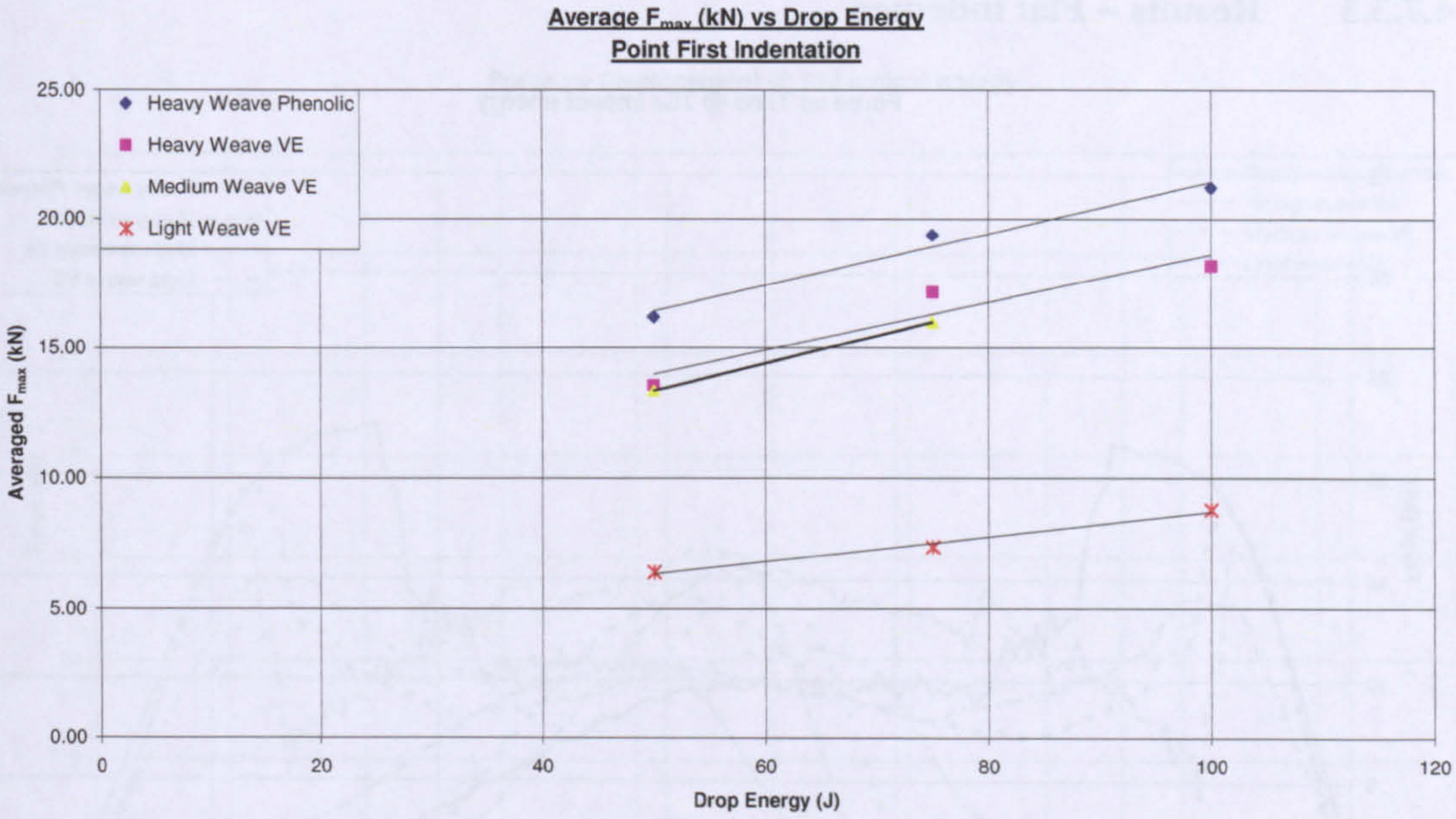

Graph 4.18: Average max force trends with increasing impact energy

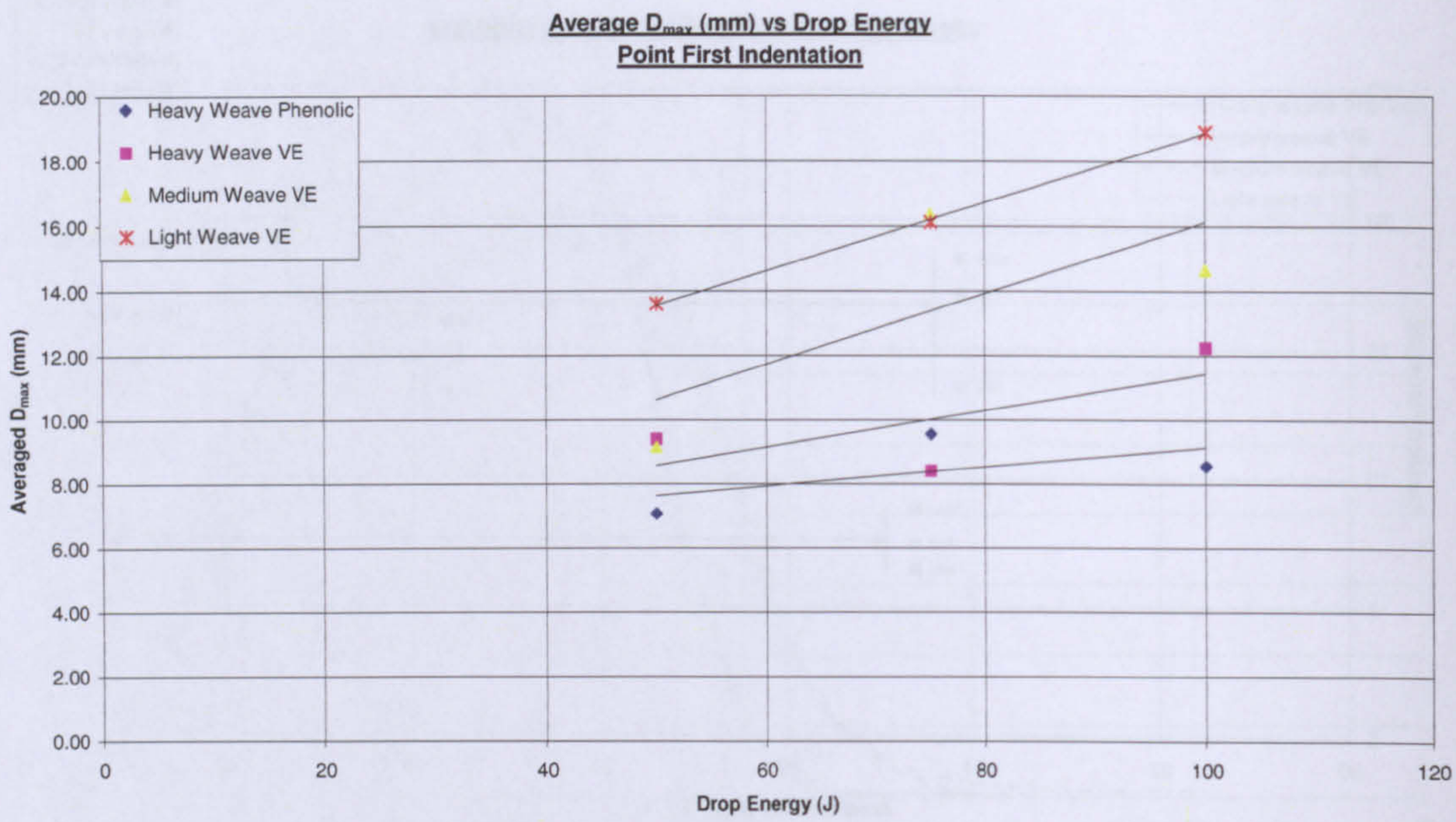

Graph 4.19: Average indentation depth trends with increasing impact energy

4.7.3.5 Results – Flat indenter

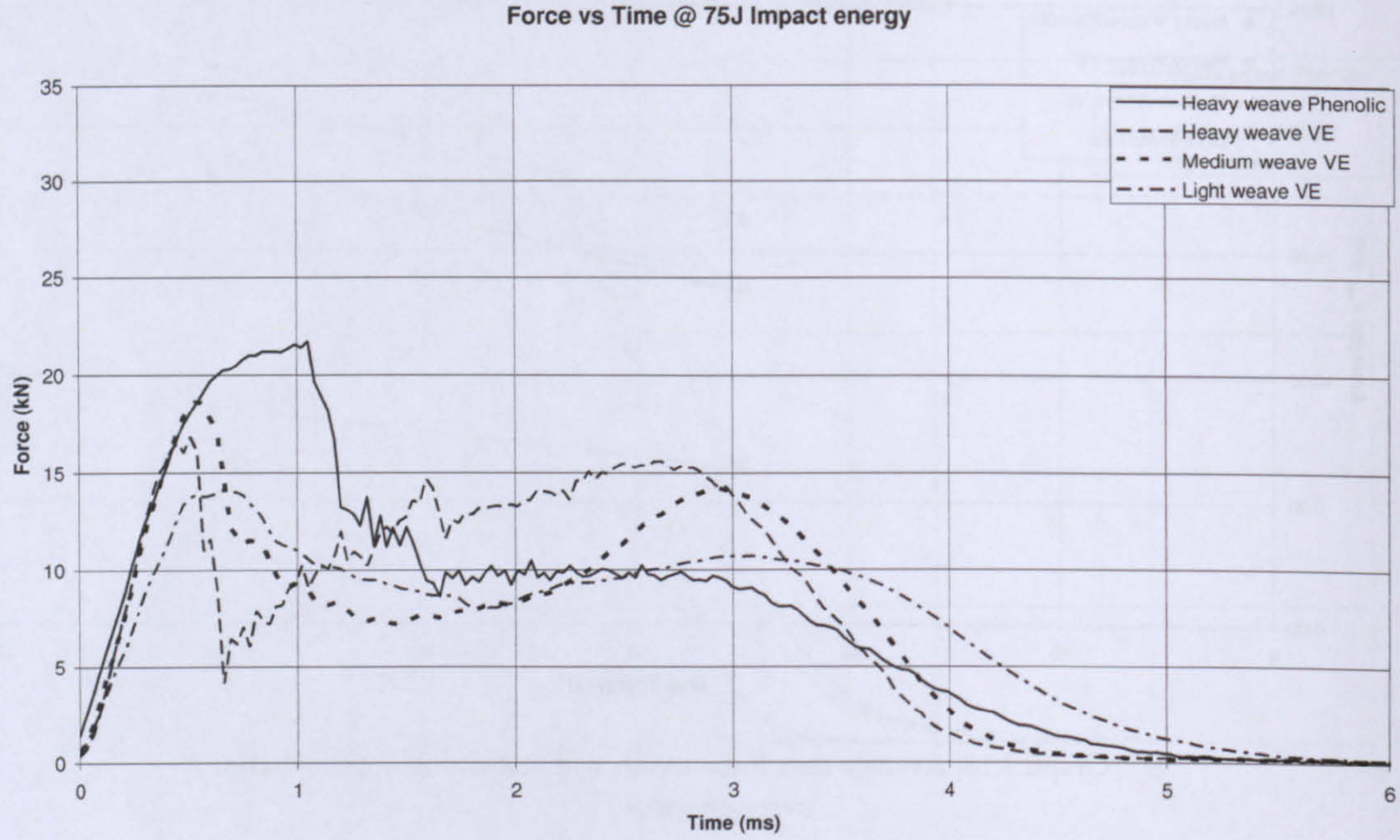

Graph 4.20: Force/Time response at 75J

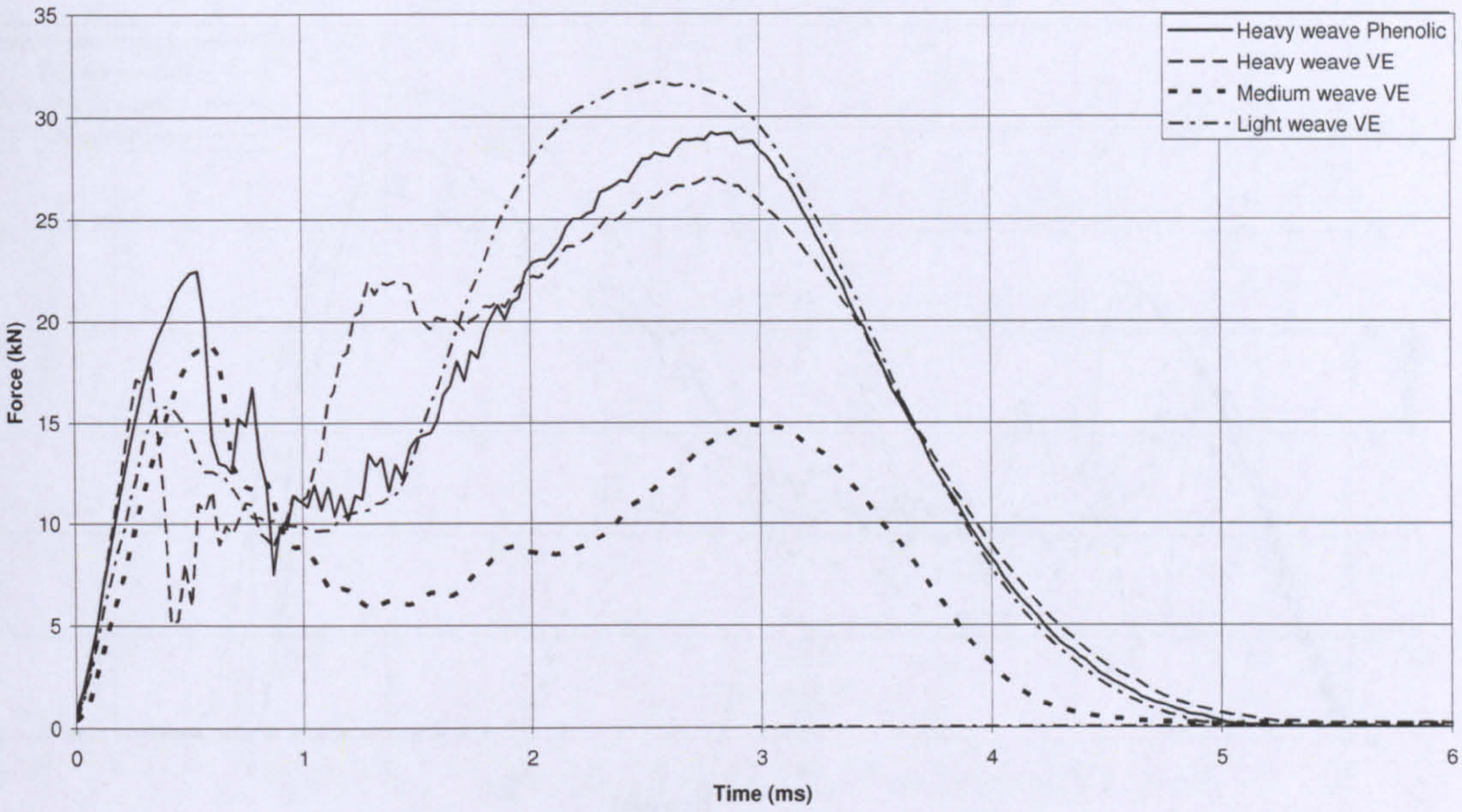

Graph 4.21: Force/Time response at 150J

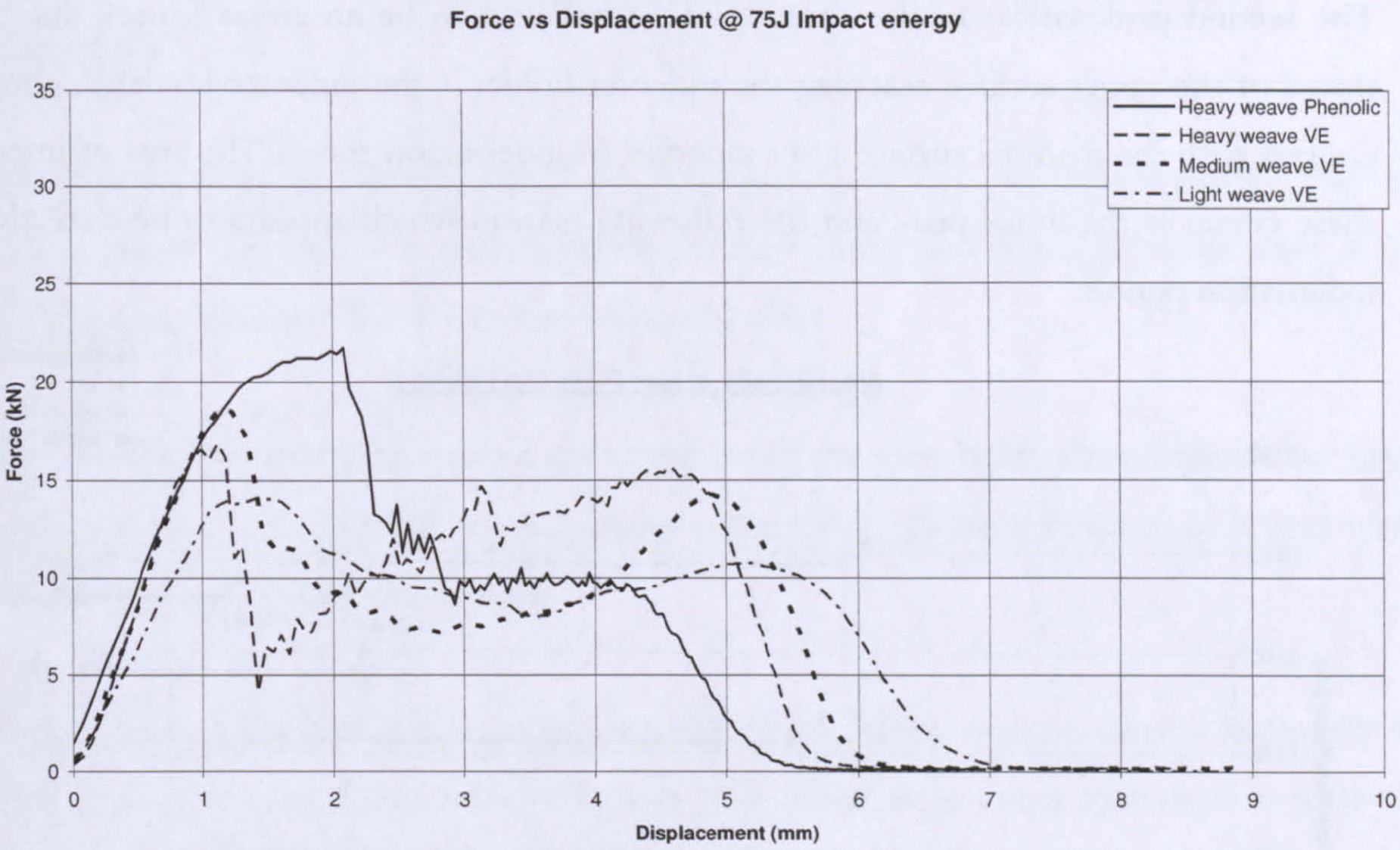

Graph 4.22: Force/Displacement response at 75J

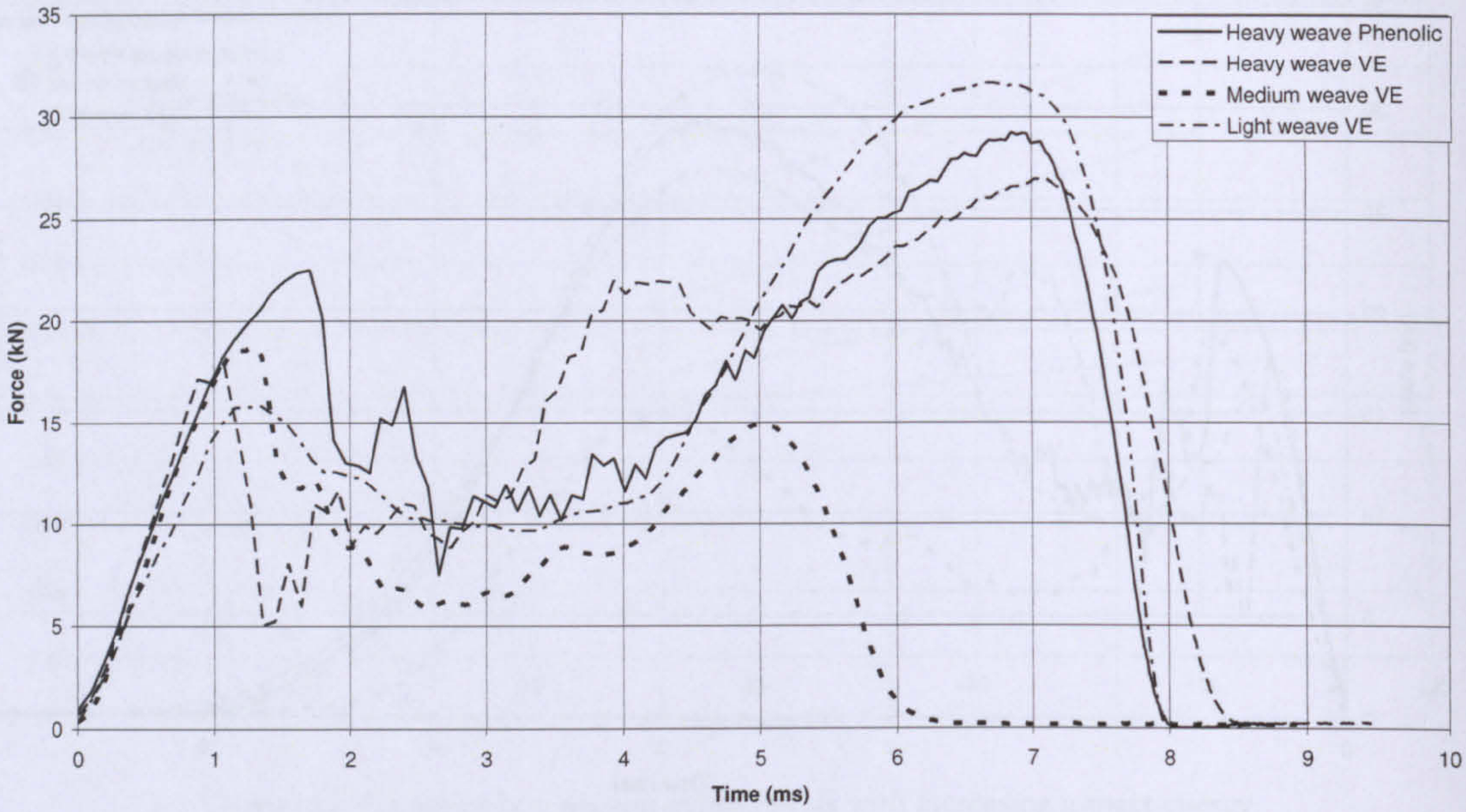

Graph 4.23: Force/Displacement response ar 150J

The second peak visible in the above plots is believed to be an arrest feature due to up-thrust of the target surface reaching the indenter holder / the indenter holder coming into contact with the material surface after a period of indentation travel. The area of interest in these curves is the initial peak and the following plateau which appears to be a steady state indentation period.

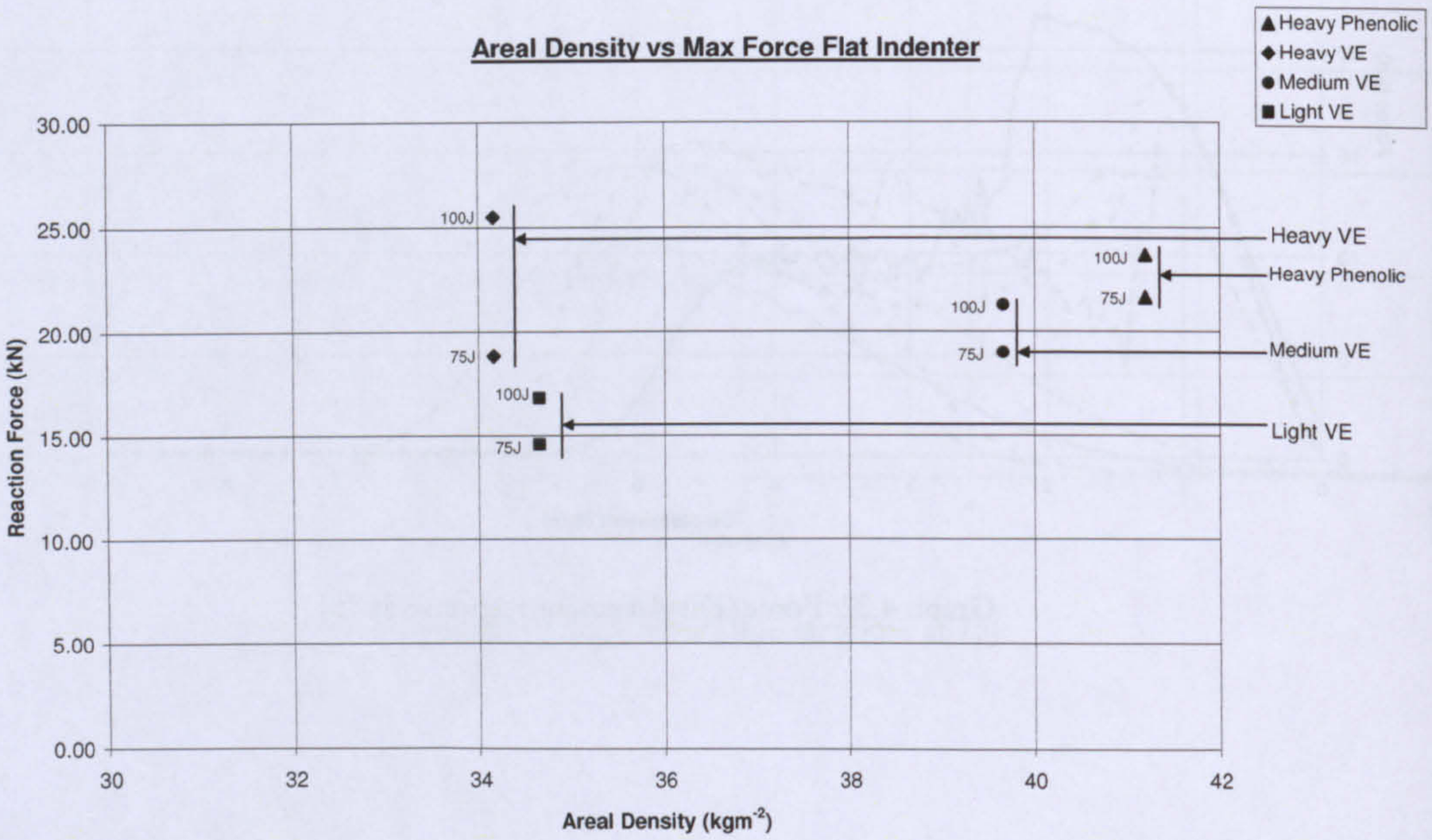

Graph 4.24: Average max force for 3 impact energies vs material areal density

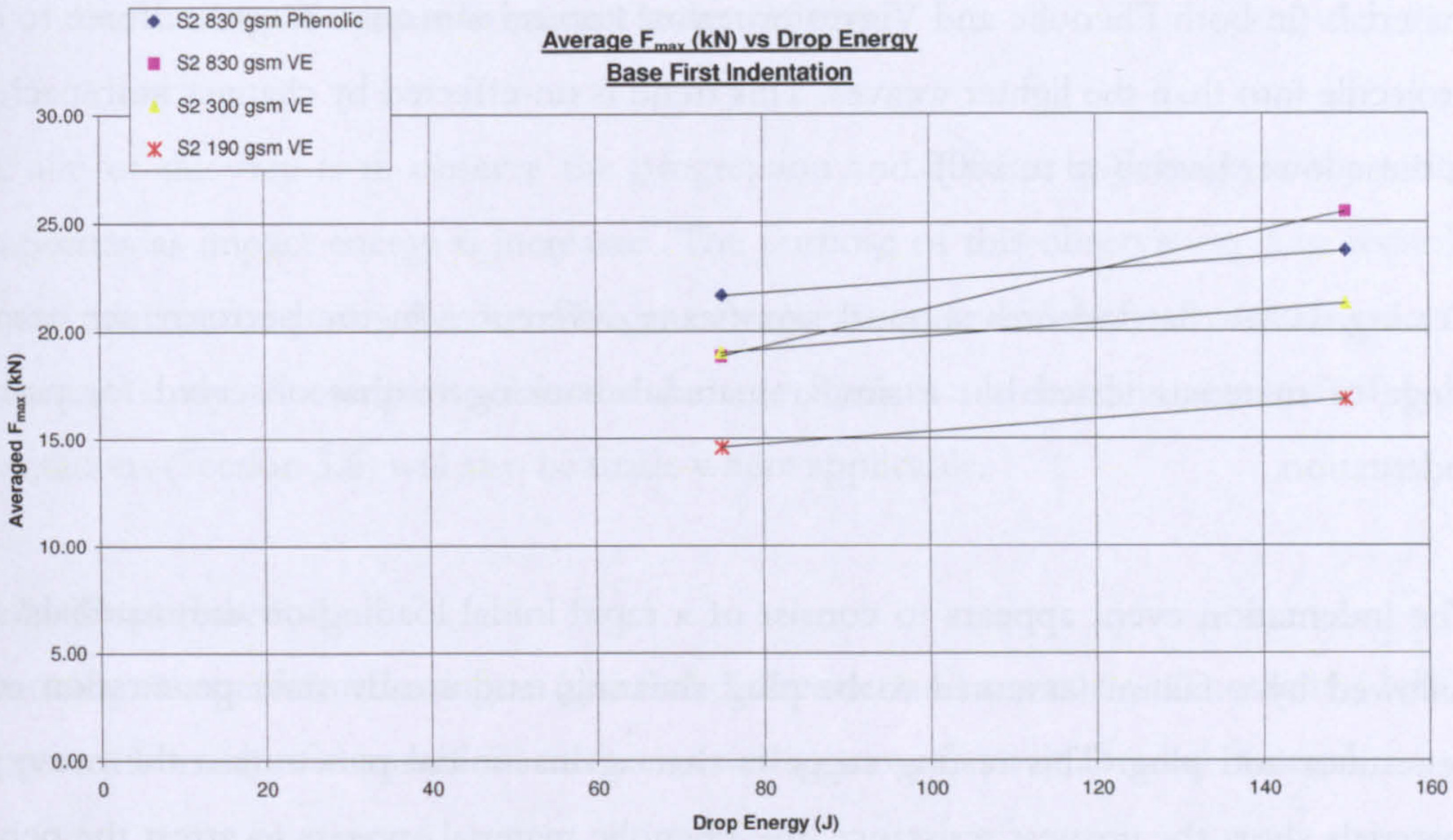

Graph 4.25: Average max force trends with increasing impact energy

4.7.3.6 Discussion

Testing with a pointed indenters showed significant differences in performance between the materials tested.

The force resisting the projectile as it entered the material was the highest for the Phenolic material (i.e. it put up the most resistance), slightly lower was the equivalent heavy weave VE. The light VE recorded the lowest resistance force.

The material ranking order seen in the force tests was seen again when indentation depth was investigated, the Phenolic material again being evidently the hardest to penetrate whilst the light weave VE being the easiest.

This testing suggests that against initial penetration the heavy weave materials (especially the Phenolic tested) show the greatest resistance. The indentation event appears to consist of a rapid initial loading followed by a rapid arrest and in the case of the heavy weave materials a small degree of elastic recovery during which the penetrator 'bounces' back out of the material. The arrest event is far more rapid for the coarse weave materials, the lighter weaves appear to unload the material more gradually.

Evaluating indentation force with increasing impact energy suggests that there are two very distinct material performance groups, heavy weave and lighter weaves. The heavy weave

materials (in both Phenolic and Vinyester resins) appear to require far more force to drive a projectile into than the lighter weaves. This trend is un-effected by changes in impact energy at these lower levels (up to 100J).

Testing with a flat indenter showed significant differences in the performance across the range of materials tested but a similar materials ranking to that observed for point first indentation.

The indentation event appears to consist of a rapid initial loading on the materials surface followed by a failure (assumed to be plug shearing) and steady state penetration of both penetrator and plug. This testing suggests that against initial penetration the heavy weave materials show the greatest resistance, the Phenolic material appears to arrest the penetrater in the shortest amount of time and sustain load longer (with respect to indentation depth) than the other materials tested, this corresponds with earlier testing (section **4.7.1**) which found the material 'hard'.

The force returned in stopping the projectile as it entered the material was the highest for the Phenolic material (i.e. it put up the most resistance), only slightly lower was the equivalent, heavy weave Vinylester. At the lower energy level (75J) the medium weave Vinylester material was of comparable performance (in terms of reaction force) to the heavy weave Vinylester however, at 100J there was a large difference between the two materials, the medium weave material appeared not to be especially sensitive to the increase in impact energy. The light weave material had the lowest reaction force. Of interest is the observation that the difference in reaction force for the two drop energies tested is far larger for the coarse weave materials whilst the lighter weaves tested resulted in very similar reaction forces for both energy levels.

The variation of indentation depth with increasing energy was not analysed as it became apparent that the indenter holder was coming into contact with the front surface of the specimen material thus invalidating any measurement of ultimate indentation depth.

4.8 Sectioning of dynamic impact indentations

4.8.1 Aims

The aim of this trial is to observe the progression and change in damage in the indented composites as impact energy is increased. The purpose of this observation is to record any trends which occur during the initial stages of penetration and identify any which are worthy of further study. A comparison to the damage features observed in sections of ballistic indentations (Section **3.6**) will also be made where applicable.

4.8.2 Experimental

Sectioning was performed using an abrasive disk cutter and a water / oil coolant / lubricant to prevent burning of the material surface as well as to wash away abraded material.

4.8.3 Panels tested

Examples of all panels tested as part of the droptower trials (Section **4.7.3**) have been subjected to sectioning. Sections were cut from examples of each drop energy and of both indenter orientations.

4.8.4 Results

These sections showed clear evidence of internal damage geometry which bears resemblance to some of the damage seen in previous mechanical evaluation, especially compressive testing. The damage increases in size with impact energy as might be intuitively expected.

Sections of indentations by flat indenters suggest that when a plug is formed it posses a flattened conical / spherical cap shape which may affect the way in which it can be treated by any mathematical model.

Sections of indentations caused by an Ogival penetrator are as follows:

Image 4.11: Heavy Phenolic indentations(L-R; 50J, 75J, 100J)

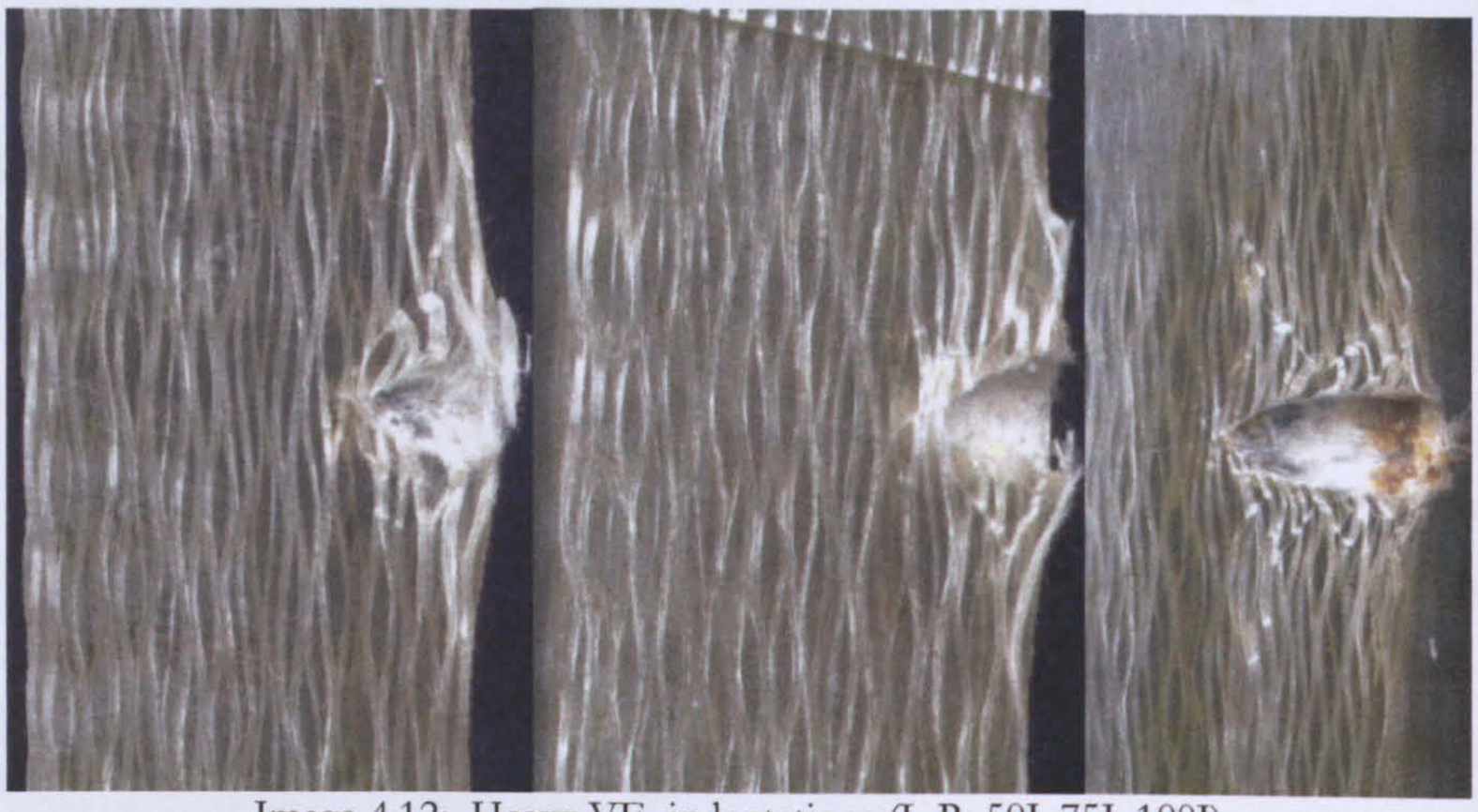

Image 4.12: Heavy VE indentations (L-R; 50J, 75J, 100J)

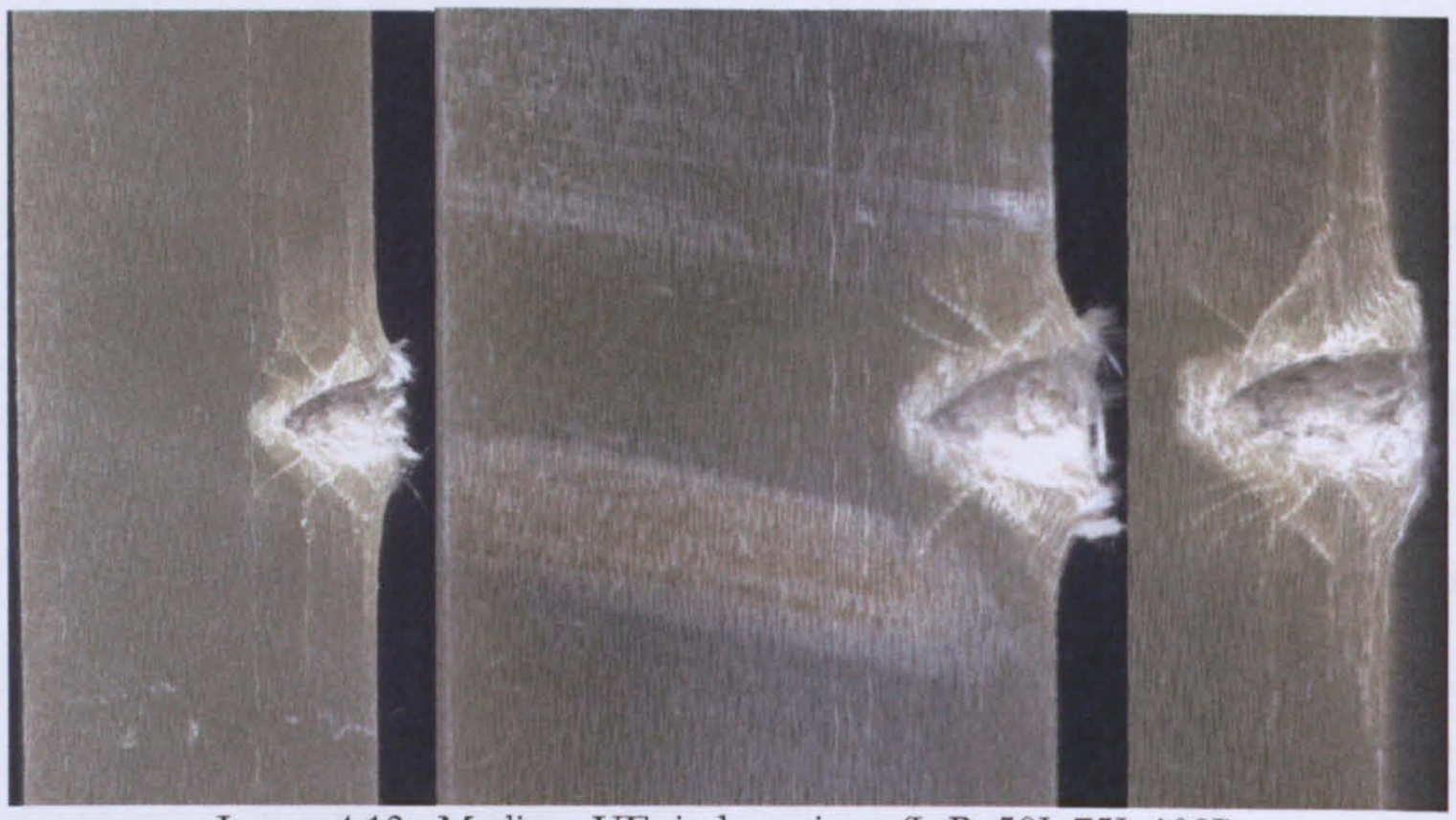

Image 4.13: Medium VE indentations (L-R; 50J, 75J, 100J)

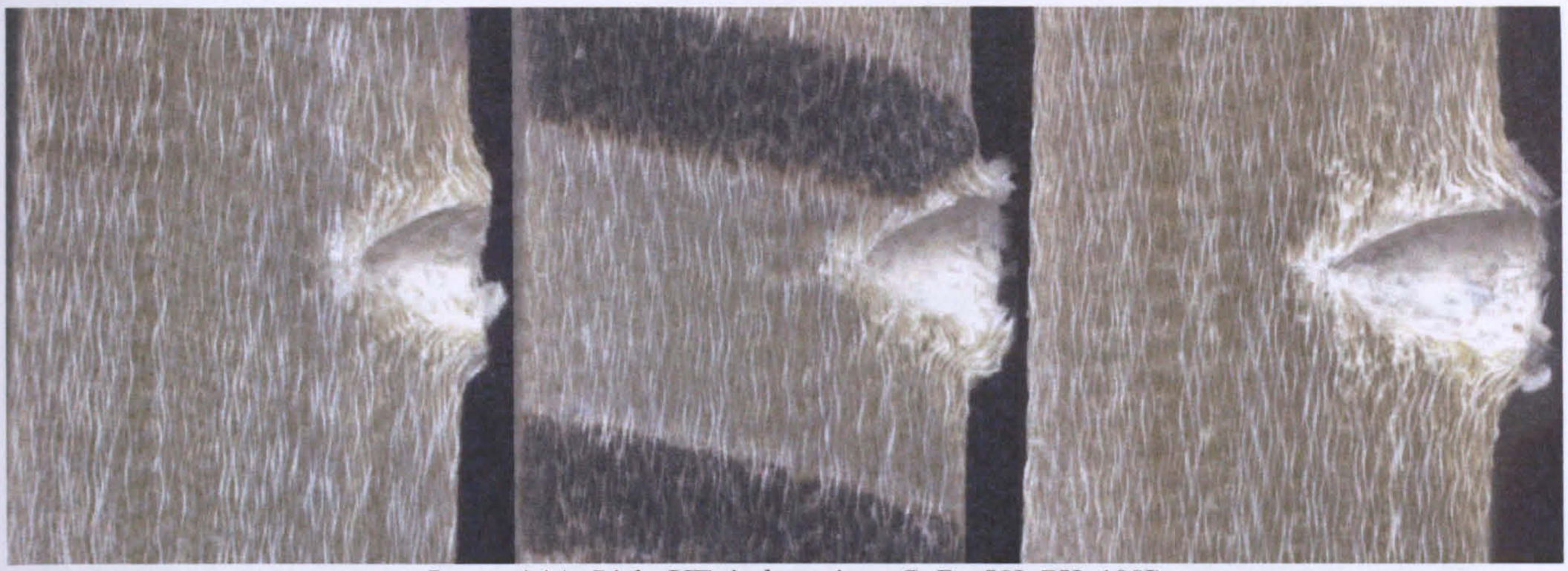

Image 4.14: Light VE indentations (L-Rt; 50J, 75J, 100J)

The sections of the indented material show clearly a difference in damage appearance between material types.

The heavy weave Phenolic material shows evidence of plastic deformation of material local to the indentaion and faint planes of buckling / shear damage extending at an angle from the indentaion both towards the front surface and into the depth of the material. Lower impact energies only seem to exhibit localised fibre deformation and failure.

The equivalent VE material seems to exhibit more plastic deformation local to the indention compared to the Phenolic the extent of this deformation area also appears less. The planes of buckled fibres observed in the 100J impacts against the Phenolic material are more visible and to a greater extent in this material however only in the 100J sections. The final shape of the indentation is far cleaner and crisper than the Phenolic material, almost a perfect impression of the indenter rather than a ragged hole.

The medium weave material appears to have far more visible buckling planes which appear to be due to radial motion of material away from the indentation. These damage planes extend both into the bulk of the material as well as up to the surface, upon reaching the surface these dislocations are manifested by a bulk up-thrust of material in far greater volumes than observed for the other materials tested. The local fibre deformation appears to be limited to a narrow band bordering the indention, the angular deflection of the fibres appears to be more severe than observed in other materials.

The lightest weave material tested because of its slightly coarser construction (due to its open weave, discussed in section **3.3.3**) seems to behave in a manner resembling the heavy weave materials, deformation of material (due to matrix plasticity) appears to take place over a wider area and there is limited evidence of buckling planes. The indentation is very crisp and clean, a feature which seems present in all Vinylester materials.

Radial movement of material away from the indentation site visible in all materials as angled planes of buckling damage, buckling / shear planes are visible travelling to the front surface as well as into the material. The medium weave VE material showed the most evidence of this kind of damage.

All materials show areas of displaced material which has caused buckling damage as the compressive buckling strength along the fibre axis has been exceeded. This process could be responsible for the onset of delamination damage following initial penetration and is most apparent in the medium weave material tested. The evidence of this radial loading during indentation suggests the compressive strength of the material with loading applied parallel to the laminate direction is of more importance than the compressive strength evaluated by loading perpendicular to the laminate surface. These sections also indicate that the coarser weave materials distribute plastic damage over a wider area than finer, lighter weaves.

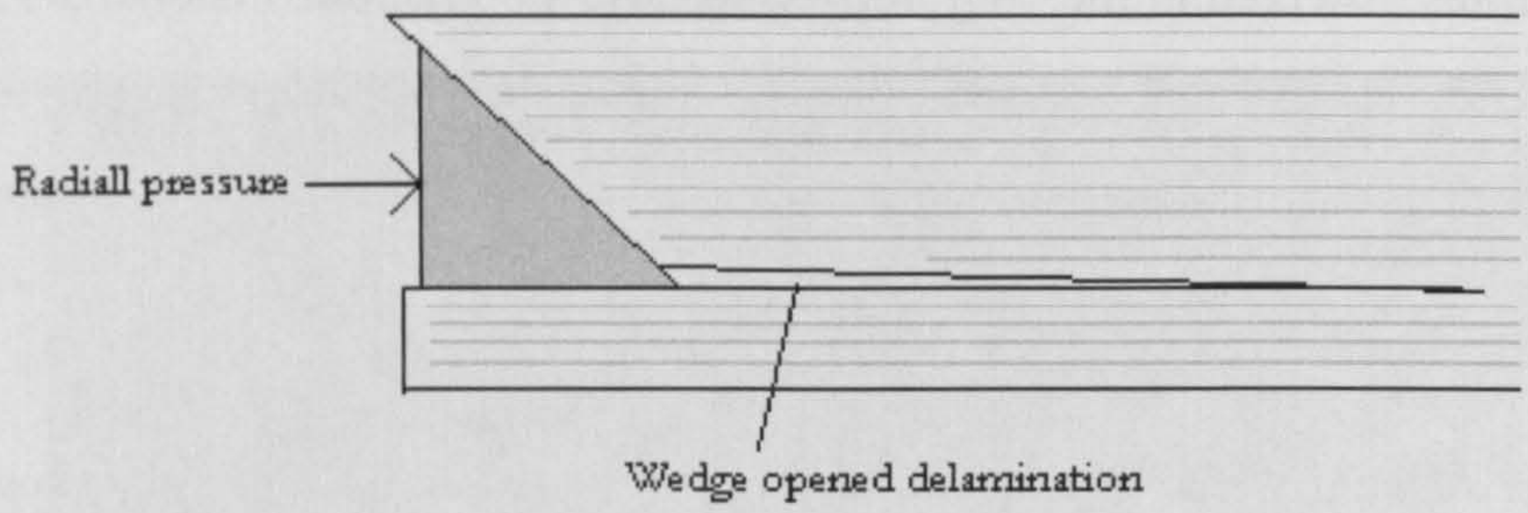

Figure 4.4: Wedge delamination

The amounts of plastic deformation visible in the materials is greater than anticipated, this suggests that upon initial penetration the 'stickiness' of the material may contribute to energy absorption from the indenter, thus the influence of friction between the indenter and the material is of interest, evaluating this for ballistic indentation rates could be difficult.

Testing with a flat indenter did not allow for an evaluation of energy absorbed per mm of penetration (over the depth of the indentation) to be fully evaluated as the indenter holder contacted the target before the indentation was complete.

However, it is possible to evaluate the energy required to separate a plug / break the surface of the material and also the energy to progress the indentation from the force displacement curves. The difference between these curves and those seen for indentation of the ogival indenter is clear to see from the following samples (Graph 4.26 & 4.27). The initial peak is due to the loading of the target surface to a point of maximum stress whereupon a plug is sheared from the material, load then reduces as the plug is compressed and driven through the remaining material. Penetration by ductile flow such as that seen by the ogival indenter results in an increasing load up to the point at which the penetrator is fully embedded within the material and begins to be arrested.

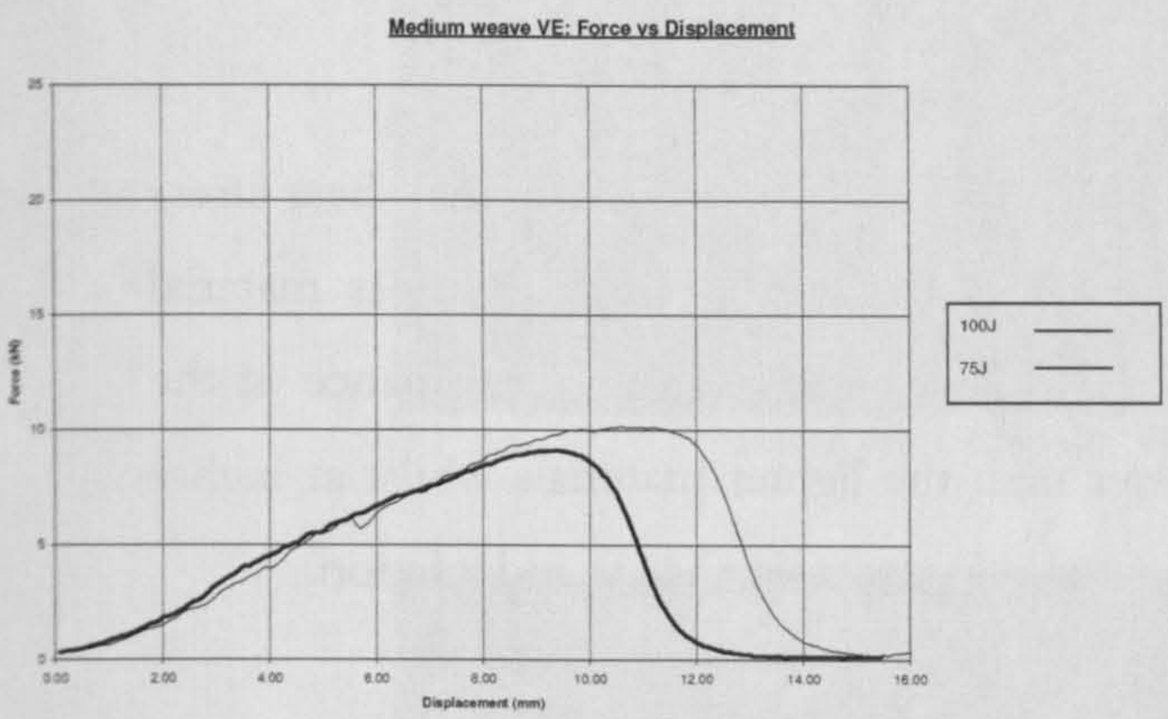

Graph 4.26: Typical Force/Displacement curves – Ogive

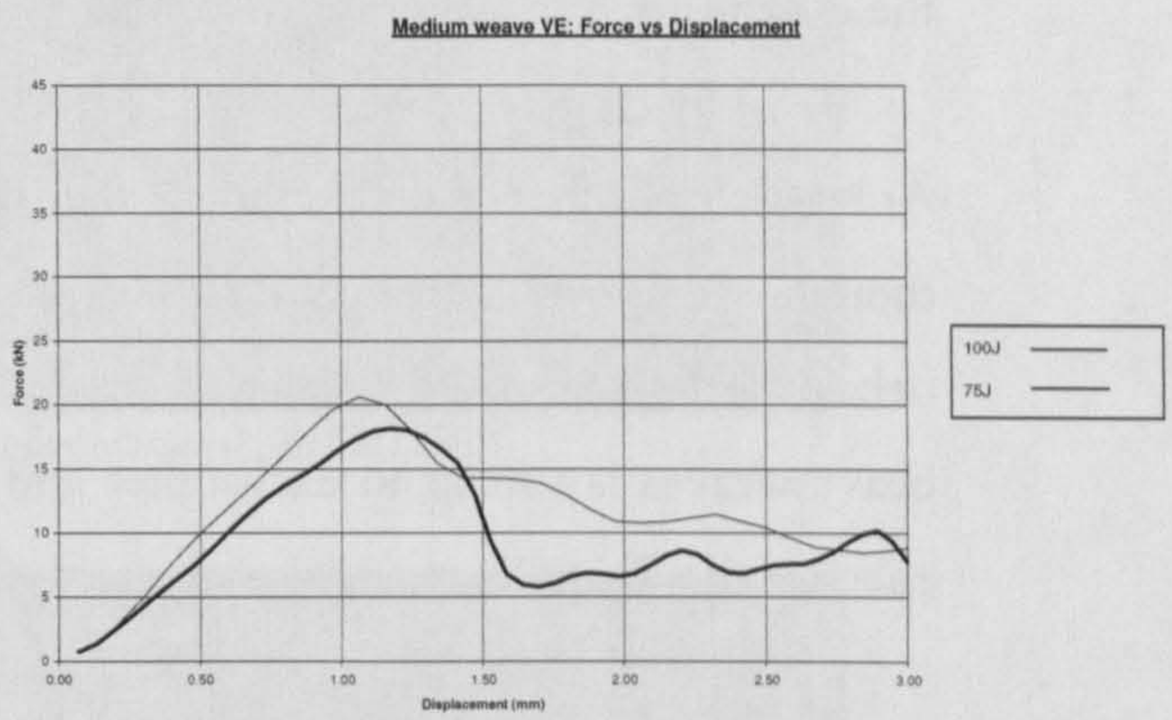

Graph 4.27: Typical Force/Displacement curves - Flat

The shear stress caused by the indenter was calculated using equation ***4.9*** this result was based on both the maximum force measured upon initial penetration as well as the sustained force value for continued penetration.

Shear Strength MPa	**Drop Energy** Peak		Continuation	
Material	**75J**	**150J**	**75J**	**150J**
S2 830 gsm Phenolic	741	811	342	376
S2 830 gsm VE	645	873	342	342
S2 300 gsm VE	651	729	274	342
S2 190 gsm VE	499	576	274	342

Table 4.6: Shear strength for initial penetration, and continuation

The results in Table 4.6 above show that at lower impact energies the Phenolic material has a far higher shear strength than the other materials. This confirms the findings from non penetrating indentation (Section **4.7**) using a ball indenter which found the Phenolic material to be 'harder' than the equivalent Vinylester material. Such a finding is unlikely to have an influence on hard indenters but the penetration of a deformable projectile (such as a fragment or a ball round) will be affected by this initial resistance to penetration.

As with the point first indentation there appears to be a distinct difference between heavier weave and the lighter weave materials. The heavy weave materials return the highest resistance force whilst the lighter weave materials perform less well. The medium weight material seems to perform better than it did against point first indentation, especially at low energy levels (see Graph 4.25). The performance gap between the heavy weave materials and the light weave materials diverge as the energy increases indicating that against blunt impact the coarser weaves will perform far better than the light weave materials.

At higher impact energies the heavy weave materials still resist the highest initial shear stress though the Phenolic material falls behind the VE. After the initial peak stress material behaviour is far closer between all panels tested, at lower energies the performance of the heavy weaves is similar to each other and better than the lighter materials whilst at higher energies the Phenolic material once again shows the greatest resistance to indentation.

The resulting indentations were sectioned to allow examination of the indentation and to search for evidence of the shear plug believed to exist. These sections are illustrated as follows:

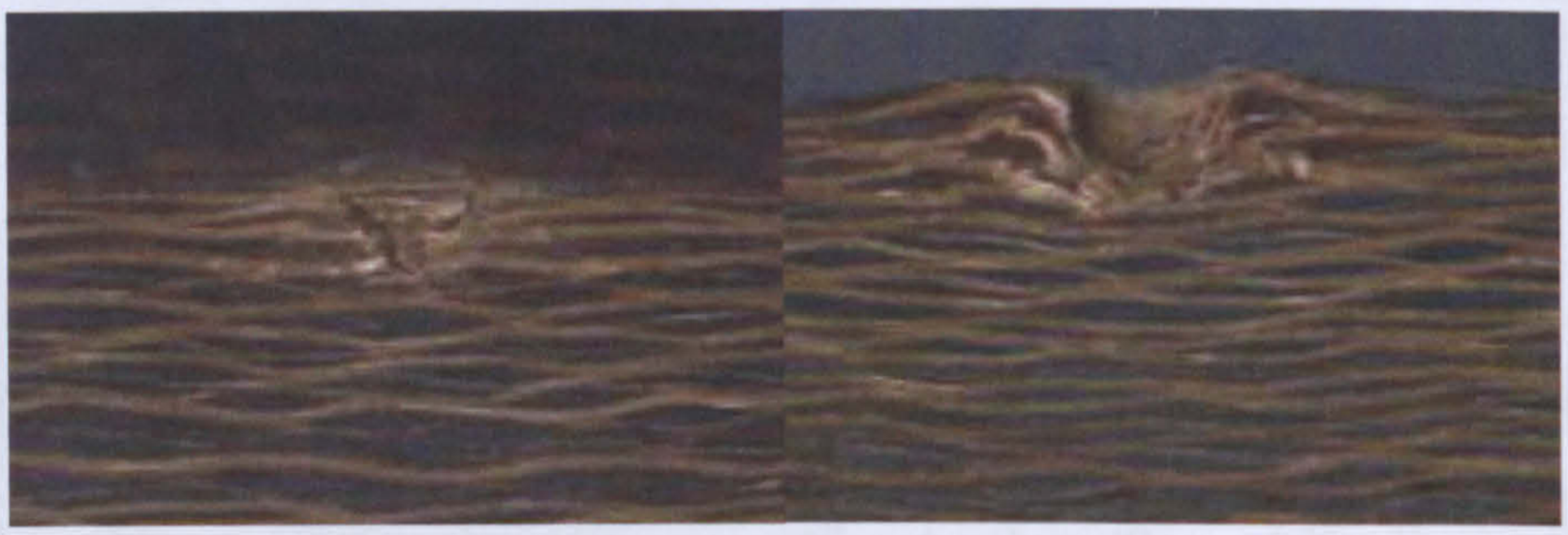

Image 4.15: Heavy Phenolic indentations(TL-TR; 75J, 150J, Bottom; Plug in 75J indentation)

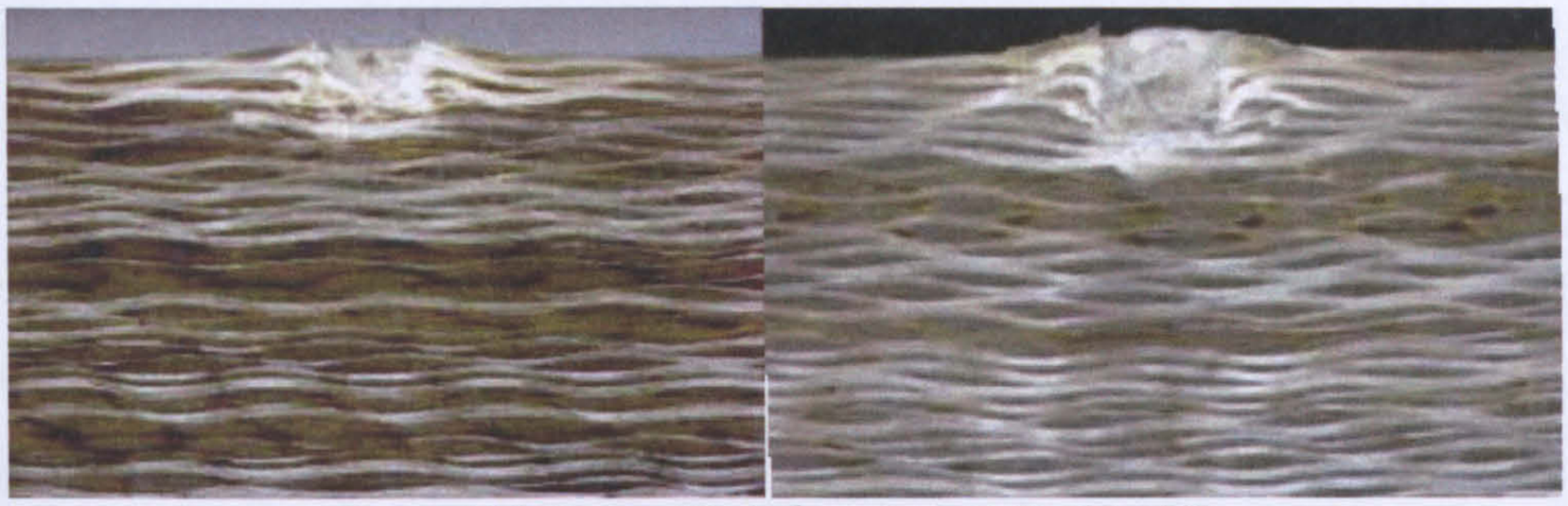

Image 4.16: Heavy VE indentations (L-R; 75J, 150J)

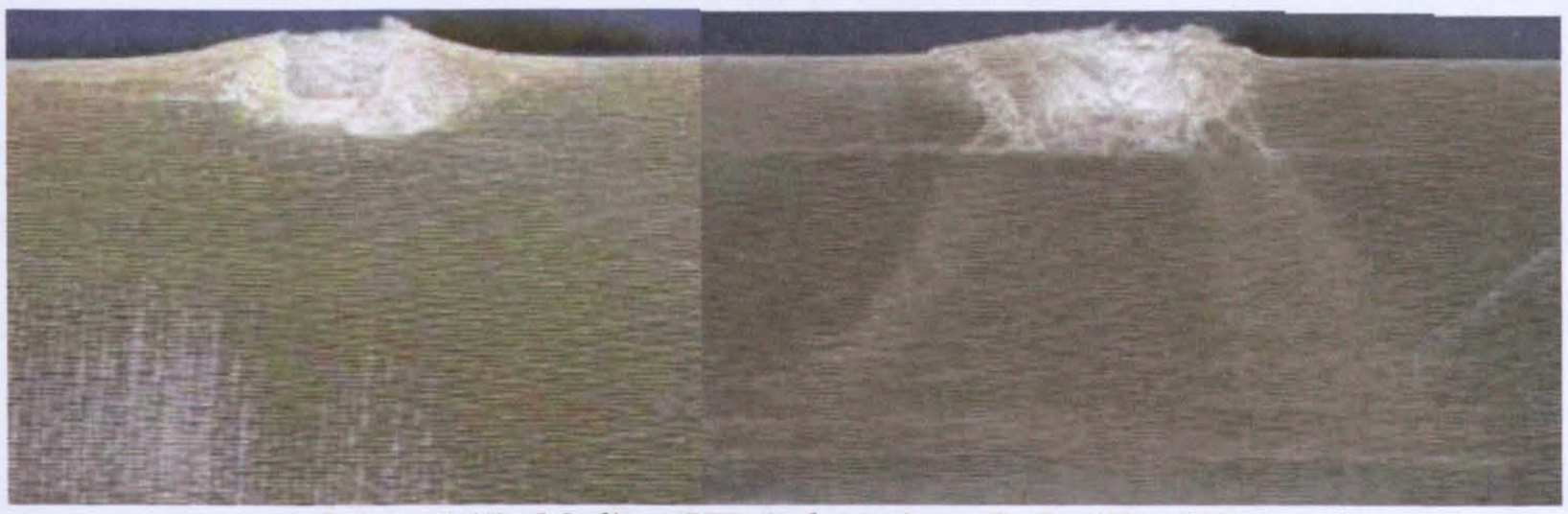

Image 4.17: Medium VE indentations (L-R; 75J, 150J)

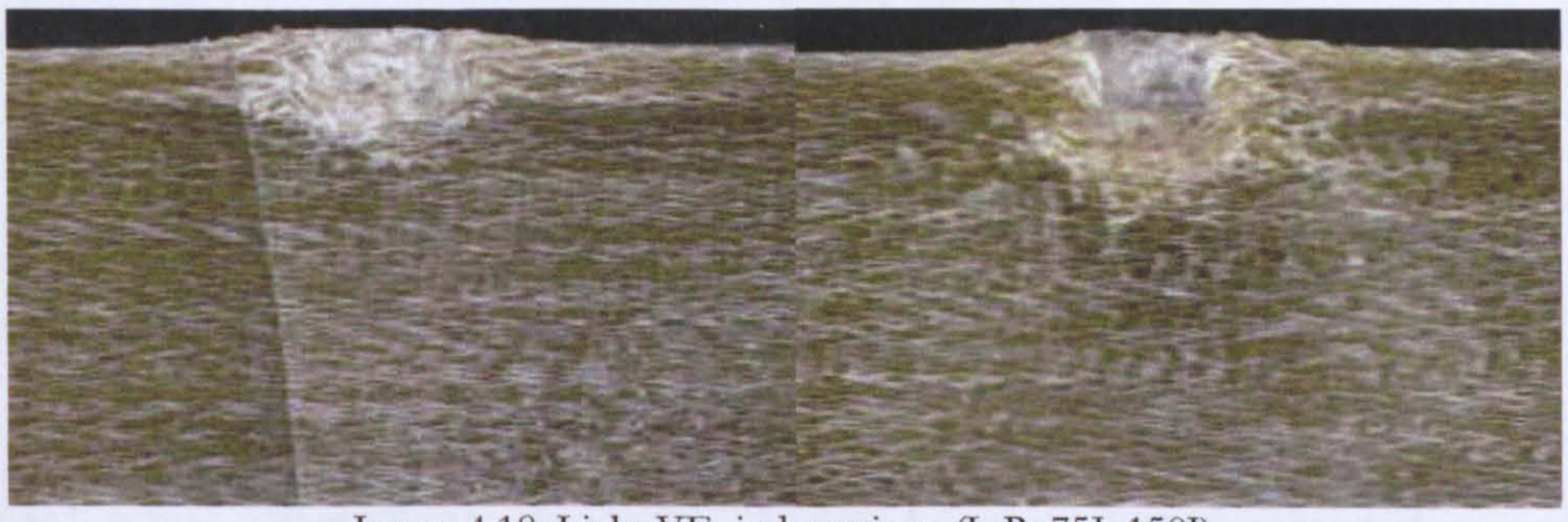

Image 4.18: Light VE indentations (L-R; 75J, 150J)

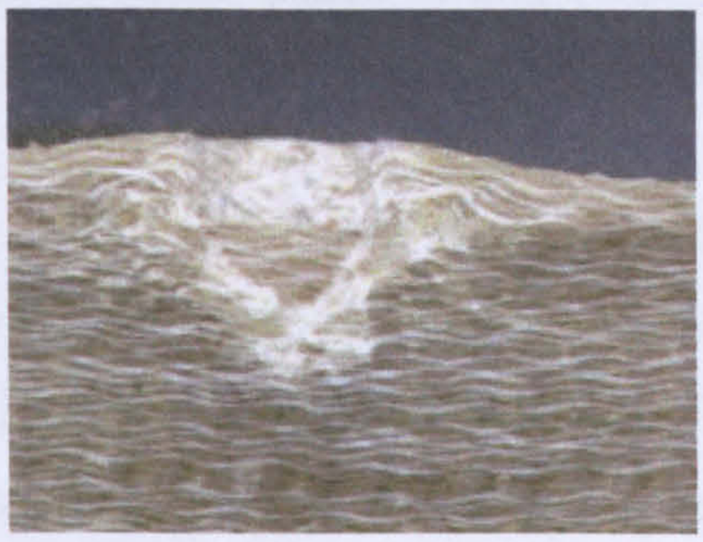

Image 4.19: Plug in light / medium VE

There is less variation visible between sections of material and the next for base first indentations than was observed for point first indentation. One important observation not shown by the indentations was that the impact had caused damage to the back surface of the material (visible from the rear surface) however whilst delamination damage was not visible to the naked eye sections of the higher impact energy showed permanent deformation of the panel by the force of the indentation. As a result it is expected that either a matrix cracking mechanism or partial delamination failure (which has not opened enough for a clear crack to be visible) is present.

Visible in the sections of the lighter weave materials (most visible in the medium weave VE; Image 4.17) is an angled shadow from the bottom corners of the indentation extending into the material, this bears resemblance to the shear planes observed in high speed video of compressive testing (Images 4.5).

4.9 Discussion of indentation testing

A considerable amount of indentation testing has been carried out. This testing has involved a number of different methods, the results of which require further discussion.

Testing with an ogival indenter gave the following results for indentation energy absorbed per mm of penetration:

Jmm^{-1}	Drop Energy			
Material	**50J**	**75J**	**100J**	**Ave**
Heavy Phenolic	7.1	7.9	11.7	8.9
Heavy VE	5.3	8.9	8.2	7.5
Medium VE		4.6	6.8	5.7
Light VE	3.7	4.6	5.3	4.5

Table 4.7: Impact energy per mm of penetration, for 3 drop energies (ogival penetrator)

The observation that the lighter weave materials suffered greater indentation depths which also increased faster relative to impact energy than those in heavy weave materials suggests the lighter weaves are a softer material. Indentation testing reviewed in section **4.7.1** supports this as the light weave materials appeared softer than the heavy weave Phenolic.

Indentation testing suggests that the use of a conical indenter can be used successfully to evaluate the resistance to indentation and successfully derive the yield strength along the laminate direction for fibre reinforced materials. The fact that yield strength perpendicular to the laminate direction is not predicted suggests that instead of compressive strength it is rather the resistance to axial displacement of the material that controls indentation.

Comparing this finding to the trends observed in compressive testing however shows better agreement with compression perpendicular to the laminate direction which ranks the materials in the same order as that of supported mean indentation pressure.

The results of dynamic indentation using flat and ogival indenters did not return the same material ranking trends as those seen in indentation testing. In an attempt to see if a similar trend of indentation pressure vs cone semi-angle existed the ogive was treated as a cone of 35.1 semi-angle and the flat indenter as a 90 semi-angle. Based on sections of indentation the plug was also treated as a conical indenter with a semi-angle of 80.

The force values for the indentation continuation rather than initial peak values were taken from the flat-faced, base-first indentations. The resulting curves looked as follows:

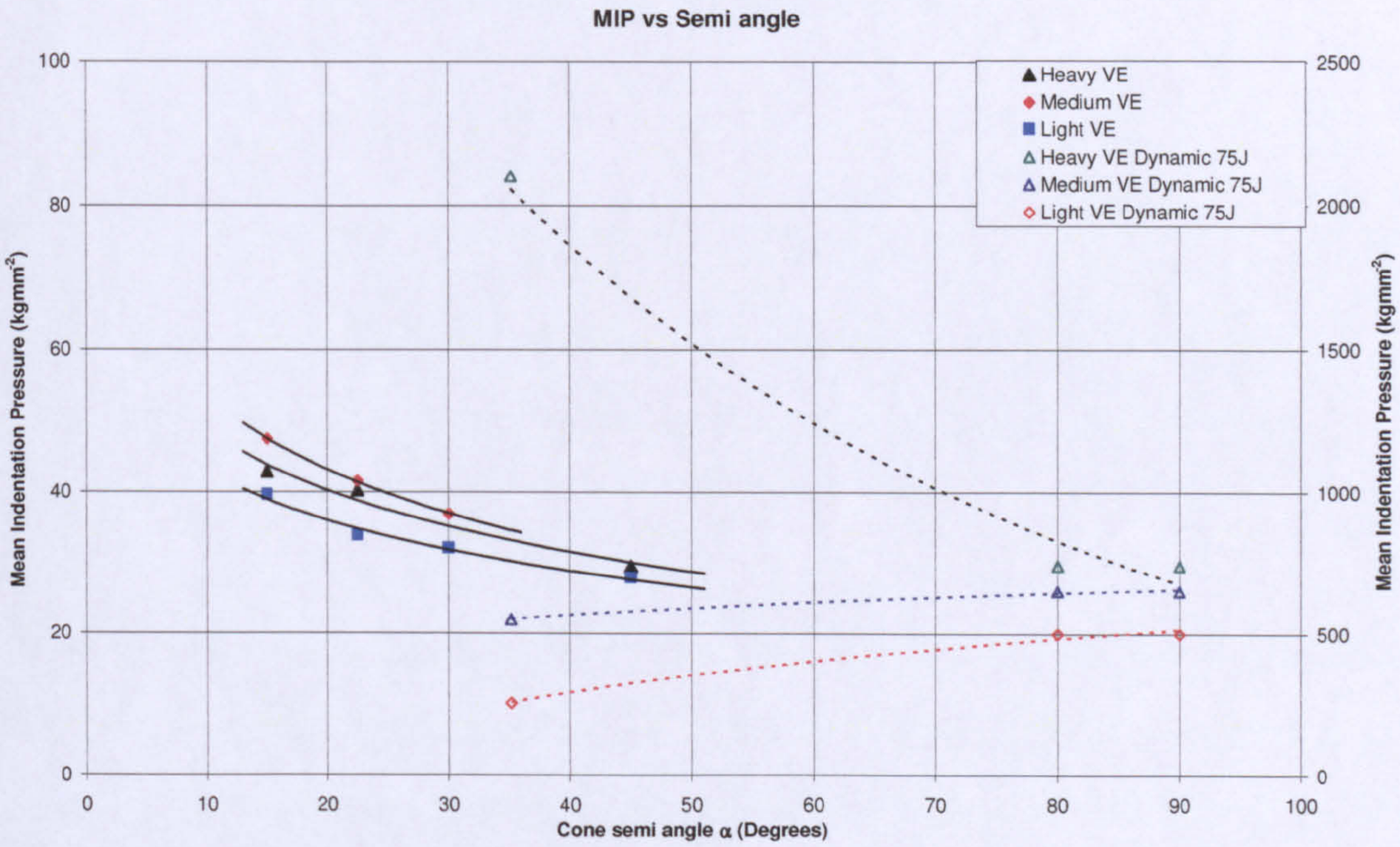

Graph 4.28: MIP calculated from droptower values (note Droptower values relate to RH axis)

The calculated yield strength and friction values are as follows, as can be seen these are far greater than quasi-static values as well as behaving in an un-expected manner:

	Results of curve Fit	
	μ	P_o (MPa)
Heavy VE Dry	1.17	7848.0
Medium VE Dry	-0.43	5591.7
Light VE Dry	-0.15	6180.3

Table 4.8: Yield strength and friction values from droptower testing.

The curves do not appear to follow the same basic trend of rising indentation pressure with decreasing cone angle. The resultant pressures and yield strengths calculated are far higher than those seen for quasi-static indentation however, it has already been discussed that the compressive behaviour of fibre reinforced plastics has been found to be highly rate sensitive. It is however suspected these are entirely incorrect as the μ values required to fit the measured data range from the highly unlikely to the utterly impossible.

-Page left intentionally blank-

CHAPTER 5:

EXPERIMENTAL INVESTIGATIONS;

REAR FACE PENETRATION MECHANISMS

This chapter will cover the experimental testing carried out to investigate physical mechanisms which occur at the rear face of a composite armour subjected to impact.

These tests have been carried out on the same set of materials initially supplied by VT Halmatic for ballistic testing (detailed in Chapter 3) and are identical to the materials evaluated in the preceding chapter. A range of different types of testing will be covered in the investigation of this material.

5.1 Overview

As discussed previously there are a number of mechanical properties which are of relevance to the rear surface performance of a composite armour undergoing ballistic impact, of interest to this work is mechanical stiffness of the composite material, inter-lamina fracture toughness and tensile strength. These will be discussed individually and tested

5.2 Rear surface properties

5.2.1 Toughness

When a projectile is caught in the rear face of a composite armour (especially a soft projectile) large amounts of delamination are often observed. This is a distinctly different defeat / failure mechanism than that seen on the front face. What is un-known is how much these delaminations contribute to absorbing impact energy; are numerous small delaminations better than fewer, larger delaminations? Relating the material toughness to ballistic performance is potentially very useful as it will enable the rear surface of an armour to be better optimised relative to the front face. A study by Laine and Vahakangas[59] has indicated that significant amounts of projectile kinetic energy is transferred to the delaminated plies during impact highlighting the importance of understanding failure in this part of an armour.

As well as outright ballistic performance damage tolerance is important for a future combat vehicle, it is likely that a composite armour will also be a load bearing component of a vehicle structure. A significant loss of strength as a result of a ballistic impact may cause the failure of an entire vehicle due to unacceptably low mechanical stiffness. As well as purely survivability concerns there is also in-service durability to consider. A tougher material will be more durable in service, as it will be more resilient to the rough handling of equipment often associated with military service.

The propagation of cracks between reinforcement lamina is one of the most common failure types seen in composite materials. The resistance of a material to the propagation of a crack is known as fracture toughness and is often ascribed the notation 'K_c' and describes the crack tip stress intensity ($MPam^{-2}$). The energy required to extend a crack through a material is known as the critical energy release rate and is notated 'G_c' and is notated (Jm^{-2}).

Fracture toughness can be evaluated in three separate ways; 'Mode I', 'Mode II' and 'Mode III'. Each one of these failure modes used to assess fracture toughness is based on a distinct

type of mechanical loading responsible for fracture. The types of loading responsible for fracture growth are as follows:

5.2.1.1 Mode I

This is a 'peeling' type of failure, two laminates are pulled apart by loading perpendicular to the plane of the reinforcement. This 'Y' shaped loading causes a crack to propagate away from the point of loading.

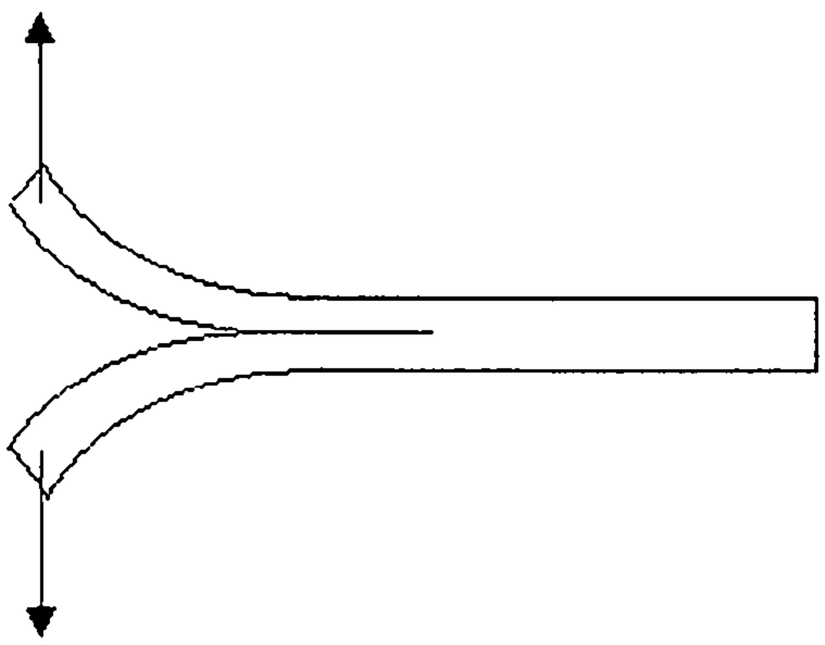

Figure 5.1: Mode I 'crack opening' fracture [60]

5.2.1.2 Mode II

This type of failure is due to shear forces. These shear forces are most often generated as a result of a bending moment being applied to the material which attempts to slide one lamina over another. A crack will grow along or close to the plane in which the shear loading is the greatest and usually propagates towards the point of maximum deflection. There is some debate regarding the validity of Mode II as a method due to the numerous problems encountered in its use and evaluation.

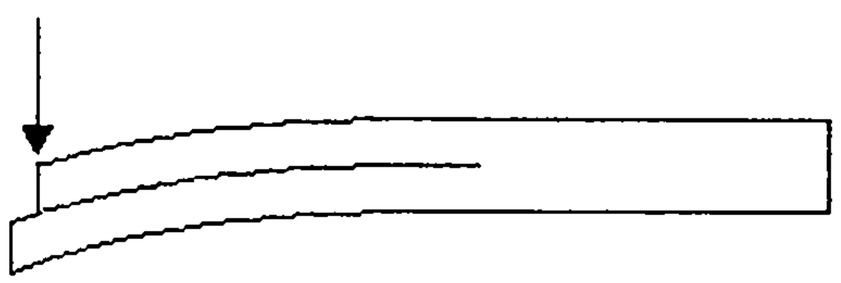

Figure 5.2: Mode II 'in plane shear' fracture [60]

5.2.1.3 Mode III

Mode III failure is caused by out of plane shear which causes a crack to progress into a laminate away from the point at which the load is applied. The areas of material separated by the fracture move sideways over and in opposing directions to each other. This is illustrated in the following diagram.

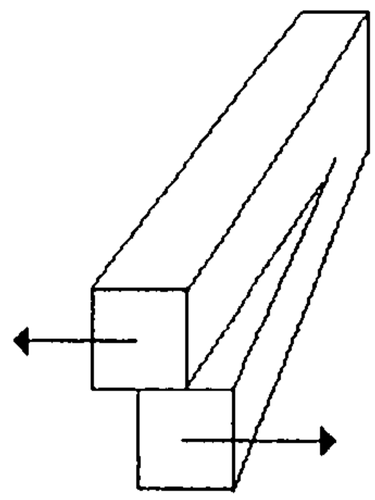

Figure 5.3 Mode III 'anti-plane shear' fracture [60]

5.2.1.4 Testing and evaluation

There has been a significant amount of work undertaken under the auspices of technical committee 'TC4' of the European Structural Integrity Society (ESIS) and other research groups (Including the International Standards Organisation - ISO) to develop test methods for Mode I and Mode II loading. So far the most significant progress has been made with Mode I loading and as such it shall be discussed here with a view to experimental work being carried out in this report.

Delamination damage from a ballistic impact is progressed by mostly mode I loading as one lamina is peeled from the other. Mode II loading may require consideration should the deflections of delaminated material be large. Mode II loading has been considered as the sole cause of loading by some authors [61][62], however as Mode I loading often results in the lowest G_c values of the loading methods discussed it will be considered as the results will err on the side of caution.

G_{Ic} (Mode I fracture energy) is measured through the use of a double cantilevered beam (DCB) test where loading is applied to the upper and lower surfaces of a beam, either side of a mid-plain crack. The propagation of the crack is measured as well as incremental force and beam end displacement values. The test specimens recommended by ISO standard 15024 are illustrated below.

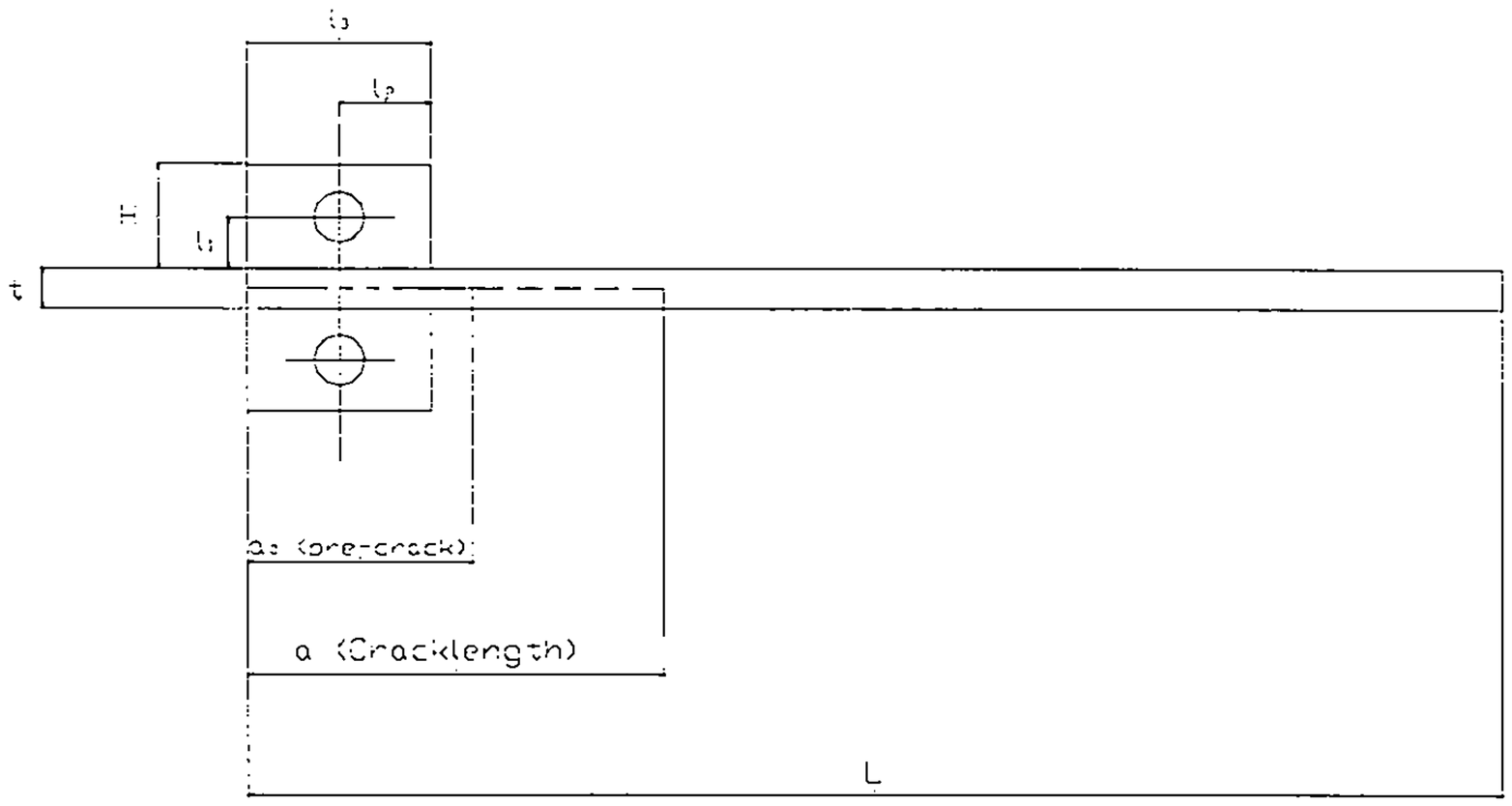

Figure 5.4: ISO 15024 DCB Specimen [63]

Data reduction allows a plot of delamination resistance against crack length to be plotted which typically increases before reaching a roughly constant value of G_c for long delamination lengths [63].

There are a number of methods for calculating G_{Ic}, ISO 15024 [39] supports the use of 'Corrected Beam Theory' (CBT) and the ESIS TC4 group have also had some success with an 'Experimental Compliance Method' (ECM).

CBT works by initially establishing the relationship between compliance and the crack length. Compliance is evaluated by dividing the displacement (δ) by the load required to produce such a displacement (F) as described below.

$$C = \frac{\delta}{F}$$

Equation 5.1: Compliance calculation

By plotting the cube root of the compliance against delamination length a y-axis intercept (Δ) can be recorded as shown below.

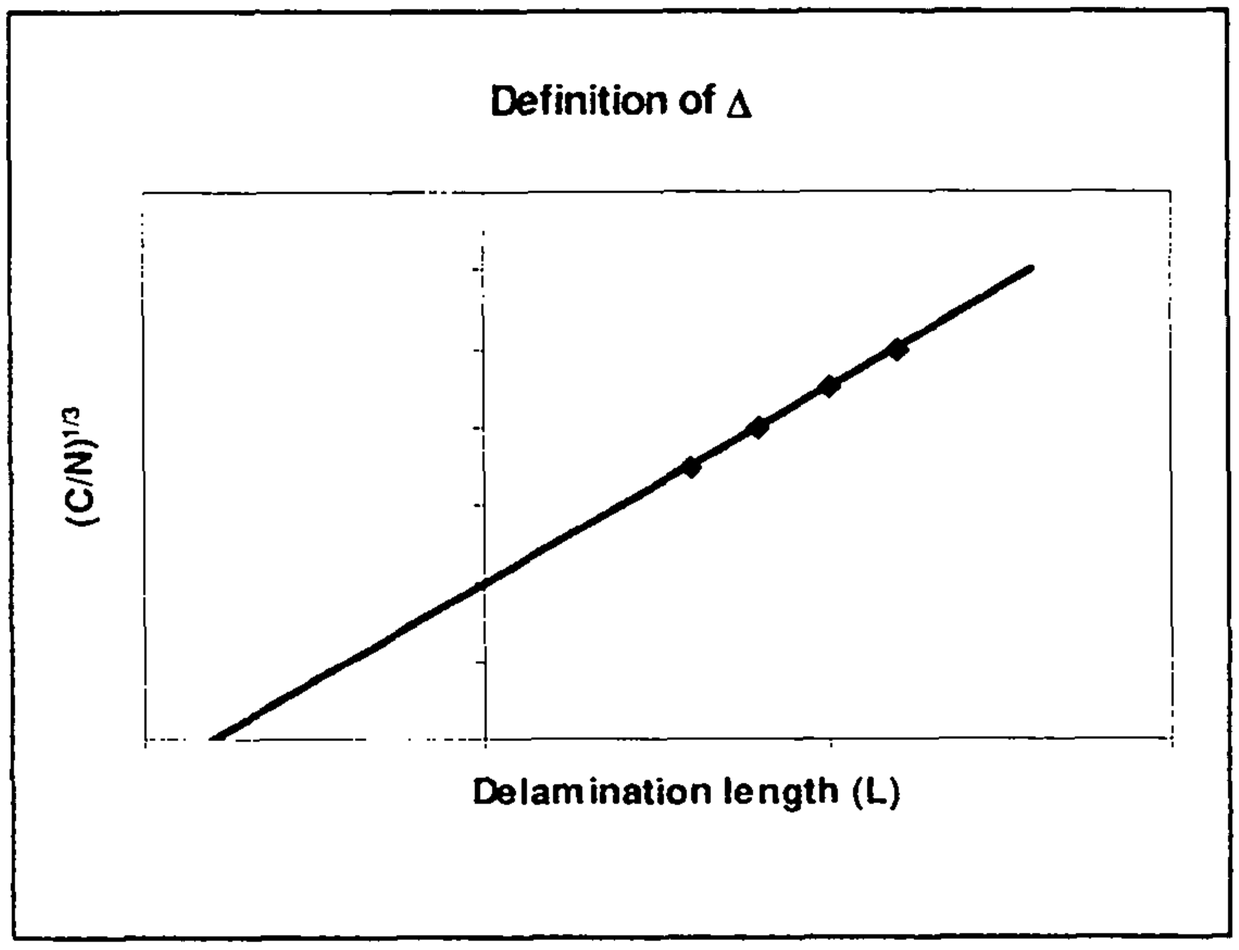

Graph 5.1 Definition of Δ [63],[64]

The mode I fracture toughness described as the critical energy release rate (G_{Ic}) is then described by the following equation and can thus be calculated for any crack length. For large displacements of the loaded ligaments a correction factor F is used as per ISO15024[63].

$$G_{Ic} = \frac{3F\delta}{2B(a+|\Delta|)Q}$$

Where: F = Applied load

δ = Displacement

B = Sample width

a = Crack length

Q = Large displacement correction

Δ = Y-axis intercept

Equation 5.2: Fracture toughness calculation

This method for determining fracture toughness is most suitable for unidirectional laminates, however some work has been carried out applying this method to so called 'Engineering Laminates' [65] with modest success, despite this these materials remain challenging to test.

The most common problem observed with these materials is that the crack can often skip from the central plane and begin to progress in neighbouring lamina. This invalidates the test as the total energy being used to propagate a crack is spread over at least three different sites. This phenomena is shown in the following diagram and image. Image 5.1 shows an initial

feasibility test where another crack has began several lamina away from the material neutral plane almost immediately after the initial crack has left the (short) insert and is now progressing through the sample in another lamina completely.

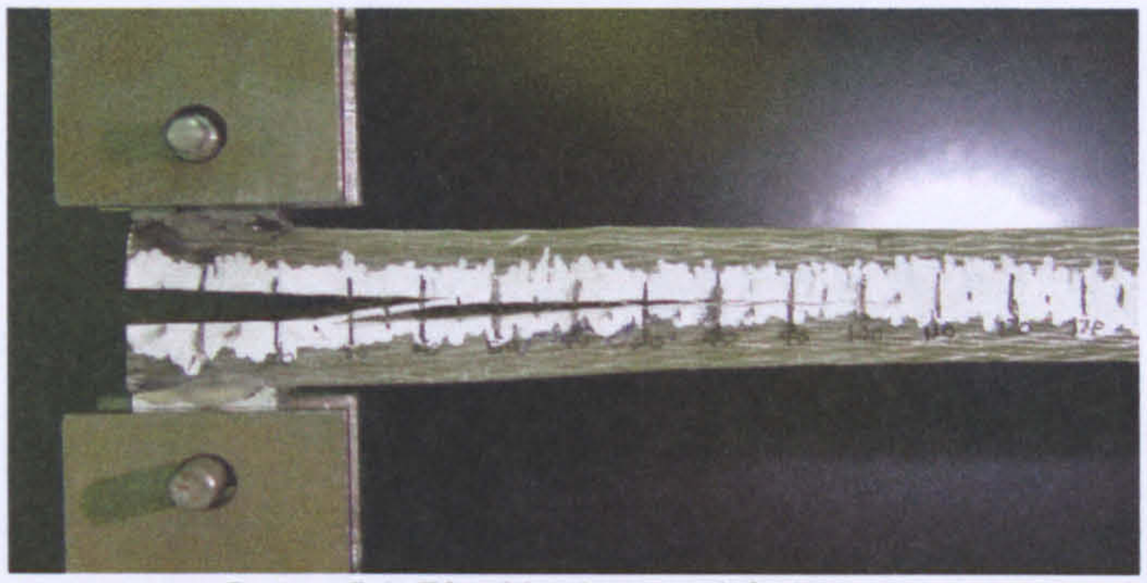

Image 5.1: Ply skipping invalidating test

5.2.2 Mechanical stiffness

Mechanical stiffness is of interest for structural as well as ballistic reasons, a stiff target will often have less impact resistance than a compliant target. As previously discussed however an impact event leads to delamination damage towards the rear face of the struck target. The stiffness of these delaminated layers is now of interest as the material is light enough to be motivated by the projectile in such a way that it may in fact contribute to the final arrest through their deformation. Stiffer materials will require more energy to deflect, however if a material is too stiff it may be perforated by means of another type of failure (such as tensile strength etc). Flexural strength is defined as the maximum stress in the outermost fibre. This is calculated at the surface of the specimen on the lower tensile loaded face

Mechanical stiffness is evaluated in terms of a flexural modulus, this material property is evaluated by a three point bend type test in the style of ASTM D790[66]. Flexural modulus is derived using the following standard formula which relates beam size, applied load, observed deflection and second moment of area.

$$E = \frac{L^3 m}{4bw^3}$$

Where:

E = Modulus (MPa)

L = Beam Span (mm)

w = Beam Width (mm)

d = Beam Depth (mm)

m = Slope of tangent to initial straight-line portion of σ/ε curve

Equation 5.3: Calculation of flexural modulus [66]

Flexural stress is at a maximum at the midpoint of the lower beam surface and can be calculated for any point during loading as thus:

$$\sigma = \frac{3FL}{2wd^2}$$

Where:

σ = Stress (MPa)

L = Beam Span (mm)

w = Beam Width (mm)

d = Beam Depth (mm)

F = Load (N)

Equation 5.4: Calculation of flexural stress [66]

Flexural strain is also evaluated for the lower beam surface and can be calculated for any point during loading as thus:

$$\varepsilon = \frac{6D_f d}{L^2}$$

Where:

ε = Strain (mm/mm)

D_f = Deflection of lower surface of beam (mm)

d = Beam Depth (mm)

L = Beam Span (mm)

Equation 5.5: Calculation of flexural strain [66]

The ASTM standard sets out specimen geometry requirements, however, when dealing with thick engineering composites it is not always possible to satisfy the requirements. Some deviation from these geometry requirements is possible however care must be taken that the failure remains in a form which can be analysed by the standard equations.

For ASTM D790:

Parameter	**Value**
Thickness (d)	1mm - 10mm
Width (w)	15mm or 30mm
Supported Length (L) / Thickness (d) ratio	L/d: 15 – 17

Table 5.1: ASTM D790 geometry

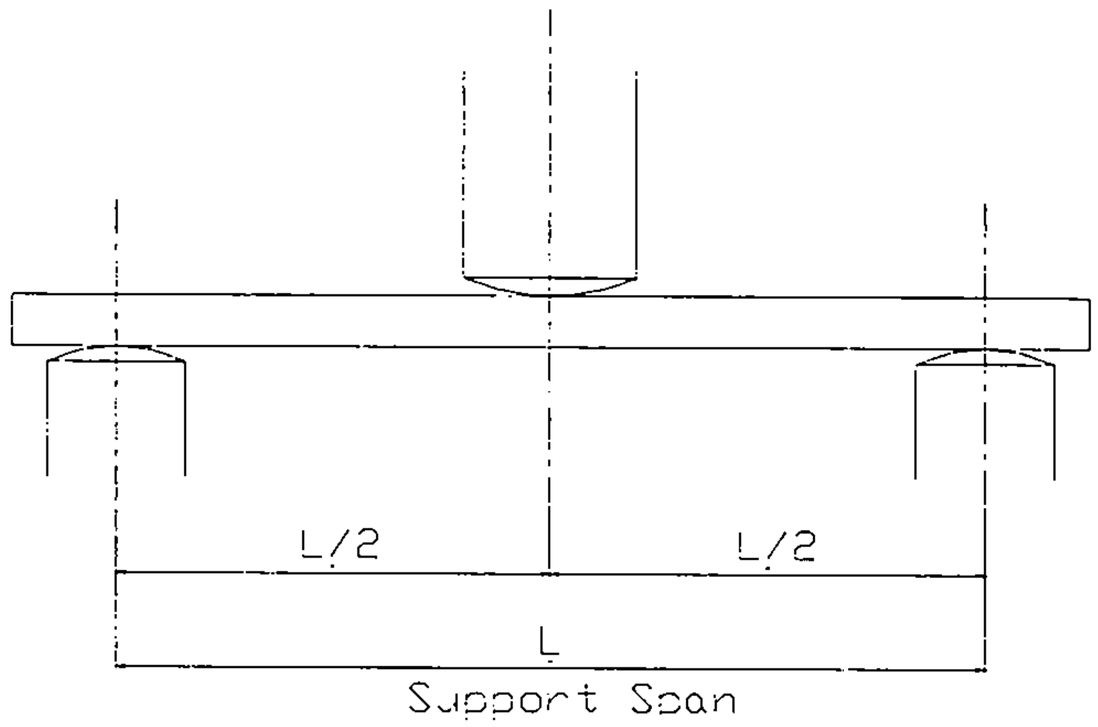

Figure 5.5: ASTM D790 3 point bend

The energy required to bend an a delaminated element of a composite target has been dealt with by Jones and Slater [61] who defined the flexural rigidity of the delaminated material as per the following equation:

$$D = \frac{E \times t^3}{12\left(1 - \upsilon^2\right)}$$

Where:

D = Flexural rigidity (J)

E = Modulus (GPa)

t = Thickness (m)

υ = Poissons ratio

Equation 5.6: Flexural rigidity of delaminated material [61]

This value is then used as follows to calculate the required bending energy:

$$U_b = \frac{55.9\pi D\varpi^2}{\alpha^2}$$

Where:

U_b = Bending energy (J)

D = Flexural rigidity (J)

ω = Depth of deformation (m)

α = Radius of bending zone (m)

Equation 5.7: Bending energy[61]

5.2.3 Tensile strength

As well as the indentation resistance and fracture toughness discussed in previous chapters the tensile behaviour of the composite is also important, especially so on the rear face of the armour. It is this face which often deforms due to impact and as a result owes much of its strength to the tensile strength of the fibres.

When a delaminated area of material deflects under loading the reinforcement fibres are stressed in tension. Whilst a sharp indenter will be more inclined to cut through fibre bundles by parting the fibres, a blunted projectile or fragment will not. This means that the failure of each reinforcement ply is dependent on its tensile strength. Laine and Vahakangas[59] have calculated that during fragment loading of fabric armour the force applied to the projectile is roughly half of the force required to break the fibres under pure tension, the weave geometry is likely however to affect this due to non-straightness of fibres and crimping effects.

The strain behaviour of the fibres is also of interest. As a cone of damage and deformation is forced away from the back of the armour panel the tensile loaded fibres will stretch. This strain will reduce as the damage cone increases in size and allows more material deformation.

Edwards [14] commented that the main deceleration of a projectile occurs when the fibres are moved in the direction of the projectile, it follows from this that tensile strength of the fibre is then of importance.

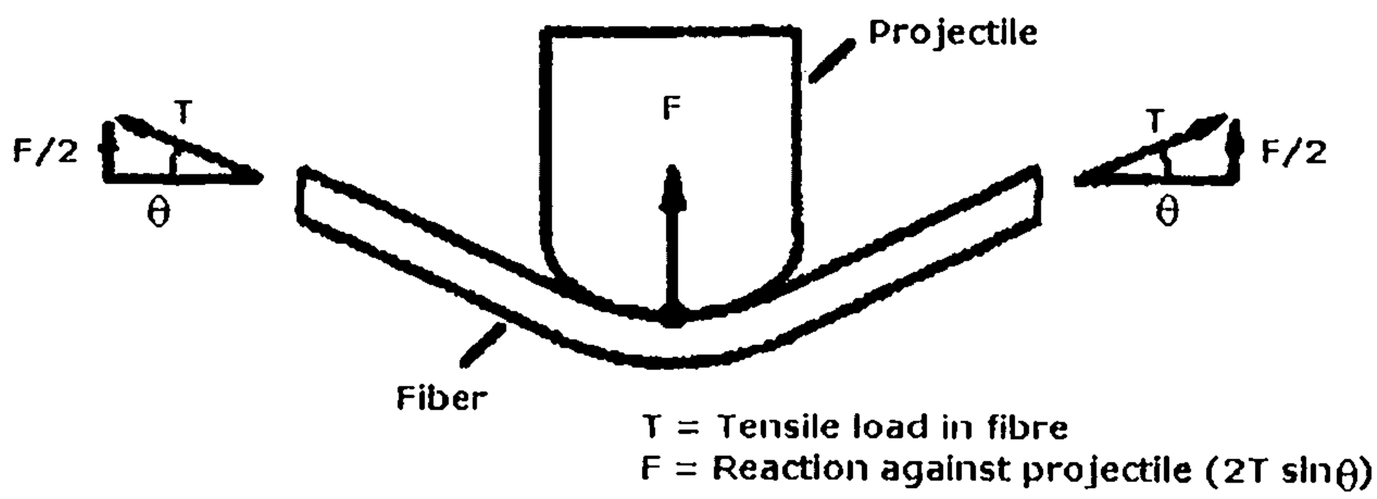

Figure 5.6: Fibre loading due to projectile impact (after Edwards [14])

Edwards was making his observations with regards to fabric armours however it is believed that the principle applies to laminated composite materials.

Tensile strength data for most reinforcement fibres is readily available and is usually in the range of 4.89 GPa for ideal S2 glass fibres (Though the respective strand strengths are usually 20-30% lower than this for real world fibres [50]). When woven into a laminate however the crimping effect of warp fibres overlapping weft fibres affects the laminates strength. Similarly whilst the tensile properties of the matrix material may be known the performance of the same material as part of a laminate complete with air pockets or resin rich areas is harder to evaluate.

Tensile testing is required to evaluate this however, tests of this type are hard to do on engineering composites of the thickness used for armour due to the physical size of the specimens.

Where possible tensile tests are simple to evaluate, the stress in the loaded material being described by the following standard equation:

$$\sigma = \frac{F}{A_x}$$

Where:

σ = Stress (Pa)

F = Applied load (N)

A_x = Cross-sectional area of specimen (mm^2)

Equation 5.8: Stress in a tensile loaded specimen

This only gives data for the material as a whole, it is important to note however that the internal stresses within the material may be locally far higher due to the woven nature of the reinforcement fibres and their associated crimping, resin rich pockets and voids.

5.3 Aims of mechanical testing

The purpose of the testing carried out in this chapter is to evaluate the mechanical properties of armour materials which are likely to contribute to the arrest of a projectile in the rear surface of a composite material.

Tests will be carried out to evaluate:

1. Mechanical stiffness
2. Mode I fracture toughness at a quasi-static rate
3. Mode I fracture toughness at dynamic rates
4. Tensile strength of laminates

5.4 Experimental Facilities

The experimental facilities of the Engineering Systems Department of Cranfield Universities Shrivenham campus (DCMT) were utilised for this work. Mechanical testing was carried out on a range of instrumented Zwick and Instron tensile/compression machines with a high load capability as well as the Imatek droptower facility in the Bashforth Laboratories.

5.5 Material available for testing

The experimental work will be carried out on the same thick, structural composite panels evaluated previously for ballistic and front surface testing and described in section **3.3.3**.

5.6 Mode I fracture toughness testing

5.6.1 Aims

Two types of testing are required, one with a quasi-static loading rate and one with a dynamic loading rate. The reason for this is that a dynamic loading rate is more representative of the conditions likely to be seen during an impact. It is however far harder to perform these tests due to the equipment and methods required. By performing both types of tests the data is cross checked for accuracy as well as determining if any degree of rate sensitivity exists.

5.6.2 Experimental

Mode I testing has been chosen to determine the material toughness, a Double Cantilevered Beam (DCB) Mode I fracture specimen was used with an adapted ESIS test method[64]. Tests were carried out at both quasi-static and dynamic loading rates.

All samples for both test types were manufactured with a PTFE film insert at the material mid-plane. Samples were then pre-cracked from this insert for both quasi-Static and dynamic testing.

5.6.2.1 Quasi-static Mode I DCB

As previously discussed the ISO standard 15024 covers the Mode I testing of composite materials. This standard is limited however to uni-directionally reinforced materials and does not cover the sizes of engineering composites available for this testing. The geometry of the standard test will be scaled as far as possible and observations of bulk effects / crack skipping taken to ensure testing is as close to a recognised form as possible. The thickness of the material available for testing will ultimately define specimen size

Testing was carried out on a Zwick Tension / Compression machine, force and deflection values are recorded by the machine and crack length is measured visually. This is done by the observation of crack progression through white correction fluid applied to each side of the specimen with marked graduations every 5mm to an accuracy of 0.5mm. The load and displacement values are recorded as the crack reaches every graduation, additional measurements between graduations were carried out through the addition of a 1mm graduated scale held against the specimen during the test.

This test is Quasi-static therefore has to be carried out at a slow a rate as practically possible, for this reason a crosshead displacement rate of 1mm/min was chosen. This allows a very slow crack propagation for accurate crack length measurements.

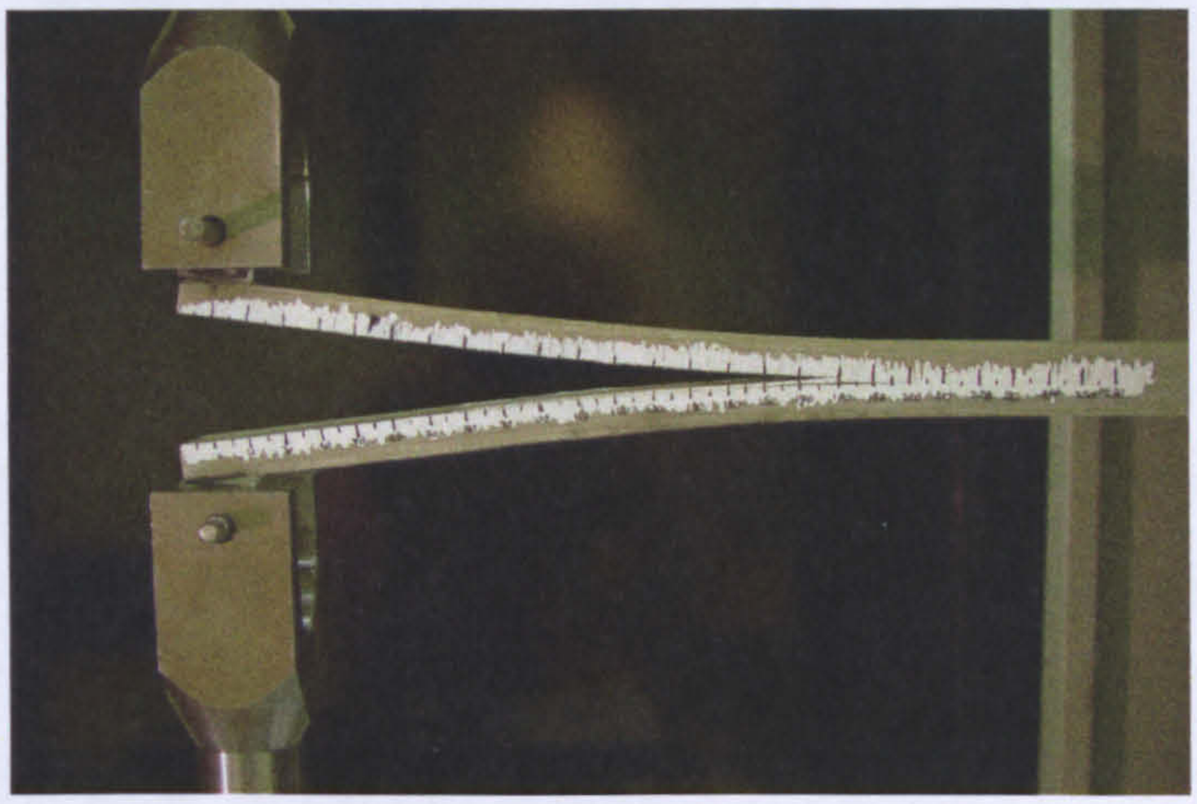

Image 5.2: Q/S mode I test (note ply skip)

5.6.2.2 Dynamic Mode I DCB

A bespoke rig designed for conducting dynamic mode I DCB tests in a droptower was designed and constructed. This rig consisted of a three sided, square tower (as illustrated in Image 5.4-6) made from 10mm thick steel plate, this thickness was chosen to ensure stiffness of the rig as well as being an easily available material size.

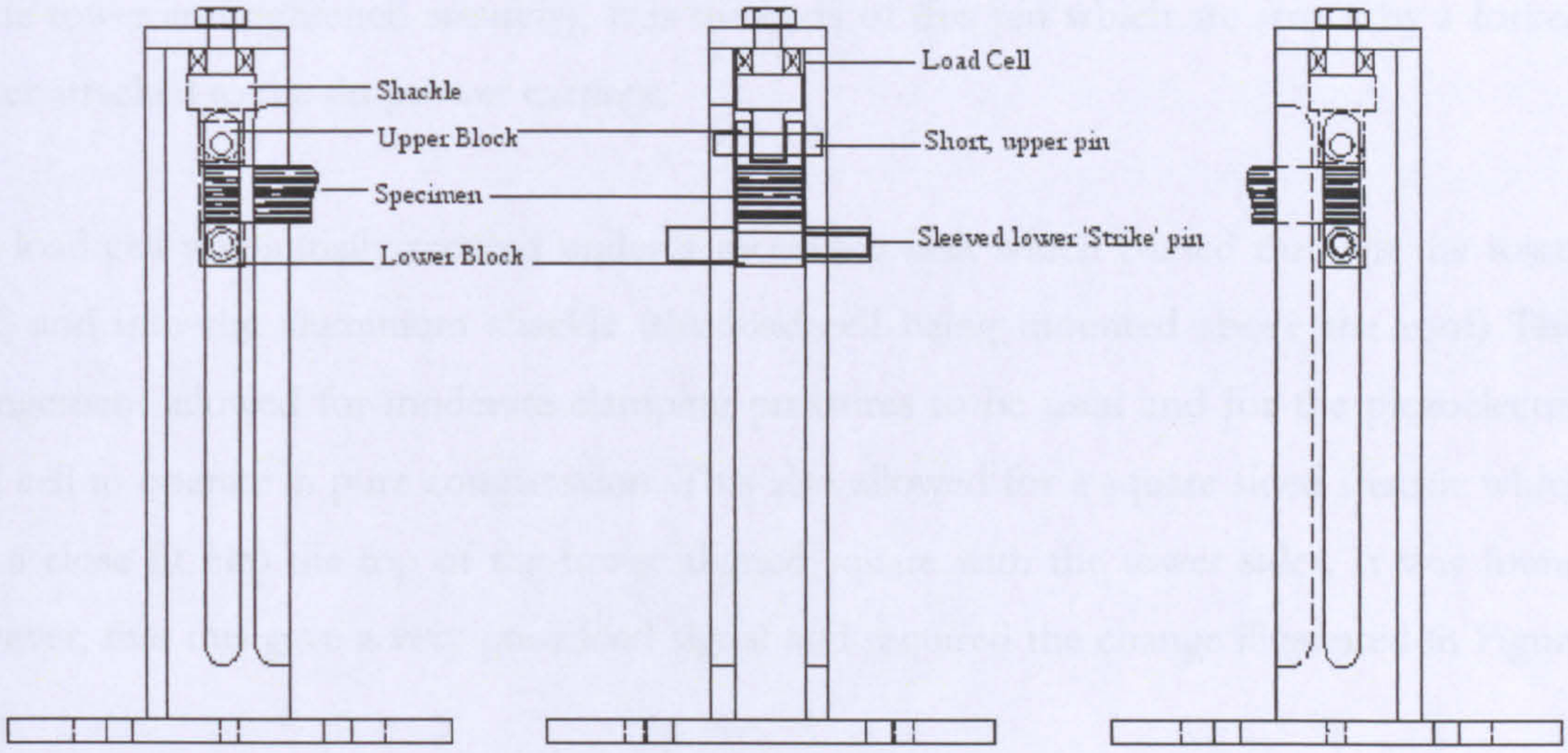

Figure 5.7: Dynamic rig schematic

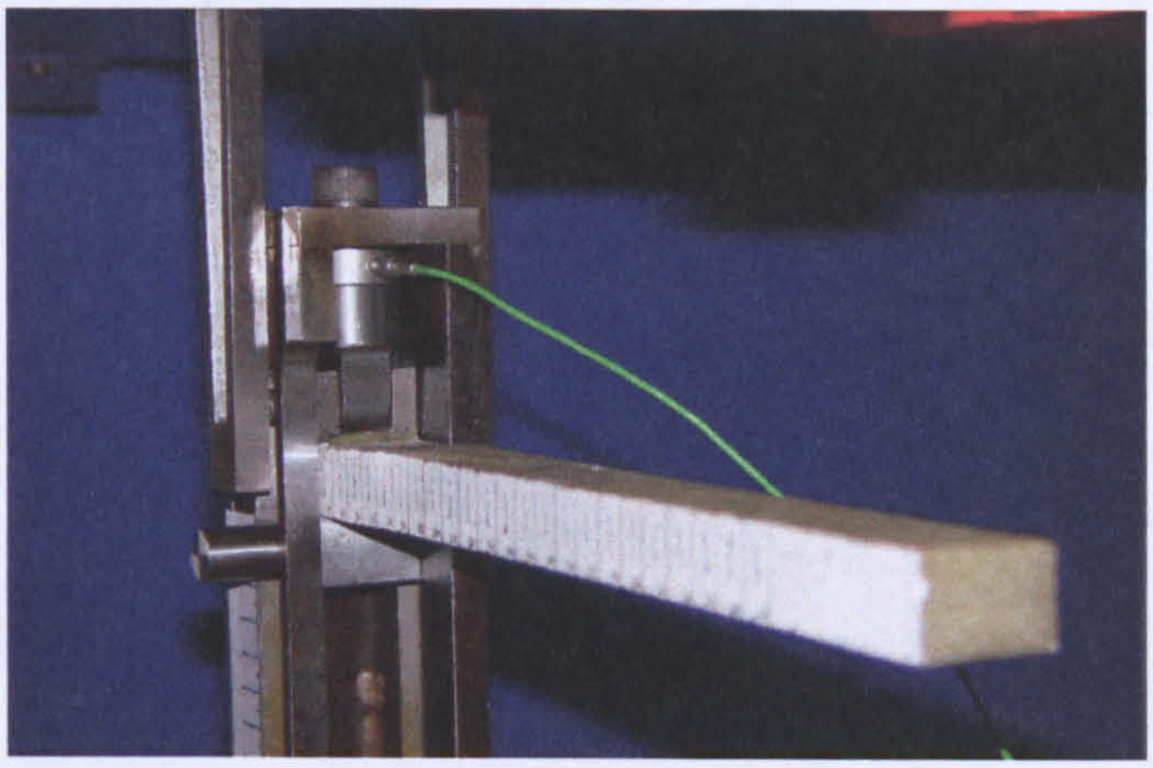

Image 5.3: Mode I sample in dynamic rig with forks visible (second rig version, note loadcell location)

A mild steel shackle sits under the roof and is the upper point of attachment for the DCB specimen, this is the weakest part of the rig (limited to 700 N load with approximately a 15% safety factor to ensure no deformation of the shackle) but is easily replaced with stronger material if required. The specimen projects through the open fourth side of the square tower and is attached to the shackle via a slotted steel load block (adhesively bonded to sample)

and a 10mm steel pin. A second pin is inserted through grooves machined in the sidewalls of the tower into the lower (aluminium) load block (This is clear in Figures 5.7 & 5.8)

This lower loading pin projects from the load block and through the sidewalls of the tower (The load pin is a two part assembly consisting of a stepped pin inserted through one tower side wall and load block from and a sleeve screwed over the stepped pin from the other side of the tower and tightened securely). It is the ends of this pin which are struck by a forked striker attached to the droptower carriage.

The load cell was initially secured under a mounting bolt which passed through the tower roof, and into the aluminium shackle (the load cell being mounted above the roof) This arrangement allowed for moderate clamping pressures to be used and for the piezoelectric load cell to operate in pure compression. This also allowed for a square sided shackle which was a close fit into the top of the tower aligned square with the tower sides. It was found however, that this gave a very poor load signal and required the change illustrated in Figure 5.8.

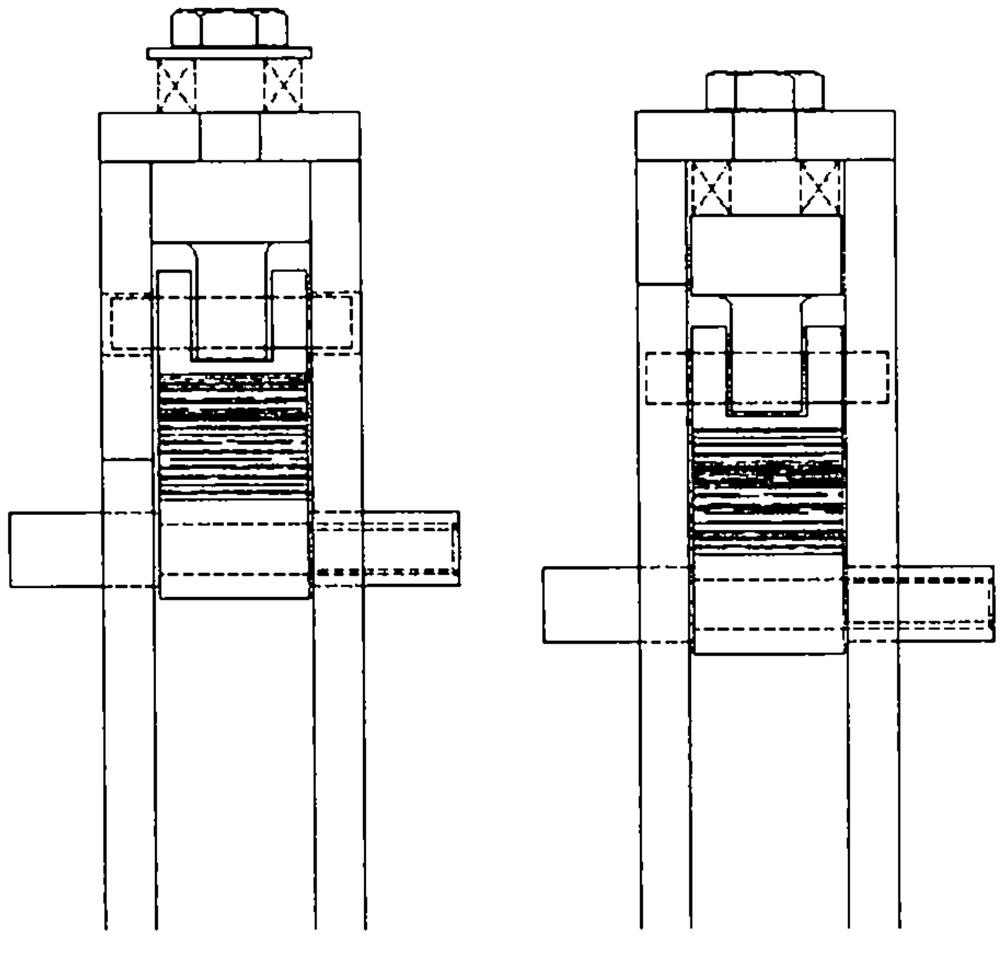

Figure 5.8: Changes to load cell location (L-R; Version 1, Version 2)

Placing the load cell below the roof, clamped above the shackle greatly improved the force signal. This arrangement required a significant clamping torque to be applied so that to pre-load the cell such that test loading actually removed compressive load but not so much to remove load completely. It was also necessary to modify the shackle, this however removed

the built in positive location and alignment, as such great care was required in rig assembly to ensure all components were square.

The striker assembly consists of a guided drop carriage to which the striker forks are attached. This carriage has the provision for considerable amounts additional weight to allow sufficient kinetic energy to be transferred into the sample to fail it at very low velocities.

The striker itself consists of a steel base to which are welded a pair of slender steel arms supported by steel gussets. When released the striker falls with the striker arms passing either side of the tower until they simultaneously strike either end of the lower pin and thus loading the sample. The striker arms are machined for reduced weight so that high strike velocities can be achieved if desired.

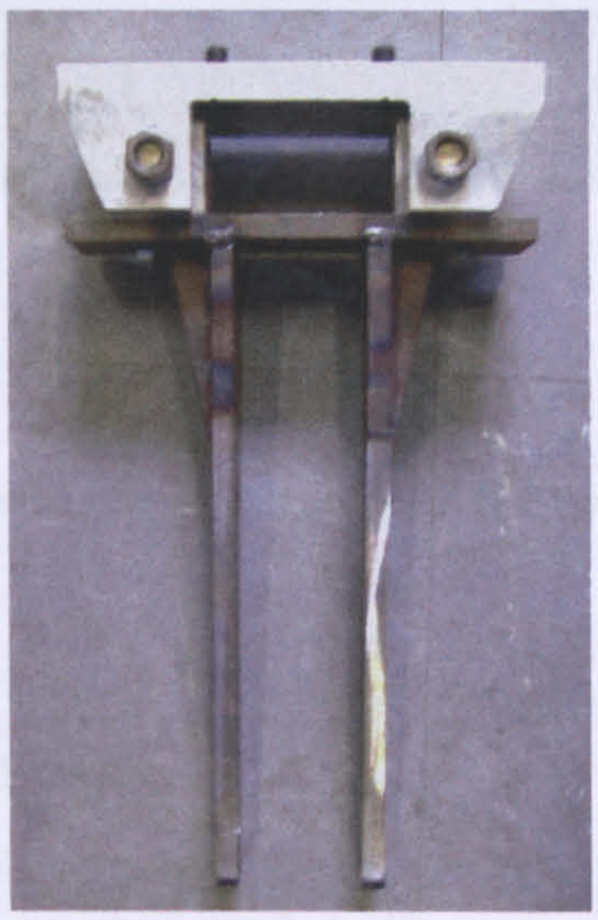

Image 5.4: Droptower striker forks, these attach to the drop carriage via four bolts (visible at top of image)

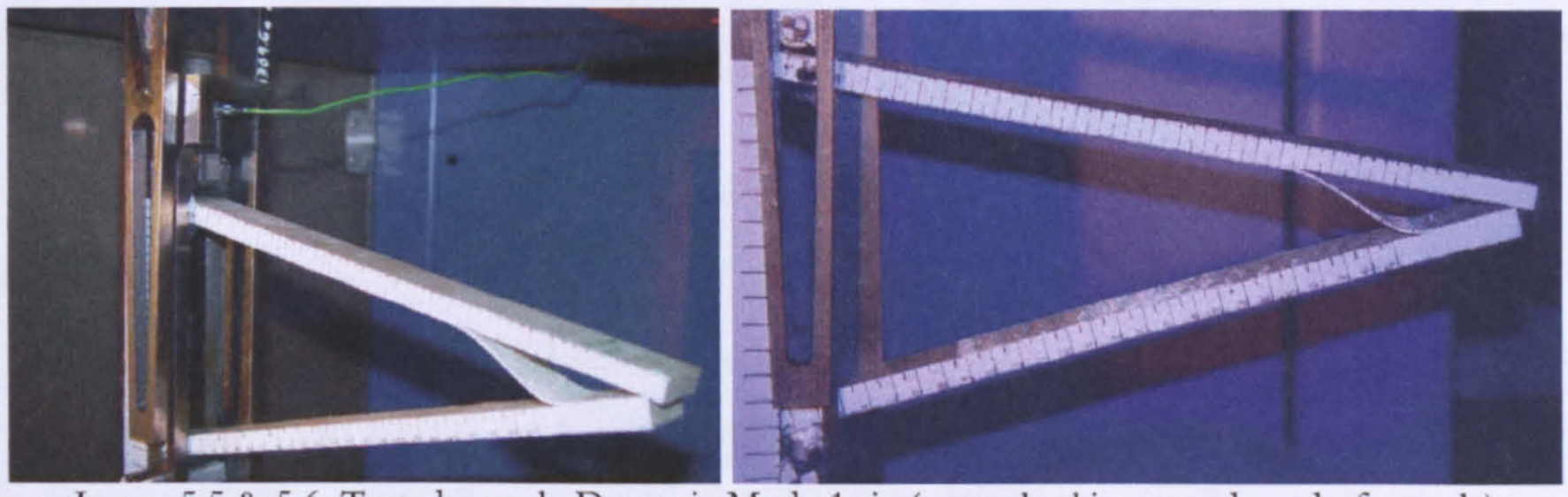

Image 5.5 & 5.6: Tested sample Dynamic Mode 1 rig (note ply skip towards end of sample)

The same data requirements and analysis as the quasi-static tests are required for these dynamic tests. Crack propagation was measured though the use of a high speed digital camera mounted at perpendicular to the specimen face. This camera can also be used to

double check displacement data should the load pin loose contact with the face of the striker forks.

The Imatek® software allows the impact event video to be replayed in such a way that measurements of crack length can be taken directly from the video and the force / displacement data for that moment recorded.

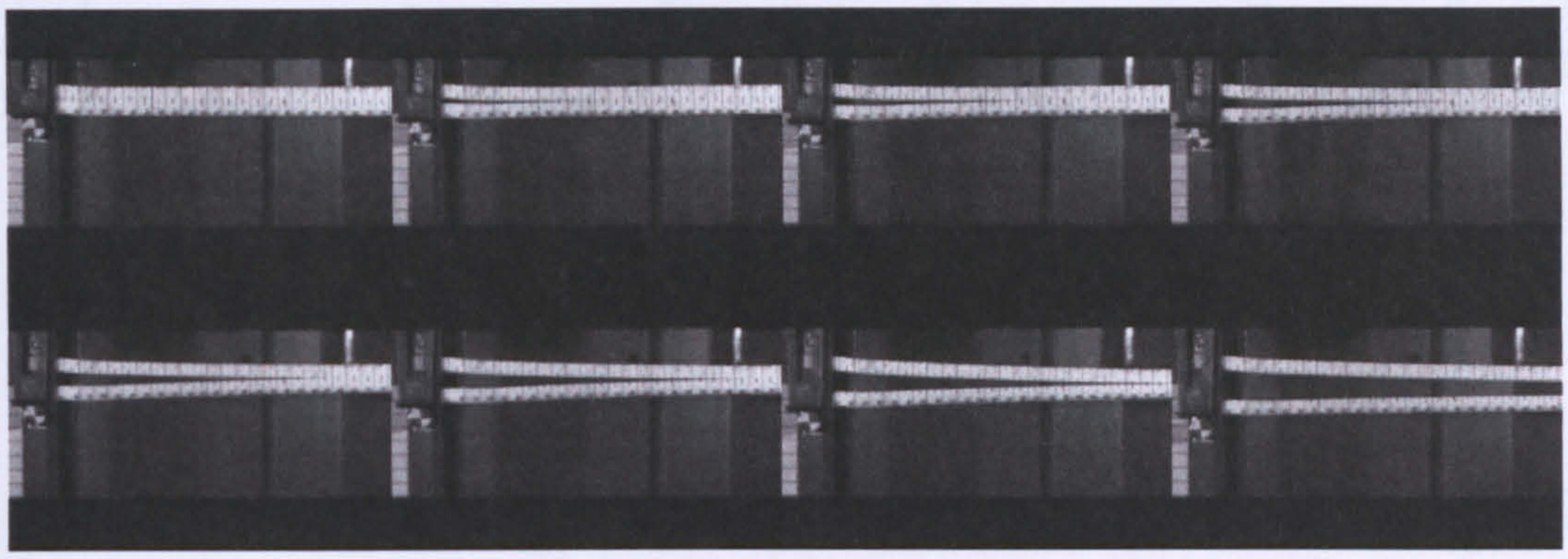

Image 5.7: High speed stills of dynamic failure

5.6.3 Panels Tested

Examples of the four main materials being tested were evaluated:

1. 830gsm S2 Glass / Phenolic
2. 830gsm S2 Glass / Vinylester
3. 300gsm S2 Glass / Vinylester
4. 190gsm S2 Glass / Vinylester

Due to a manufacturing flaw (no PTFE insert) Phenolic samples had to be initially cracked by forcing a wedge into the material

5.6.4 Results

For processing of results a spreadsheet was obtained courtesy of Dr A Brunner from EPFL Switzerland. This sheet has been developed by the ESIS technical committee TC4 as part of their investigations into Mode I testing which later contributed significantly to ISO 15024 [67] This sheet was employed to determine G_{Ic} against crack length using Corrected Beam Theory (CBT) and Experimental Compliance (ECM) methods as discussed in section **5.2.1.4**.

5.6.4.1 Quasi-Static results

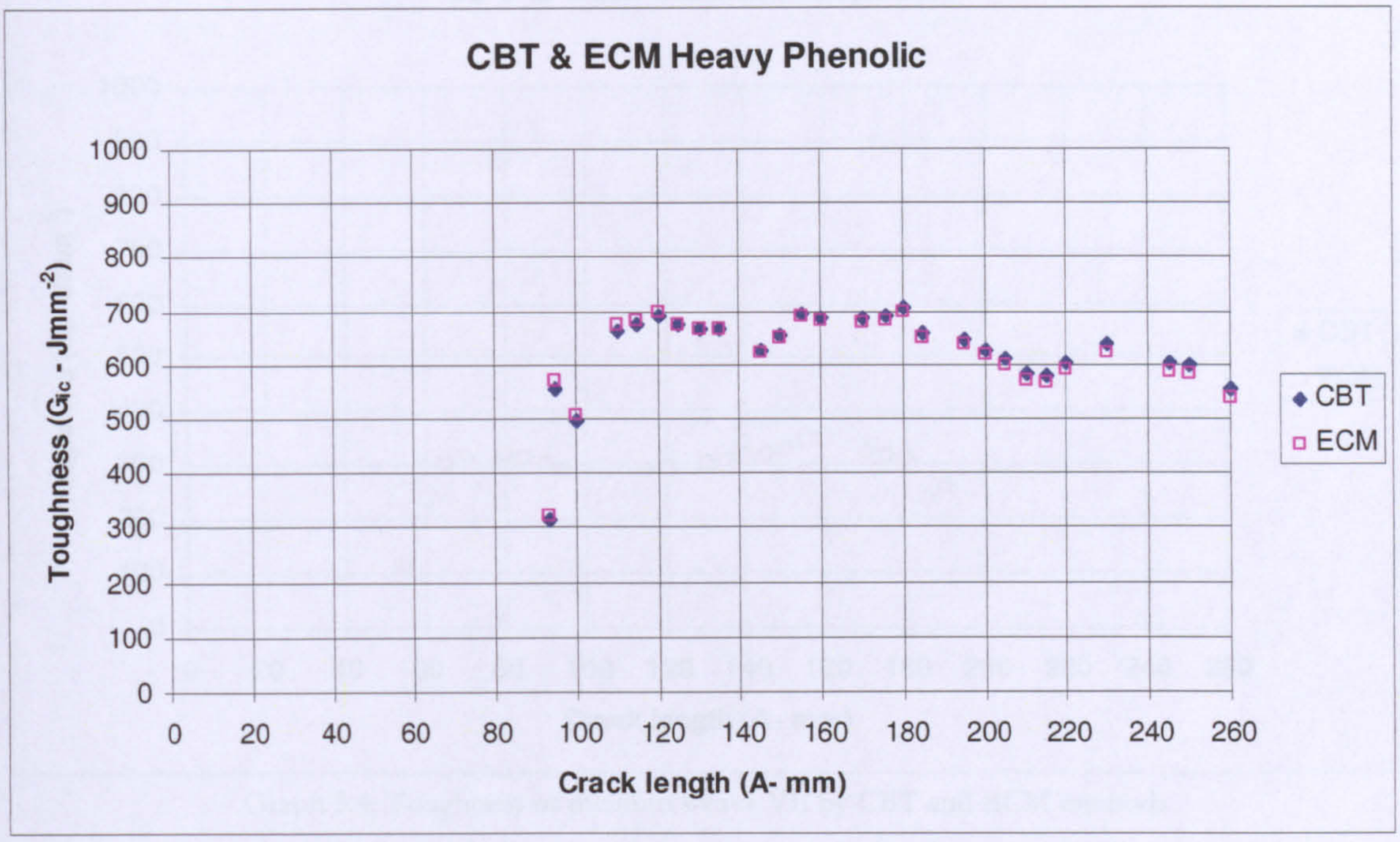

Graph 5.2: Toughness of heavy weave Phenolic by CBT and ECM methods

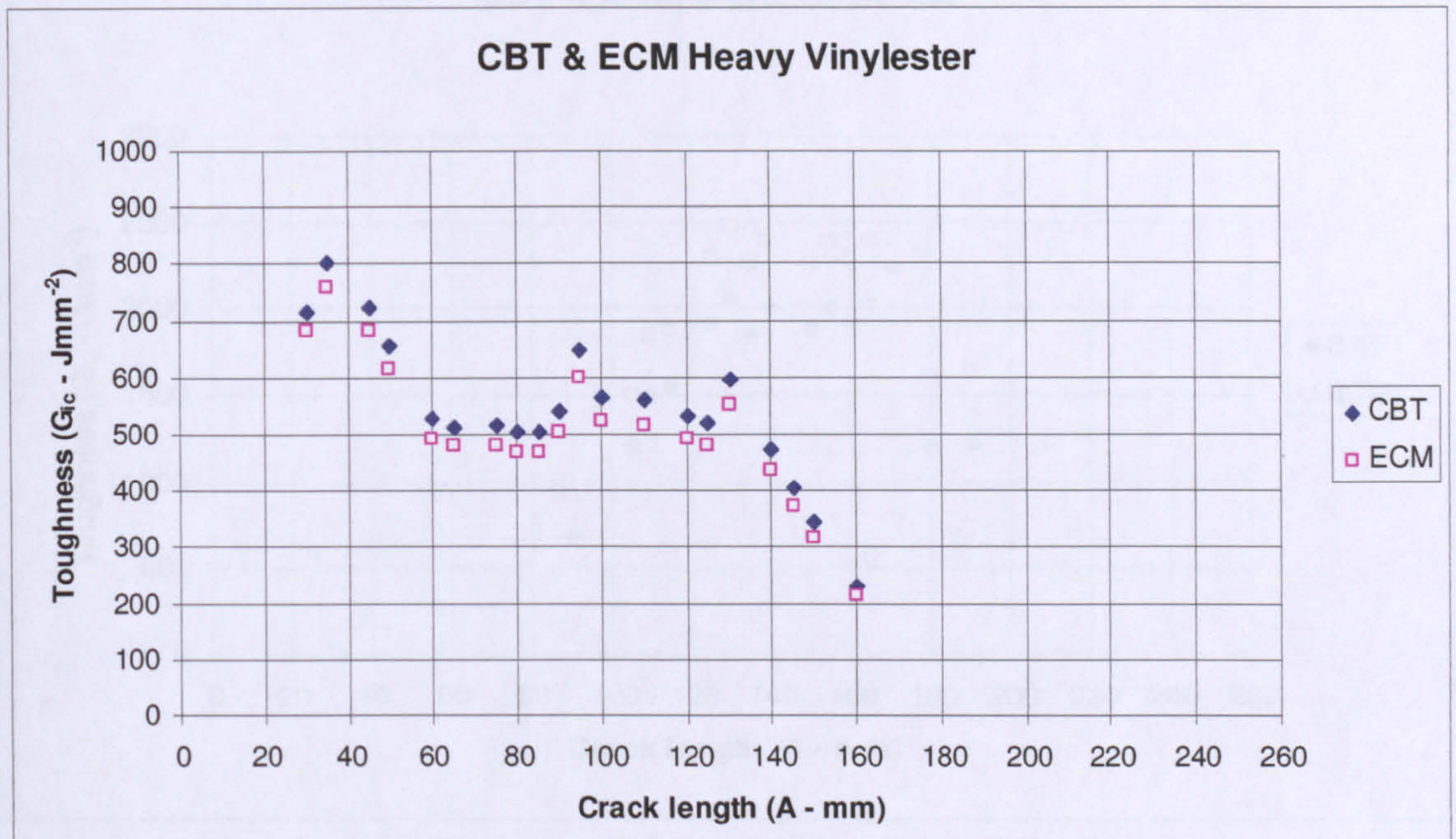

Graph 5.3: Toughness of heavy weave VE by CBT and ECM methods

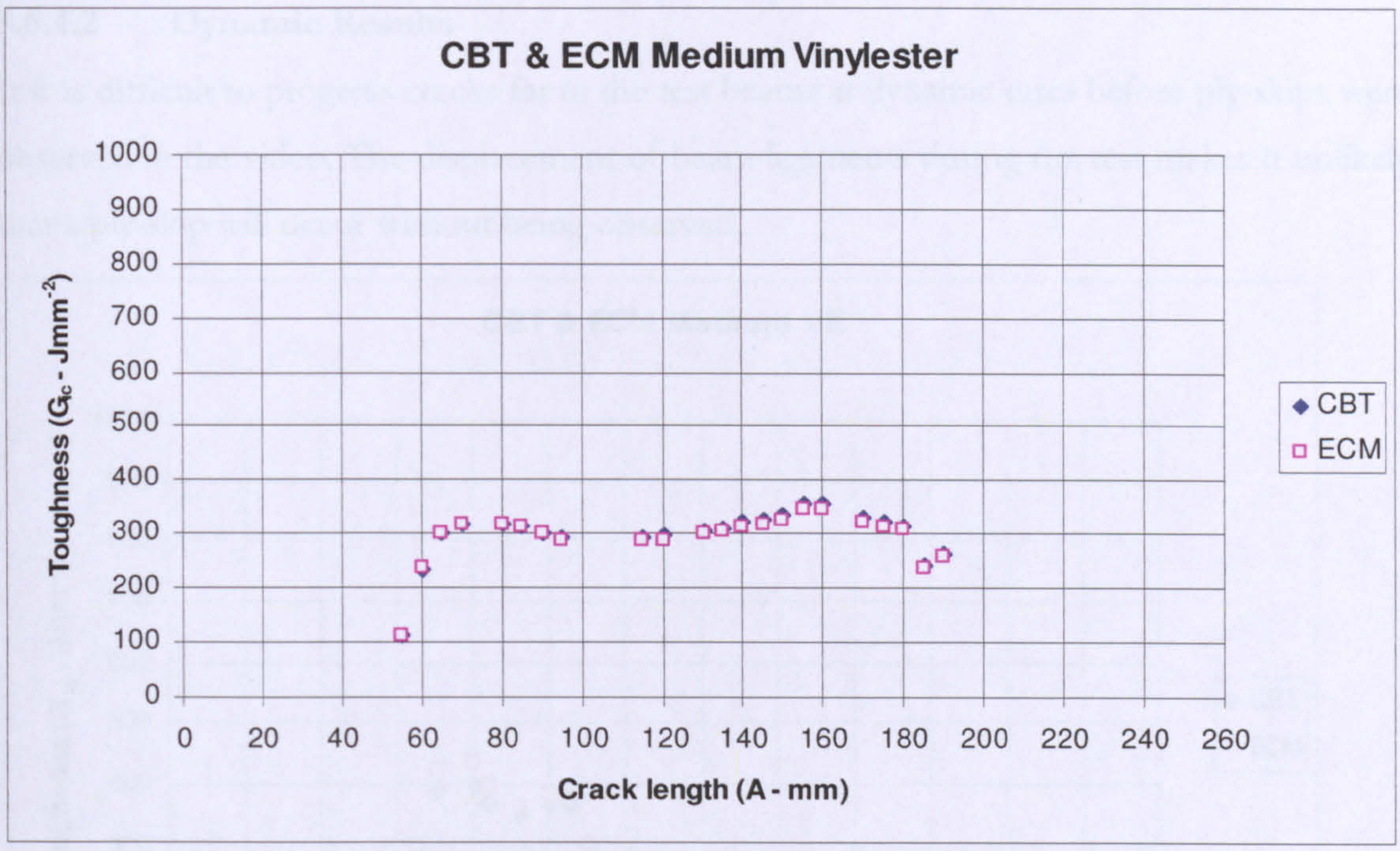

Graph 5.4: Toughness of medium weave VE by CBT and ECM methods

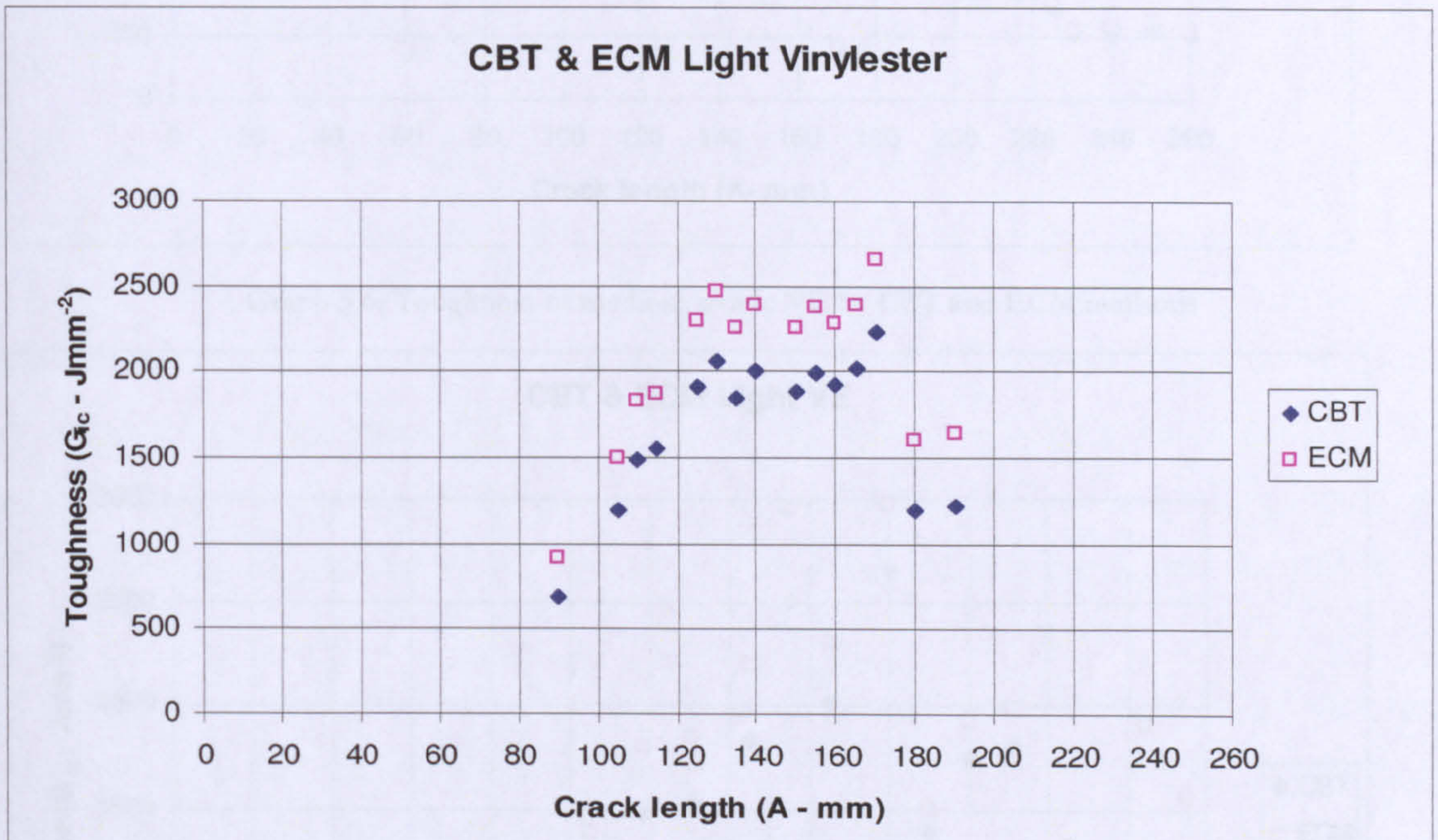

Graph 5.5: Toughness of light weave VE by CBT and ECM methods

These trials showed good agreement between both calculation methods, the agreement was best for the medium weave VE which co-incidentally was the easiest material to test. It should be noted that Graph 5.5 has a Y-axis scale three times that of Graphs 5.3 and 5.4 (for heavy and medium weave materials) this because of the high toughness of the light weave material compared to others, a variance of this magnitude between materials was not anticipated.

5.6.4.2 Dynamic Results

It was difficult to progress cracks far in the test beams at dynamic rates before ply-skips were observed in the video. The displacement of beam ligaments during the test makes it unlikely that a ply-skip will occur without being observed.

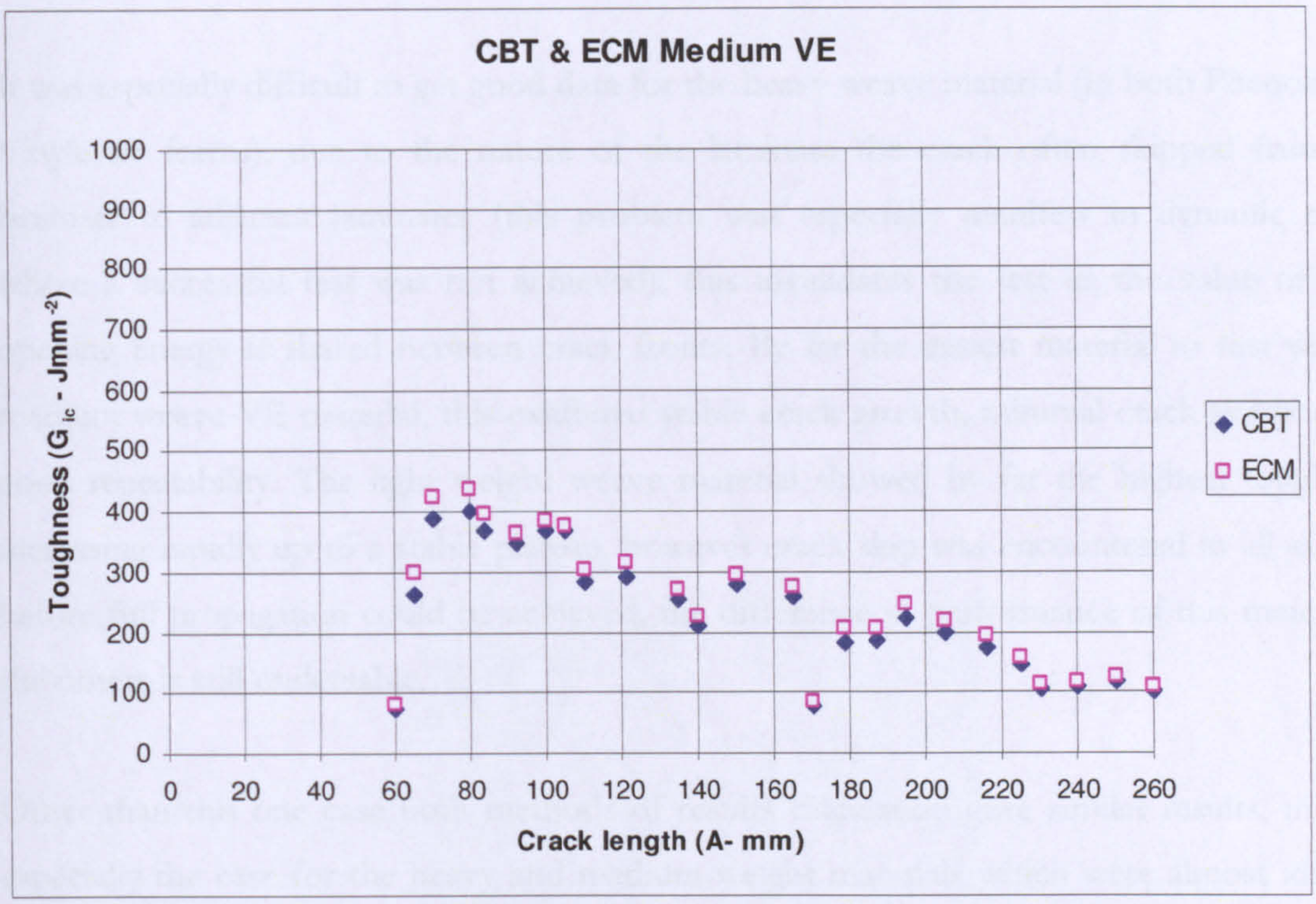

Graph 5.6: Toughness of medium weave VE by CBT and ECM methods

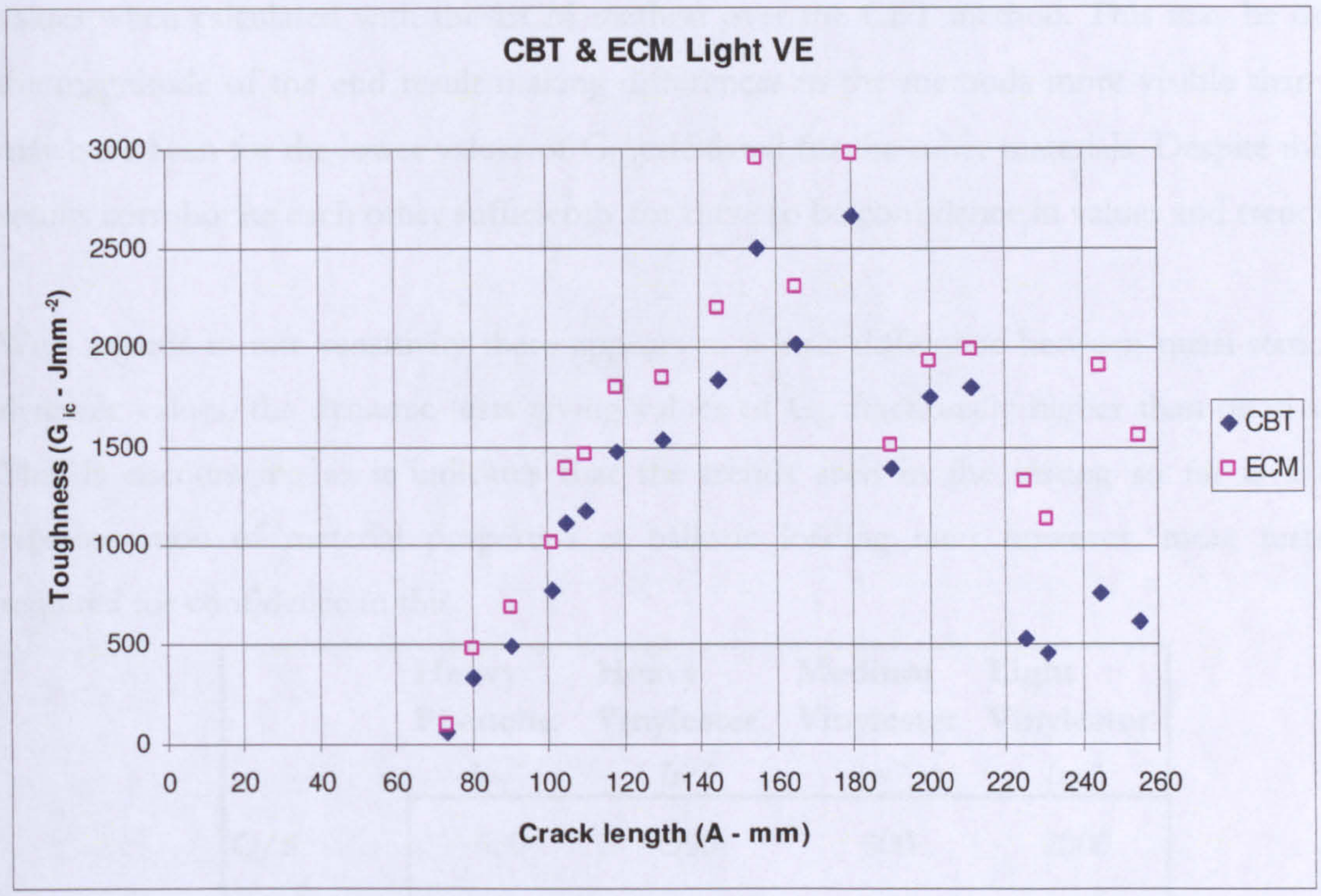

Graph 5.7: Toughness of light weave VE by CBT and ECM methods

5.6.5 Summary and discussion

It is apparent from the testing which has been carried out that there is significant difference in the Mode I fracture toughness (G_{Ic}) values observed between the materials tested at both quasi-static and dynamic loading rates.

It was especially difficult to get good data for the heavy weave material (in both Phenolic and Vinylester forms), due to the nature of the laminate the crack often skipped from one laminate to adjacent laminates (this problem was especially manifest in dynamic testing where a successful test was not achieved), this invalidates the test as the value of crack opening energy is shared between crack fronts. By far the easiest material to test was the medium weave VE material, this exhibited stable crack growth, minimal crack skipping and good repeatability. The light weight weave material showed by far the highest toughness, increasing rapidly up to a stable plateau, however crack skip was encountered in all samples before full propagation could be achieved, the difference in performance of this material to the others is still undeniable.

Other than this one case both methods of results calculation gave similar results, this was especially the case for the heavy and medium weight materials which were almost identical for both methods. The lightest weave material however exhibited slightly increased G_{Ic} values when calculated with the ECM method over the CBT method. This may be due to the magnitude of the end result making differences in the methods more visible than they may have been for the lower values of G_{Ic} calculated for the other materials. Despite this the results corroborate each other sufficiently for there to be confidence in values and trends.

With regards to rate sensitivity there appears to a little difference between quasi-static and dynamic values, the dynamic tests giving values of G_{Ic} fractionally higher than quasi-static. This is encouraging as it indicates that the trends seen in the testing so far is a close representation of material properties at ballistic loading rates however. more tests are required for confidence in this.

	Heavy Phenolic Jm^{-2}	**Heavy Vinylester** Jm^{-2}	**Medium Vinylester** Jm^{-2}	**Light Vinylester** Jm^{-2}
Q/S	680	500	300	2000
Dynamic			300	1700

Table 5.2: Mode I Toughness values

5.7 Three point bend

5.7.1 Aims

A simple three point bend test was employed to determine the modulus of the materials being tested. This is important information required for understanding the structural properties of the materials being tested. A good degree of stiffness is required if this material is to be used as a structural hull member of a vehicle.

5.7.2 Experimental

Testing was carried out on an Instron 4206 machine utilising a standard three point bend fixture with force and deflection being recorded. Due to the physical size of the samples available the conventional ASTM D790 standard would not accommodate the specimen size because of thickness.

Image 5.8: Three point bend test [68]

5.7.3 Panels tested

Specimens cut from each of the S2 glass reinforced armour materials tested were available for testing. The panel materials tested in this work are listed as follows:

1. Heavy weave S2 Glass, Phenolic Matrix
2. Heavy weave S2 Glass, Vinylester Matrix
3. Medium weave S2 Glass, Vinylester Matrix
4. Light weave S2 Glass, Vinylester Matrix

5.7.4 Results

Due to the thickness of the materials being tested it was always a possibility that they would not fail in the correct manner (tensile failure of the rear surface). This was indeed the case and all materials failed in a mode II fashion as shown in Image 5.9 which also shows evidence of buckling failure in the upper part of the failed specimens.

The results from testing are shown in Table 5.3, data taken in the elastic region is believed to be valid however caution should be expressed regarding failure values. Derived values were calculated using equations *5. 3*, *5.4* and *5.5* as described in section **5.2.2** and ASTM D720.

	Heavy Phenolic	Heavy VE	Medium VE	Light VE
Modulus	12.1	13.0	13.9	12.7
UTS (MPa)	146.0	316.9	247.4	236.8
F_{max} (kN)	15.0	14.9	15.5	12.3
ε_{fail}	1.93	2.23	2.57	3.11
ε_{yield}	0.23	0.23	0.25	0.29
D_{yield}	0.50	0.50	0.46	0.60

Table 5.3: Results of 3 point bend testing

A typical stress-strain curve is shown in the following Graph 5.8

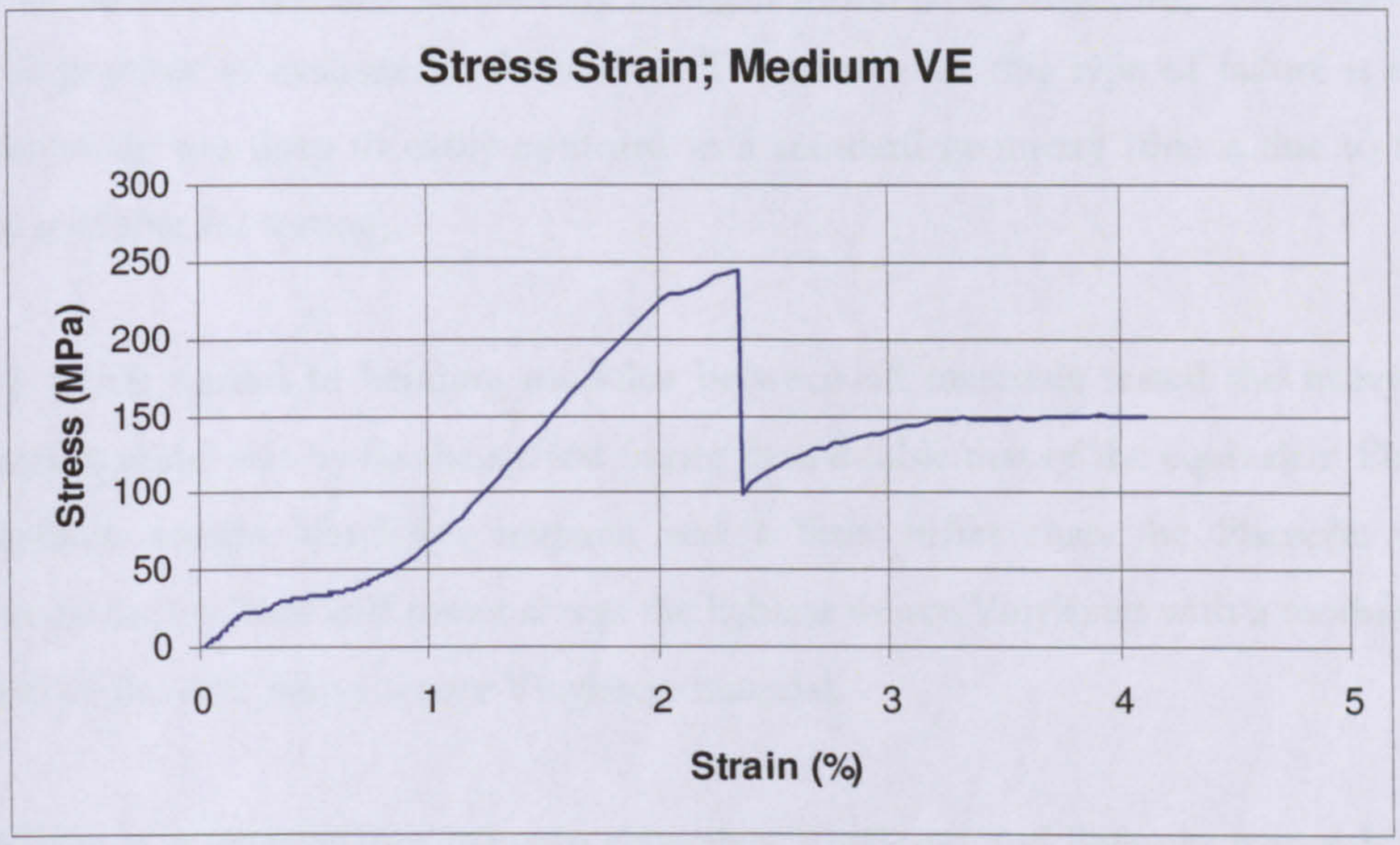

Graph 5.8: Medium Vinylester Stress/Strain trend

Failure of these specimens was not by tensile failure on the lower face or by crushing below the load roller (or a combination of both) but was as previously mentioned by sudden, uncontrolled mode II shearing failure of the laminate. This is believed to be due to the extreme thickness of the laminate causing high shear stresses below the neutral plane as the beam deflected.

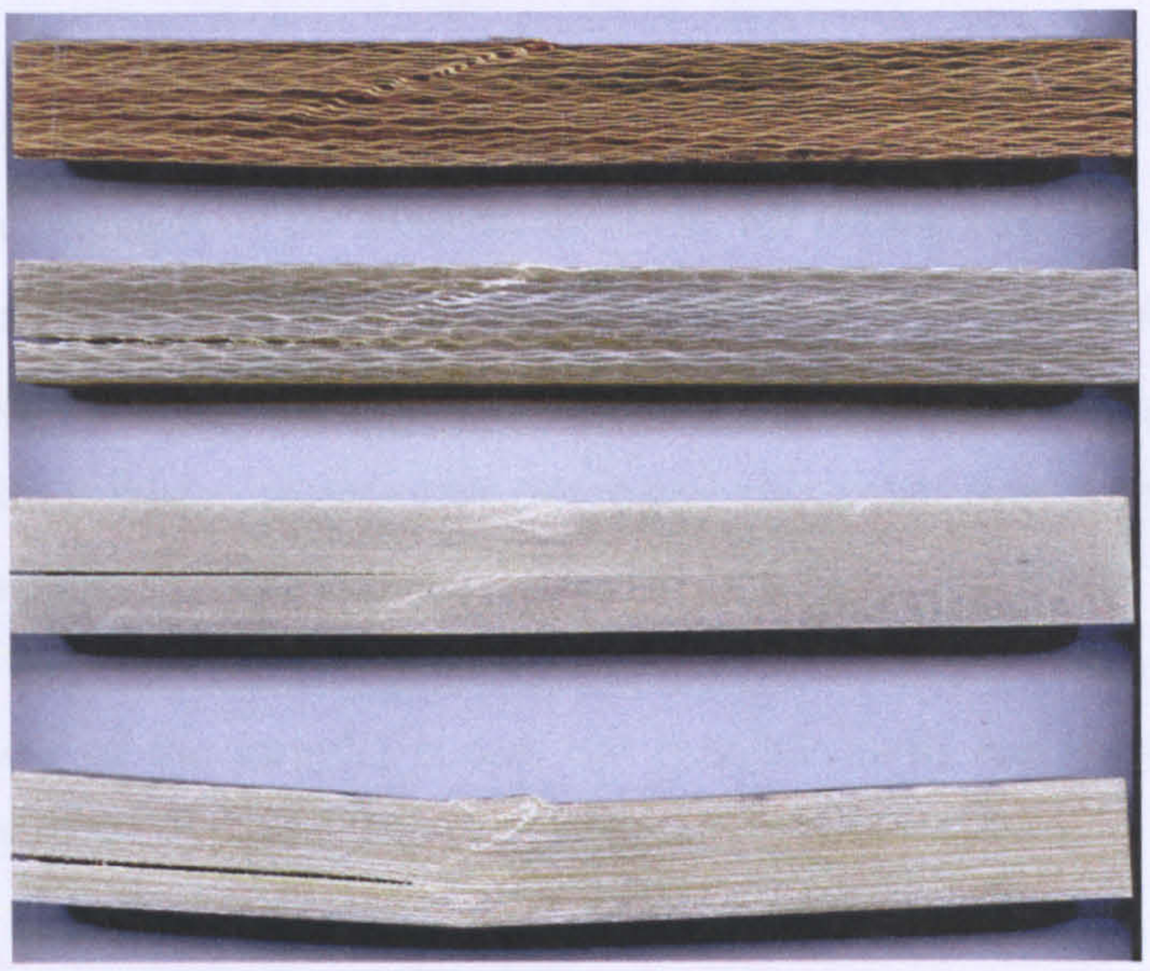

Image 5.9: Failed bend specimens (Top-Bottom: Heavy Phenolic, Heavy, Medium & Light Vinylester)

5.7.5 Summary and discussion

The materials tested all failed in Mode II shearing and as such values of maximum force cannot be used as a measure of bending strength however by observing the elastic region only it is possible to evaluate modulus data. The reason for this type of failure is that the specimen is far too deep to easily conform to a standard geometry (this is due to the raw material available for testing).

There is a fair spread in bending modulus between all materials tested the heavy weave Vinylester material was by far the stiffest (more than double that of the equivalent Phenolic). The medium weight Vinylester material was a little stiffer than the Phenolic samples however by far the least stiff material was the lightest weave Vinylester with a modulus close to a third of the stiff, heavy weave Vinylester material.

The difference in performance between equivalent Vinylester and Phenolic materials was not expected, similarly the performance of the medium weave Vinylester system (being slightly greater than the heavy weave Phenolic material) suggests that a Vinylester system will be a far better candidate for a structural system which also requires ballistic strength.

5.8 Tensile strength testing

5.8.1 Aims

As discussed in section **5.2.3**. The tensile strength of a composite armour is important to the performance of the rear surface of a target. This is especially the case when large, bulging deformations are formed where lamina are bent and fail by tensile rupture.

5.8.2 Experimental

Due to the size and strength of the material available for testing exceeding the load capacity of the test machines available (250kN Zwick 1484) reduced thickness samples had to be cut from existing material thickness. This was achieved by splitting rectangular samples in a Mode I fashion with a wedge to produce two equal specimens which were then measured and examined individually before testing.

Due to the thickness of the samples it was not possible to fit end tabs as the grip width available was insufficient.

Samples were tested at 2mm/min until final failure.

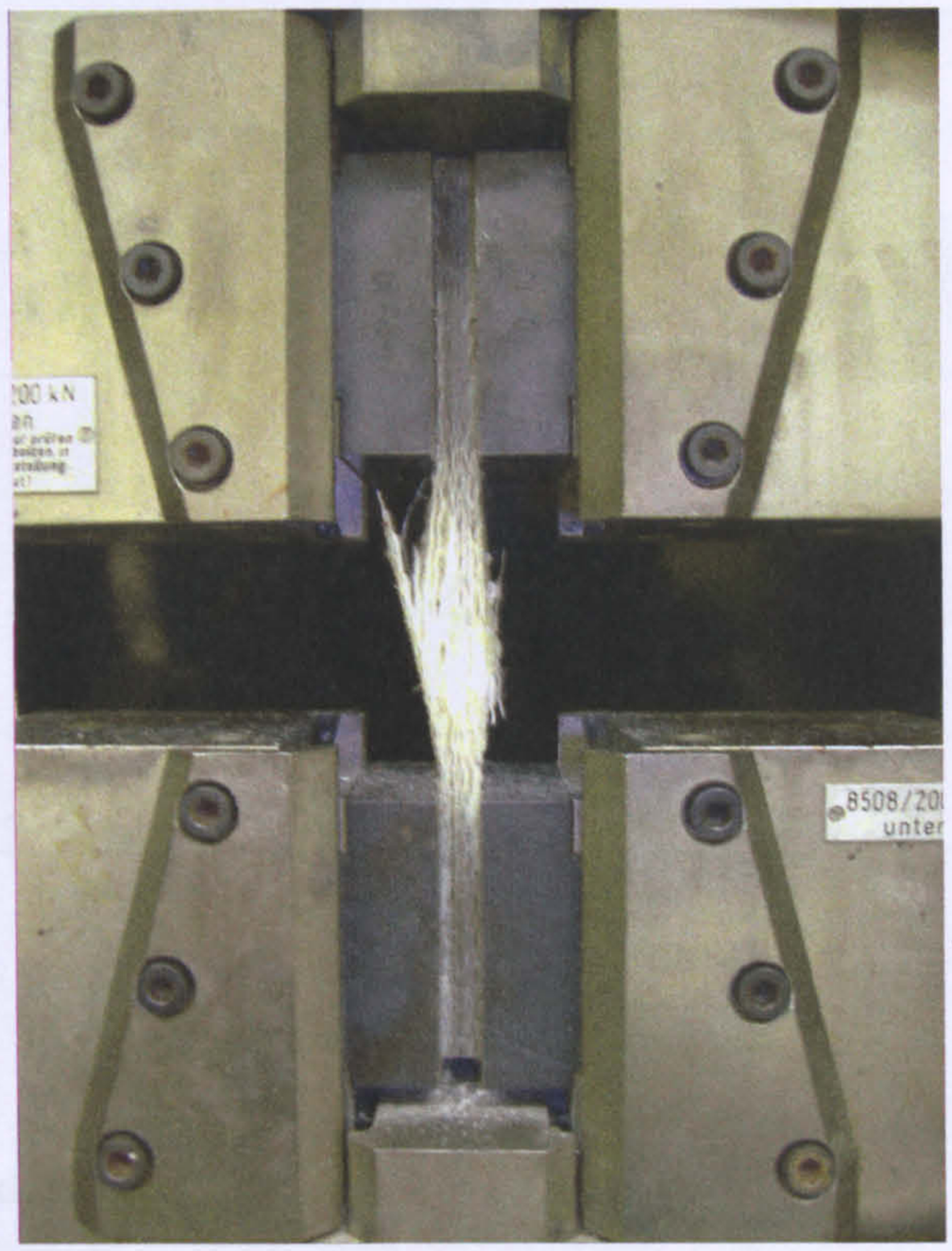

Image 5.10: Tensile failure

5.8.3 Panels tested

Specimens cut from each of the S2 glass reinforced armour materials tested were available for testing. The panel materials tested in this work are listed as follows:

1. Heavy weave S2 Glass, Phenolic Matrix
2. Heavy weave S2 Glass, Vinylester Matrix
3. Medium weave S2 Glass, Vinylester Matrix
4. Light weave S2 Glass, Vinylester Matrix

5.8.4 Results

	UTS (MPa)	Failure strain (%)	Modulus GPa
Heavy Phenolic	408.0	15.9	3.18
Heavy VE	549.4	21.7	3.18
Medium VE	381.5	16.6	3.18
Light VE	328.4	14.1	3

Table 5.4: Results of tensile testing

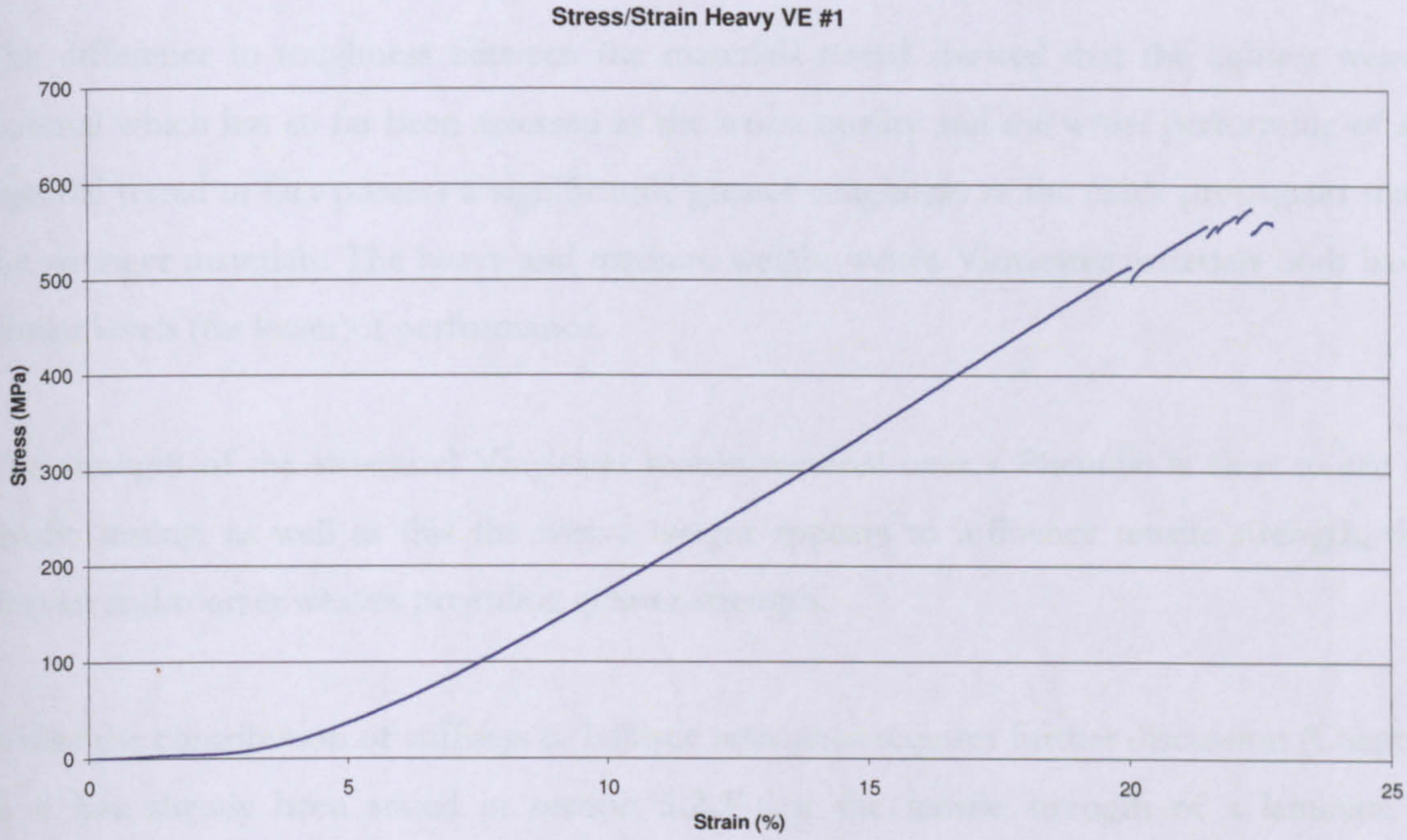

Graph 5.9: Sample Stress/Strain curve

5.8.5 Summary and discussion

The tensile testing of these laminates showed as expected the structural VE resin gives a far stronger and surprisingly more ductile material than the equivalent Phenolic material, additionally the weave weight appears to have a significant effect, the heavy weave with

coarser, larger fibre bundles is significantly stronger. The high strain supported by the heavy weave VE material is due to its ability to support a progressive failure as the load was increased.

5.9 Overall summary of rear surface testing

The testing in this chapter shows some interesting trends, it was expected for instance that the Phenolic material would be the stiffest of the materials tested and that the light weave material would have the highest fracture toughness. This suggests that in terms of a structural material the Vinylester materials offer a better solution. It was not possible to assess maximum bending strength of these materials as they failed in a mode II fashion rather than a conventional bending failure.

Interlamina fracture toughness testing indicates that there is relatively little rate sensitivity in Mode I crack length. This is encouraging as it means that data obtained with only moderate loading rates is a valid assessment of target behaviour under ballistic impact.

The difference in toughness between the materials tested showed that the lightest weave material which has so far been assessed as the worst quality and the worst performing of all material tested in fact possess a significantly greater toughness as the crack propagates than the stronger materials. The heavy and medium weight weave Vinylester materials both have similar levels (far lower)of performance.

The strength of the structural Vinylester matrix material over a Phenolic is clear to see in tensile testing, as well as this the weave weight appears to influence tensile strength, the heavier and coarser weaves providing greater strength.

Whilst the contribution of stiffness to ballistic resistance requires further discussion (Chapter **6**) it has already been stated in section **5.2.3** that the tensile strength of a laminate is important in stopping a blunt projectile.

CHAPTER 6:

GENERAL DISCUSSION

In this chapter the results of previous mechanical and ballistic testing will be connected and discussed. This chapter will aim to connect the importance of the various mechanical properties tested and their direct effect on ballistic performance. Theoretical expectations will be compared to actual findings and the resulting difference will be evaluated. An energy model based on observations of visible damage will be constructed and validated.

6.1 General discussion

This chapter will bring together the findings of all the mechanical and ballistic testing detailed and discussed in previous chapters. Findings of mechanical testing will be directly linked with ballistic testing in order to tie specific mechanical properties to ballistic performance.

6.2 Ballistic testing against soft projectiles (Ball ammunition, STANAG level I)

Mechanical testing allowed the materials available for ballistic testing to be characterised and evaluated. The results which came from this mechanical testing were evaluated with a view of making predictions of material behaviour when subjected to ballistic testing.

Ballistic testing generated the following results:

Material	Thickness (mm)	Areal Density (kgm^{-2})	V_{50} (ms^{-1})	Damage Front (mm)	Damage Rear (mm)
Heavy weave Phenolic	21	40.6	773	36	150
Heavy weave VE	21	34.4	651	51	252
Medium weave VE	23	39.5	645	75	192
Light weave VE	21	34.6	430	28	103

Table 6.1: Testing results - V_{50}, Visible damage and areal density

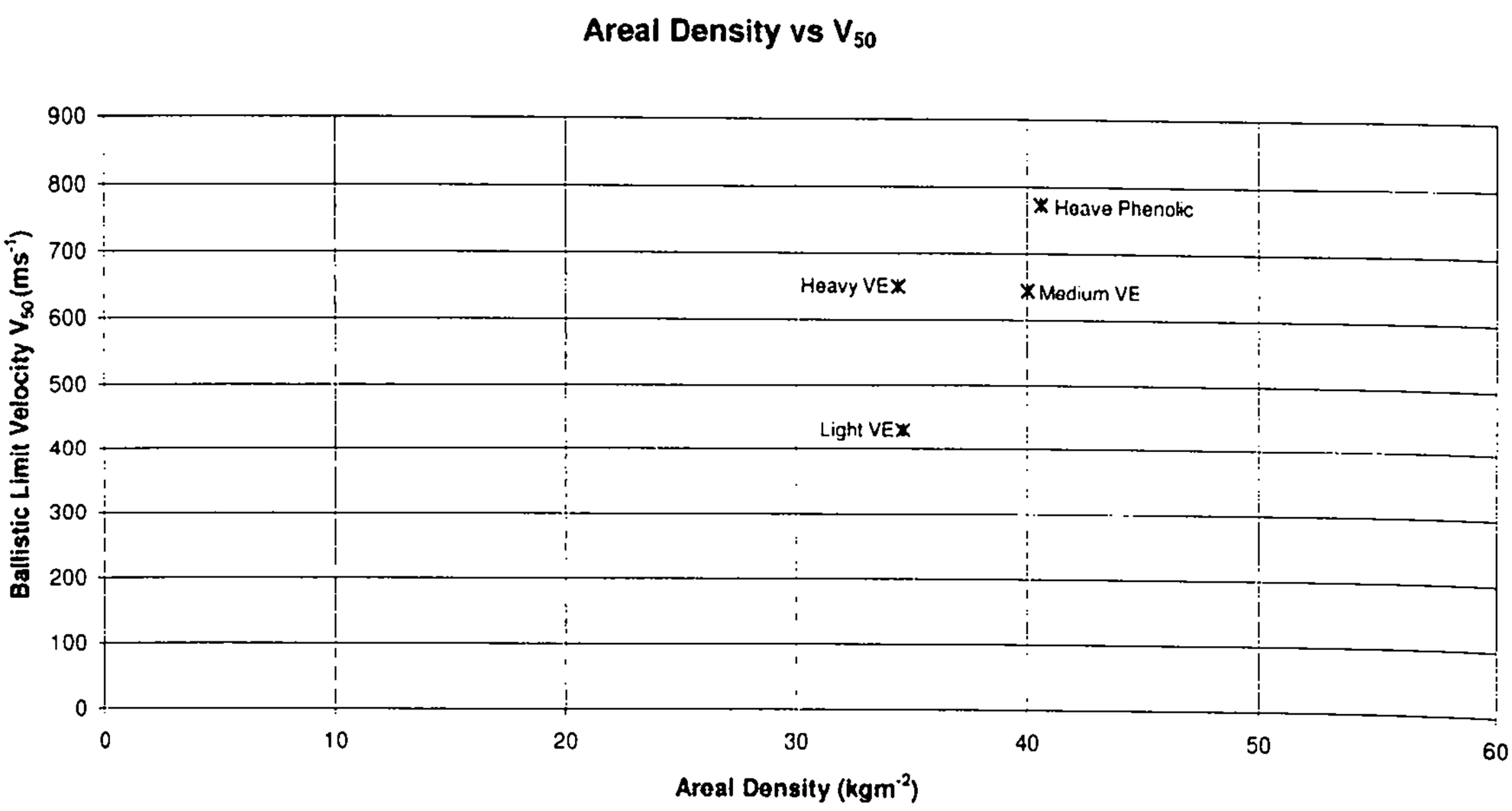

Graph 6.1: Ballistic testing vs Ball ammunition

Looking at the impact energy at the V_{50} velocities obtained for these materials gives the following values based on a projectile weight of 9.65g from section **2.9**:

- Heavy weave Phenolic: 2,838J @ 773ms^{-1}
- Heavy weave Vinylester:: 2,045J @ 651ms^{-1}
- Medium weave Vinylester: 2,009J @ 645ms^{-1}
- Light weave Vinylester:: 888J @ 430ms^{-1}

Mechanical testing has covered a range of failure mechanisms which contribute to projectile defeat. Mode I fracture toughness testing (section **5.6**) has suggested an inverse material performance ranking to that seen in ballistic testing with the heavy weave Phenolic, medium and heavy weave Vinylester materials being of similar performance whilst the light weave Vinylester material proving far tougher. This finding is borne out by sectioning of impacts (section **3.6**) which show significantly less delamination damage in the light weave material compared to the other Vinylester materials tested. As well as this the large amounts of delamination visible in the Phenolic material correspond to its modest toughness and the high velocity at which the projectiles struck the armour.

Mechanical testing has also evaluated the tensile properties of the laminates being tested. The importance of tensile strength has already been covered. Of the laminates tested it was shown that coarser weaves had significantly higher strengths than the lighter weaves tested. It was also shown that the Vinylester resin system was stronger than the equivalent Phenolic material and also had a significantly greater strain to failure than any of the materials tested.

The understanding of tensile strength does not complete the full picture, intuitively the heavy weave VE material with its high strength and high strain to failure was expected to be the best performer (especially compared to the equivalent Phenolic material), however the results of ballistic testing show the weaker and less ductile Phenolic material is in fact the better performer.

Laminate stiffness ranked the VE materials in order of ballistic performance however the Phenolic material did not fit into this relationship, but had a lower stiffness.

Non-penetrating indentation testing (Section **4.7.1**) does not however reflect the trends seen in ballistic performance, especially with regards the heavy weave VE material which was found to be the 'softest'. However, the use of penetrating indenters (Section **4.7.2**) suggests that the heavy weave Vinylester material (followed by medium and light respectively) has the highest resistance to penetration over a range of indenter angles. Interestingly, whilst this type of testing was found to predict compressive yield strength (in plane with the laminate (Section **4.6**)) compressive testing itself did not achieve great success in predicting ballistic performance. The Phenolic material, which was the best performer ballistically was also by far the strongest when compressed with a load perpendicular to the laminate. Impact force trends from dynamic indentations also matches the ballistic relationships well. Agreement is found for both flat and ogival indenters, though is better for the latter.

The following table shows the ranking of mechanical properties and ballistic limit velocity in order of performance from 1-4, i.e. the best/strongest/toughest/stiffest material is ascribed a rank of one and vice versa the worst/weakest a rank of 4.

	Compression		**Indentation**			
	Parrallel	**Perpendicular**	**Q/S Ball**	**Q/S Cone**	**Dyn Ogive**	**Dyn Flat**
Heavy Phenolic	*4*	*1*	*1*	*-*	*1*	*1*
Heavy VE	*1*	*3*	*4*	*1*	*2*	*2*
Medium VE	*2*	*2*	*2*	*2*	*3*	*3*
Light VE	*3*	*4*	*3*	*3*	*4*	*4*

	Mode I		**Bend**	**Tensile**	
	Q/S	**Dyn**	**Modulus**	**Modulus**	**Strength**
Heavy Phenolic	*3*	*-*	*2*	*3*	*2*
Heavy VE	*2*	*2*	*1*	*2*	*1*
Medium VE	*4*	*-*	*3*	*1*	*3*
Light VE	*1*	*1*	*4*	*4*	*4*

	Ballistic (V_{50})			**Weight**
	Ballistic	**AP (Thin)**	**AP (Thick)**	**Areal density**
Heavy Phenolic	*1*	*1*	*1**	*4*
Heavy VE	*2*	*2*	*2*	*2*
Medium VE	*3*	*3*	*1**	*3*
Light VE	*4*	*4*	*3*	*1*

Table 6.2: Material performance ranking (* equal performance)

In summary, against ball ammunition no one mechanical property appears to be dominant to the extent that ballistic performance ranking can be estimated.

6.3 Ballistic testing against hard projectiles (AP ammunition, STANAG level II)

Testing against a non-deforming AP round (rather than a soft 'ball' round) is of interest simply because this ammunition is a more dangerous threat and harder to protect against. Testing was carried out in two stages, initially against a single thickness target followed by testing against double and treble thickness targets.

This threat is significantly more difficult to stop than STANAG level I. STANAG level II requirement is to stop this round at 695ms^{-1}. The best performing materials in the higher areal density group are very close to this.

Against AP ammunition the difference between ballistic performance of materials tested is much smaller. At the lowest weight tested the Phenolic material once again showed the best ballistic performance though it was also the heaviest. The medium weave Vinylester material performed only slightly worse than the Phenolic material however it is significantly lighter. Interestingly the medium weave panel has a marginally better performance than the heavy weave (a 30ms^{-1} higher V_{50}) though it is still significantly heavier (not as heavy as the Phenolic however). The lightest weave material which is only a little heavier than the heavy weave Vinylester has noticeably poorer ballistic performance, some 70 ms^{-1} lower than the other targets– worst of all materials tested.

Ballistic testing generated the following results:

Material	Thickness (mm)	Areal Density (kgm^{-2})	V_{50} (ms^{-1})	Damage diameter (mm) Front	Rear
Heavy weave Phenolic	21	41.9	436	48	130
	40	84.3	683	-	-
Heavy weave VE	21	33.9	394	50	111
	40	73.9	626	56	96
Medium weave VE	23	38.9	424	64	119
	44	78.6	683	57	132
Light weave VE	21	34.7	362	33	77
	41	67.7	619	45	75

Table 6.3: Testing results - V_{50}, Visible damage and areal density

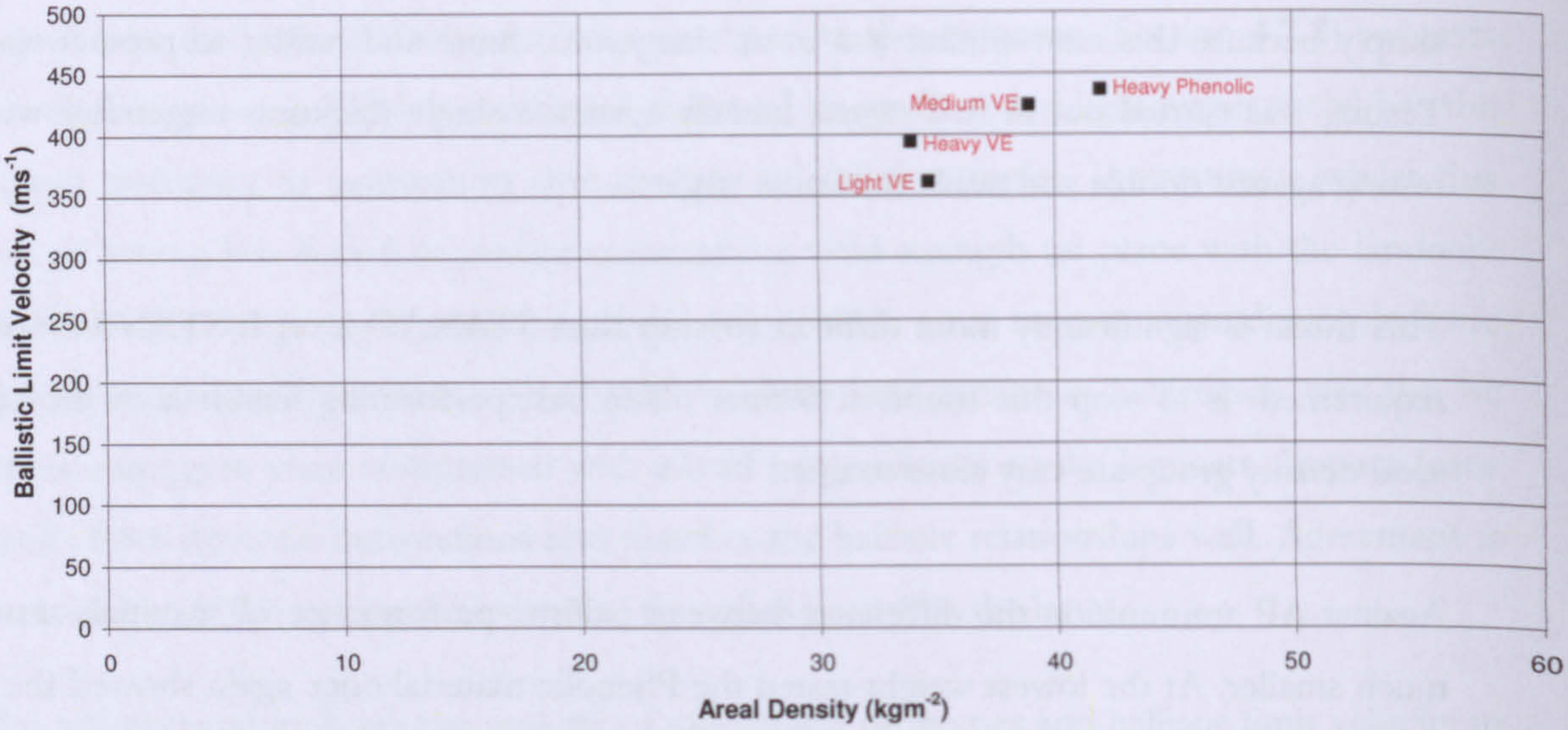

Graph 6.2: Ballistic testing of thin targets vs AP ammunition

Looking at the impact energy at the V_{50} velocities obtained for these materials gives the following values based on a core weight of 4.04g[27] (the jacket and gilding metal has been ignored from this value as it is the core which is designed to lead penetration:

- Heavy weave Phenolic: 381J @ 436ms^{-1}
- Heavy weave VE: 310J @ 394ms^{-1}
- Medium weave VE: 359J @ 424ms^{-1}
- Light weave VE: 261J @ 362ms^{-1}

The second series of testing with the same AP ammunition tested thicker targets generating the remaining results recorded in Table 6.2. The damage visible on the front and rear faces was different only in scale from the damage previously recorded.

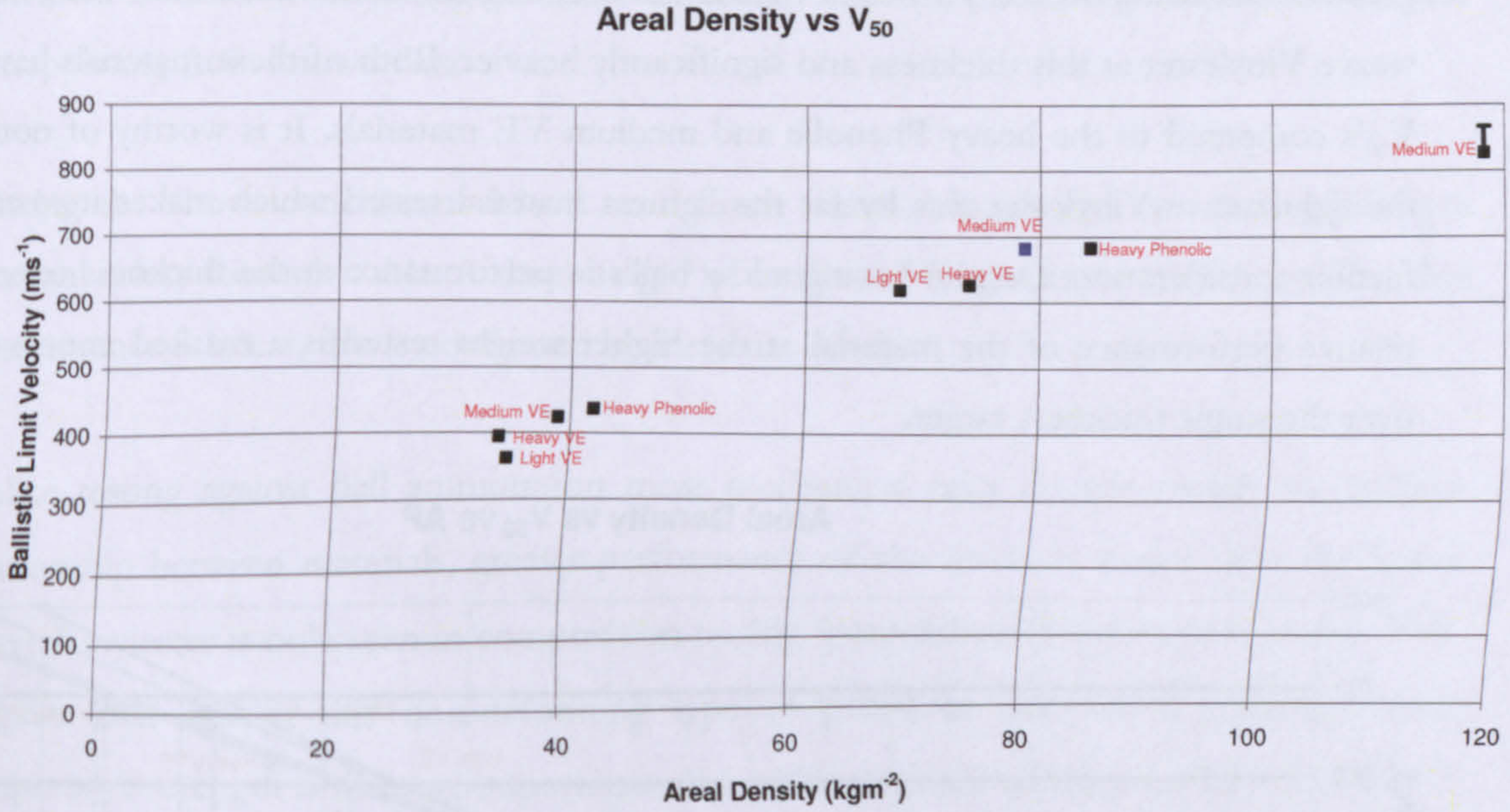

Graph 6.3: V_{50} vs Areal density, all panels tested against AP

The energy absorbed by these materials is once again based on the recorded V_{50} (Table 6.2) and is as follows:

- Heavy weave Phenolic: 934J @ 683ms^{-1}
- Heavy weave VE: 785J @ 626ms^{-1}
- Medium weave VE: 933J @ 683ms^{-1}
- Light weave VE: 766J @ 619ms^{-1}

The treble thickness target could not be perforated therefore at a velocity of 827 ms^{-1} all 1381.5J of core energy was absorbed by the target.

It is noted that the thick sections have the an internal defect in the form of the join between panels, sectioning indicated that these panels also appear to experience projectile yaw to a far greater degree. Whilst the two panels can be dealt with individually, no provision has been made for yawing of the projectile which may as a result cause some error in the estimation of energy absorbed.

At the higher areal densities the weight advantage of the medium weight Vinylester material over the heavy weave Phenolic material is significant, its ballistic performance is also slightly

greater. The heavy weave Vinylester material is only slightly better ballisticaly than the fine weave Vinylester at this thickness and significantly heavier. Both of these materials have low V_{50}'s compared to the heavy Phenolic and medium VE materials. It is worthy of note that the light weave Vinylester was by far the lightest material tested which makes it worthy of further consideration. Despite having a low ballistic performance at the thickness tested, the relative performance of the material at the higher weight tested is a marked improvement over the single thickness target.

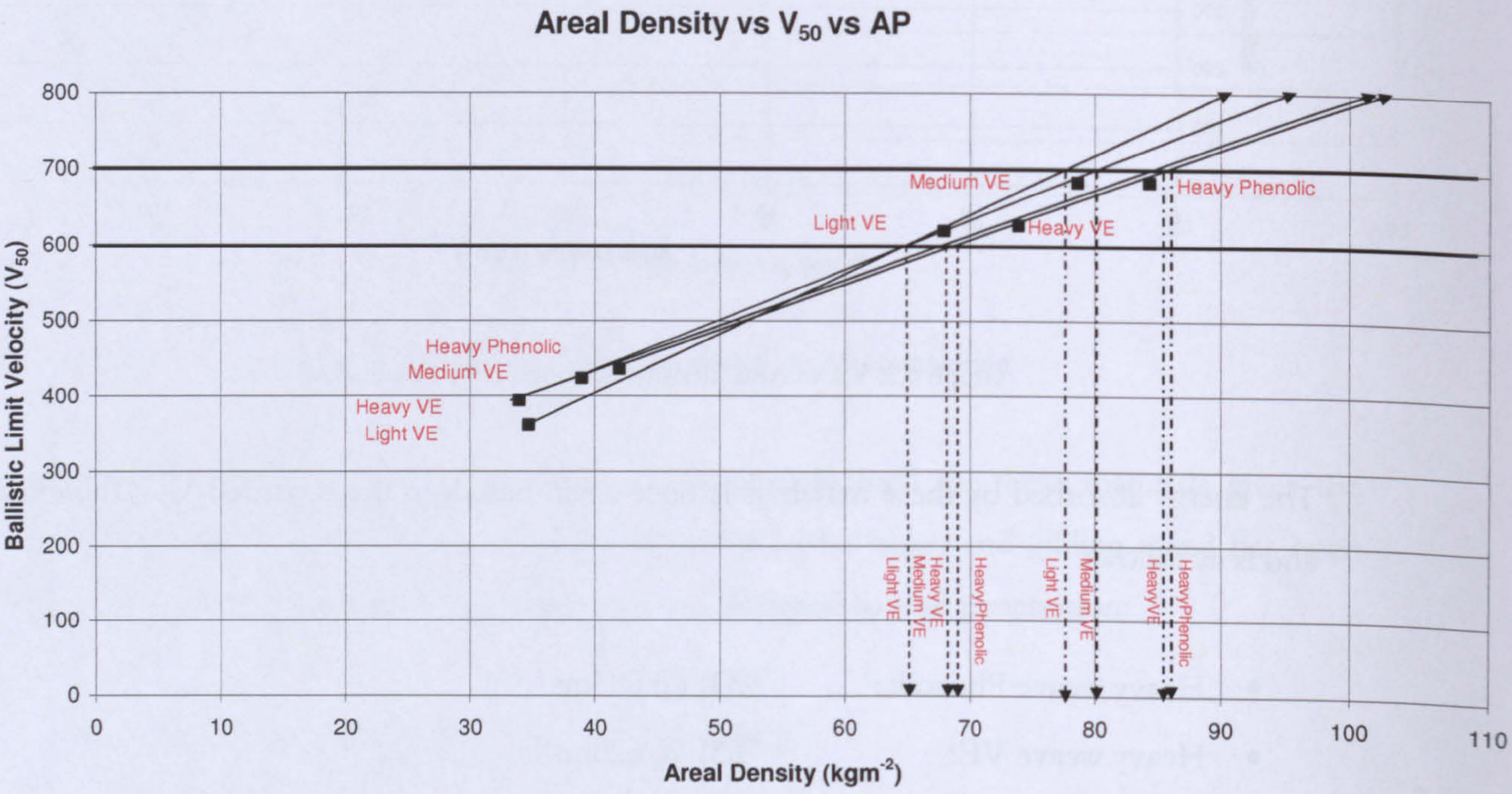

Graph 6.4: V_{50} trends. STANAG Level II; 7.62x39 AP

The preceding graph shows the trends which appear to be emerging with regards to ballistic performance as the impact velocity increases. In all cases it appears that the medium Vinylester based material is superior to the Phenolic material in terms of weight for equivalent ballistic performance.

More interestingly is that assuming the linear trend is correct the lighter weight composites appear to become more attractive as the impact velocity is increased. At an arbitrary projectile impact velocity of $700ms^{-1}$ the heavy weave materials (Phenolic and Vinylester) are comparable however the finest weave material seems to offer equivalent protection for $10kgm^{-2}$ less weight. It is anticipated that to defeat a STANAG level II threat a Vinylester based system will provide a noticeable weight saving over a Phenolic based system. This

statement is based on assuming a linear relationship between panel areal density and V_{50} and extrapolating from known data.

Making the above conclusions based on a linear trend through just two data points per material is less than advisable. A third weight of medium VE was tested which confirms that performance is linear, this is confirmed by literature results.

Unlike testing against ball ammunition most mechanical tests do not match the ballistic relationship between materials, greater performance of the medium weave over the heavy weave Vinylester is only seen in compression testing (perpendicular to laminate plane). This suggests that against this non-deforming type of projectile indentation resistance and compressive strength is of more importance due to the tendency of the pointed projectile to pierce through laminates by parting and shearing fibre bundles rather than by tensile rupture and deformation.

6.4 Hybrid targets against hard projectiles (AP ammunition, STANAG level II)

Ballistic testing also extended to the testing of two hybrid targets.

The first hybrid target tested in Section **3.4** had an estimated V_{50} of 632 ms^{-1} which corresponds to an energy capability against the AP ammunition used of 799J.

Hybrid #1:

Front surface - 300gsm S2/Vinylester

Rear surface - 830gsm S2/Vinylester

Resultant areal density: 74.kgm^{-2}

This configuration was chosen as previous testing had indicated the medium weave material performed well against AP ammunition and the heavy weave material well against a more deformable projectile. It was hoped that by the time the projectile reached the rear surface it would be sufficiently slowed and damaged that accompanied by bulk material deformation the rear surface would act as if under a blunt impact and absorb energy through deformation and delamination. The intention was that this material would have a higher V_{50} than equivalent double thickness targets of each of the constituent materials.

The second hybrid target tested in Section **3.4** had an estimated V_{50} of 605 ms^{-1} which corresponds to an energy capability against the AP ammunition used of 732J.

Hybrid #2:

Front surface - 20mm unknown CFRP

Rear surface - 830gsm S2/Vinylester

Resultant areal density: 61.15kgm^{-2}

This configuration was trialled as mechanical testing had indicated that the medium weave material which has performed well against AP ammunition is hard to indent. As a result a material which was even harder to indent was chosen, the CFRP panel was available for testing and was used as such. The intention was to increase the indentation resistance of the front face and thus observe the resultant effect on ballistic performance. The rear surface was chosen for the same reasons as Hybrid #1.

The results are as follows, material constraints did not allow for complete V_{50}'s to be obtained however the error bars indicate the range of values in between which the V_{50} is expected.

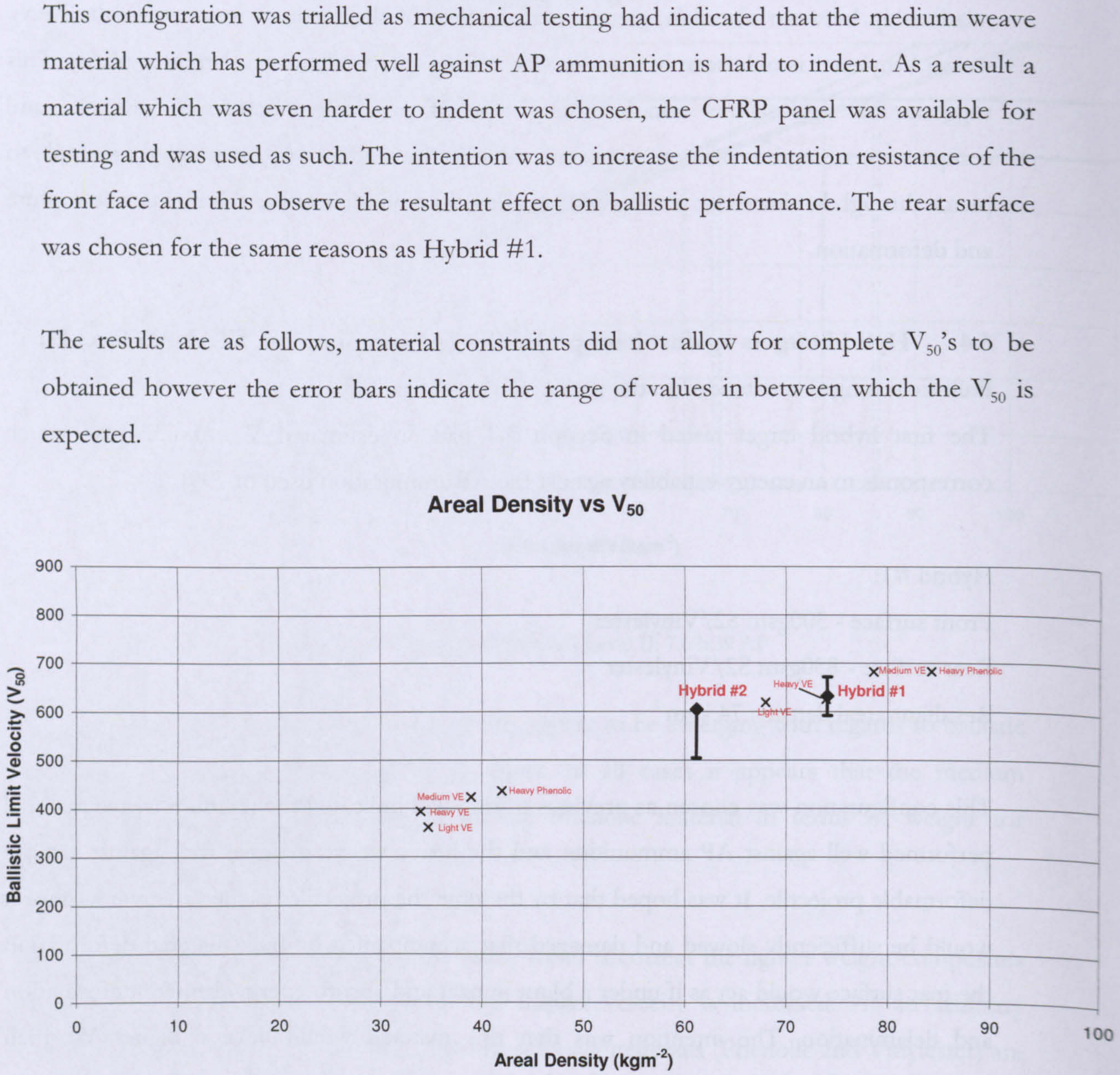

Graph 6.5: Performance of Hybrid materials #1 & #2 relative to other materials tested (7.62x39 AP)

The 'Hybrid #1' material was approximately the same areal density as the all heavy weave target and around 5 kgm^{-2} lighter than the all medium weave target material. However the resultant performance was worse than expected, the material appearing to have a V_{50} very close to the heavy weave material. This suggests that the delamination mechanisms alone may not be as important as initially anticipated, as by adding a material with a tendency to delaminate to a material which exhibits much damage in the front surface region has reduced ballistic performance (over an equivalent target of entirely 'front surface' material) and vice versa

It was noted that the target used was too small and delaminations in the rear material ran out to the surfaces this may have adversely affected performance. Additionally the small size resulted in a far greater degree of restraint between front and rear faces being imposed by the clamps when compared to the larger targets tested.

6.5 Damage Investigation

The amount of damage an impact caused to the test materials was also investigated. An ideal test would be a 'Compression after impact' test in which a impacted sample is crushed in a compression machine, the more damage the weaker the buckling strength of the panel. This was not possible, the physical thickness and strength of these panels even the most powerful machines available (used for crushing concrete blocks) did not have a high enough capacity and suitable data logging.

Visible damage was less easily assessable for the Phenolic panel due to the opacity of the resin. The front surface is similar for both Ball and AP ammunition. Of all panels the medium weight material appears to have the greatest amount of damage visible on the surface.

It can be seen from the following Graphs (6.6& 6.7) that the visible damage on the front surface is similar for both Ball and AP ammunition. It is interesting to note that the medium weave material appears to have the greatest damage visible on the surface. Against AP ammunition the rear surface damage can be seen to follow the same trend as the front surface damage but at higher values. Against AP ammunition however damage is worse in the medium weave panel (which performs well for its weight).

Against soft, deformable Ball ammunition it can be seen how the spreading of the projectile and thus the impact loading over a wide area drastically increases the rear surface damage as

the projectile is caught by delamination failure and deformation of laminates. It should be noted that the data for damage was averaged across the V_{50} shots. Whilst the heavy weave material had the highest rear surface damage area against ball ammunition it also was stopping these projectiles at the highest velocity of all the panels evaluated therefore a greater damage area would be expected. The charts plot damage in terms of V_{50} and indicate that against the more damaging ball ammunition the heavy weave material suffers more rear surface damage and less front surface damage than the medium weight material with a similar V_{50}.

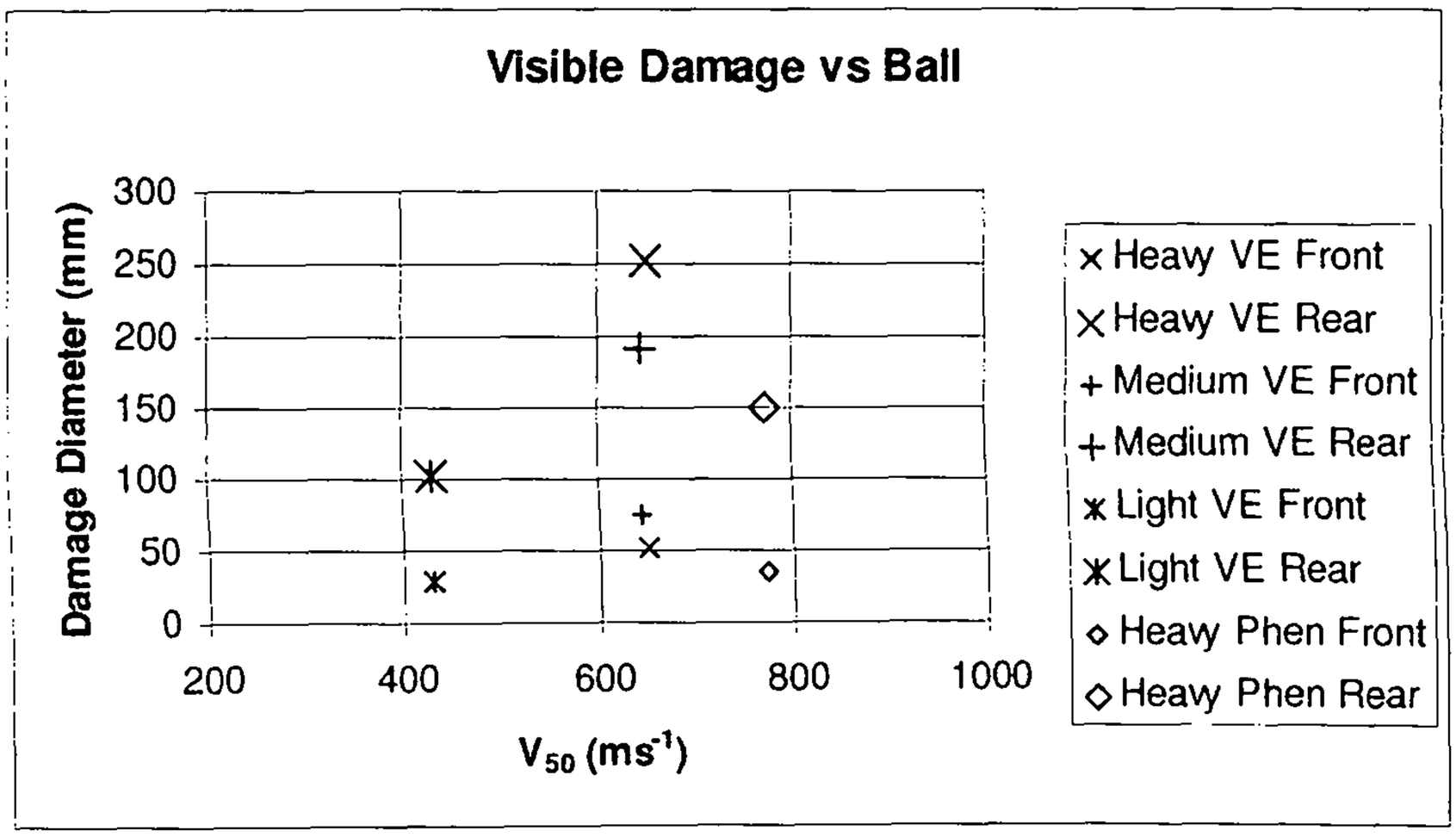

Graphs 6.6: Visible damage vs V_{50} 7.62mm Ball (lower values are for front face)

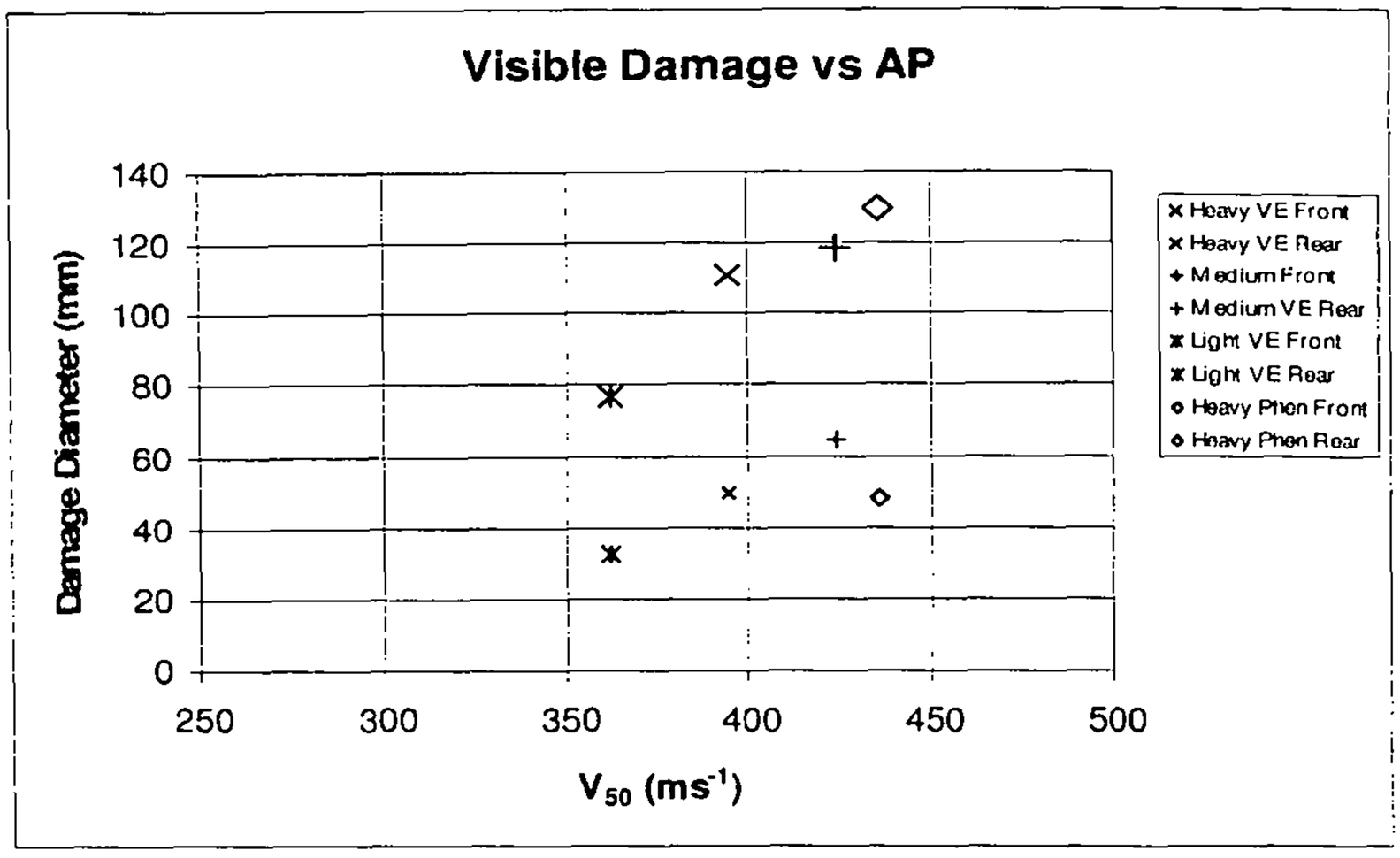

Graphs 6.7: Visible damage vs V_{50} 7.62mm AP (lower values are for front face)

The damage on the exit face of all materials was low due to the jacket and gilding metal of the bullet remaining embedded within the panel and only the armour piercing core exiting

the panel. The damage trends seem to be concurrent with ballistic performance trends i.e. the materials with larger amounts of visible damage appear to have higher V_{50} values.

The amount of visible rear face damage sustained by these materials increases with reinforcement weave weight, whilst on the front face it peaks with the medium weight material. The exit damage observed in perforated panels was low for the heavy weave materials, the medium and light weave reinforced materials tore over a significant area and ejected debris.

The effect of weave weight on damage was assessed. Against Ball ammunition it is noted that whilst the medium Vinylester panel is only marginally poorer ballistically it is far heavier than the heavy weave Vinylester panel. The light weave panel is even worse ballistically though has a comparable weight to the heavy weave material.

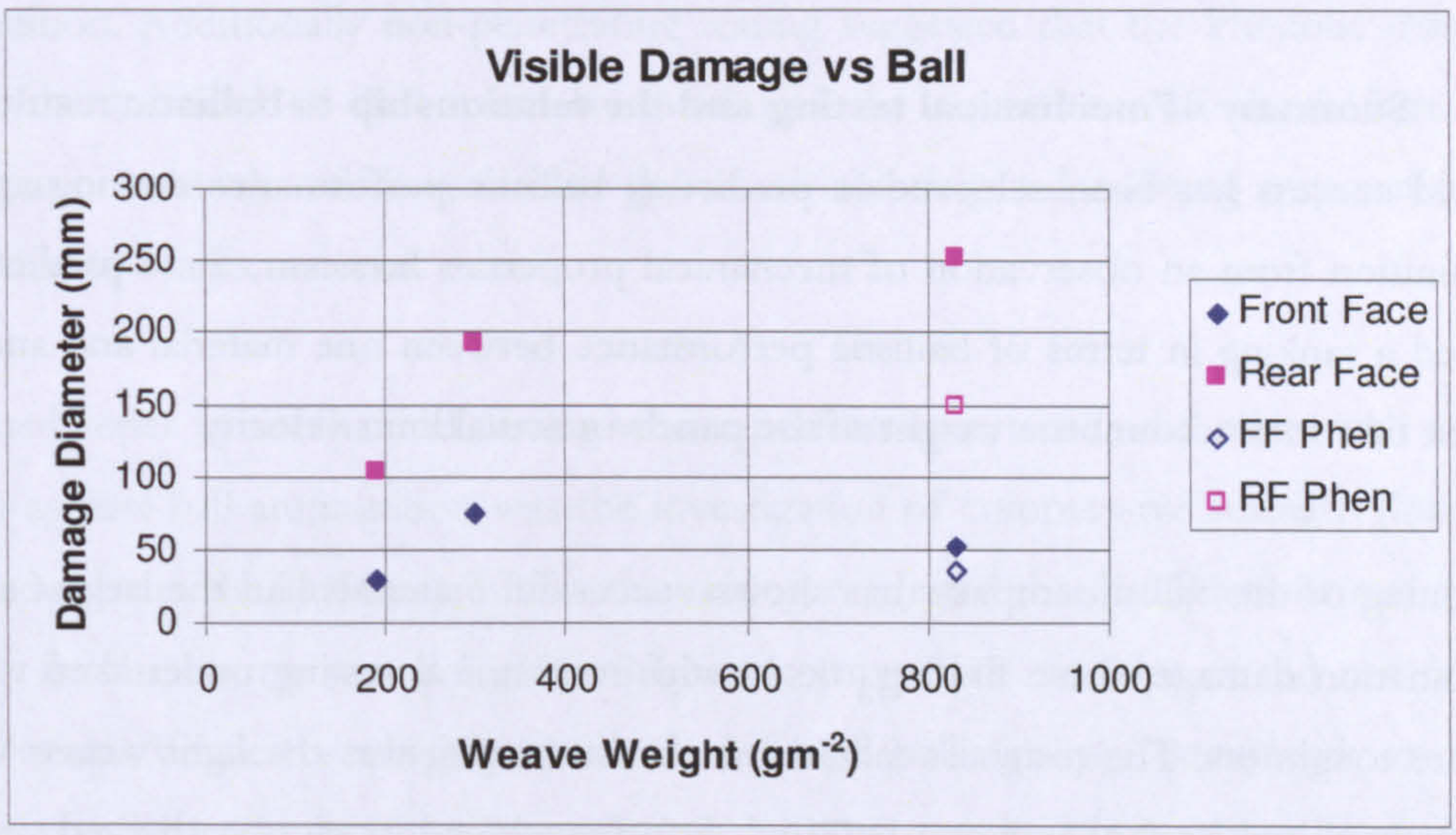

Graphs 6.8: Visible damage vs weave weight 7.62mm Ball (lower values are for front face)

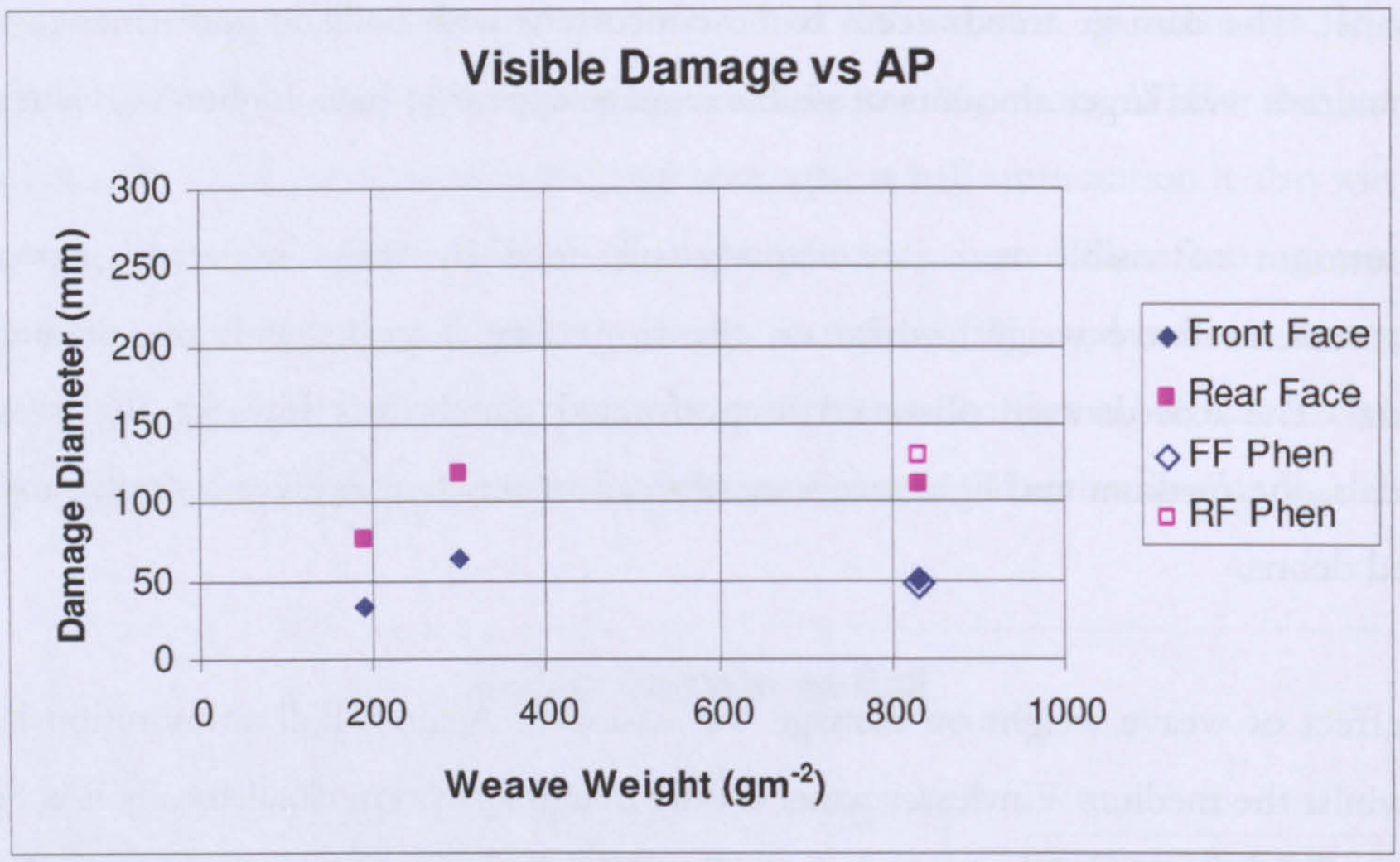

Graphs 6.9: Visible damage vs weave weight 7.62mm AP (lower values are for front face)

6.6 Summary of mechanical testing and the relationship to ballistic results

Limited success has been achieved in predicting ballistic performance ranking against ball ammunition from an observation of mechanical properties however, these predictions only enabled a ranking in terms of ballistic performance between one material and another and did not take into account the weight of the panels or actual limit velocity.

Sectioning of the ballistic impacts has shown successful materials had the largest amount of delamination damage, these findings tie in with mechanical testing undertaken to evaluate fracture toughness. The toughest material from this testing was the light weave Vinylester, this material had by far the worst ballistic performance and in section showed very limited delamination damage, this backs up the supposition that fracture toughness is vitally important to ballistic performance and that better performing materials appear to have low toughness values. This is especially important in the defeat of soft projectiles.

High fracture toughness implies a lot of energy is needed to open a crack, this is only possible if the tensile strength of the laminate is sufficient to resist the loads which result in crack opening. In the case of the light weave material lowest tensile strength and highest toughness combined to result in poor performance whilst the heavy weave material with the lowest toughness and far higher tensile strength performed better. The deformed laminates were able to hold the projectile for longer before tensile failure, thus allowing a greater

through-thickness (equivalent to crack opening) displacement and as a result a longer crack length.

Adding the findings of bending resistance to this problem suggests that one of the reasons for the Phenolic materials better performance over the equivalent VE material (despite the VE materials tensile strength) was due to its far lower bending stiffness. This means that it is far easier to deform delaminated material and transfer projectile energy to tensile strain energy. The VE material may simply not deform quickly enough to allow this to take place before local stresses fail the fibres.

The results of penetration resistance testing by the impact of a blunt cylindrical impacter matches the trends seen in ballistic testing quite well, certainly at higher indentation energies the droptower rankings bear striking similarities to the ballistic performance rankings of ball ammunition. Additionally non-penetrating testing suggested that the Phenolic material was by far the 'hardest' of the materials tested and the equivalent VE the softest. This in combination with the stiffness already discussed is anticipated as being responsible for the performance of this material.

A related series of mechanical testing whose performance trends did relate well to ballistic testing against ball ammunition was the investigation of compressive strength (load applied perpendicular to the laminate). Whilst this testing suggested that the Phenolic material tested was by far the strongest and had the highest compressive modulus, it did not favour the heavy weave Vinylester which performed very well ballistically. Concurrently compressive loading parallel to the laminate plane found the heavy weave Vinylester to be the strongest and stiffest whilst the equivalent Phenolic material was the least strong and of the least stiff. Despite this the Phenolic material had the highest V_{50} against this type of ammunition.

6.7 Behind armour effects

As discussed in Chapter 2 spall refers to the debris ejected behind an armour when it is perforated. Metallic armours suffer badly for this and often require a composite spall liner to catch this debris as composite materials in general have very good spall characteristics.

Image 6.1: spall of aluminium

Out of the materials tested there were two very distinct forms of failure of perforated armours. The heavy weight weave materials experienced very little damage, a small tuft of fibres a few calibres in diameter was torn out of the bulk of the armour. The lighter weight materials failed in a more dramatic fashion, they tore in the *x* and *y* planes and folded open over a large area ejecting debris and bullet fragments. This debris is still far more benign than spall from a metallic armour.

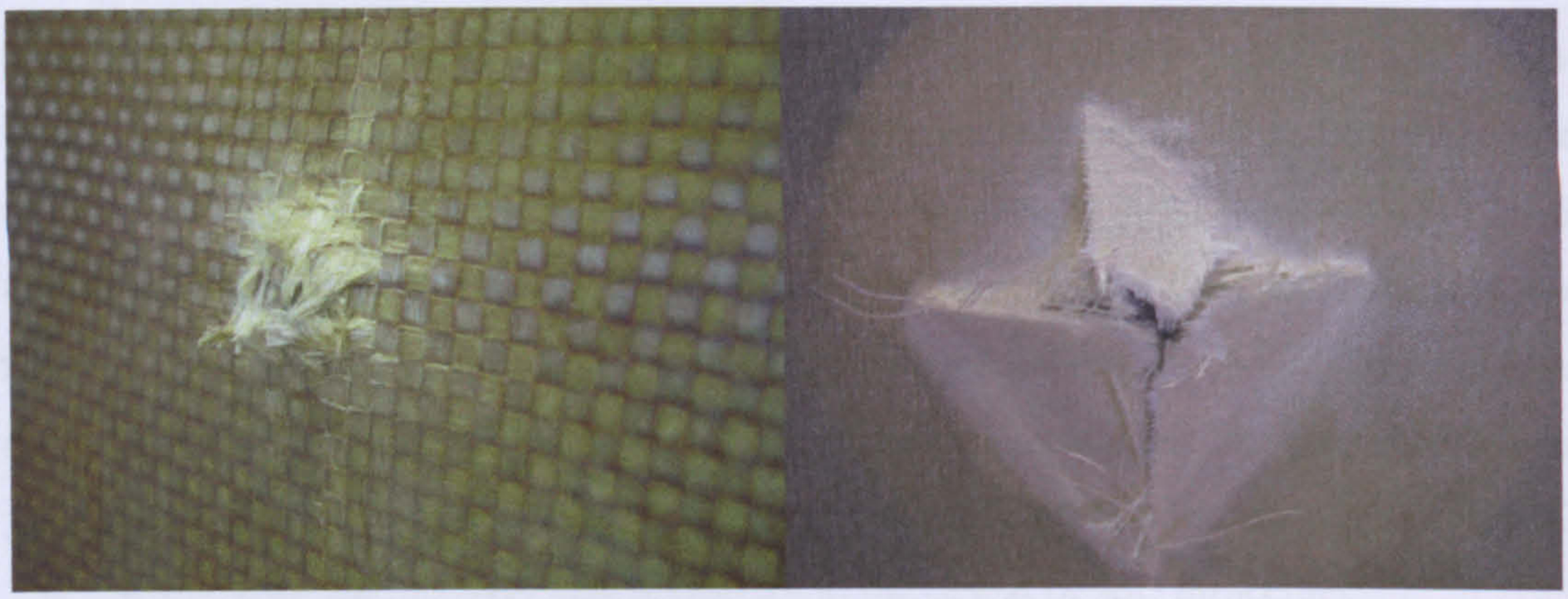

Image 6.2: Rear surface damage of heavy (left) and light (right) weave materials (different magnifications)

The material which generated the greatest amount of spall debris when perforated by damaging ball ammunition was the medium weave Vinylester material, as can be seen from the high speed video stills in Image 6.3 that the amount of spall is still remarkably small.

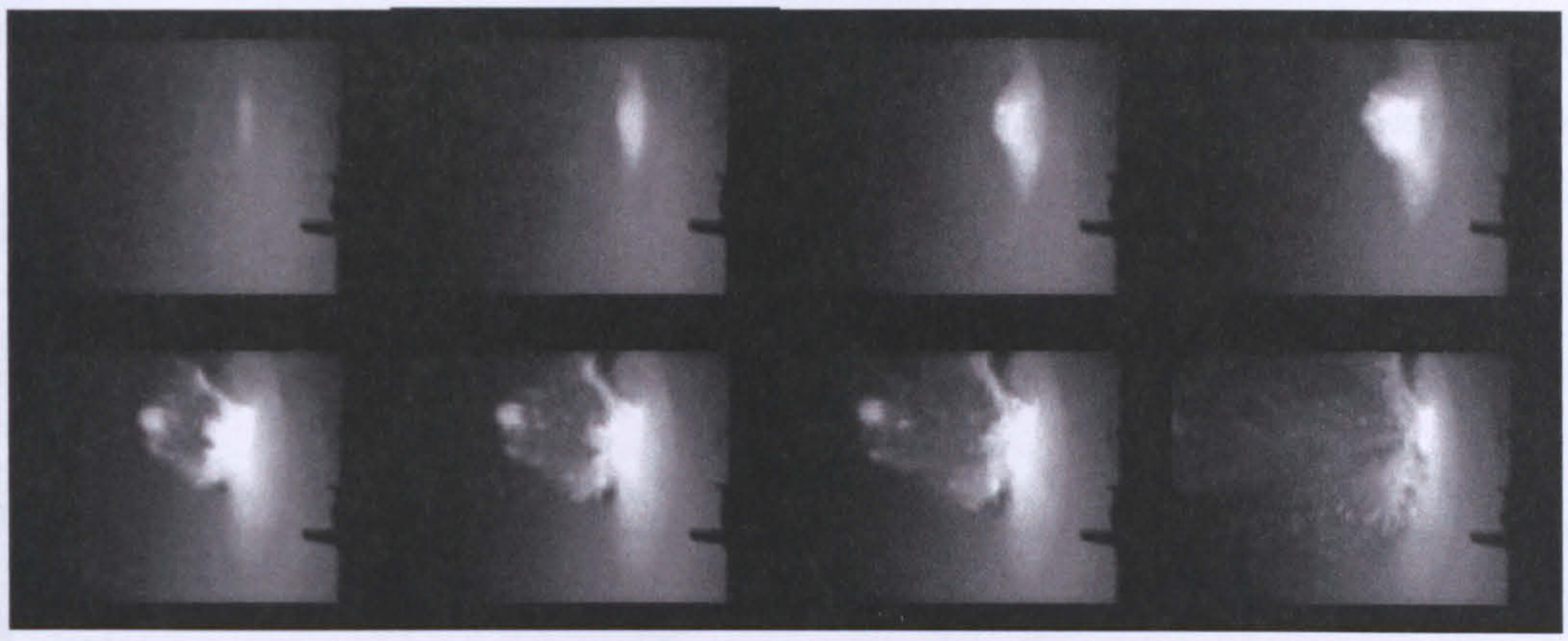

Image 6.3: High speed camera stills of a light weave Vinylester material being perforated by 7.62 ball

6.8 A model to predict ballistic limit velocity

As a result of the mechanical testing carried out to characterise the materials tested it is possible to further evaluate the damage observed in sections of ballistic impacts.

By identifying individual failure modes and applying standard formulae for these failures it will be possible to calculate the energy absorbed (by each individual mechanism) in the damage process. By evaluating the observed damage in this way it will be possible to identify significant mechanical properties and to evaluate the effect of ballistic performance of mechanical changes.

As a result of these trials and based on observations from impact sectioning it is hypothesized that the main mechanisms involved in defeating a soft, deformable projectile are as follows:

On the front face of the armour energy is absorbed via, compressive strength and indentation resistance, friction between projectile and the material will also be responsible for some energy absorption. On the rear surface, energy is absorbed through Mode I fracture (delamination), bending of delaminated plies and subsequent tensile loading of fibres.

This hypothesis is based on the observations that when a projectile is successfully stopped, large amounts of delamination are observed along with significant material deformation. The failure of this deforming material which has delaminated from the bulk of the armour appears to be due to tensile rupture (not always directly below the broken up projectile) after bending loading and not by a ductile penetration mechanism. The front surface of impacted

targets show significant plastic deformation of material and radial displacement of material away from the bullet path. This the initial impact phase which includes projectile break-up must involve indentation resistance / compressive strength mechanism the effectiveness of which will significantly contribute to the eventual defeat of the projectile (the more broken up and deformed the projectile, the better).

Against hard cored AP ammunition it is anticipated that the same properties will be of importance though in different proportions.

To develop a model which can be used for a range of hypothetical materials based on a small amount of testing a method of predicting damage is first required. Once the damage morphology can be estimated the energy absorbed by the various failure modes assumed to be present can be calculated and thus summed to give a value of maximum energy absorption thus allowing a V_{50} for a projectile to be calculated.

6.9 Modelling impact damage; Gellert analysis

As discussed in section **2.12.2** work by Gellert et al[45] has linked perforation energy to a defined damage geometry, for low thicknesses / grossly over matched targets projectile energy is absorbed at a lower rate (Joules per mm of thickness) than that for thicker targets. Gellert [45] defined a bi-linear energy/thickness trend and linked each portion of the trend to a certain type of damage geometry. Thin targets when sectioned were shown to have damage in the form of a cone expanding in diameter from front surface to the rear. Thick targets were shown to have a waisted 'hourglass' shape.

By testing a third thickness of medium weave VE material confirmation of the Gellert [45] bi-linear perforation energy / thickness relationship discussed in section **2.12.2** has been possible. Plotting penetration energy based on core weight alone (4.04g) results in the following graph (the treble thickness V_{50} value is estimated based on testing carried out, see section **3.3.7**).

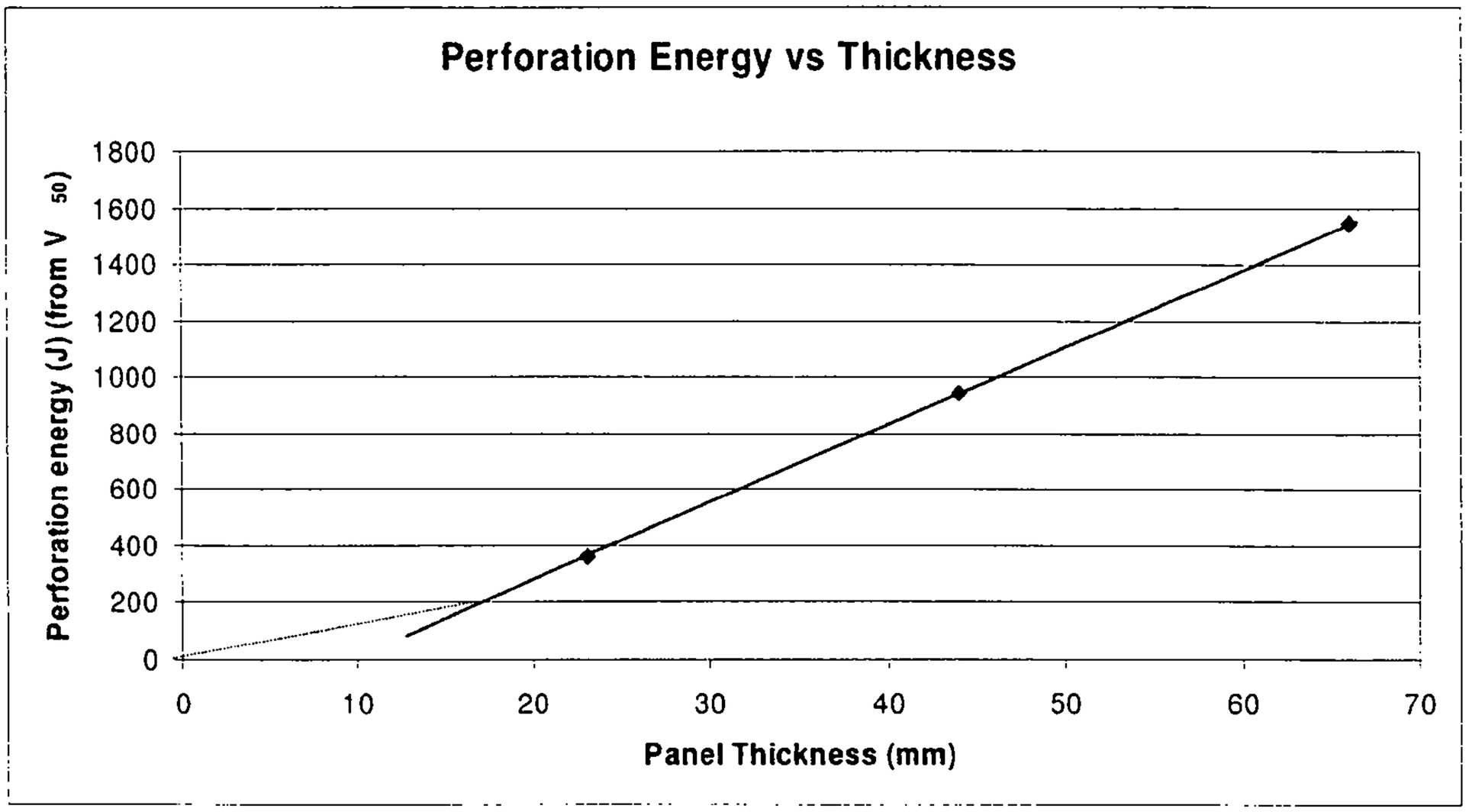

Graph 6.10: Confirmation of Gellert[45] relationship using existing and predicted data

The data on its own does not exhibit a bi-linear relationship, it is highly likely that sufficiently thin materials have not been tested (sectioning and damage observation confirm this). A bi-linear relationship must however exist for perforation energies at low material thicknesses, as a simple linear fit through the existing data would otherwise suggest a zero penetration energy at thickness less than around 10mm. A suggested definition of 'thin' in the data is expressed with the dotted line in the Graph 6.10. It must be noted however that the definition of 'thin' may be closely related to projectile properties and impact velocity and as such may vary dependent on these variables.

The first step in producing any model which might link mechanical properties to ballistic performance is the definition of the physical dimensions of the damage. The confirmation of similar energy behaviour to that found by Gellert leads to confidence in the use of the damage geometry system proposed by the same author.

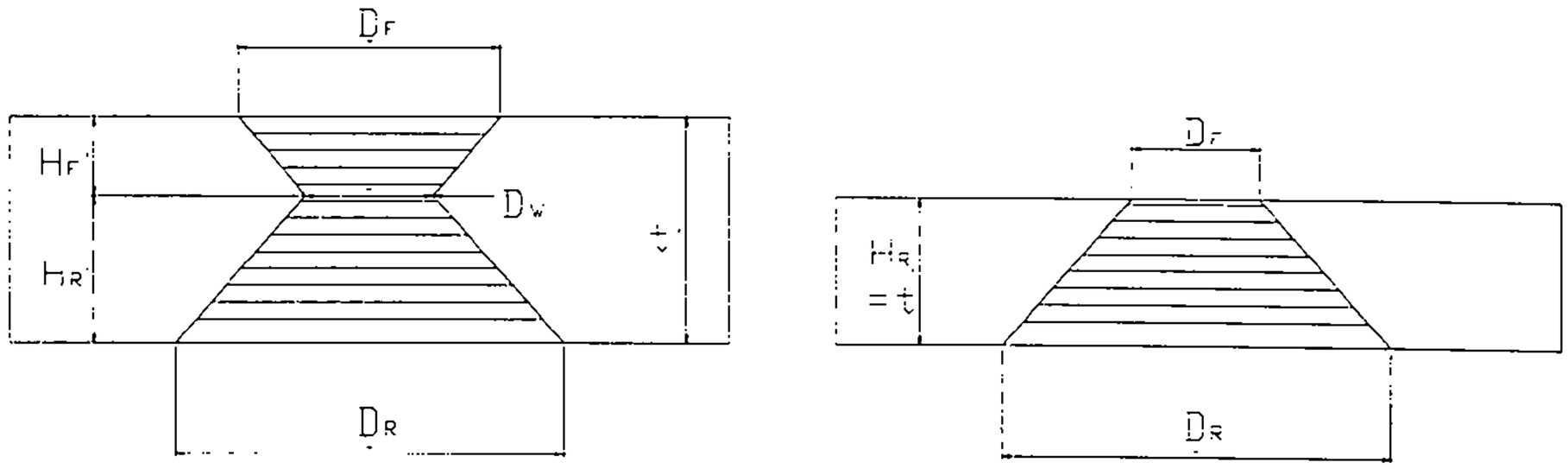

Figure 6.1: Gellert 'hourglass' geometry definitions for 'thick' and 'thin' materials[38]

The following tables record the geometric parameters observed in sections of ballistic impacts against Ball and AP ammunition. The sections have been from shots either side of the V_{50} velocity and have been averaged to give a V_{50} damage geometry.

Dimensions						
	T	**H_R**	**D_F**	**D_W**	**D_R**	**t/H_R**
Heavy Phenolic	21	13	36	30	150	1.62
Heavy VE	21	14	51.3	39	252	1.50
Medium VE	23	14	74.6	27.5	192	1.64
Light VE	21	16	28.2	25	103	1.31

Table 6.4: Damage geometry against Ball ammunition

Dimensions	T	H_R	D_F	D_W	D_R	t/H_R
Heavy Phenolic	21	13	48	21	130	1.62
Heavy VE	21	13	50	37.5	111	1.62
Medium VE	23	18.5	64.4	30	119	1.24
Light VE	21	13	32.8	24	76.5	1.62
Heavy Phenolic	42					
Heavy VE	42	28	56.3	30.5	96.3	1.50
Medium VE	46	26	56.7	35	131.7	1.77
Light VE	42	21	45	12.5	75.3	2.00
Medium VE	66	46	73	35	150	1.43

Table 6.5: Damage geometry against AP ammunition

From these values a graphical representation of their change with material thickness can be made such that the damage sustained by a V_{50} impact of a similar material can be estimated for a range of thicknesses.

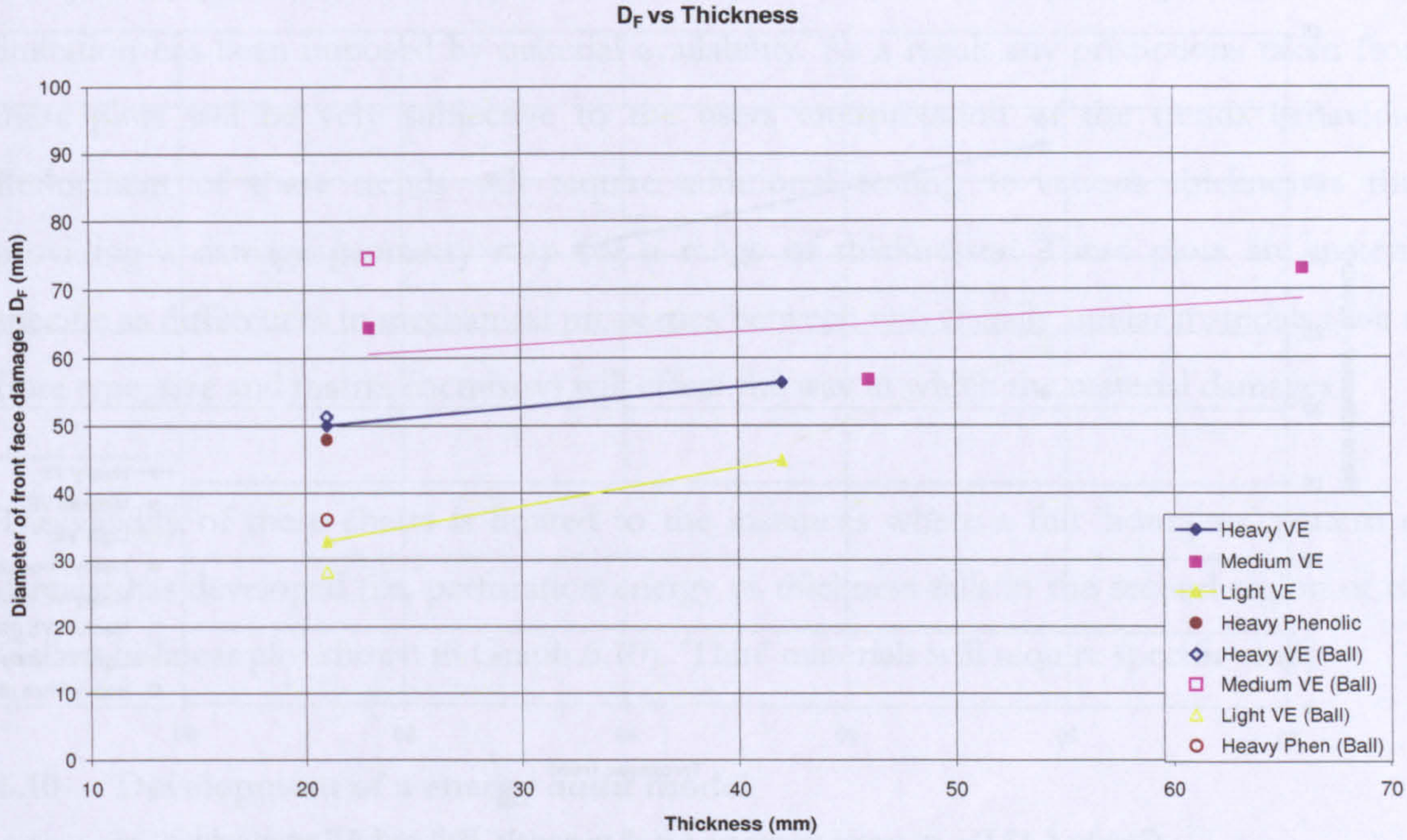

Graphs 6.11: D_F vs target thickness for all materials, Ball and AP ammunition

Graphs 6.12: D_R vs target thickness for all materials, Ball and AP ammunition

Graphs 6.13 D_W vs target thickness for all materials, Ball and AP ammunition

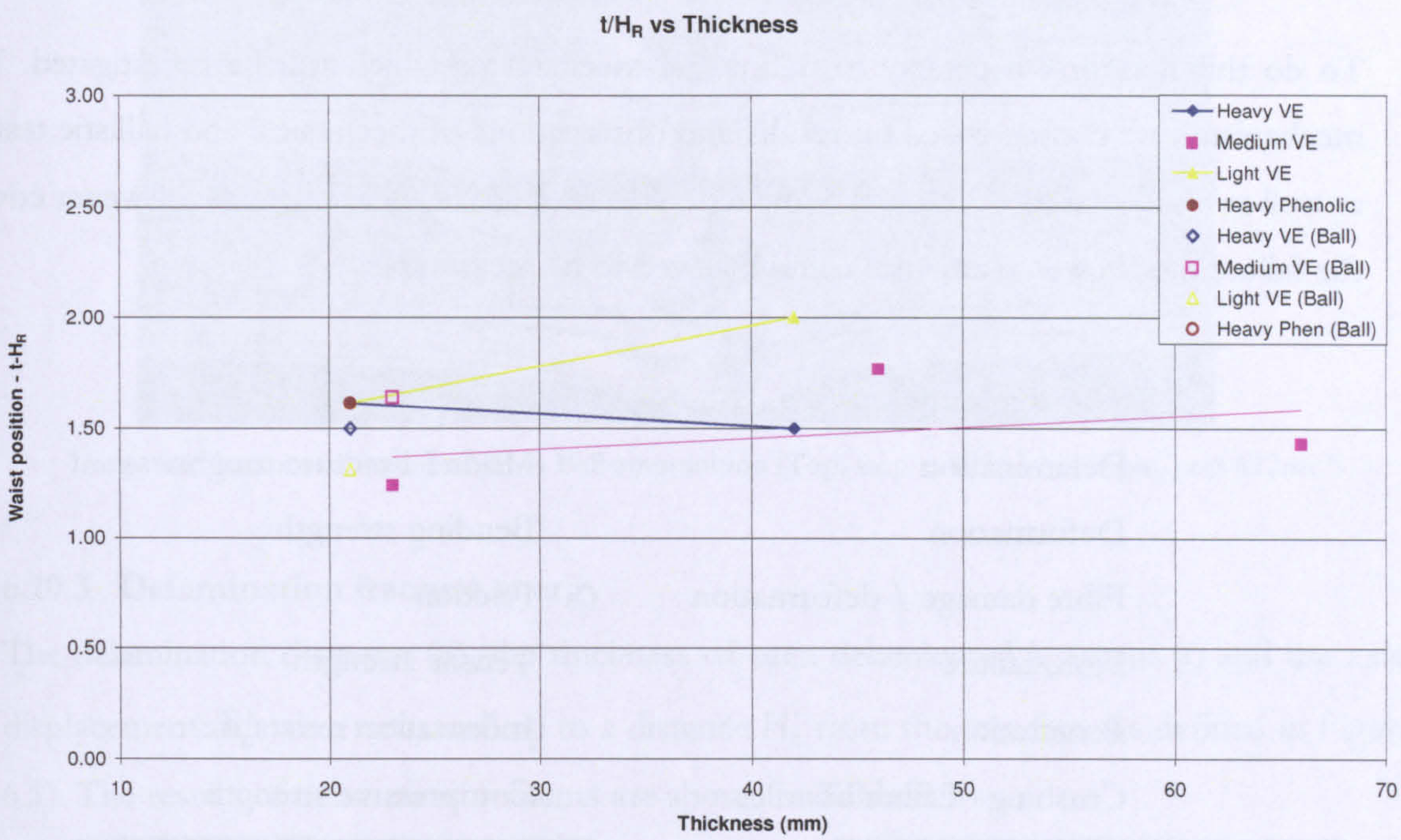

Graphs 6.14: t/H_R vs target thickness for all materials, Ball and AP ammunition

The preceding charts are based on at the very most, three data points per material, this limitation has been imposed by material availability. As a result any predictions taken from these plots will be very subjective to the users interpretation of the trends behaviour. Refinement of these trends will require additional testing at various thicknesses thus providing a damage geometry map for a range of thicknesses. These plots are material specific as differences in mechanical properties between two visually similar materials (due to fibre type, size and matrix chemistry) will effect the way in which the material damages.

The validity of these charts is limited to the instances where a full 'hourglass' pattern of damage has developed (i.e. perforation energy vs thickness falls in the second region of the Gellert bi-linear plot shown in Graph 6.10). 'Thin' materials will require specific study.

6.10 Development of a energy audit model

6.10.1 Defining mechanisms

Based on the successful identification of material properties which appear to have an effect on ballistic performance, as well as the development of method to estimate the extent and geometry of damage for various material thicknesses, a simple energy audit model can be developed. This model shall attempt to link the energy required to create the observed post-impact damage with the kinetic energy of the projectile which caused the damage.

To do this it is first necessary to define the mechanisms which will be investigated. The mechanisms are chosen based on results and observations of mechanical and ballistic testing as well as observations of sectioned impacts. This may not be a definitive list however covers the failure modes which are visible and believed to be measurable.

Damage mechanism	*Mechanical property*
Delamination	Mode I Fracture toughness
Deformation	Bending strength
Fibre damage / deformation	Friction
Fibre failure	Tensile strength
Penetration	Indentation resistance
Crushing of fibre bundles	Compressive strength

The following text will follow the development of a model for the medium weave material against ball ammunition. The same process was followed for all materials and against both ball and AP ammunition.

Using the formulae defined in previous chapters to deal with each individual mechanical property the energy required to produce the damage observed in material sections (section **3.6**) will be calculated. Once all the individual components have been evaluated they will be summed to produce a value of energy absorbed by observed physical damage. This value can then be compared to the projectile impact energy. A successful audit of damage will mean that the sum of damage energy will be equivalent to projectile impact energy for a successful stop and less than projectile impact energy for a successful perforation.

6.10.2 Model for medium weave VE against Ball ammunition

The results of impacts just above and just below the V_{50} velocity are shown in Image 3.16 which is repeated below for reference:

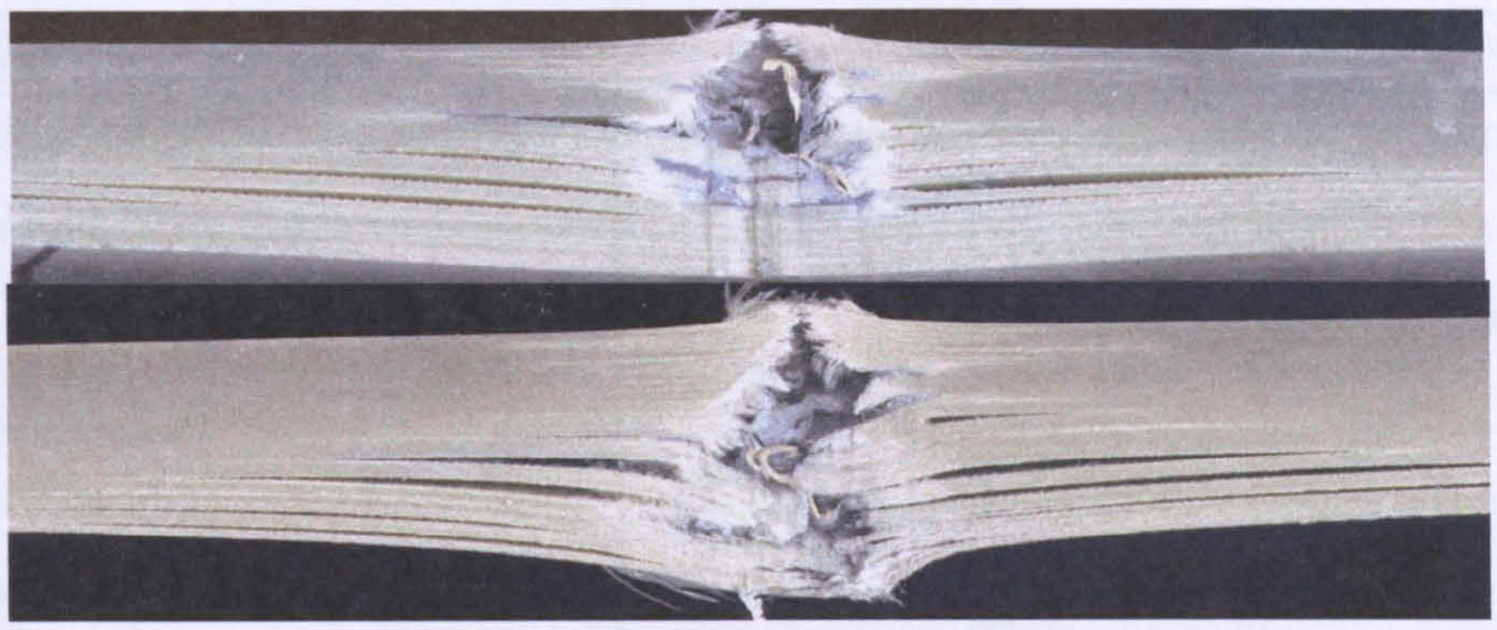

Image 6.4: Sections of medium VE vs Ball ammunition (Top, stop at 625ms^{-1}, bottom, perf 622ms^{-1})

6.10.3 Delamination fracture energy

The delamination diameter (d), the thickness of each delaminated ligament (t) and the axial displacement (δ_z) were measured up to a distance H_R from the rear face (as defined in Figure 6.1). The results of these measurements are shown in Table 6.5.

Perforation @ 625ms^{-1}		
r	*t*	δ_z
120	1	8.00
115	1.5	10.00
98	1	9.00
98	1.5	8.50
86	1.75	8.00
73	2	4.00
50	2.5	2.00
22	1.5	0.50
19	1.5	0.50
32	1.5	
25	1.5	
25	1.5	
37	1.5	
35	1.5	
35	1.5	

Stop @ 622 ms^{-1}		
r	*t*	δ_z
110	2.5	4.00
110	1.5	4.00
110	1.5	4.00
110	1	4.00
116	1.5	3.00
106	1.5	3.00
100	1.5	3.00
87	1.5	1.50
52	1.5	1.00
35	1.5	1.00
44	1.5	
36	1.5	
26	1.5	
36	1.5	
44	1.5	

Table 6.6: Fracture geometry

By assuming the delaminations were perfectly circular the area of each individual delamination could be calculated. This may not be a valid way to deal with crack opening as the following calculations are based on a straight crack progressing through a rectangular beam rather than a circular crack growing from a central point however, for the first iteration of this model it is a good approximation.

The areas of each individual delamination were summed to give a total delaminated area. Multiplying this area by the previously derived Mode I crack opening energy (G_{Ic}) (from equation *5.2*) for the material gives the energy (J) required to cause an equivalent crack of such an area through Mode I loading.

As previously discussed Mode I fracture toughness was evaluated in preference to Mode II due to it being less complicated to test and analyse. This ease of testing allowed dynamic toughness values to be obtained which are of more relevance to ballistic impact work than quasi-static values. It has been noted however that Mode I toughness generally has a lower value than those obtained through other modes, this may have an effect of the final performance of the model.

Whilst the visible delaminations could be easily measured and recorded there is a large area of damaged material (visible in sections as a pale area), whilst there are no delaminations visible to the eye other than those already recorded, it is possible that the damaged area also contains delamination cracks which have not been opened sufficiently to be visible to the eye.

To account for this an assumption was made that every ply in the damaged region was in fact delaminated. The required energy required to produce such damage was calculated as before. Both values for delamination energy were then compared to the ballistic energy (calculated from the standard formula for kinetic energy Equation *6.1*) as a percentage, the results are illustrated in Table 6.6.

$$KE = \frac{1}{2}mv^2$$

Where:

KE = Kinetic energy (J)

m = Projectile mass (Kg)

v = Projectile velocity (ms^{-1})

Equation 6.1: Standard Equation of Kinetic Energy

Perforation @ 625ms^{-1}	
Ballistic energy (J)	1884.77
Delaminated	
Area (m^2) Vis	0.217
Energy required (J)	65.03
Proportion (%)	**3.45**
Delaminated	
Area (m^2) max	0.767
Energy required (J)	229.76
Proportion (%)	**12.19**

Stop @ 622 ms^{-1}	
Ballistic energy (J)	1866.72
Delaminated	
Area (m^2) Vis	0.319
Energy required (J)	95.88
Proportion (%)	**5.14**
Delaminated	
Area (m^2) max	1.15
Energy required (J)	345.16
Proportion (%)	**18.49**

Table 6.7: Proportion of projectile energy absorbed by delamination (visible and max possible)

6.10.4 Deformation energy

Measurement of the through thickness displacement (δ) was carried out on sectioned impacts and is recorded in Table 6.6. The definition of the bending deflection was not straightforward due to the significant local deformation of failed plies close to the projectile path (this was especially the case when observing ligament deflection in materials struck by AP ammunition). The deformation recorded was that described by a constant radius of bending thus discounting the very localised bending due to projectile effects. See Figure 6.2 below.

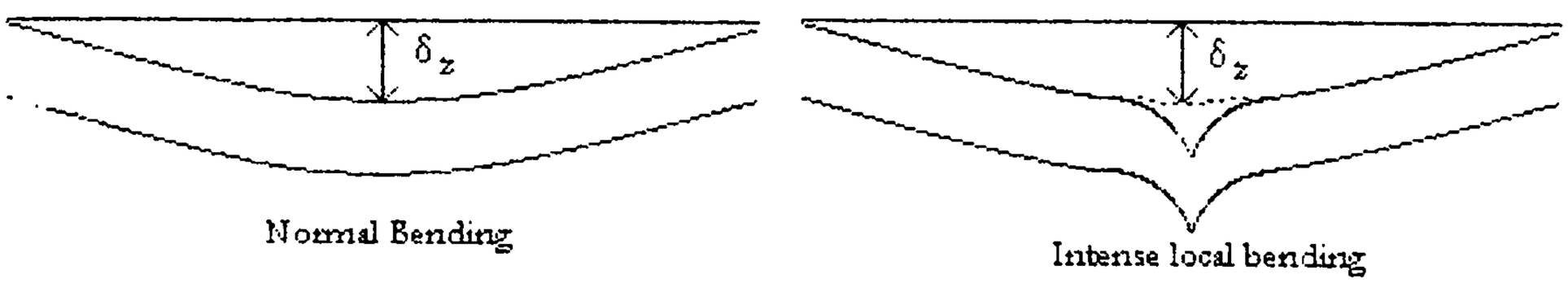

Figure 6.2: Definition of through thickness deformation (δ_z) for laminates

It is important to note that these values of bending are measured from the permanent plastic deformation observed in sections of ballistic impacts rather than the instantaneous dynamic deflection observed in high speed film. This is for two reasons, firstly there is insufficient film footage to allow measurement of the dynamic deflection and secondly that the dynamic motion of the delaminated ligaments depends on their kinetic energy. This energy can only be estimated as the velocity of the moving ligaments is only measurable (Via dedicated high speed filming) for the rearmost face of the target. As such this effect will not be dealt with in this iteration of energy model.

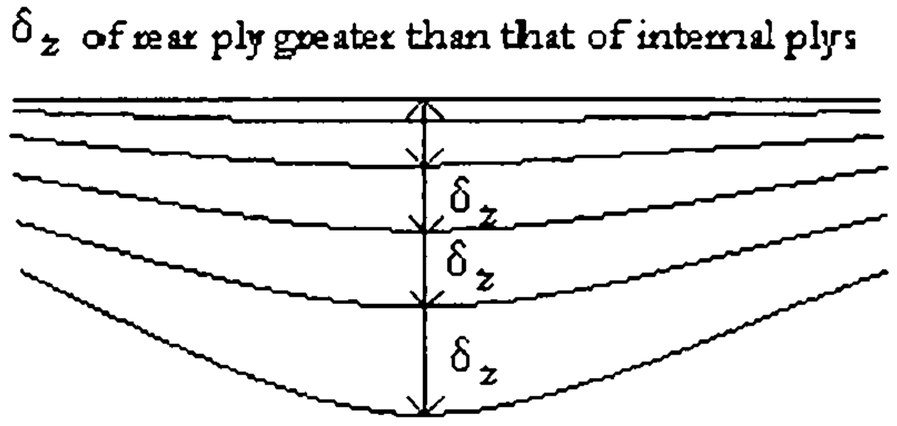

Figure 6.3: Definition of through thickness deformation (δ_z) for instantaneous bending

To calculate the energy required to produce the bending deflection work by Jones and Slater [55] (who treated bending in the manner discussed in section **5.2.2)** resulted in the use of Equation *5.6* to first calculate the flexural rigidity of a circular membrane from recorded membrane size, thickness and displacement data. This value for rigidity is then used in Equation *5.7* to calculate the bending energy. The contribution of bending energy to the arrest of the projectile was for both cases (perforation and penetration) a very small percentage as can be seen in the following table.

In an attempt to evaluate instantaneous bending energy high speed film was used to roughly estimate the instantaneous bending deflection on the rear face. Applying the estimated difference in δ_z between the instantaneous and final values to existing data gave the following results:

Perforation @ 625ms^{-1}	
Ballistic energy (J)	1884.77
Final deformation	
Bending energy (J)	10.42
Proportion (%)	**0.55**
Instantaneous deformation est	
Bending energy (J)	76.47
Proportion (%)	**4.06**

Stop @ 622 ms^{-1}	
Ballistic energy (J)	1866.72
Final deformation	
Bending energy (J)	2.8
Proportion (%)	**0.15**
Instantaneous deformation est	
Bending energy (J)	25.63
Proportion (%)	**1.67**

Table 6.8: Estimated proportion of projectile energy absorbed through permanent and instantaneous bending

Despite the difference between these values and those based on final displacement values the overall percentage contribution to the projectile defeat is small. As a result of this the intrinsic error present when final values are used is not of great significance. Additionally the approach to membrane bending in the literature has dealt with a single membrane rather

than a delaminated series of membranes. The treatment of individual delaminated plies and the summation of the resultant bending energies may not be entirely valid as it ignores any interaction effects between laminates.

Equation *5.7* as proposed by Jones and Slater is not supported with a full derivation and as such should be used with caution.

6.10.5 Friction energy

Friction is present during the interaction of all forms of indenters and target materials, it is simply the energy required to push the projectile through the crater created by ductile hole expansion or plugging[69]

The effects of friction are expected to be important for both ammunitions, however due to the nature of penetration of AP ammunition (continuous indentation of a pointed, non-deformable indenter) it is estimated that the importance of friction will be greater than for ball. Investigations of recovered AP cores suggest that very significant loading is placed on the surface of the indenter. The extremely hard cores (900Hv) displayed significant amounts of scratching concurrent with the spinning projectile passing through the target. These scratches would have required a significant surface pressure to be caused by a soft polymer composite.

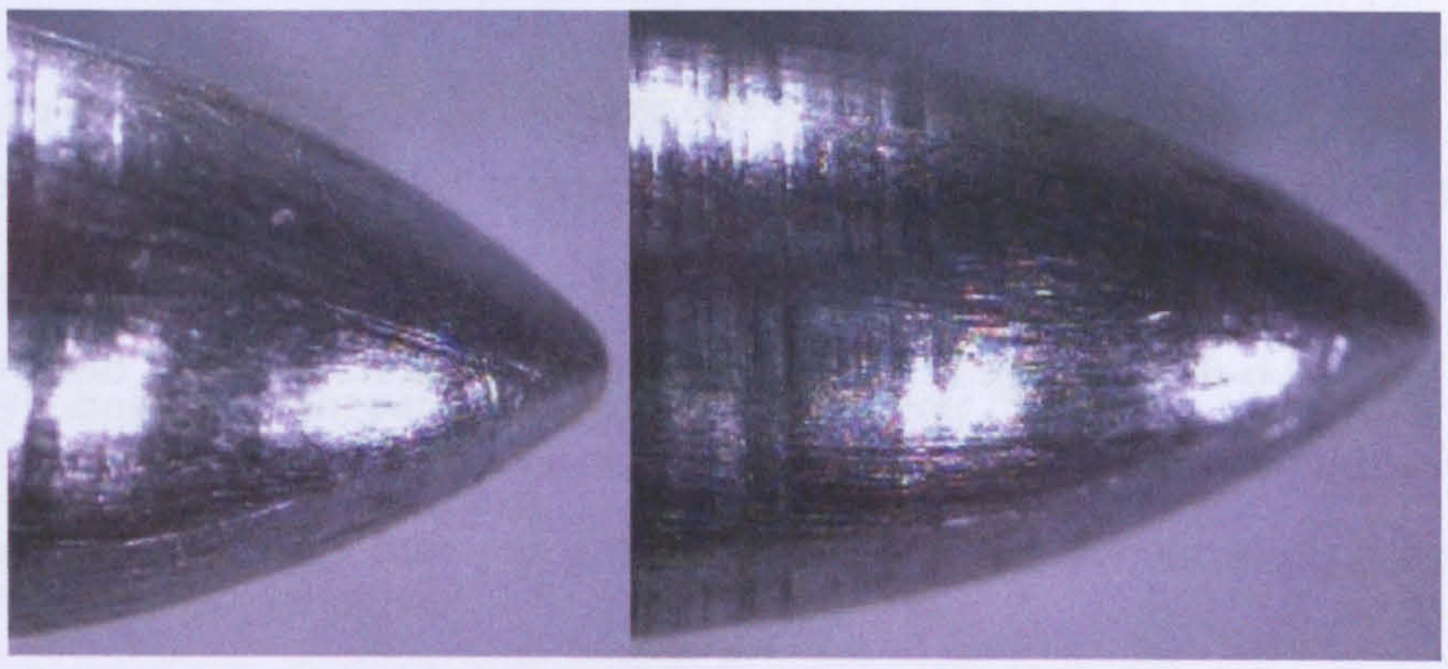

Image 6.5: Damage to recovered cores

From indentation testing (Section **4.7.2**) values for coefficient of friction (μ) have been calculated. It was not possible to check these values against literature data as it not available for the materials being tested. As a result the values of μ should be treated with caution, that is not to say however that an attempt to use them to evaluate friction energy should be ignored.

Indentation testing has provided two values for μ, these were generated by 'dry' indentation (steel indenter against composite) and 'wet' indentation using a dry PTFE lubricant, both values will be evaluated as whilst the indention is essentially 'dry' dynamic effects (such as fibre melting for instance) could contribute to a lower coefficient of friction than that measured at quasi-static indentation rates.

Friction is a complex and contentious subject, especially at high slip-rates. Whilst there is some literature which investigates the friction behaviour between steel and FRP composites at moderate rates there are no studies of friction at the slip velocities and high contact pressures likely to be seen between a ballistic projectile and an armour.

It has been found that the coefficient of friction between a steel and FRP composite surface is at its lowest when the fibres are orientated normal to the sliding surface [70]. Research on the frictional behaviour of FRP's has been conducted with sliding rates of up to $4ms^{-1}$ and for varying loads which indicates that in many cases the value of μ generally decreases with increasing slide velocity [71],[72],[73] though some work suggests that this reduction may be limited and that as slip velocity is increased further μ begins to rise [74].In addition to slip velocity the contact pressure has an effect on the friction between laminates, there is evidence that this peaks sharply at low loads after which mechanisms such as fibre softening [70] rapidly reducing the coefficient value to a constant value. Work by other authors suggests a clear trend of reducing μ with increasing pressure.

High speed film showing the perforation of targets by ball ammunition suggests that a reasonable amount of the projectile has remained intact as a flattened disk of core and jacket material. Based on this footage it is estimated that the diameter of this disk is approximately 10mm. For the purposes of evaluating the frictional energy during the impact of a ball round the indenting projectile will be modelled as having assumed a hemispherical shape of 10mm diameter.

Evaluating the shape of the AP indenter is however less straightforward. The nose of the indenter (as seen in Image 6.5) is an ogive. Ogives fall into two shape categories, Tangent ogive and Secant ogive as defined in Figure 6.3 below).

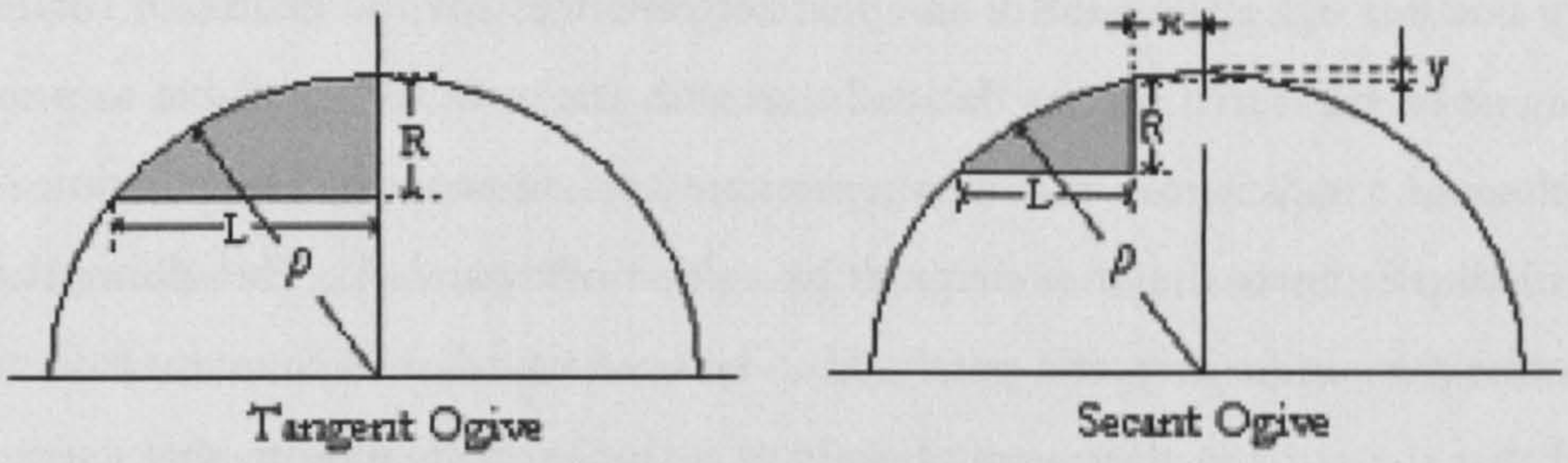

Figure 6.3: Tangent and Secant Ogive nose shapes

The nose shape of the 7.62x39 indenter is a secant ogive, the surface area of which is defined by integrating Equation *6.2* for 2π radians about the indenters z-axis.

$$y = \sqrt{\left(d_2\left(C^2 + \frac{1}{4}\right)\right)^2 - x^2} - \left(d\left(C^2 - \frac{1}{4}\right)\right)$$

$$x_{off} = -r \times \sin\left[-\beta + \frac{\alpha_o}{2}\right]$$

$$y_{off} = r \times \cos\left[-\beta + \frac{\alpha_o}{2}\right]$$

$$d_2 = d + 2\left(r - y_{off}\right)$$

$$C = \frac{L}{d}$$

Where:

y = y co-ordinate y_{off} = Centre of rotation y offset (mm)

x = x co-ordinate x_{off} = Centre of rotation x offset (mm)

d = Cone base diameter (mm)

d2 = Equivalent tangent ogive cone base diameter (mm)

r = Radius of curvature (mm)

L = Base length of ogive

β = Angle between secant and x-axis centreline

α_o = Angle between radial lines from centre of rotation to either end of chord

Equation 6.2: Length of a secant ogive

To carry out this calculation the x and y offset distances for the centre of rotation of the surface must be measured. It was decided that with the resources available measurement of these values to a satisfactory accuracy represented an un-economic use of time. Instead it was decided to estimate the nose shape as being that of a parabola. This allows the standard equation for the surface area of a parabolid to be used based on definite measurements. It is believed that the error in this assumption is of a similar magnitude to that encountered by estimating the x and y offset values for a secant ogive.

$$A = \frac{2\pi}{3P}\left[\sqrt{\left(\left(\frac{d^2}{4} + P^2\right)^3\right)} - P^2\right]$$

$$P = \frac{d^2}{8h}$$

Where:

d = Diameter of base of paraboloid (mm)

h = Depth of paraboloid (mm)

Equation 6.3: Surface area of a prabolid

The total surface area of the indenter can then be calculated by adding the surface area of the paraboloid to that of the cylindrical body of the indenter using the standard formula for defining the surface area of a cylinder.

$$A = \frac{2\pi}{3P}\left[\sqrt{\left(\left(\frac{d^2}{4} + P^2\right)^3\right)} - P^2\right] + \pi dh$$

$$P = \frac{d^2}{8h}$$

Where:

d = Diameter of base of paraboloid (mm)

h = Depth of paraboloid (mm)

r = Radius of cylinder / base of paraboloid

Equation 6.4: Surface area of 7.62x39 AP core (Paraboloid + cylinder)

In the case of an indenter passing through a laminate the friction will come as a result of the force perpendicular to the surface of the indenter[69] rather than the through thickness resistance which will be evaluated via compressive strain energy later. Assuming that the material immediately adjacent to the surface of the indentation has been displaced it is fair to define the force required to displace the material as being equal to or greater than the compressive yield stress of the material in the failed direction.

As the data does not exist for compressive strength for at a range of angles to the laminate (other than parallel to the reinforcement and perpendicular to the reinforcement) a full picture cannot yet be constructed. For the sake of simplicity the compressive failure strength in plane with the reinforcement will be used to calculate the force applied to the indenter and thus, the frictional energy. This is a valid simplification as it is in this plane which material has been observed to fail when moved axially away from the path of the indentation.

Thus as:

$$\sigma = \frac{F}{A}$$

Equation 6.5: Standard stress equation

Then:

$$F = \sigma A$$

Where:

σ = Stress (Pa)

F = Force (N)

A = Area (m^2)

Equation 6.6: Equation 6.5 re-arranged for force

Using the previous simplification that this force is equal to that perpendicular to the indenter surface we can say that:

$$F_y = R$$

Where:

Fy = Yield force (N)

R = Reaction force perpendicular to projectile surface (N)

Equation 6.7: Definition of reaction force

Thus:

$$F_f = \mu F_y$$

Where:

F_f = Force due to friction (N)

μ = Coefficient of friction

Fy = Yield force (N)

Equation 6.8: Force due to friction on projectile

The frictional energy can then be derived from calculating the area under the force/ distance curve by making the simplification that the indentation distance is equal to target thickness for full perforation and equal to indentation depth for a successful stop. This can be revisited after initial validation of the model to take into account the entry and exit portion of the impact event however, it is worth noting that against the impact of AP ammunition the penetrating core which is being considered separate of the complete bullet in this instance will not immediately leave its jacket and begin penetrating the composite material on its own (see Image 2.12 for AP bullet construction).

The results of this analysis for the medium weave Vinylester material are as follows:

Perforation @ 625ms^{-1}	
Ballistic energy (J)	1884.77
Friction energy (J)	1356.81
Dry μ	
Proportion (%)	**71.99**
Friction energy (J)	705.54
Lubricated μ	
Proportion (%)	**21.6**

Stop @ 622 ms^{-1}	
Ballistic energy (J)	1866.72
Friction energy (J)	914.37
Dry μ	
Proportion (%)	**48.98**
Friction energy (J)	475.47
Lubricated μ	
Proportion (%)	**14.69**

Table 6.9: Proportion of projectile energy absorbed through friction (medium weave VE vs Ball ammunition)

The values of frictional energy recorded are larger than anticipated and suggest that the initially suspect coefficient of friction values may indeed be unreliable (though the values calculated in section **4.7.2** compare well with literature values for similar glass/plastic systems [70],[71],[72],[73]). This was encountered for all materials tested as illustrated in the following table.

Perforation	
Dry	**Proportion (%)**
Heavy Phenolic (est μ-0.3)	10.92
Heavy VE	37.68
Medium VE	71.99
Light VE	60.01
Lubricated	**Proportion (%)**
Heavy Phenolic (est μ-0.15)	5.46
Heavy VE	13.37
Medium VE	21.6
Light VE	17.78

Stop	
Dry	**Proportion (%)**
Heavy Phenolic (est μ-0.3)	10.16
Heavy VE	30.16
Medium VE	48.98
Light VE	18.66
Lubricated	**Proportion (%)**
Heavy Phenolic (est μ-0.15)	5.08
Heavy VE	10.99
Medium VE	14.69
Light VE	5.5

Table 6.10: Proportion of projectile energy absorbed through friction (Ball ammunition vs all materials)

The highest values of energy have been calculated for un-lubricated steel-on-composite μ values, the projectile however is constructed from soft lead with a copper jacket, the difference in μ values between the bullet materials and the indenter material may also be responsible for some error. The values using the lubricated μ are still higher than expected but are of much more reasonable values.

The possible errors in this part of the energy model come from unreliable μ values, incorrect compressive strength values or inappropriate attention to the shape of the indenter and the presence of friction as an energy absorption mechanism for the impact of a deformable projectile. If this latter possibility held true then performing the same friction energy analysis on AP impacts should show less error as the indenter is a finite shape and remains so through out the impact (rather than a deforming indenter which changes shape throughout the impact).

Interestingly, this is not the case as illustrated in Table 6.11 the values of friction range from higher than expected to completely improbable.

Perforation	
Dry	**Proportion (%)**
Heavy Phenolic (est μ-0.3)	38.36
Heavy VE	124.2
Medium VE	172.6
Light VE	100.9
Lubricated	**Proportion (%)**
Heavy Phenolic (est μ-0.15)	19.18
Heavy VE	44.08
Medium VE	51.78
Light VE	29.9

Stop	
Dry	**Proportion (%)**
Heavy Phenolic (est μ-0.3)	22.96
Heavy VE	62.08
Medium VE	113.84
Light VE	54.61
Lubricated	**Proportion (%)**
Heavy Phenolic (est μ-0.15)	11.48
Heavy VE	22.03
Medium VE	34.15
Light VE	16.18

Table 6.11: Proportion of AP projectile energy absorbed through friction

Once again the values of frictional energy only appear more sensible for the lubricated coefficient of friction values. There are a number of factors which could cause the coefficient of friction between indenter to be lower than anticipated. The high rate of indentation could cause melting of the fibre tips, the indenter may possess a covering of lead metal for at least some of the indentation acting as a lubricant or the presence of combusting incendiary material in the AP rounds used could have had an effect.

This incendiary material is located behind the core and ignites upon impact with a target, this material begins to combust whilst the projectile is passing through the armour therefore it is possible that this hot gas could force its way between the indenter and the material acting as a lubricant.

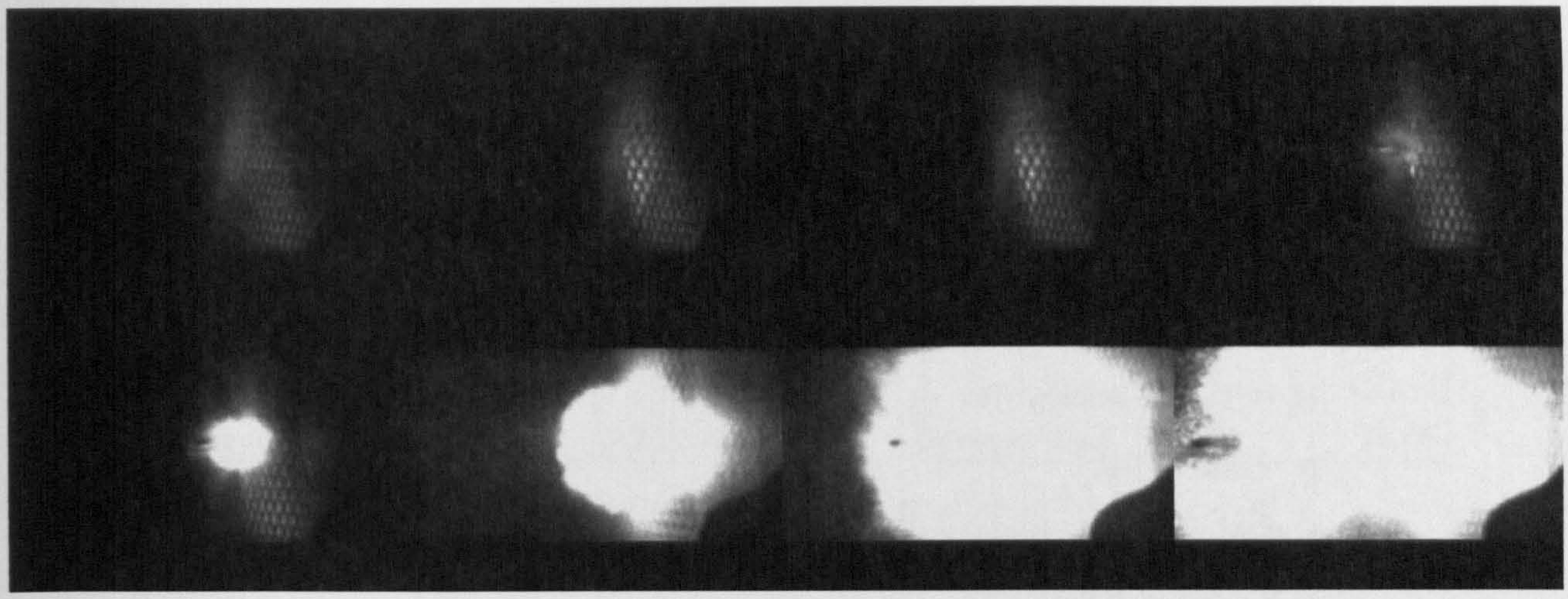

Image 6.6: High speed camera stills of burning incendiary material

Despite the difficulties encountered in this analysis, evidence suggests that friction is an important energy absorbing mechanism in ballistic impact. A study of the literature suggests that high slip rates and high contact pressures all contribute to a reduction in coefficient of friction values over those which might be derived from quasi-static experimentation. The definition of friction from indentation testing needs confirming by other means to ensure the validity of this analysis. Equally there is further study required into the treatment of friction in a ballistic impact to ensure that all areas are accounted for.

6.10.6 Tensile strain energy

As well as the bending strength of the reinforcement fibres it is also a known fact that the tensile strength of the reinforcement material has a positive effect on the ballistic performance, this is discussed in Chapter **2** and Section **5.8**.

Due to the popularity of the tensile test as a material testing method there are established formulae for the analysis of such loading. Of these formulae is an expression for tensile energy absorption for elastic materials shown in the following equation *6.9*.

$$U_t = \frac{\sigma^2}{2E}$$

Where:

U_t = Tensile energy (J)

σ = Stress (Pa)

E = Modulus of elasticity (Pa)

Equation 6.9 Tensile energy absorption [75]

Applying this equation to the failed material as a result of impact requires the area of tensile failure to be considered.

$$U_t = \frac{\sigma^2}{2E} A_r$$

Where:

U_t = Tensile energy (J)

σ = Stress (Pa)

E = Modulus of elasticity (Pa)

A = Area of failure (m^2)

Equation 6.10: Energy absorbed by finite amount of failed fibre

Additionally material is being loaded in both the *x* and *y* directions, as such Equation *6.10* becomes:

$$U_t = \left(\frac{\sigma_x^2}{2E_x} \times A_{tx}\right) + \left(\frac{\sigma_y^2}{2E_y} \times A_{ty}\right)$$

$$= 2\left(\frac{\sigma^2}{2E} \times A_t\right)$$

Where:

U_t = Tensile energy (J)

σ_x & σ_y = Stress (Pa)

E_x & E_y = Modulus of elasticity (Pa)

A = Area of failure (m^2)

Equation 6.11: Energy absorbed by finite amount of failed fibre

This energy calculation only considers tensile energy for the elastic behaviour portion of the laminates stress/strain curve. The laminates tested in section **5.8** have only shown limited plastic behaviour (this can be seen in Graph 5.9) and thus the consideration of energy calculations valid for elastic behaviour is unlikely to be a significant source of error.

The fibres which failed by tensile rupture are found in the rear portion of the damage hourglass, the size of the rupture dependent on the size of the projectile. The area of fibres failed was defined as being the diameter of the projectile and the depth of the rear hourglass. This is defined in the *x* and *y* planes, treating the failure as a square area. This is valid as the

reinforcement is also aligned in the x and y planes, therefore the area of fibres failed is rectangular (across the diameter) in each plane. Results are as follow in Table 6.12.

Perforation @ 625 ms^{-1}	
Ballistic energy (J)	1866.72
Tensile energy (J)	417.78
Proportion (%)	**22.17**

Stop @ 622 ms^{-1}	
Ballistic energy (J)	1866.72
Tensile energy (J)	348.15
Proportion (%)	**18.65**

Table 6.12: Proportion of projectile energy absorbed through tensile loading

6.10.7 Indentation resistance

Whilst both the tensile and bending energy in the fibres has been assessed for the global extent of the damage region, the local energy expended during ductile indentation remains undefined. Pointed indenters penetrate a composite by pushing through fibre bundles with only limited and very localised bending or tensile loading of fibres and by ductile displacement of material without compressive failure.

This indentation energy was evaluated from the results of droptower testing in section **4.6.3**. Using values for drop energy and the maximum penetration achieved it was possible to derive an arbitrary figure for energy absorption per mm of indentation for both ogival and flat indenters. This value was multiplied by the indentation depth to determine indentation energy.

The use of a flat indenter encourages shear failure rather than ductile hole growth, and as such the value reported for indentation energy of a flat indenter is at least partially attributable to this phenomena. Sectioning of droptower impacts has however shown the presence of a spherical-cap shaped shear plug ahead of the indenter as illustrated in Image 4.19, it will be this plug which leads the indentation and due to its shape will be less prone to cause a shear failure mechanism.

Indentation depth can be defined in two distinct ways. The first uses the standard damage geometry developed at the beginning of this model, the indentation failure region being defined as being the front face damage region of the hourglass damage shape (i.e. t-H_R). The results of applying the findings of indentation testing to the indentation of the front surface is shown in the following table.

Perforation of t-H_R	
Ballistic energy (J)	1884.77
Flat Indentor	
Indentation energy (J)	144.2
Proportion (%)	**6.82**
Ogival Indentor	
Indentation energy (J)	61.5
Proportion (%)	**2.91**

Table 6.13: Proportion of projectile energy absorbed through indentation (Indentation depth = t-H_R)

The second definition of indentation depth is based on the location of the projectile post impact, the indentation thickness being equal to the maximum penetration depth for a successful arrest and equal to the target thickness for a complete perforation. The results of this analysis are defined in the following table:

Perforation @ 625 ms^{-1}	
Ballistic energy (J)	1866.72
Flat Indentor	
Indentation energy (J)	383.6
Proportion (%)	**17.43**
Ogival Indentor	
Indentation energy (J)	157.1
Proportion (%)	**7.43**

Stop @ 622 ms^{-1}	
Ballistic energy (J)	1866.72
Flat Indentor	
Indentation energy (J)	248.4
Proportion (%)	**13.31**
Ogival Indentor	
Indentation energy (J)	105.9
Proportion (%)	**5.67**

Table 6.14: Proportion of projectile energy absorbed through Indentation (Indentation depth max pen or target thickness)

Whilst the amount of projectile energy absorbed in this fashion is not vast it is important to note that the indentation resistance will influence other forms of energy absorption. This is due to that fact that a material with a higher indentation resistance will deform a soft projectile more than a low resistance material. This will then influence the final damage geometry and the proportion of energy absorbed by delamination and tensile rupture mechanisms. This treatment of indentation depth may not be a correct estimation as it assumes the same penetration mechanism as taking place throughout the entire event. Despite this simplification however it is believed that this is a good approximation for penetration of hard, non-deformable projectiles, the change in shape of deformable projectiles requires further research.

6.10.8 Compression energy

The through thickness compressive strength is likely to have the most influence on the impact of flat faced or deformable projectile. Once again the energy absorbed through compressive deformation can be evaluated by calculating the area below the compressive force deflection curve for the material under loading.

At the point of compressive failure we can assume that the compressive stress is equal to the previously recorded UCS of the material, as the recorded compressive modulus is derived from dividing compressive stress over compressive strain we can rearrange for a value of compressive strain at the point of compressive failure.

Defining the area in which compression is believed to be dominate the displacement can be calculated. Force is derived from the standard stress equation linking force and area using the known failure stress and area to give failure coordinates in terms of compressive loading and resultant displacement.

The area which is subjected to significant amounts of compressive loading can be either defined as the front surface section of the 'hourglass' or can be based on observation of the projectile position. For a perforation we can assume that the material failed in compression is equal to the target thickness, for a successful stop the penetration depth can be used as the value of compressively failed material. Assuming the material behaves in a linear-elastic manner the compressive energy can be calculated from the energy below this elastic curve, the results are illustrated as follows.

Perforation @ 625ms^{-1}	
Ballistic energy (J)	1884.77
Compressive energy (J)	73.64
Proportion (%)	**3.91**

Stop @ 622 ms^{-1}	
Ballistic energy (J)	1866.72
Compressive energy (J)	48.02
Proportion (%)	**2.57**

Table 6.15: Proportion of projectile energy absorbed through compression

The proportion of compressive energy is small, as such there is not likely to be a large error if compressive failure depth is defined as the thickness of the front face damage region (t-

H_R) or is based on target thickness / penetration depth (though the latter will give the higher result).

It is important to note however, that compressive strength is expected to be rate sensitive. The preceding analysis only uses compressive strength values evaluated from quasi-static testing, the magnitude of strength at ballistic leading rates is un-known and hard to evaluate. Despite this simplification, the percentage of energy absorbed is still expected to be relatively small based on the values calculated in table 6.15.

6.10.9 Summarised values

There are several combinations of energy contributions which can be assembled and evaluated as an audit of the energy absorbed during the damage process. As anticipated in most cases the calculated energy is less than the full ballistic impact, this is due to the examination of the post impact damage rather than the instantaneous damage (i.e. elastic deformation) which is recovered after impact. Kinetic energy effects have also been ignored.

The resulting audit for the medium VE material against ball ammunition is show in Table 6.16 below along with four possible combinations of variables which give sensible and justifiable results.

	Perforation @ 625ms^{-1}		Proportion
	Ballistic energy (J)	1884.8	100%
	Delamination energy (J):		
1	*Visible*	65.0	3.45%
2	*Max possible*	229.8	12.19%
3	Bending energy (J)	10.4	0.55%
	Friction energy (J):		
4	*Dry* μ	1356.8	71.99%
5	*Lubricated* μ	407.0	21.60%
6	Tensile energy (J)	417.8	22.17%
	Indentation energy (J):		
	Indent zone = t-H_R:		
7	*Flat indenter*	144.2	6.82%
8	*Ogival Indenter*	61.5	2.91%
	Indent zone = pen depth:		
9	*Flat indenter*	383.6	17.43%
10	*Ogival Indenter*	157.1	7.43%
11	Compressive energy (J)	73.6	3.91%

Total:	**Energy (J)**	**Proportion (%)**
(2,3,4,6,9,11)	2472.0	128.2
(2,3,5,6,9,11)	1522.3	77.9
(2,3,4,6,7,11)	2232.6	117.6
(2,3,5,6,7,11)	1282.9	67.2

	Stop @ 622 ms^{-1}		Proportion
	Ballistic energy (J)	1866.7	100%
	Delamination energy (J):		
1	*Visible*	95.9	5.14%
2	*Max possible*	345.2	18.49%
3	Bending energy (J)	2.5	0.15%
	Friction energy (J):		
4	*Dry* μ	914.4	48.98%
5	*Lubricated* μ	274.3	14.69%
6	Tensile energy (J)	348.2	18.65%
	Indentation energy (J):		
	Indent zone = t-H_R:		
7	*Flat indenter*	144.2	6.82%
8	*Ogival Indenter*	61.5	2.91%
	Indent zone = pen depth:		
9	*Flat indenter*	248.4	13.31%
10	*Ogival Indenter*	105.9	5.67%
11	Compressive energy (J)	73.6	3.91%

Total:	**Energy (J)**	**Proportion (%)**
(2,3,4,6,9,11)	1587.0	103.5
(2,3,5,6,9,11)	947.0	69.2
(2,3,4,6,7,11)	1482.8	97.0
(2,3,5,6,7,11)	842.8	62.7

Table 6.16: Energy audit for Medium weave Vinylester

Four combinations of damage parameters have been assembled from the data, these arise from there being a number of options available for the evaluation of indentation and friction energy. These are explained as follows:

(2,3,4,6,9,11) 2472J/128.2% Delamination energy assuming all damage area has suffered from cracking (to take account of matrix cracking not visible to the eye), Bending energy, Friction energy (based on a dry value of μ), Tensile strain energy, Indentation energy based on a flat indenter with indentation depth equal to maximum penetration depth and Compressive energy.

(2,3,5,6,9,11) 1522J/77..9% As above but using friction energy values based on a lubricated coefficient of friction value.

(2,3,4,6,7,11) 2232J/117.6% Delamination energy assuming all damage area has suffered from cracking (to take account of matrix cracking not visible to the eye), Bending energy, Friction energy (based on a dry value of μ), Tensile strain energy, Indentation energy based on a flat indenter with indentation depth equal to the front surface damage depth (t-H_R – i.e. the depth of the upper portion of the hourglass) and Compressive energy.

(2,3,5,6,7,11) 1283J/67.2% As above but using friction energy values based on a lubricated coefficient of friction value.

The favoured combination which appears to work well across the VE materials tested is as follows:

- Mode I delamination energy applied throughout visible damage zone (i.e. assuming every ply is delaminated this accounts for any invisible delaminations and matrix cracking damage)
- Bending energy of the delaminated plys
- Frictional energy using the coefficient of friction derived for dry indentations
- Tensile strain energy in the ruptured plys
- Indentation energy for the front face damage zone defined by t-H_R (flat indenter)
- Compressive energy for the area below the projectile in the front face damage zone

The other combinations listed in Table 6.16 follow the same lines but use frictional values derived from wet indentation and values of indentation zone thickness based on observed penetration depth. These other methods are not necessarily incorrect rather present an alternative interpretation of the impact energy absorbed based on slightly different conditions.

The results for all materials tested against ball ammunition are shown for comparison in the following Table 6.17. It is interesting to notice that whilst the Vinylester panels show a similar level of success the equivalent Phenolic material has less than 60% of the ballistic

impact energy absorbed accounted for. The individual energy contributions are listed in Appendix C.

	Perforation *Sum total % of projectile energy*				*Stop* *Sum total % of projectile energy*			
	Heavy Phenolic	**Heavy VE**	**Medium VE**	**Light VE**	**Heavy Phenolic**	**Heavy VE**	**Medium VE**	**Light VE**
(2,3,4,6,9,11)	50.9	45.4	128.2	154.7	58.7	89.2	103.5	90.1
(2,3,5,6,9,11)	45.5	72.3	77.9	128.3	53.6	60.0	69.2	75.6
(2,3,4,6,7,11)	43.8	85.9	117.6	127.0	52.4	80.2	97.0	87.4
(2,3,5,6,8,11)	38.4	62.8	67.2	84.9	47.9	53.1	67.7	72.9

Table 6.17 Complete summary of energy audit

An interesting observation is that the energy absorption through the damage mechanisms studied has calculated that in many cases a higher amount of projectile energy is being absorbed for a perforation than for a successful stop. Intuitively as the successful stop has resulted in a complete transfer of energy from the projectile to the armour there would be more damage visible and thus calculated than for a perforation where the projectile carries a residual amount of kinetic energy with it.

Observation of the individual mechanism energy suggests that the energy absorbed through friction and tensile failure is significantly higher for the perforated material than for the successful stop.

The frictional energy may well be higher for the perforation case, as the projectile has had to pass through more material. The reported error of coefficient of friction values in section **6.10.5** may also be compounded by the treatment of the indenter as a hemispherical solid instead of a ductile, transient shape. The amount of this error suggests refinement is required when dealing with friction especially as the model suggests more than a 100% energy absorption through friction alone in some cases (especially against AP ammunition) as seen in Tables 6.10 and 6.11.

6.10.10 Material hardness effects

One reason for this under-estimation of the Phenolic materials energy could be due to the hardness of the material relative to the equivalent VE panels. This was assessed in section **4.7** which showed that there is a variation in the 'hardness' of the composites tested. This will have a significant effect on the penetration of deformable projectiles, the harder a

surface is the more deformation will be imparted to the projectile. This change in projectile shape with hardness will mean that harder materials will be penetrated by a flatter projectile likely to spread material damage over a considerably greater area than a little deformed projectile impacting a soft target.

As a result of this it will be important to make a correction for this effect for a model to work against deformable projectiles. This correction will be based on the Brinel indentation data assessed in section **4.6.1** and the results of the initial model presented in section **6.10.9**.

Comparing the indentation diameters of the tested composite panels to RHA gives a value of difference in indentation size (between the composite and RHA) as seen in Table 6.18.

The amount by which the audit under-accounts for projectile energy is then used to calculate a correction factor (i.e if the audit accounts for 80% of projectile energy a correction of 1.2 is required).This process needs to be repeated for each set of variables (as the total amount of projectile energy accounted for will vary depending on which choices have been made) used in the audit (i.e. those in Table 6.17), correction tables for all variable sets are listed in Appendix C.

Material	Ave indentation Diameter (mm)	Relative to RHA Difference (mm)	Relative to RHA Difference multiplyer
RHA	1.5	N/A	N/A
Heavy Phenolic	3.00	1.50	1.527
Heavy VE	4.67	3.17	1.064
Medium VE	3.67	2.17	0.979
Light VE	3.67	2.17	1.0147

Table 6.18: Indentation results comparable to RHA and model error factor (2,3,4,6,9,11)

By plotting the required multiplier against the difference in initial hardness, a curve is formed which links material hardness to the model error (i.e. based on hardness relative to RHA a correction can be applied to the energy audit results to bring them closer to total projectile energy). This allows a model which is based at present on a Vinylester material system to be applied to other materials with different indentation resistance, stiffness and compressive strength.

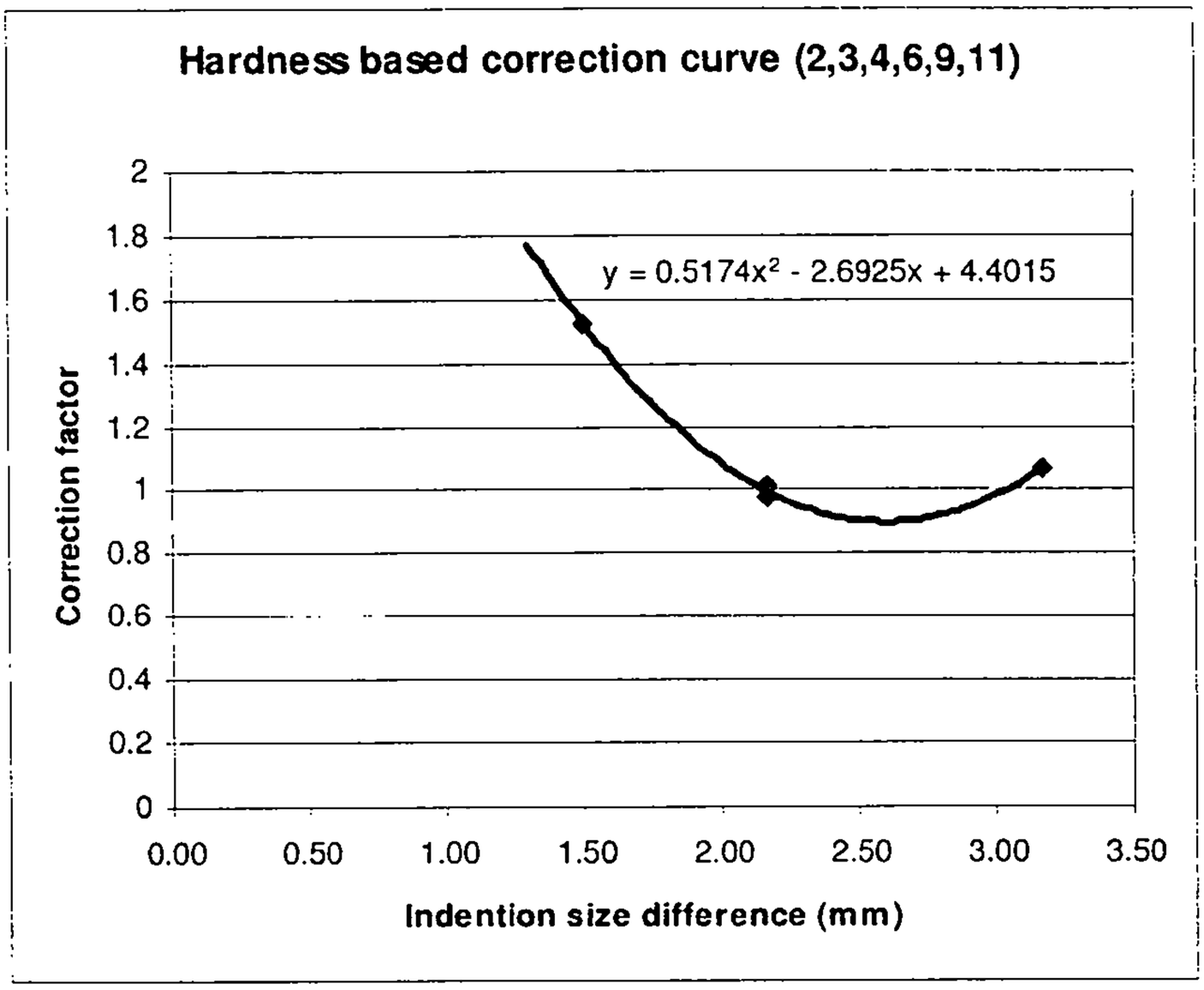

Graph 6.15: Sample hardness correction curve, and equation.Combination (2,3,4,6,9,11),table 6.16

This correction is calculated using the equation of the correction curve seen in Graph 6.15 and is based on the individual analysis of the indentation resistance of the test material. The correction is not valid the non-deformable AP model as the hardness difference between projectile and target is so significant that the projectile will not change shape / be broken up.

Due to the shape of the correction curve estimation of material hardness values in the absence of actual indentation test data should be avoided, only a small change in indentation difference could result in a significant difference in correction factor.

6.10.11 Model for AP ammunition (pointed, non-deformable)

The application of this modelling process to the impact of AP ammunition has been less successful. The main indenter in this case is the hardened steel core, as such the core was initially dealt with as the sole penetrator. This was justified as the core leaves the bullet almost immediately after the projectile strikes the front face of the target, it is the core which does the penetration whilst the jacket material folds into the front face of the target and the gilding material and other debris fills the empty cavity behind the core.

Despite this simplification however the energy predicted by the model far exceeds the core energy, in some cases a single mechanism appeared to absorb more energy than the core

itself possessed. This was especially the case for the evaluation of tensile energy and friction energy.

As mentioned in section **6.10.5** there may be cause to suspect that the frictional energy values are being over-estimated which may explain the values calculated. The errors in calculated tensile energy absorption suggest that the volume of fibres assumed to have failed in tension has been estimated incorrectly.

The complete audit for the medium weave VE material is shown in Table 6.19 followed by the complete summary of all test materials both with and without the suspect results discussed above. The possible combinations of variables which give sensible and justifiable results are listed at the end of the table and include combinations which exclude tensile energy (denoted by *) and which exclude both tensile energy and friction energy (denoted by **).

	Perforation @ 432ms^{-1}		Proportion
	Ballistic energy (J)	377.7	100%
	Delamination energy (J):		
1	*Visible*	22.0	5.83%
2	*Max possible*	64.8	17.16%
3	Bending energy (J)	1.5	0.39%
	Friction energy (J):		
4	*Dry μ*	1546.1	410.14%
5	*Lubricated μ*	464.7	123.04%
6	Tensile energy (J)	390.2	103.31%
	Indentation energy (J):		
	Indent zone = t-H_R:		
7	*Flat indenter*	72.1	19.10%
8	*Ogival Indenter*	30.7	8.14%
	Indent zone = pen depth:		
9	*Flat indenter*	368.6	97.60%
10	*Ogival Indenter*	157.1	41.60%
11	Compressive energy (J)	41.6	11.04%

Total:	**Energy (J)**	**Proportion (%)**
(2,3,4,6,9,11)	2412.8	639.6
(2,3,5,6,9,11)	1331.4	352.5
*(2,3,4,10,11)**	1811.1	480.3
*(2,3,5,10,11)**	729.7	193.2
*(2,3,4,8,11)**	1684.7	446.9
*(2,3,5,8,11)**	603.3	159.8
*(1,3,5,10,11)**	686.9	181.9
*(2,3,10,11)***	265.0	70.2

	Stop @ 415ms^{-1}		Proportion
	Ballistic energy (J)	348.4	100%
	Delamination energy (J):		
1	*Visible*	9.9	2.85%
2	*Max possible*	58.5	16.79%
3	Bending energy (J)	11.0	3.16%
	Friction energy (J):		
4	*Dry μ*	941.1	270.52%
5	*Lubricated μ*	282.8	81.16%
6	Tensile energy (J)	334.4	95.99%
	Indentation energy (J):		
	Indent zone = t-H_R:		
7	*Flat indenter*	72.1	19.10%
8	*Ogival Indenter*	30.7	8.14%
	Indent zone = pen depth:		
9	*Flat indenter*	368.6	97.60%
10	*Ogival Indenter*	157.1	41.60%
11	Compressive energy (J)	51.2	14.72%

Total:	**Energy (J)**	**Proportion (%)**
(2,3,4,6,9,11)	1764.9	498.8
(2,3,5,6,9,11)	1106.5	309.4
*(2,3,4,10,11)**	1218.9	346.8
*(2,3,5,10,11)**	560.6	157.4
*(2,3,4,8,11)**	1092.5	313.3
*(2,3,5,8,11)**	434.2	124.0
*(1,3,5,10,11)**	512.0	143.5
*(2,3,10,11)***	277.8	76.3

Table 6.19: Energy audit for medium weave Vinylester against AP (* denotes summaries excluding tensile energy, ** denotes summaries excluding tensile and friction energy)

(2,3,4,6,9,11) Delamination energy assuming all damage area has suffered from cracking (to take account of matrix cracking not visible to the eye), Bending energy, Friction energy (based on a dry value of μ), Tensile strain energy, Indentation energy based on a flat indenter with indentation depth equal to maximum penetration depth and Compressive energy.

(2,3,5,6,9,11) As above but using friction energy values based on a lubricated coefficient of friction value.

(2,3,4,10,11) Delamination energy assuming all damage area has suffered from cracking (to take account of matrix cracking not visible to the eye), Bending energy, Friction energy (based on a dry value of μ), Tensile strain energy, Indentation energy based on a ogival indenter with indentation depth equal to maximum penetration depth and Compressive energy.

(2,3,5,10,11) As above but using friction energy values based on a lubricated coefficient of friction value.

(2,3,4,8,11) Delamination energy assuming all damage area has suffered from cracking (to take account of matrix cracking not visible to the eye), Bending energy, Friction energy (based on a dry value of μ), Tensile strain energy, Indentation energy based on a ogival indenter with indentation depth equal to the front surface damage depth ($t-H_R$ – i.e. the depth of the upper portion of the hourglass) and Compressive energy.

(2,3,5,8,11) As above but using friction energy values based on a lubricated coefficient of friction value.

(1,3,5,10,11) Delamination energy based on visible delaminations, Bending energy, Friction energy (based on a lubricated value of μ), Tensile strain energy, Indentation energy based on a ogival indenter with indentation depth equal to maximum penetration depth and Compressive energy.

(2,3,10,11) Delamination energy assuming all damage area has suffered from cracking (to take account of matrix cracking not visible to the eye), Bending energy, NO friction energy (due to concerns regarding accuracy), Tensile strain energy, Indentation energy based on a

ogival indenter with indentation depth equal to maximum penetration depth and Compressive energy.

	Penetration @ 415.3 ms^{-1} *Sum total % of projectile energy*				*Stop @ 432.4 ms^{-1}* *Sum total % of projectile energy*			
	Heavy Phenolic	**Heavy VE**	**Medium VE**	**Light VE**	**Heavy Phenolic**	**Heavy VE**	**Medium VE**	**Light VE**
(2,3,4,6,9,11)	703.7	639.6	682.3	359.5	294.6	575.5	498.8	543.2
(2,3,5,6,9,11)	513.3	442.8	433.6	255.4	240.0	480.3	368.8	408.6
*(2,3,4,10,11)**	144.4	480.3	235.5	271.1	125.7	153.3	346.8	233.1
*(2,3,5,10,11)**	106.3	283.5	153.1	167.0	102.8	113.4	216.8	176.8
*(2,3,4,8,11)**	202.7	446.9	654.9	646.2	149.4	228.6	313.3	420.7
*(2,3,5,8,11)**	101.4	250.0	446.7	346.1	87.9	124.4	183.4	197.8
*(1,3,5,10,11)**	96.1	272.1	141.7	115.5	95.9	104.3	202.9	88.4
*(2,3,10,11)***	80.8	70.2	63.8	92.6	87.6	83.5	76.3	136.5

Table 6.20 Complete summary of energy audit against AP

It is clear from Table 6.20 above that the success seen when dealing with ball ammunition has not been immediately met against AP. In most cases the energy calculated is far greater than the projectile energy (based on the core alone).

It is apparent that of the values calculated both those for friction and those for tensile strain energy are higher than might be expected, whilst potential errors in the evaluation of friction energy have already been discussed the difficulties encountered with tensile energy have been unexpected. These are believed to be due to inappropriate selection of the areas of fibres believed to have been failed through tensile rupture. It is believed that those fibres said to have failed in tension are more likely to have failed as a result of the indentation process and in fact little in the way of tensile fibre rupture has occurred.

This supposition is valid due to the manner in which the AP projectile defeats the armour, there is insufficient indentation resistance to the projectile to delaminate, deform and tear a laminate in the same way a deformed ball round might, evidence of this is clear from post impact sectioning analysis.

Despite these changes in interpretation the model still over-predicts impact energy and it is only when the frictional energy is removed from the analysis that a sensible result is achieved.

As previously mentioned the energy analysis has concentrated on the KE of the AP core only and has ignored the energy possessed the rest of the projectile, this may be an invalid assumption, especially for front surface mechanisms. Re-modelling for the entire projectile energy gives the following results:

	Perforation @ 432ms^{-1}		Proportion
	Ballistic energy (J)	902.1	100%
	Delamination energy (J):		
1	*Visible*	22.0	2.44%
2	*Max possible*	64.8	7.19%
3	Bending energy (J)	1.5	0.16%
	Friction energy (J):		
4	*Dry μ*	1546.1	171.39%
5	*Lubricated μ*	804.0	89.12%
6	Tensile energy (J)	390.2	43.25%
	Indentation energy (J):		
	Indent zone = t-H_R:		
7	*Flat indenter*	72.1	7.99%
8	*Ogival Indenter*	30.7	3.40%
	Indent zone = pen depth:		
9	*Flat indenter*	368.6	40.86%
10	*Ogival Indenter*	157.1	17.41%
11	Compressive energy (J)	41.6	4.61%

Total:	**Energy (J)**	**Proportion (%)**
(2,3,4,6,9,11)	2412.8	267.5
(2,3,5,6,9,11)	1670.7	185.2
*(2,3,4,10,11)**	1811.1	200.8
*(2,3,5,10,11)**	1069.0	118.5
*(2,3,4,8,11)**	1684.7	186.8
*(2,3,5,8,11)**	942.6	104.5
*(1,3,5,10,11)**	1026.2	113.7
*(2,3,10,11)***	265.0	29.4

	Stop @ 415ms^{-1}		Proportion
	Ballistic energy (J)	832.19	100%
	Delamination energy (J):		
1	Visible	9.93	1.19%
2	Max possible	58.48	7.03%
3	Bending energy (J)	11	1.32%
	Friction energy (J):		
4	*Dry μ*	941.12	113.09%
5	*Lubricated μ*	489.38	58.81%
6	Tensile energy (J)	334.44	40.19%
	Indentation energy (J):		
	Indent zone = t-H_R:		
7	*Flat indenter*	72.1	8.66%
8	*Ogival Indenter*	30.7	3.69%
	Indent zone = pen depth:		
9	*Flat indenter*	368.6	44.29%
10	*Ogival Indenter*	157.1	18.88%
11	Compressive energy (J)	51.23	6.16%

Total:	**Energy (J)**	**Proportion (%)**
(2,3,4,6,9,11)	1764.87	212.08
(2,3,5,6,9,11)	1313.13	157.80
*(2,3,4,10,11)**	1218.93	146.48
*(2,3,5,10,11)**	767.19	92.20
*(2,3,4,8,11)**	1092.53	131.29
*(2,3,5,8,11)**	640.79	77.01
*(1,3,5,10,11)**	718.64	86.36
*(2,3,10,11)***	277.81	33.39

Table 6.21 Energy audit for medium weave Vinylester against AP, full projectile mass considered (* denotes summaries excluding tensile energy, ** denotes summaries excluding tensile and friction energy)

These results still over-estimate the energy absorbed with tension and friction once again being the main apparent sources of error, the full summary is shown in the following table.

	Penetration @ 415.3 ms^{-1} *Sum total % of projectile energy*				*Stop @ 432.4 ms^{-1}* *Sum total % of projectile energy*			
	Heavy Phenolic	**Heavy VE**	**Medium VE**	**Light VE**	**Heavy Phenolic**	**Heavy VE**	**Medium VE**	**Light VE**
(2,3,4,6,9,11)	299.8	267.4	267.5	285.4	130.2	245.8	212.1	227.8
(2,3,5,6,9,11)	220.2	185.1	185.2	181.4	107.3	205.9	157.8	171.4
*(2,3,4,10,11)**	180.6	200.8	200.8	217.1	81.6	109.6	146.5	154.0
*(2,3,5,10,11)**	100.9	188.5	118.5	113.1	58.7	69.8	92.2	97.7
*(2,3,4,8,11)**	166.3	186.8	186.8	207.4	66.0	95.3	131.3	144.4
*(2,3,5,8,11)**	86.5	104.5	104.5	103.4	43.2	55.5	77.0	88.0
*(1,3,5,10,11)**	94.8	113.8	113.7	91.6	55.8	66.0	86.4	60.7
*(2,3,10,11)***	41.1	29.4	29.4	38.8	43.5	29.4	33.4	57.4

Table 6.22 Complete summary of energy audit against AP (full projectile mass considered)

6.11 Model validation

6.11.1 Defining parameters

As with all models it is important to test the results against wider data before it can be used with confidence. There is however a lack of data in the literature which lists values for all the mechanical properties required by this model. Work by Wong [65] did investigate toughness, bending and tensile properties of a number of thin E-Glass-Phenolic armour materials which were later subjected to ballistic impact by 7.62mm (.30cal) FSP's. Of the results chosen for examination two materials were commercial armour laminates and one was a developmental material, all materials were manufactured by Permali Gloucester (UK).

The three materials with the most consistent data (values of G_{Ic} were averaged from only two tests. The results excluded from this validation varied significantly between tests) were chosen ("DV8912", an E-Glass, SC1008/10% PVB matrix developmental laminate. "SL 209", an E-Glass, SC1008 laminate. "SL302", an E-Glass, SC1008/amino-silane matrix laminate[65]). The damage geometry was then estimated from trends in Graphs 6.11- 6.14), at this stage this is a slightly subjective process based on the data available in the damage charts, however if more data points are added in the future the potential for user error will fall. The

values of damage geometry were predicted to fall in between a maximum and a minimum value, model calculations will be performed using both values to predict a range within which the V_{50} should lay.

	Max	Min
D_F	*48.0*	*40.0*
D_R	*140.0*	*120.0*
D_W	*35.0*	*30.0*
H_F	*12.0*	*12.0*
H_R	*9.6*	*6.9*
H_F/H_R	*1.3*	*1.8*
α	*77.1*	*74.2*

Table 6.23: Predicted damage geometry for Wong's material

Coefficient of friction data is not available for this material, a value of 0.45 was chosen based on an average of the (dry) values of the other composites tested in this work.

Using the damage geometry as well as the other material property data it was possible to make a prediction of ballistic energy capacity of the material. The model developed for flat or deformable indenters was used as although FSP's are unlikely to deform significantly they present a large and flat contact area to the armour when compared to an AP projectile, as well as this the design of the projectile is such that plugging and shearing failure in the target material is encouraged.

Image 6.7: 7.62mm/.30cal FSP

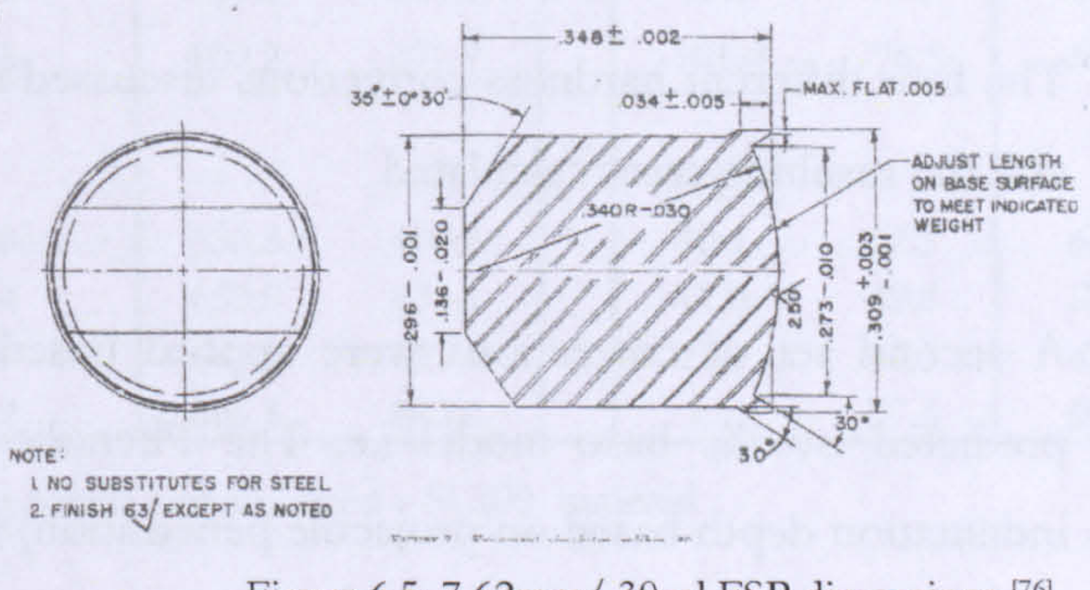

Figure 6.5: 7.62mm/.30cal FSP dimensions [76]

The indentation diameter caused by a 10mm Brinell ball with 750kg equivalent force was not available for the material, fortunately some material from this testing still existed and was tested so a hardness correction factor could be calculated and applied.

The energy proportions developed in section **6.9** are as listed in Table 6.24 (see Appendix C). The proportions calculated for the heavy Phenolic material will be used at this material is the most representative of the validation materials.

			Heavy Phenolic	
1	**Mode I -**	***Max***	18.0	9.2
2		***Visible***	8.6	4.1
3	**Bending**		0.8	0.5
4	**Friction -**	***Dry μ***	16.9	35.0
5		***Lubricated μ***	6.8	15.0
6	**Tensile**		16.5	34.8
7	**Indentation**	***Ball-Point 1st***	7.2	6.6
8		***Ball-Base 1st***	10.1	11.7
9		***t-H_R Point***	3.1	2.7
10		***t-H_R Base***	4.4	4.8
11	**Compression**		3.2	2.8

Table 6.24 Energy proportions from model

6.11.2 Results

The calculated results were tabulated and compared to actual V_{50} data, the resulting error being calculated for the V_{50} estimation based on minimum as well as maximum values (see Table 6.23 for max and min geometry values).

The four different hardness corrections discussed in section **6.10.10** were applied to the data and the resulting error calculated.

A second set of corrections were applied based on the proportion of projectile energy predicted by the base model i.e. The Phenolic material model (using dry friction and indentation depth based on projectile penetration) accounts for a total of 65.49% (from table 6.17) of the impact energy, thus multiplying the result of the validation energy audit by 1.3451 gives 100% of projectile impact energy from which the velocity can be calculated.

6.11.2.1 "DV8912"

DV8912			Energy Absorbed (J)		Derived V_{50} (ms^{-1})			V_{50} Error (ms^{-1})		V_{50} Error (%)	
Measured V_{50} = 670.9ms^{-1}			*Max*	*Min*	*Max*	*Min*		*Max*	*Min*	*Max*	*Min*
	Calculated:		532.5	508.5	607.7	593.8		63.2	77.1	***9.4***	***11.5***
	Corrected:										
	Hardness corrections										
	Dry μ	(2,3,4,6,9,11)	481.4	459.7	577.8	564.6		93.1	106.3	***13.9***	***15.9***
	Lub μ	(2,3,5,6,9,11)	626.8	598.5	659.3	644.2		11.6	26.7	***1.7***	***4.0***
t-H_R	*Dry* μ	(2,3,4,6,7,11)	483.7	461.8	579.1	565.9		91.8	105.0	***13.7***	***15.7***
t-H_R	*Lub* μ	(2,3,5,6,7,11)	635.8	607.0	664.0	648.8		6.9	22.1	***1.0***	***3.3***
	General Corrections										
	65.49%		716.3	683.9	704.8	688.7		-33.9	-17.8	***-5.1***	***-2.7***
	55.33%		770.4	735.6	730.9	714.2		-60.0	-43.3	***-8.9***	***-6.5***
	59.73%		747.0	713.2	719.7	703.3		-48.8	-32.4	***-7.3***	***-4.8***
	49.57%		801.1	764.9	745.4	728.3		-74.5	-57.4	***-11.1***	***-8.6***

Table 6.25: Modelling results and V_{50} error – DV8912 material

6.11.2.2 "SL209"

SL209			Energy Absorbed (J)		Derived V_{50} (ms^{-1})			V_{50} Error (ms^{-1})		V_{50} Error (%)	
Measured V_{50} = 601.2ms^{-1}			*Max*	*Min*	*Max*	*Min*		*Max*	*Min*	*Max*	*Min*
	Calculated:		426.2	397.0	543.6	524.7		57.6	76.5	***9.6***	***12.7***
	Corrected:										
	Hardness corrections										
	Dry μ	(2,3,4,6,9,11)	543.0	505.9	613.6	592.3		-12.4	8.9	***-2.1***	***1.5***
	Lub μ	(2,3,5,6,9,11)	660.1	615.0	676.6	653.1		-75.4	-51.9	***-12.5***	***-8.6***
t-H_R	*Dry* μ	(2,3,4,6,7,11)	577.8	538.3	633.0	611.0		-31.8	-9.8	***-5.3***	***-1.6***
t-H_R	*Lub* μ	(2,3,5,6,7,11)	710.9	662.3	702.2	677.7		-101.0	-76.5	***-16.8***	***-12.7***
	General Corrections										
	65.49%		573.2	534.0	630.5	608.6		40.4	62.3	***6.0***	***9.3***
	55.33%		616.5	574.4	653.9	631.1		17.0	39.8	***2.5***	***5.9***
	59.73%		597.8	556.9	643.8	621.4		27.1	49.5	***4.0***	***7.4***
	49.57%		641.1	597.2	666.8	643.6		4.1	27.3	***0.6***	***4.1***

Table 6.26 Modelling results and V_{50} error – SL209 material

6.11.2.3 "SL302b"

SL302b Measured V_{50} = 670.48ms^{-1}		Energy Absorbed (J)		Derived V_{50}			V_{50} Error (ms^{-1})		V_{50} Error (%)	
		Max	*Min*	*Max*	*Min*		*Max*	*Min*	*Max*	*Min*
Calculated:		514.0	491.1	597.1	583.6		73.4	86.9	***11.0***	***13.0***
Corrected:										
Hardness corrections										
	Dry μ	(2,3,4,6,9,11)	464.7	444.0	567.7	554.9	102.8	115.6	***15.3***	***17.2***
	Lub μ	(2,3,5,6,9,11)	605.0	578.1	647.7	633.1	22.7	37.3	***3.4***	***5.6***
t-H$_R$	*Dry* μ	(2,3,4,6,7,11)	466.8	446.1	569.0	556.2	32.2	45.0	***5.4***	***7.5***
t-H$_R$	*Lub* μ	(2,3,5,6,7,11)	613.7	586.3	652.3	637.7	-51.1	-36.5	***-8.5***	***-6.1***
General Corrections										
65.49%			691.4	660.6	692.5	676.9	-21.6	-6.0	***-3.2***	***-0.9***
55.33%			743.6	710.5	718.1	702.0	-47.2	-31.1	***-7.0***	***-4.6***
59.73%			721.0	688.9	707.1	691.2	-36.2	-20.3	***-5.4***	***-3.0***
49.57%			773.3	738.8	732.3	715.8	-61.4	-44.9	***-9.1***	***-6.7***

Table 6.27 Modelling results and V_{50} error – SL302b material

6.11.3 Discussion

In all cases the Phenolic material model predicts the V_{50} for the validation panels well, the worst error of all three materials is 13% under-estimation of the V_{50}. As a general observation it appears that all uncorrected values are close to 10% under the correct V_{50}.

There are eight possible corrections trialled with varying levels of success, these corrections and their origin have been described previously.

The 'hardness' based corrections have produced individual results within 2% of V_{50} and with a spread between max and min predicted values of less than 4%. At the same time however some versions of this type of correction have worsened the accuracy of the results, the worst recorded being a 17% under-estimation. Of the three materials tested the hardness correction based on a lubricated μ value has returned significantly better results than the correction based on a dry μ value in two of the three cases.

The general corrections based on the proportion of impact energy calculated by the original model have produced results with a greater accuracy and lower spread than those based on the hardness correction. A best result of 0.6% V_{50} error and 2.1% spread between max and

minimum values has been achieved with a worst result of 11.1% error and 3.3% spread between values. It should be noted that the V_{50} does not generally lie in-between the predicted maximum and minimum values.

6.12 Modelling summary

The energy audit method of modelling V_{50} values for fibre reinforced plastic composites appears to be successful. The use of a geometry plot to estimate material damage at the limit velocity makes it easy to apply this model to a wide variety of similar materials. The applicability of this model to other materials of similar construction (i.e. woven laminates of tough fibres in a Phenolic or Vinylester thermoplastic matrix) is good requiring only basic, easy to perform mechanical testing for definition of material properties

A series of corrections have been defined which should be applied to any results, the type of correction used is at present up to the user as there is a range to choose from. It appears from the validation testing carried out thus far that the corrections based on material hardness require further refinement, validation testing has not been carried out for a soft deformable projectile which might see the most benefit from this type of correction. The second type of correction based on total energy accounted for by the model has been used to greater success, once again the choice of correction is in the hands of the user though in this case there is scope for an educated choice to be made based on the confidence in input data and projectile type.

For the model to be applied to significantly different materials it would be prudent to perform a limited ballistic trial and post impact sectioning in addition to mechanical testing. This would allow an audit process to be carried out and model parameters defined in the same way as used in this report.

As it stands the model appears to be most promising when applied to flat or deformable projectiles, further work and a through validation is required before the same approach can be used for AP projectiles.

CHAPTER 7:

SUMMARY AND CONCLUSIONS

This chapter will summarise the findings discussed in previous chapters and draw appropriate conclusions.

7.1 Overview

The bulk of the experimental work has been carried out on the following core group of materials manufactured by VT Halmatic using fibres supplied by AGY and resin supplied by Reichold for use in this project, other materials subjected to brief testing will be otherwise introduced where required. These material are as follows:

1. S2 glass / Phenolic. 830gsm 2000 tex reinforcement weave (Coarse)
2. S2 glass / Vinyl Ester. 830gsm 2000tex reinforcement weave (Coarse)
3. S2 glass / Vinyl Ester. 300gsm 66 tex reinforcement weave (Medium)
4. S2 glass / Vinyl Ester. 190gsm 66/33 tex reinforcement weave (Fine)

A wide variety of testing has been carried out to evaluate the mechanical properties which are believed to influence ballistic impact performance. Testing has been carried out at quasi-static and dynamic rates. Ballistic testing and evaluation has also been carried out such that mechanical properties and ballistic performance can be directly related.

7.2 Summary of Ballistic testing

A range of ballistic testing as been carried out on a number of structural composite materials. The main materials tested have been a series of S2-glass reinforced panels of Phenolic and Vinylester reinforcement of varying weave weight.

Testing has shown that against ball ammunition (STANAG level I) and similar deformable projectiles that heavy weave weight and coarse yarns perform better than equivalent materials with a finer and lighter reinforcement weave. Press-cured Phenolic out-performs identically reinforced Vinylester matrix material in terms of ballistic limit velocity however is somewhat heavier.

The post impact damage recorded from the test panels is significant, especially in the case of heavy weave materials (though these were stopping projectiles at a higher velocity than the light weave materials). The lightest weave material tested had less than half the amount of visible damage compared to the other Vinylester materials tested (for roughly half the ballistic performance). The medium and heavy weave VE panels had more comparable ballistic performance however the heavy weave panel suffered more damage on the rear face (though interestingly this material suffered less front surface damage).

Several weights of material have been tested against AP ammunition (STANAG level II) and testing indicates a linear performance trend between V_{50} and areal density. At lower velocities the Phenolic material is once again the heaviest but the best performer in terms of V_{50}. At higher velocities however it has equivalent performance to the best Vinylester material though for significantly greater weight. The finer weave Vinylester materials appear to perform better against this threat than the heavy weave materials, despite this their performance was still amongst the worse of the materials tested.

Against AP ammunition the medium weave material (which had the highest V_{50}) suffered the most damage on both front and rear surfaces than the other materials tested. For a velocity spread of roughly $100ms^{-1}$ there was a significant difference in damage area between the lightest weave panel and the heavier weaves.

With regards to behind armour effects once a target is perforated; it appears that the heavy weave materials behave in a far more favourable way against ball ammunition. Against AP ammunition there is negligible spall, save for either a complete bullet or bullet core depending on how over-matched the panel is. Against incendiary ammunition (AP(I)) the impact was only sufficient to detonate the incendiary when the heavier group of materials was tested

In an attempt to optimise a material solution a hybrid target combining the heavy weave Vinylester material, (which performed well against ball ammunition) and the medium weave material, (which performed well against AP ammunition) as a single target was tested. It was hoped that performance would be in excess of a target made entirely of either one of the components. The resultant performance was better than a target made entirely of the heavy weave material but worse than a target made from the medium weave material. This indicates that the addition of the heavy weave material has had a detrimental effect on the target performance and that the mechanisms at work in the medium weave material during an AP projectile impact are of more importance than those taking place in the heavy weave material. A CFRP faced hybrid material was also tested against AP ammunition but returned disappointing results.

7.3 Summary of mechanical testing

The testing undertaken in this project has attempted to evaluate the mechanical properties of thick structural engineering composites intended for use as vehicle armour. The mechanical properties have been evaluated in such a way as to allow later investigation of the relationship between certain mechanical properties and the ballistic performance of the composite materials tested. This investigation of impact and penetration events has been evaluated in terms of front surface and rear surface mechanisms, the approach made to testing has assumed that there are unique properties relevant to each. Testing of properties concerned with the front face is covered in Chapter 4 and those relevant to the rear face in Chapter 5.

Mechanical testing was carried out to establish a range of properties, these were:

- Fracture toughness
- Tensile strength
- Bending strength
- Compressive strength in two laminate orientations, (ultimate and yield)
- Indentation resistance
- Coefficient of friction

Fracture toughness, Tensile and Bending strength were identified as dominant properties on the rear surface whilst compressive strength, indentation resistance and friction were considered as front surface energy absorption mechanisms.

Fracture toughness was evaluated at quasi-static and dynamic loading rates (using specially constructed apparatus). This testing established that whilst most materials had similar fracture toughness (Heavy VE, medium VE and heavy Phenolic in order of rising magnitude) the lightest weave Vinylester material had a significantly higher fracture toughness. Dynamic testing has shown little rate sensitivity of G_{Ic}. Testing of heavy weave laminates was difficult due the tendency of cracks to appear and propagate in plies other than the centreline, this invalidated the test for the period that these cracks were growing in addition to the main crack. It is possible that small cracks not visible to the eye have had a slight positive effect on G_{Ic} values.

Tensile testing established that in tension the heavy weave materials were stronger than those of equivalent matrix but with a lighter weave reinforcement. Of the equivalent Vinylester and Phenolic materials the highest strength was attained by the Vinylester. The strain to failure of the VE materials was also in excess of the Phenolic laminated tested.

Bending strength was evaluated through a simple three point bend flexure test, whilst ultimate bending strength was not evaluated due to incorrect failure of the test samples (material available forced an incorrect sample geometry) modulus data was recorded. The modulus data suggests that once again the heavy weave VE material is by far a better performer than the lighter weave VE materials. The Phenolic tested was ranked third of the four materials tested.

Compressive strength was evaluated for loading applied both parallel and perpendicular to the laminate direction. With loading parallel to the laminate plane the heavy weave Phenolic material performed the least well of the materials tested. The Vinylester materials were once again ranked in terms of weave weight with the heaviest weave material performing the best.

Loading applied perpendicular to the laminate showed the Phenolic material to be, in fact by far the strongest of the materials tested, the medium weave material was the best of the Vinylester specimens followed by the heavy and light weaves.

Indentation testing was evaluated in a number of ways, quasi-static testing was carried out in a style similar to that of a Ludwick hardness test and built on literature work of a number of authors. This work was successful in evaluating the yield strength of the composite material parallel with the laminate, this confirmed that for the penetration of hard indentators radial flow away from the indentation (and thus compressive yield strength parallel with the laminate) has an important influence on energy absorption. As well as successfully determining compressive strength values this indentation testing was also able to derive the coefficient of friction between the composite being tested and both lubricated and dry steel.

Dynamic indentation using both flat and ogival penetrators (an AP bullet core) were use to characterise ballistic indentation. The flat indenter generated a spherical-cap shaped shear plug ahead of the indenter which lead the penctration process. An attempt to apply the indentation theory used for quasi-static indentations failed, it is believed that this is due to the compressive rate sensitivity of composite materials, especially in compression.

A summary of the ranking is shown in Table 6.2 and is repeated below.

	Compression		Indentation			
	Parrallel	Perpendicular	Q/S Ball	Q/S Cone	Dyn Ogive	Dyn Flat
Heavy Phenolic	4	1	1	-	1	1
Heavy VE	1	3	4	1	2	2
Medium VE	2	2	2	2	3	3
Light VE	3	4	3	3	4	4

	Mode I		Bend	Tensile	
	Q/S	Dyn	Modulus	Modulus	Strength
Heavy Phenolic	3	-	2	3	2
Heavy VE	2	2	1	2	1
Medium VE	4	-	3	1	3
Light VE	1	1	4	4	4

	Ballistic (V_{50})			Weight
	Ballistic	AP (Thin)	AP (Thick)	Areal density
Heavy Phenolic	1	1	1	4
Heavy VE	2	2	2	2
Medium VE	3	3	1	3
Light VE	4	4	3	1

Table 7.1: Material performance ranking

7.4 Sectioning of ballistic impacts

There is a clear difference between the local impact damage caused by deformable ball and un-deforming AP ammunition. Despite this the geometry of material damage retains the same general 'hourglass' shape regardless of the damage local to the axis of penetration.

Sectioning of the materials has suggested that heavy weave materials which are susceptible to delamination yet strong enough to contain the projectile material in the front face are the better performers against soft ammunition, lighter weaves showed significant amounts of damage. Sections of impacts in which the projectile had been

successfully stopped showed far more delamination damage and deformation than sections of perforations indicating that to stop a projectile the target material has to be able to damage rather than remaining perfectly intact with the exception of a small core of damage where a projectile has cut through.

Sectioning indicated that AP rounds penetrated the armour to a significant degree before the core exited the jacket. Again materials with greater amounts of delamination damage tend to be successful, the sooner this damage starts (relative to the struck face) the better. The fine weave materials fail on the front face by bulk radial flow of material away from the indentation and resultant buckling of fibres because of this, heavy weaves appeared to exhibit less of this damage but did suffer more plastic deformation adjacent to the indentation path.

Sectioning of the first hybrid material indicated that the deflection of the front face observed during testing of the standard panels was not observed here due to the smaller panels being more tightly clamped together. This seems to have delayed the beginning of delamination in the rear surface. Sectioning of the second hybrid material tested showed that the CFRP front face did not appear to have suffered widespread damage and had absorbed relatively little projectile energy.

7.5 Modelling

A link between damage morphology and ballistic performance has been established and used to extrapolate damage for a range of target thicknesses.

A successful model was produced based on an audit of the energy required to produce visible post impact damage. This model calculated the energy absorbed through a range of damage mechanisms by measurement of sectioned impacts and application of mechanical test data recorded as part of this report. The contribution of this mechanism to absorbing projectile energy can then be calculated.

A model has been constructed to calculate the energy absorbed by failure mechanisms, this model calculated the energy absorbed through a range of damage mechanisms by measurement of sectioned impacts and application of mechanical test data recorded as

part of this report. The contribution of these various mechanisms to the absorption of projectile was then calculated.

An audit of the studied mechanisms has been carried out and the sum total of the accounted energy compared to the projectile impact energy with a range of success. The audit process has been most successful for soft, deformable projectiles. Some concern exists with the treatment of friction and tensile fibre failure, especially when non-deforming AP ammunition is considered. Removing these uncertain parameters from the analysis suggests the model is still valid.

A series of correction curves were generated to take into account the 'hardness' of the composites being tested (using RHA as a reference) when struck by a deformable projectile (as harder targets will cause more projectile deformation and promote break-up).

The model was validated against three thin glass/Phenolic armour composites attacked by .30cal FSP's good agreement was found between theoretical and experimental data. After standard behaviour of the test materials was established it was possible to predict the damage geometry suffered by the thinner validation panels at their limit velocity. This was done using a rigid definition of damage geometry which was plotted against thickness to create a 'material map' allowing predictions of a range of material thicknesses to be made.

7.6 Other observations from modelling exercise

It was noted that there appears to be a strong inter-dependency between tensile strength, bending strength and fracture toughness. Whilst it was noted that delamination energy made a low contribution to energy absorption, materials which failed to delaminate sufficiently and deform quickly enough did not realise significant tensile loading and energy abosrbtion in the delaminated plys.

The indentation hardness varies between materials and in the case of soft (ball) ammunition promotes earlier projectile break-up. The use of this hardness knowledge allowed a correction to be applied to the data based on individual material properties.

Mechanical properties rank materials in (generally) the same order as ballistic teting against ball ammunition (especially the VE based materials). Less success is achieved in predicting material ranking against AP from mechanical performance, compressive properties however appear to be important and do correspond to ballistic trends.

Modelling showed a greater dependency on friction than first thought (especially in the case of AP ammunition) however the calculations are sensitive to coefficient of friction values. The measurement of these values is difficult and there is literature to suggest that the value of the coefficient varies with slip velocity and contact pressure. It is very difficult to measure friction values at ballistic slip-rates and contact pressures, literature suggests that these values if they were to be recorded may be less that those measured at quasi-static rates.

7.7 Conclusions

The work in this project has reached a number of clear conclusions, the linking of mechanical properties to ballistic performance has not previously been investigated in this way. As such elements of this work (such as the damage energy audit model) deserve careful consideration and further work.

The main conclusions are.

Materials with a heavy reinforcement weave perform well against a soft projectile threat whilst those with medium weave reinforcement perform better against hard, non deformable projectiles.

Ballistic performance follows a linear trend with increasing target thickness. It was noted that unconstrained interfaces within a composite target appear to promote projectile yaw

Pointed, non-deformable indenters penetrate the target material by causing radial flow of material away from the indentation path, material fails under compressive loading parallel to the reinforcement direction exhibiting angled planes of bucking throughout the material.

Quasi-static indentation using metal cones (a la Ludwick hardness test) is successful at predicting the radial yield strength (parallel to the laminate) of a composite but not the through thickness yield strength.

Dynamic indentation using a flat cylinder in a droptower apparatus ranks materials in the same manner as ballistic testing against ball ammunition.

Damage morphology can be defined as being either 'thick' or 'thin'. A bi-linear trend of energy absorption against thickness was observed (validating literature) thus damage morphology was shown to vary with impact energy in a predictable manner.

A model based on the audit of mechanical damage mechanism energy (and morphology prediction) was constructed and successfully tested against difficult materials. Accuracy of predictions was well within 10% of measured results.

Projectile and target characteristics influence penetration mechanisms and performance. A correction for target hardness has been developed and used with moderate success, further validation is requited.

Delamination energy alone is only responsible for a small proportion of projectile energy absorption, this is contrary to popular opinion.

Delamination and deformation allows large amounts of projectile energy to be absorbed via tensile strain in reinforcement fibres.

Materials with the low fracture toughness had better ballistic performance than those with high toughness. Fracture toughness requires matching with laminate tensile strength for best ballistic performance, low toughness and high strength is desirable.

Friction appears to be responsible for a significant amount of energy absorption (especially for non-deforming projectiles) but is difficult to quantify and use successfully.

REFERENCES

1. L Hollaway, *'Polymer composites for civil and structural engineering'*, Chapman & Hall 1993.
2. M H Datoo, *'Mechanics of fibrous composites'*, Elsevier 1991.
3. R Ogorkiewicz, *'Technology of tanks'*, Jane's Information Group 1991.
4. F Grose, *'Military antiquities respecting a history of the English army from conquest to the present time'*, I Stockdale, London 1812. Copperplate engraving *'Pavisors & a Moveable Tower Assaulting a Castle'*.
5. Notebooks of L DaVinci, c1487.
6. I M Daniel & O Ishai, *'Engineering mechanics of composite materials'*, Oxford University Press 1994.
7. 'Airbus Jumbojets: First A400M wing assembled, A380 wins certification', *High Performance Composites, January 2007* (ISSN 1081-9223), ed J Sloan, Ray Publishing Inc
8. Lockheed Martin (http://www.lockheedmartin.com/wms/findPage.do?dsp=fec&ci=15046&rsbci=11165&fti=0&ti=0&sc=400)
9. Airbus Military (http://www.airbusmilitary.com/specifications.html)
10. Boeing Defence (http://www.boeing.com/defense-space/military/c17/index.htm)
11. J Hetherington, 'Mobility *and* Survivability – is 'fly-light-fight-heavy' the answer?' SLAV Symposium 2004, *RMCS, UK.*
12. W Suttie [DSTL], *'Integrated Survivability Approach for Light Weight Vehicles'.* Proceedings of CVT symposium 12/2004 RMCS,UK.
13. W L Cheng, S Langlie and S Itoh, *'High velocity impact of thick composites'*, International Journal of Impact Engineering 29 (2003) 167-184
14. M Edwards, *'Land based military applications'* sect 6.37, 'Comprehensive Composite Materials', 2000 Elsevier Science Ltd.
15. B James [Dstl], *'Techniques and Technology for Hard survivability'*, SLAV Symposium 2004, RMCS, UK.
16. K E Simkin, *'Antitank'*, ELS Ltd 1982.
17. J S Rinehcart & J Pearson, *'Behaviour of metals under impulsive loads'*, American Society of Metals, Cleveland 1954 cited in H Kolsky, *'Stress waves in penetration', Ballistic Materials and Penetration Mechanics,* R C Laible ed.
18. CEN, European Committee for Normalisation, standard.

19. N P Aerospace, http://www.np-aerospace.co.uk/
20. M Normandia & W Gooch, *'An overview of ballistic testing methods of ceramic composite materials'*, 'Ceramic Armour Materials by Design', Ceramic Transactions Vol 134, American Ceramic Soc.
21. M French, *'Composite materials for armoured fighting vehicles'*, QinetiQ SLAV Symposium 2004, RMCS, UK.
22. D Hartman, M Greenwood & M Miller; *'High strength glass fibres'*, AGY Technical Paper, 2003, Advanced Glassfiber Yarns, LLC.
23. CAV-ATD,Globalsecurity.org http://www.globalsecurity.org/military/systems/ground/cav.htm
24. R M Ogorkiewicz, *'Development of Light Armour Systems'*, LASS 1995.
25. Dynamic prices and charts for Aluminium, *Investment Mine,*WWW.Infomine.com (http://www.infominc.com/investment/metalschart.asp?c=aluminum&u=lb&submit1=Display+Chart&x=usd&r=15y#chart)
26. N P Aerospace, *'Composite Armour'*, N P Aerospace, Coventry, UK 1998.
27. T Gander & I V Hogg ed; *'Jane's ammunition handbook 1995'*, 4th edition ©Jane's Information Group 1995.
28. M V Hosur, U K Vaidya, S Myres & S Jeelani, *'Studies on the repair of ballistic impact damaged S2-glass/Vinylester laminates,* Composite Structures, 61(2003), 281-290.
29. STANAG 4569, *'Protection levels for occupants of logistic and light armoured vehicles'*, ©North Atlantic Treaty Organization 1999.
30. V Miyagi, *'7.62mm versus 5.56mm – Does NATO really need two standard rifle calibres'*, Marine Corps Command & Staff College 1986.
31. M J Iremonger, *'Polyethylene composites for protection against high velocity small arms bullets'*, Proceedings of the 18th Symposium on Ballistics, San Antonio, Texas USA 11/1999
32. S J Coburn [RAAC], *'Enhancing ballistic protection by inducing yaw'*, RMCS, UK.
33. B Wang and S M Chou, *'The Behaviour of laminated composite plates as armour'*, Journal of Materials Processing Pechnology 68 (1997), 279-287.
34. K.Herlaar & M Van der Jagt-Deutekom. *'Finite element simulations and experiments to determine the residual damage of a CFRP composite material after ballistic impacts'*, TNO Defence, Security and Safety, The Netherlands.

35. B A Cheeseman, R Jensen & C Hoppel, *'Protecting the future force: Advanced materials and alalysis enable robust composite armour',* AMPTIAC Quarterly v8, 4(37-43)US DoD.
36. M E Backman & W Goldsmith, *'The mechanics of penetration of projectiles into targets',* International Journal of Engineering science 1978 v16, 1-99, ©Pergamon Press.
37. N K Naik & P Shrirao, *'Composite structures under ballistic impact',* Composite Structures 66(2004), 579-590.
38. B A Cheeseman & T A Bogetti, *'Ballistic impact into fabric and composite laminates',* Composite Structures 61 (2003), 161-173.
39. V B C Tan & K L J Khoo, *'Perforation of flexible laminates by projectiles of different geometry',* International Journal of Impact Engineering 31(2005), 793-810.
40. H M Wen, *'Penetration and perforation of thick FRP laminates,* Composites Science and Technology 61(2001) 1163-1172.
41. T Mitrevski, I H Marshall, R Thomson, R Jones & B Wittingham, *'The effect of impactor shape on the impact response of composite laminates',* Composite Structures 67(2005), 139-148.
42. J Awerbuch, *'A Mechanics approach to projectile penetration',* Israel Journal of Technology 1970, 8:3, 75-83. Cited in X W Chen & Q M Li, *'Perforation of thick plate by rigid projectiles',* Journal of Impact Engineering 11/2002.
43. J Awerbuch & S R Bodner, *'Analysis of the mechanics of perforation of projectiles in metallic plates',* International Journal of Solids. Cited in X W Chen & Q M Li, *'Perforation of thick plate by rigid projectiles',* Journal of Impact Engineering 11/2002.
44. W Goldsmith & S A Finnegan, *'Penetration and perforation processes in metal targets at and above ballistic limit velocities',* Journal of Mechanical Science 1971, 13:843-66. Cited in X W Chen & Q M Li,' *'Perforation of thick plate by rigid projectiles',* Journal of Impact Engineering 11/2002.
45. E P Gellert, S J Cimpoeru & R L Woodward, *'A Study of the effect of target thickness on the ballistic perforation of glass-fibre-reinforced plastic composites',* International Journal of Impact Engineering 24(2000), 445-456, Pergamon Press.
46. F S Mascianica, *'Ballistic technology of lightweight armour',*_AMMRC TR 81-20 1980, Confidential, cited in Gellert.....[45]
47. D Roylance & S S Wang, *'Penetration of Textile structures',* in Methods and Phenomena 5; Ballistic materials and penetration mechanisms', R C Laible ed.

48. MIL-STD-622F, *'Department of Defence Test Method Standard V_{50} ballistic test for armour'*, United States of America Department of Defence, 12/1997.
49. B Tekyeh-Marouf & R Bagheri, *'The impact resistance of laminated structures: Influences of layers, thickness and interfacial adhesion'*, Proceedings of 4th ESIS TC4 Conference on Fracture of Polymers, Composites and Adhesives 8/2005, Les Diablerets Switzerland.
50. AGY Inc, *'High strength Glass Fibres'*, AGY Technical Paper ©2003 Advanced Glassfiber Yarns, LLC.
51. P J Hogg, *'Composites for ballistic applications'*, Report. Dept of Materials, Queen Mary, London.
52. D Tabor, Chapter, VII, *'The hardness of metals'*, Oxford at the Clarendon Press (1951).
53. E Meyer, Zeits.d. Vereines Deursch. Ingenieure (1908) cited in D Tabor, Chapter II *'The hardness of metals'*, Oxford at the Clarendon Press (1951).
54. R F Bishop, R Hill & N F Mott, *'The Theory of Indentation and Hardness Tests'*, Proceedings of the Physics Society, **57/3** (1945).
55. G A Hankins, Proceedings of the Institution of Mechanical Engineers, **1**, 611. Cited in D. Tabor, 'The Hardness of Metals' (1951).
56. I Horsfall, 'Stab *Resistant Body Armour,* PhD, College of Defence Technology, Cranfield University (2000) .
57. A G Atkins, & D Tabor, *'Plastic Indentation In Metals With Cones'*, Journal of Mechanics, Physics, Solids, **13,** 149-164 (1965).
58. A Haque & M Ali, *'High strain rate responses and failure analysis in polymer matrix composites – An experimental and finite element study'*, Journal of Composite Materials, Vol 39 No 5/2005.
59. I Laine & P Vahankangas, *'Energy absorption mechanism of FSP in aramid fabric'*, PAS Symposium,1996, Colchester, UK.
60. F L Matthews & R D Rawlings, *'Composite materials: Engineering and science'*, Imperial College, UK, ©1999, Woodhead Publishing.
61. A M Jones & A P Slater, *'The development of a model for the prediction of the ballistic performance of composite armours'*, Coulthards Aerospace, Coventry UK.
62. G Zhou and G A O Davies, *'Impact response of thick glass fibre reinforced polyester laminates'*, International Journal of Impact Engineering Vol 16, No 3, 357-374, (1995).

63. ISO 15024:2000(E), *'Fibre-reinforced plastic composites-Determination of Mode I interlaminar fracture toughness, G_{Ic}, for unidirectionally reinforced materials'*, ©ISO 2000.

64. *'Fibre reinforced plastic composites – Determination of the mode I interlaminar fracture toughtness (G_I),* an ESIS TC4 test protocol.

65. W Wong, *'The effects of composite layer design on ballistic performance'*, BEng(Hons) Aeromechanical Sys Eng Final Year Project 2000, Cranfield University, UK

66. ASTM D790, *'Standard test methods fot flexural properties of un-reinforced and reinforced plastics and electrical insulating materials'*, © 2003 ASTM International.

67. A J Brunner, S Tanner, P Davis, H Wittich, *'Interlaminar fracture testing of unidirectional fibre-reinforced composites: Results from ESIS Round-Robins'*, Composites testing and standardisation, ECCM-CTS2, Ed: P Hogg, K Schulte & H Wittich. ©Woodhead Publishing 1994

68. P Bourke, *'The effect of short term excursions to elevated temperatures on fibre re-indorced polymeric matrix composite materials'*, BEng(Hons) Aeromech Sys Eng Final Year Project 2003, Cranfield University, UK.

69. A Shahkarami, E Cepus, R Vaziri & A Poursartip, *'Material responses to ballistic impact'*, Ch3 in *'Lightweight ballistic composites, military and law enforcement applications'*, Ed A. Bhatnagar. Woodhead Publishing 2006.

70. N Sung & N Suh, *'Effect of fiber orientation on friction and wear of fiber reinforced polymeric composites'*, Wear 53 (1979), 129-141.

71. N S El-Tayeb & R M Gadelrab, *'Friction and wear properties of E-glass fiber reinforced epoxy composites under different sliding contact conditions'*, Wear 192 (1996), 112-117.

72. B Vishwanath, A P Verma & C V S Kameswara Rao, *'Effect of fabric geometry on friction and wear of glass-fibre-reinforced composites,* Wear 145 (1991), 315-327.

73. A Mimaroglu, H Unal & T Arda, *'Friction and wear performance of pure and glass fibre reinforced poly-ether-imide on polymer and steel counterface materials'*, Wear (2007) (article in press).

74. R Ramesh & Kishore; *'Dry wear studies on glass-fibre-reinforced epoxy composites'*, Wear 89 (1983), 131-136.

75. J H Faupel & F E Fisher, *'Engineering Design'*, Second edition ©1981, J Wiley & Sons inc.

76. MIL-P-46593A (ord).

APPENDIX: A

Ballistic testing of carbon fibre

Aims

There has been much debate into the usefulness of structural carbon fibre as a major component of a future armoured vehicle system. Some (particularly thick) material was made available by VT Halmatic for limited investigation. The performance of this type of material against small calibre and medium calibre threats is of interest.

Of the two panels available the thinner will be tested in a very basic manner to get a feel for material behaviour and the thicker will be tested more scientifically

Experimental

This round of ballistic testing was carried out with exactly the same equipment and experimental setup as that used in earlier testing detailed in Chapter 3 of the preceding thesis.

Due to the small amount of material available an accurate V_{50} was not attempted, however a number shots were made with different threats and protection to gain an understanding of the materials generic response.

Panels tested

Two panels of structural Carbon Fibre Re-inforced Plastic (CFRP) have been obtained, one small panel of moderate thickness and a particularly thick specimen.

1. Panel 1

   29mm thick

   Multi Phase construction:

   Appears to be alternating layers of UD tape (5mm wide fibre bundles with glass fibre binding) arranged ±45° and UD sheet arranged 0/90° through thickness.

Areal density of the panel is 44kgm^{-2}. The addition of 3mm mild steel inclined, spaced plate increases areal density to 66 kgm^{-2}. The addition of an 8mm thick alumina tile brought the areal density 78kgm^{-2}.

2. Panel 2

   65mm thick

   Multi Phase construction:

   Skins: 2 ply UD tape (5mm wide fibre bundles with glass fibre binding) arranged ±45°

   Inner skin: 7mm thick UD fibres (no binding) arranged at 0°

   Inner skin mid plane: 2 ply UD tape (5mm wide fibre bundles with glass fibre binding) arranged ±45°

   Inner skin: 7mm thick UD fibres (no binding) arranged at 0°

   Core: 32mm thick UD tape (5mm wide fibre bundles with glass fibre binding) arranged ±45°

   Outer skin as per inner skin (UD bundles with tape mid layer and tape skin)

   Areal density is: 160kgm^{-2}

Against STANAG[13] level II threat (7.62mm) the material will be tested as is however against a level IV threat a 60m^2 , 24mm thick tile of 95% purity alumina ceramic will be adhered to the composite surface.

Threats

The panels were tested against:

1. 7.62mm calibre armour piercing rounds (7.62x39 API) as per STANAG 4569 level II.
2. 7.62mm calibre armour piercing rounds (7.62x51) similar to STANAG 4569 level III (but with a steel core rather than tungsten)
3. 14.5mm calibre armour piercing rounds (14.5x114 AP) as per STANAG 4569 level IV

Image 1: Ammunition L-R: 14.5mm AP Complete, Bullet, Core, 7.62x51, 7.62x39 complete, Bullet, core

Note: The 7.62x51mm (NATO size) AP ammunition was only tested (in a very limited fashion on the thinner evaluation panel due to range facility and ammunition availability.

Results:

CFRP Panel #1

7.62x51 AP vs Carbon panel alone 44kgm^{-2}:

This shot perforated the panel ejecting a fair degree of debris and creating a delamination approximately 55mm in diameter on entry. At exit the delamination area was seen to be oval in shape, approximately 100mm x 170mm across maxima and minima.

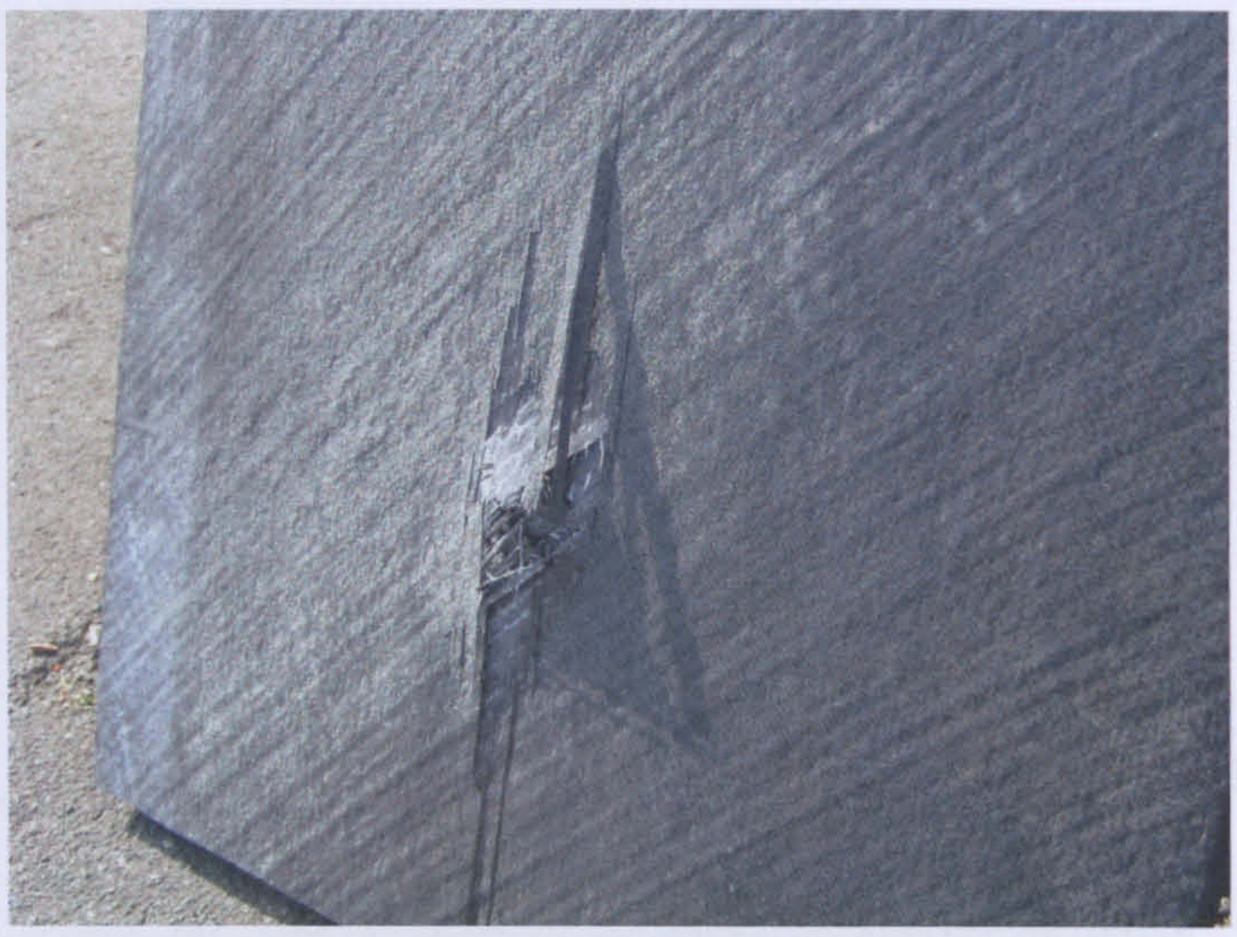

Image 2: 7.62 AP vs Carbon panel alone 44kgm^{-2}

7.62x51 AP vs Carbon panel + 3mm mild steel spaced and inclined 66kgm^{-2}:

This shot was successfully tripped by the spaced plate and caught successfully by the carbon panel. Delamination on the surface is a maximum of 70mm across and a minimum of 50mm across. The panel was penetrated to between half and two thirds of its thickness.

Image 3: 7.62 AP vs Carbon panel + 3mm mild steel spaced and inclined 66kgm^{-2}

7.62x51 AP vs Carbon panel + 8mm alumina tile 78kgm^{-2}:

This shot was easily stopped, the majority of the AP core of the round remained visible, the area of delamination was between 35 and 40mm in diameter.

Image 4: 7.62 AP vs Carbon panel + 8mm alumina tile 78kgm^{-2}

14.5mm B32 (STANAG IV) vs Carbon panel + 20mm alumina tile 126 kgm^{-2}:

These shots completely overmatched the panel causing extensive damage.

Image 5: 14.5 B32 (STANAG IV) vs Carbon panel + 20mm alumina tile 126 kgm^{-2}

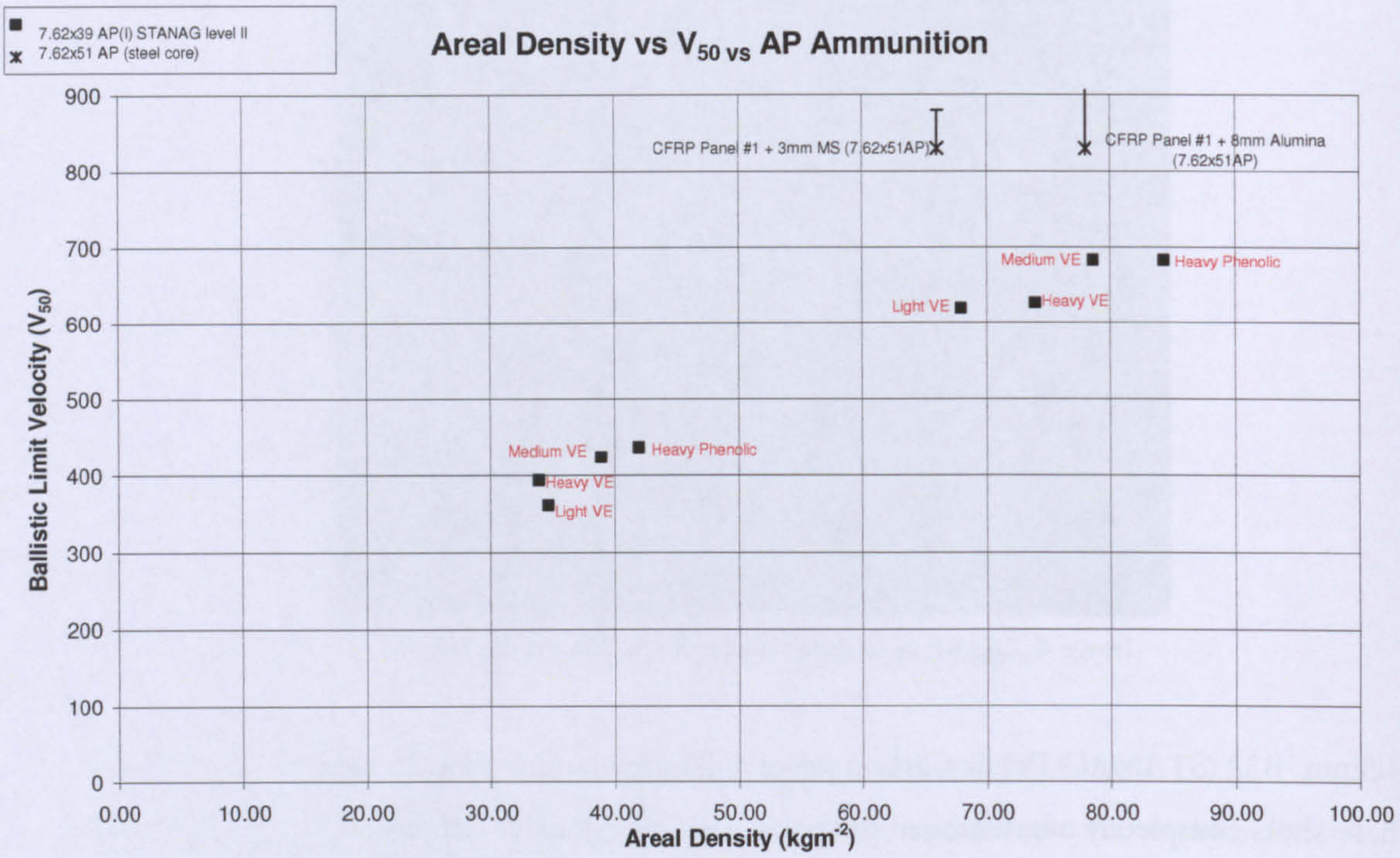

Graph 1: Summary of Carbon Panel #1 Ballistic testing with GRFP testing for reference

CFRP Panel #2:

No shots of 7.62x39 AP ammunition could penetrate this material even with the fullest charge possible. Six shots were fired in total, the highest velocity of these has been taken as the data point on the following chart. The actual V_{50} however is somewhat higher and is estimated by the error bar.

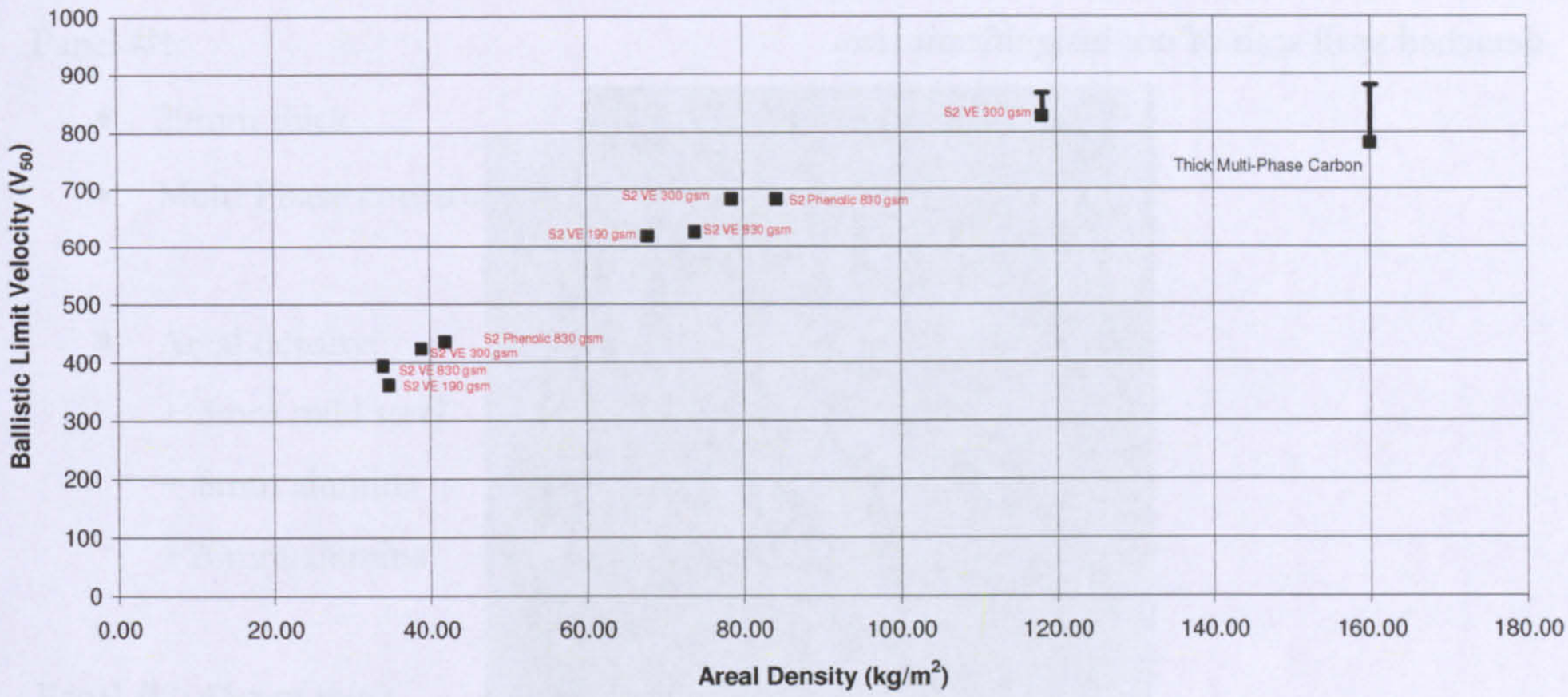

Graph 2: Summary of Carbon panel #2 Ballistic testing with GRFP testing for reference

Sectioning of the impacts revealed that there appears to be a significant yawing effect on the projectile when it encounters the interface layer between the UD reinforcement and the tape core, this is visible in every section.

Image 6: Yaw in impacted carbon

There appears to be a great deal of through thickness cracking in the outer, rear UD layer, this damage is also seen at the rear face significantly ahead of the projectile final location. These through thickness cracks progress away from the impact centre in a cone

like fashion and leave a significant amount of solid material detached from the bulk of the carbon held only by the mid-skin tape layer – this should it break free would form a detached spall scab of not insignificant size.

Image 7: Spall scab in impacted carbon

Against the Level IV threat the panel failed completely, the UD areas of laminate appearing to shatter whilst the tape areas of the laminate appearing to be more resilient

Image 8: Failure against STANAG level IV

Discussion and summary

As there is increasing interest in the use of CFRP as an armour material it was thought prudent to perform some limited testing on such material.

Two material panels were available for testing:

Panel #1:

- 29mm thick
- Multi Phase construction:
- Areal density: = 44 kgm^{-2}
  + 3mm mild steel = 66 kgm^{-2}
  + 8mm alumina = 78 kgm^{-2}
  +20mm alumina = 126 kgm^{-2}

Panel #2: 65mm thick

- Multi Phase construction:
- Areal density is: = 160 kgm^{-2}
  + 24mm alumina = 259 kgm^{-2}

Panel #1 was given a general evaluation against 7.62x51 AP (Steel core). This round has performance in excess of STANAG level II but below level II and was used due to range and ammunition availability.

At ~ 830ms^{-1} velocity panel #1 was easily defeated on its own, however the addition of a thin spaced steel plate stopped the round within the first 1/3 of the material thickness, the addition of a thin alumina tile stopped the round easily in the front face providing quite an attractive solution in terms of weight. Note on the following graph that the other data points are against the less powerful 7.62x39m AP with no surface disruption.

CFRP Panel #1

The experiments with this panel indicated that against small arms ammunition, carbon may offer reasonable protection at a good weight. However it appears that the material

does not fail in a nice way when over matched, rather it appears to shatter. This is especially evident when struck by heavier projectiles even with a lot of ceramic facing. It appears the shock caused by these higher energy impacts is enough to generate significant through thickness damage in the material.

CFRP Panel #2

Panel #2 was initially tested against STANAG level II ammunition with the intention of obtaining a V_{50} however it proved impossible due to the material thickness, the ammunition was uploaded to the highest level possible with no success. The following chart indicates the fastest stop, the error bars estimate the range in which the V_{50} is expected to fall, note the performance relative to the heaviest Vinylester material tested.

In the coarse weave material there is delamination, most of the damage is ahead of the arrest point and greater in magnitude in the direction the projectile has yawed. It appears that UD material is far more fragile than UD tape.

There is only a small amount of plastic deformation visible in the fibres and there is evidence of some fibre fracture.

When faced with a dangerous threat such as 14.5mm AP the carbon is entirely overmatched even with the addition of a significant amount of ceramic tile. The impact appears to have caused a shattering failure in the areas of the laminate made entirely from UD fibres whilst the areas made from UD tape appear more resilient. There is no visible bulk deformation.

APPENDIX: B

Effect of front surface disruption

Aims

Disruption of a projectile before it strikes an armour is an effective way of reducing the damage caused on impact. Often appliqué armour is added spaced in front of the main armour intended to cause the projectile to tumble or break up. Doing so increases the amount of armour involved in stopping penetration, i.e. the energy density is reduced.

The aim of this work is to qualitatively evaluate the response of composite armours to some spaced appliqué solutions.

Experimental

This round of ballistic testing was carried out with exactly the same equipment and experimental setup as that used in earlier testing detailed in chapter 3 of the preceeding thesis.

Panels tested

Sheets of heavy and medium weight Vinylester material were used with the following front surface disruptors:

1. EN24 Steel rods in a pack 30x30mm 30° to armour
2. 3.5mm RHA steel surface mounted as well as spaced from surface (25mm & 150mm)
3. 3.5mm perforated RHA steel surface mounted as well as spaced from surface (25mm)

Threats

The armour systems were tested against STANAG[13] level II AP ammunition concurrent with the other experimental work carried out in this project.

1. 7.62mm calibre armour piercing rounds (7.62x39 API) as per STANAG 4569[13] level II.

Results

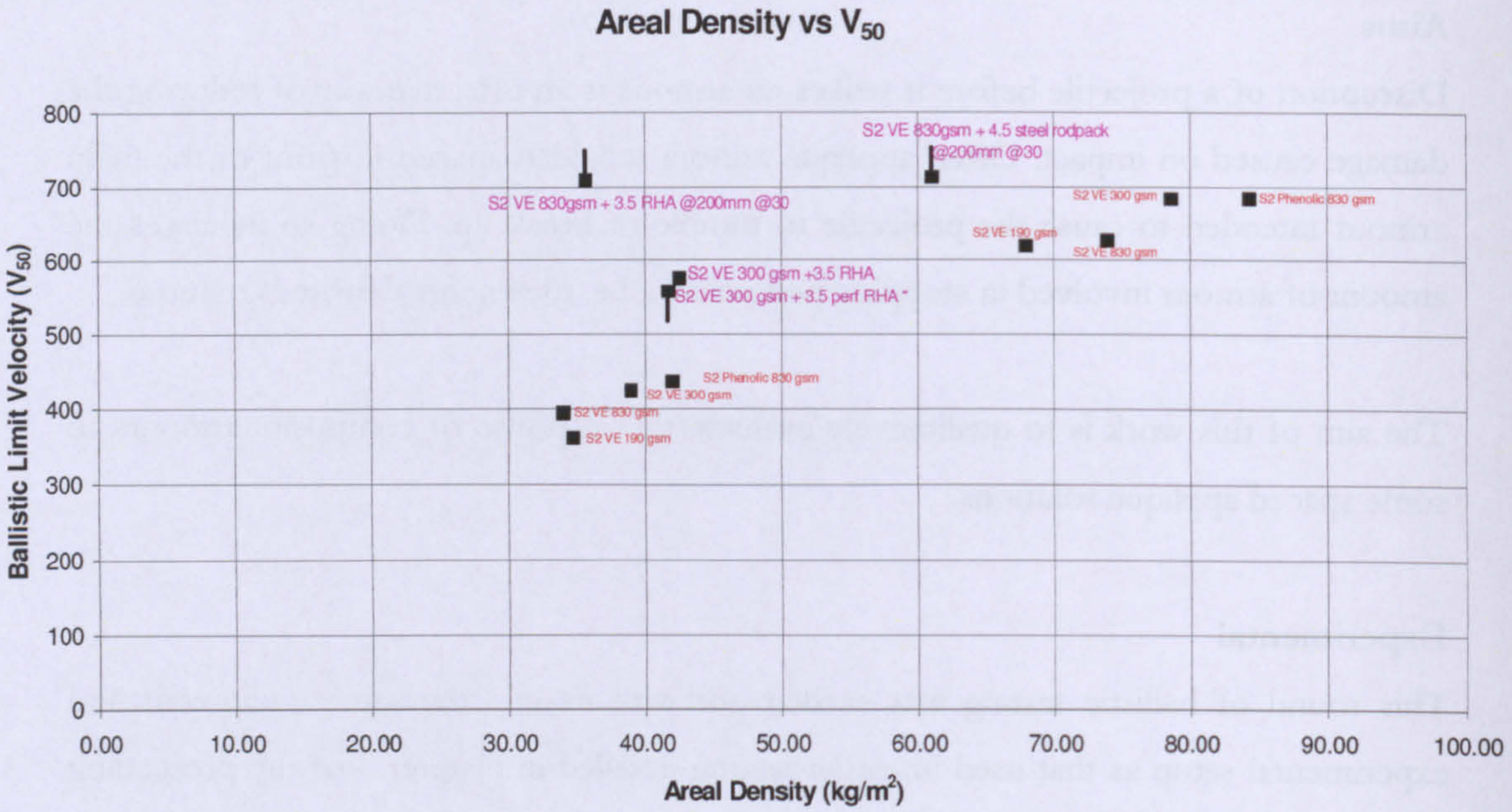

Graph 1: Effectiveness of front face disruption (Other GFRP testing included for comparison)

Discussion and summary

In practice there are advantages to having a steel skin to a composite armour system, gains in durability and easy use of conventional fastening techniques are all desirable. The use of a skin spaced from a main armour has been shown to provide significant advantages, however most systems require a significant gap between main armour and the front surface. It is believed that a composite system will respond very well to a front surface disruptor which can damage or deflect the projectile allowing a lower energy density to be applied to the soft composite. Initial testing of a CFRP system has indicated that significant gains should be possible in this area (Appendix A)

A number of different disruptor types were trialled:

1. 3.5mm RHA
2. 3.5mm RHA at 24mm
3. 3.5mm perforated RHA (5mm diameter holes every 5 mm)
4. 3.5mm perforated RHA (5mm diameter holes every 5 mm) at 25mm
5. 4.5mm Diameter EN24 steel rods (30mm long) spaced and inclined at 30°

The addition of a steel protective facing to the front face of the armour added only as much protection as the steel itself would offer, it can be seen from the following chart that for a small increase in areal density of less than $4kgm^{-2}$ $150ms^{-1}$ has been added to the V_{50} of the armour. This is roughly the performance of the plate alone i.e. there is no coupling effect between the plate and composite.

The perforation of the steel plate reduced ballistic performance but did not significantly reduce the overall areal density of the armour. The addition of 24mm of spacing to both plated brings the perforated plate to a similar level to that of the plain plate with only a small weight saving.

A small amount of spacing has had a beneficial effect but with only 25mm of spacing it is not incredible. Increasing the spacing to 200mm and introducing some obliquity has a greater effect on performance than expected, better than composite of double the thickness.

The steel rods appeared to have potential, however due to material constraints were only tested at the highest of standoffs where they gave slightly better performance than 3.5mm RHA plate but at a far higher weight, better constraint may have improved performance.

This sensitivity to spacing is believed to be due to the stripping of the bullet jacket material from the core allowing the composite to stop the core rather than being deeply penetrated by the jacket before the core can be slowed.

A brief investigation into a couple of novel disruption schemes was also undertaken, small tiles of RHA and aluminium were spaced off the surface of a target panel with the intention of both deflecting the projectile, stripping the jacket from the core and by sharing projectile energy with the motivated plate.

This testing indicated that whilst the plates used were motivated by the projectile they were too light to deflect the bullet and too heavy to be accelerated by the projectile before the plates were penetrated. The use of steel rods spaced from the target was more successful however the solution was rather heavy.

APPENDIX: C

Energy contributions: All materials vs Ball

		Ball - Stop				Ball - Perf			
		Heavy Phenolic	Heavy VE	Medium VE	Light VE	Heavy Phenolic	Heavy VE	Medium VE	Light VE
Tensile		16.45	34.84	18.65	9.04	17.33	33.87	22.17	29.98
Friction	**Dry**	10.19	30.16	48.98	18.66	10.92	35.65	71.99	59.71
	Lubricated	5.09	0.99	14.69	4.13	5.46	12.50	21.60	13.34
Bending		0.76	0.50	0.15	9.47	0.69	0.63	0.55	2.53
Indentation	**t-Hr Point**	3.12	2.68	2.91	2.90	3.12	2.68	2.91	2.90
	t-Hr Base	4.39	4.76	6.82	8.70	4.39	4.76	6.82	8.70
Mode I toughness	**All**	17.96	9.24	18.49	36.82	6.08	7.67	12.19	20.10
	Visible	8.65	4.11	5.14	1.14	3.58	3.63	3.45	5.00
Compression		3.23	2.76	2.57	4.71	4.40	3.36	3.91	5.86

Energy contributions: All materials vs AP

		AP - Stop				AP - Perf			
		Heavy Phenolic	Heavy VE	Medium VE	Light VE	Heavy Phenolic	Heavy VE	Medium VE	Light VE
Tensile		116.07	282.56	95.99	101.11	101.59	242.30	103.31	88.46
Friction	**Dry**	75.61	158.54	270.52	118.05	126.34	317.22	410.14	347.85
	Lubricated	32.55	71.38	81.16	67.80	54.38	142.82	123.04	125.31
Bending		5.26	6.67	3.16	3.09	0.71	3.88	0.39	2.74
Indentation	**AP - Point 1st**	60.02	55.30	41.60	37.36	60.02	55.30	41.60	37.36
	AP - Base 1st	60.02	98.10	97.60	112.25	84.32	98.12	97.60	112.50
	t-Hr Point	22.86	21.07	8.14	14.23	22.86	21.07	8.14	14.23
	t-Hr Base	32.12	37.38	19.10	42.76	32.12	37.38	19.10	42.76
Mode I toughness	**All**	10.60	12.99	16.79	95.68	11.99	16.98	17.16	52.31
	Visible	3.70	3.90	2,85	7.26	1.77	2.55	5.83	0.84
Compression		28.03	20.50	14.72	0.96	30.67	21.98	11.04	0.41

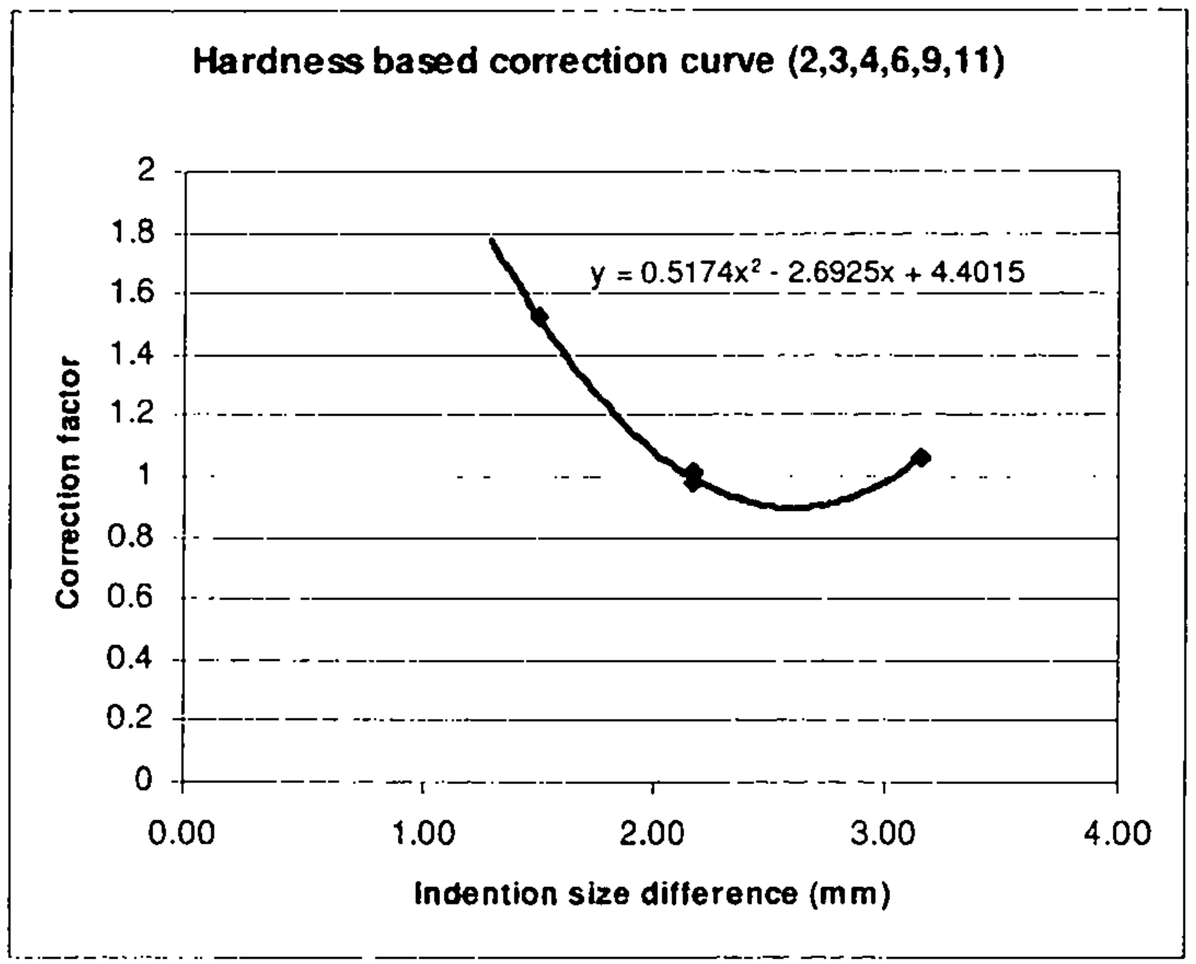
Hardness based correction curve (2,3,4,6,9,11)
y = 0.5174x² - 2.6925x + 4.4015
Correction factor
Indention size difference (mm)
0
0.2
0.4
0.6
0.8
1
1.2
1.4
1.6
1.8
2
0.00
1.00
2.00
3.00
4.00

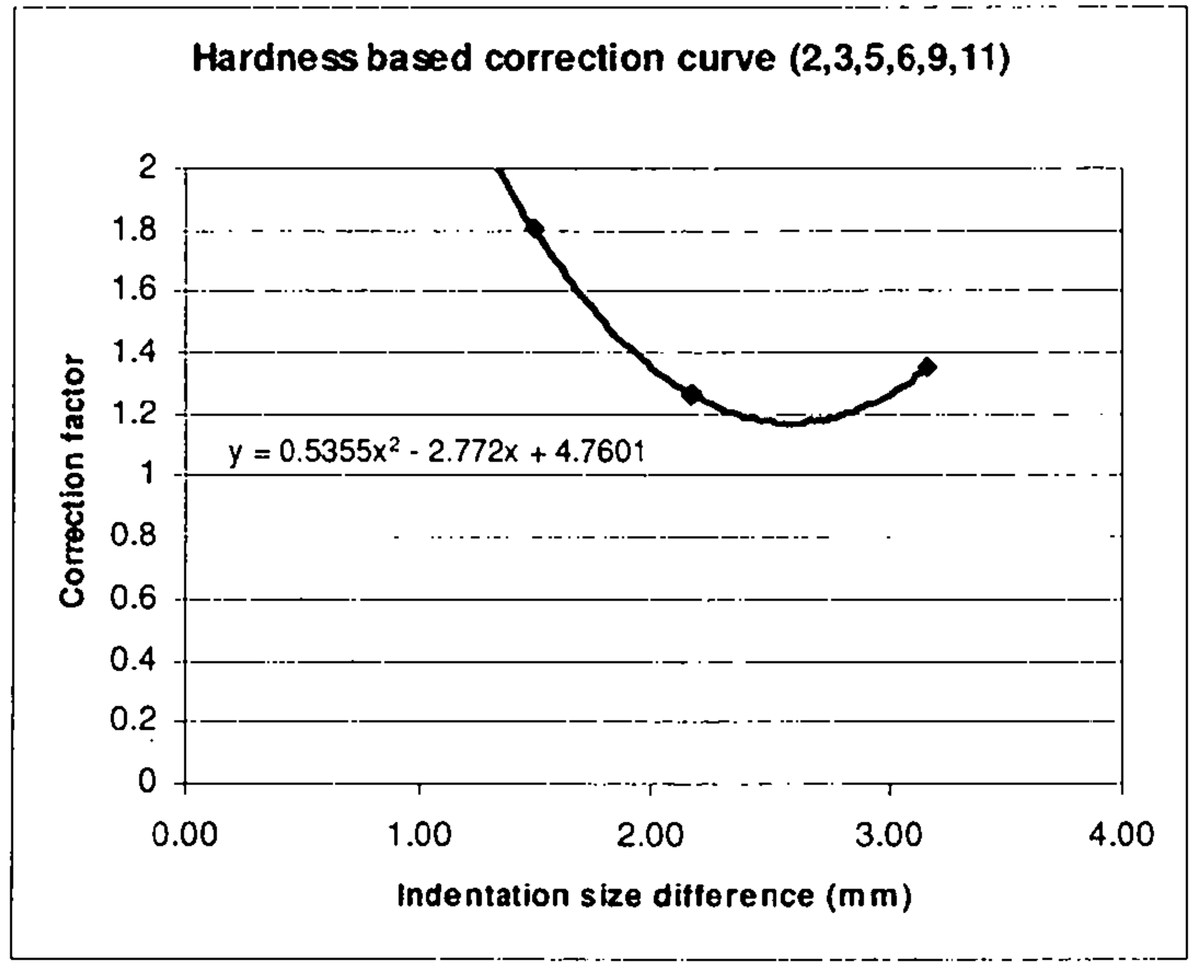
Hardness based correction curve (2,3,5,6,9,11)
y = 0.5355x² - 2.772x + 4.7601
Correction factor
Indentation size difference (mm)
0
0.2
0.4
0.6
0.8
1
1.2
1.4
1.6
1.8
2
0.00
1.00
2.00
3.00
4.00

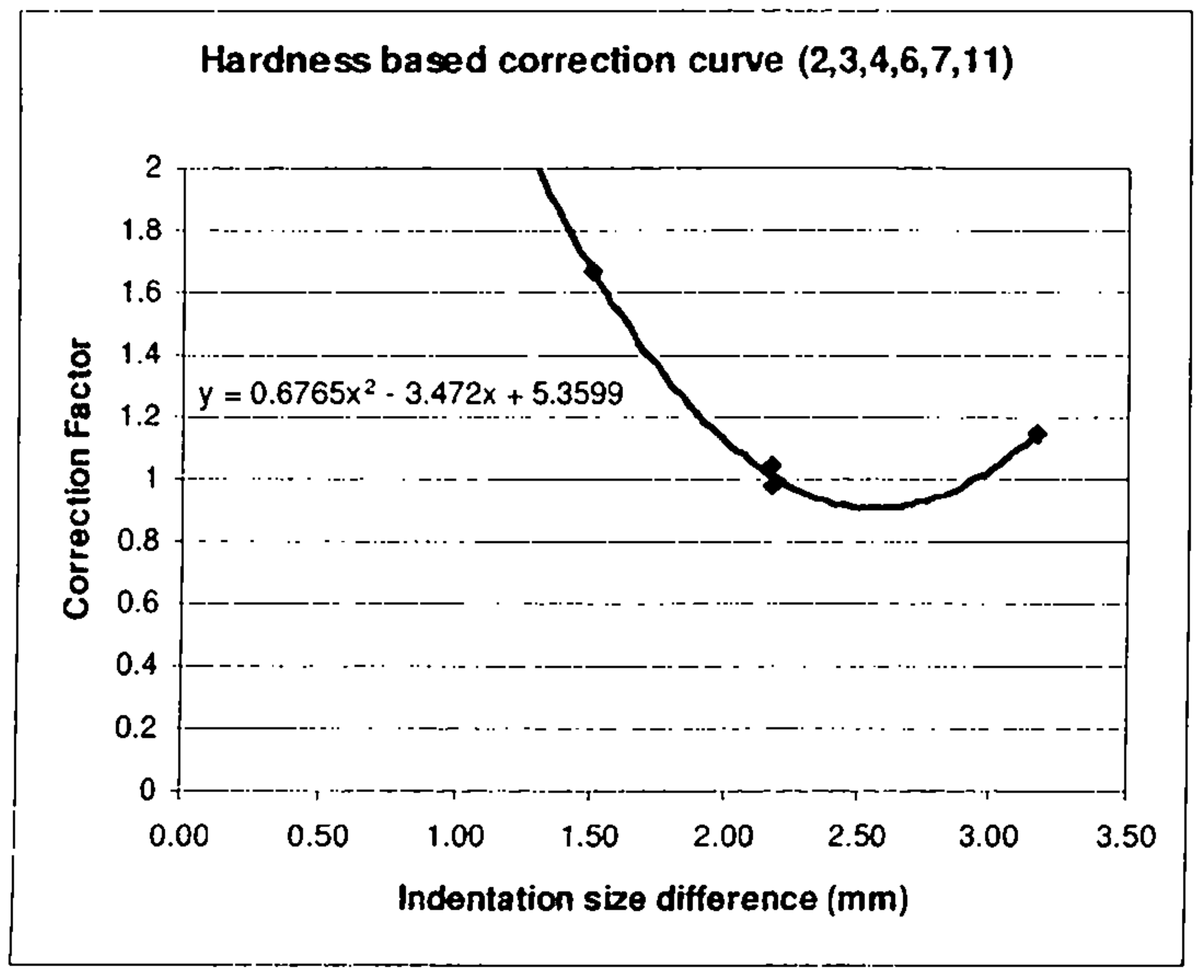
Hardness based correction curve (2,3,4,6,7,11)
y = 0.6765x² - 3.472x + 5.3599
Correction Factor
Indentation size difference (mm)
0
0.2
0.4
0.6
0.8
1
1.2
1.4
1.6
1.8
2
0.00
0.50
1.00
1.50
2.00
2.50
3.00
3.50

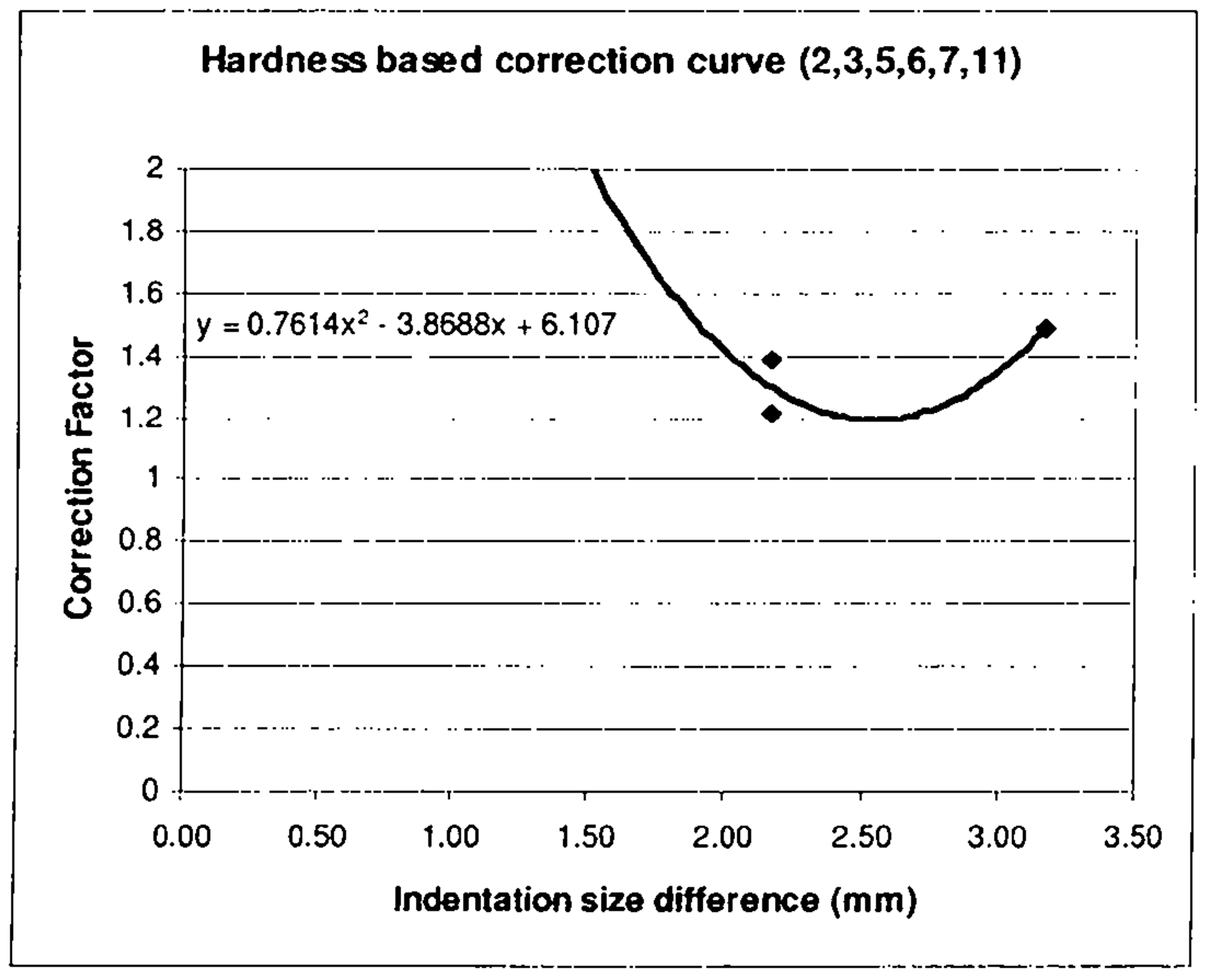
Hardness based correction curve (2,3,5,6,7,11)
y = 0.7614x² - 3.8688x + 6.107
Correction Factor
Indentation size difference (mm)
0
0.2
0.4
0.6
0.8
1
1.2
1.4
1.6
1.8
2
0.00
0.50
1.00
1.50
2.00
2.50
3.00
3.50

APPENDIX: D

Dynamic Mode I rig:

Tower

ReadMe - Sample Tower Assembly Notes

Cranfield Dynamic Rig Assembly Notes - Sample Tower

Drawings 010 - 016 & 018
Author PDB

Construction:
Towet is to be assembled by suitable welds of sufficient strength - arc welding recommended

Considerations:
Striker forks pass close to tower walls, all welds must be on the inside of tower, any welding / projections on outside of tower must be ground flat.

Roof of tower MUST be perpendicular to baseplate to ensure sample alignment

Finishing of tower roof welds may be required to allow load cell to be bolted flush to roof - large welds may intefer with this.

PART NUM	DWG NUM	PART NAME	NUM OF	MATERIAL
1	010	TOWER ROOF	1	MILD STEEL SHEET
2	011	TOWER BACK PLATE	1	MILD STEEL SHEET
3	012	TOWER SIDE PLATE (FRONT)	1	MILD STEEL SHEET
4	013	TOWER SIDE PLATE (REAR)	1	MILD STEEL SHEET
5	015	TOWER BASE PLATE	1	MILD STEEL SHEET

RMCS Cranfield UNIVERSITY

CHANGE:			No.	DATE
TITLE: DYNAMIC RIG: TOWER PARTS LIST	DRAWN: PDB	DATE: 21/04/05	APPROVED:	
	MATL:	TOL: ±0.1 UNLESS STATED	SCALE:	
DWG No. 018 / ISSUE No. 2	ACAD FILE:	3.2 SURFACE FINISH IN μm UNLESS STATED	DIMS. IN: mm	

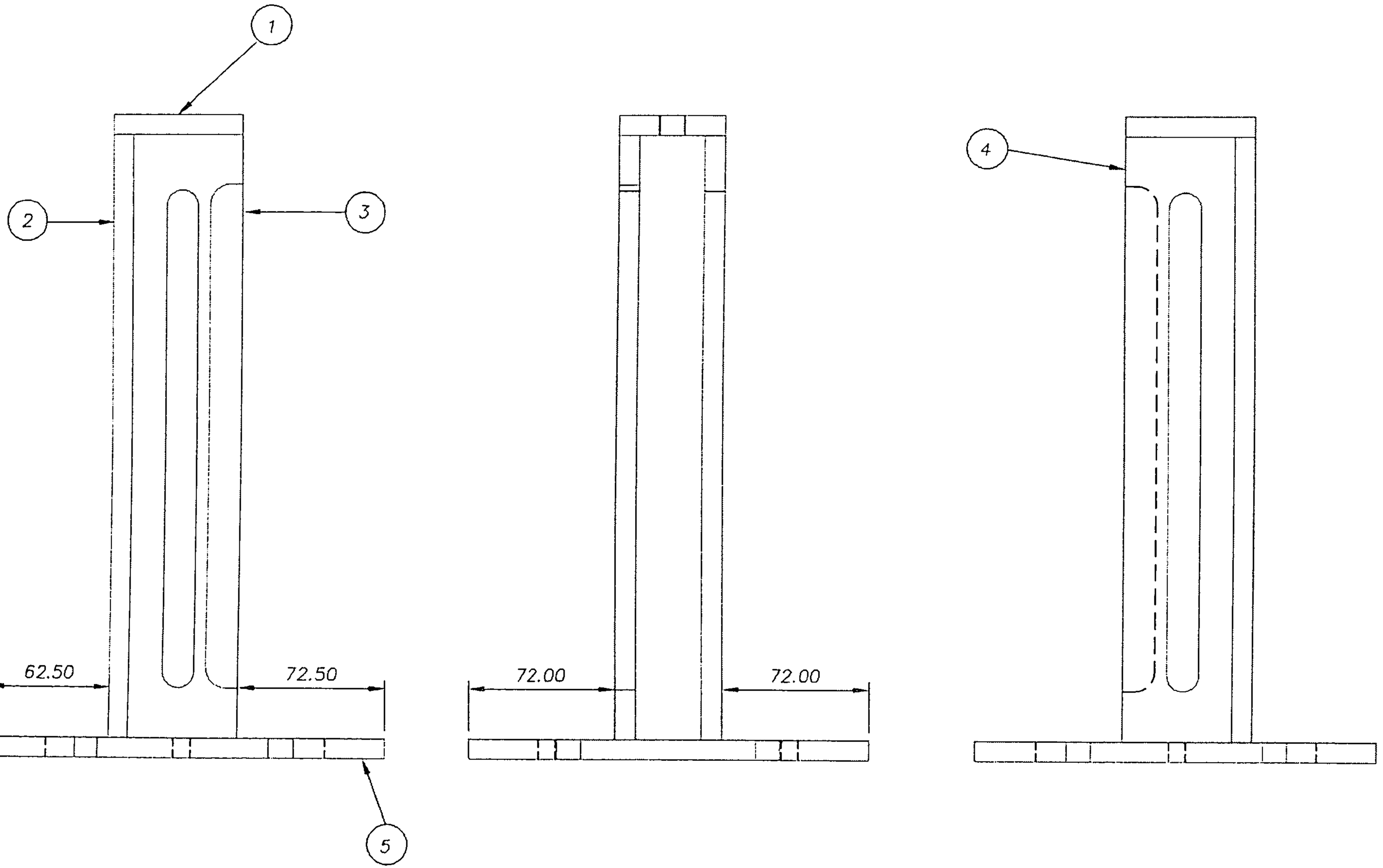

ALL JOINTS WELDED ON INSIDE FACES

CHANGE	No.	DATE
2nd generation side plates added	1	

MATL: 10mm MILD STEEL PLATE	DRAWN: PDB	DATE: 19/04/05	APPROVED:	SCALE 2:1	RMCS Cranfield UNIVERSITY	TITLE: DYNAMIC RIG – TOWER GENERAL ASSY
	FINISH:	TOLERANCES: ±0.1 UNLESS STATED	3.2 SURFACE FINISH IN µm UNLESS STATED	DIMNS. IN mm		DWG. No. 015 / ISSUE No. 4 / ACAD FILE: / A3

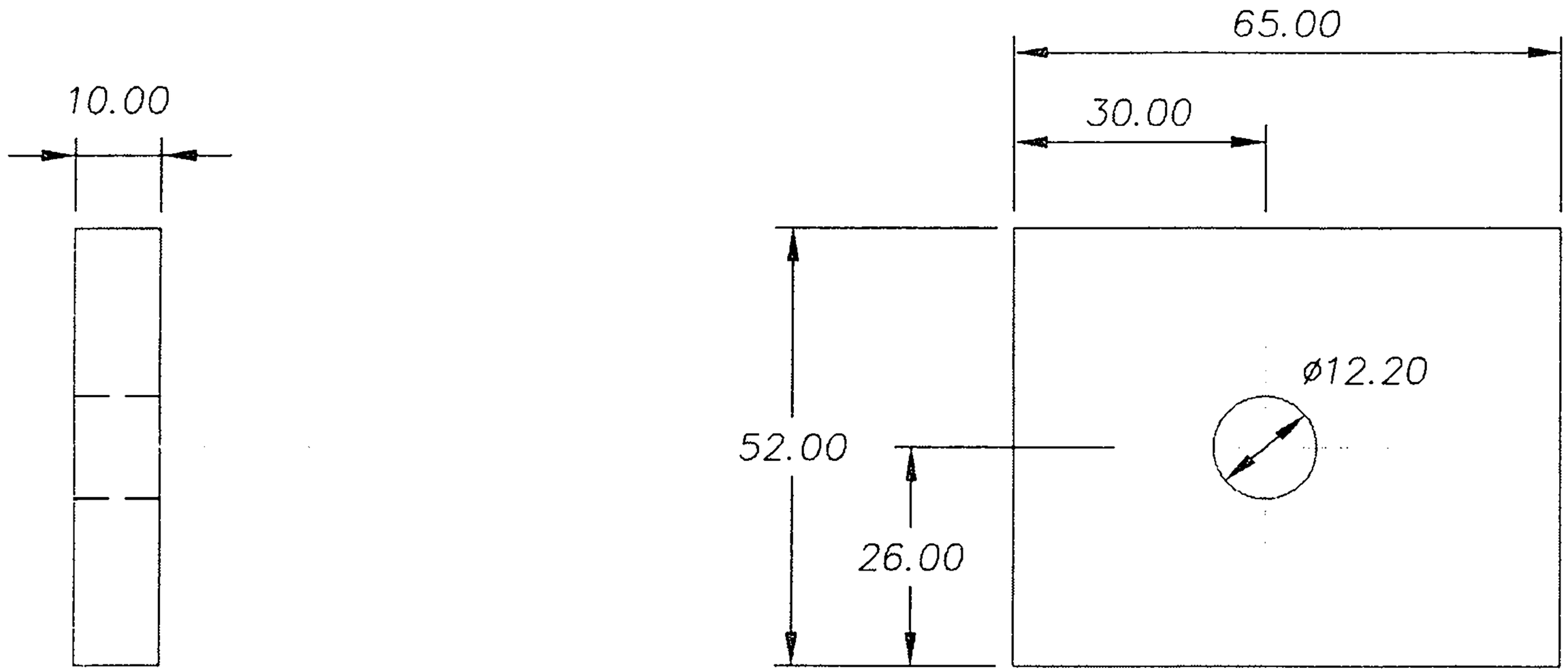

				CHANGE:	No. DATE
TITLE: TOWER ROOF				DRAWN: PDB	DATE: 15/04/05 APPROVED:
MATL: MILD STEEL PLATE			TOL: ±0.1 UNLESS STATED	SCALE : 1:1	RMCS Cranfield UNIVERSITY A4
DWG No. 010	ISSUE No. 1	ACAD FILE:	3.2 SURFACE FINISH IN μm UNLESS STATED	DIMS. IN: mm	

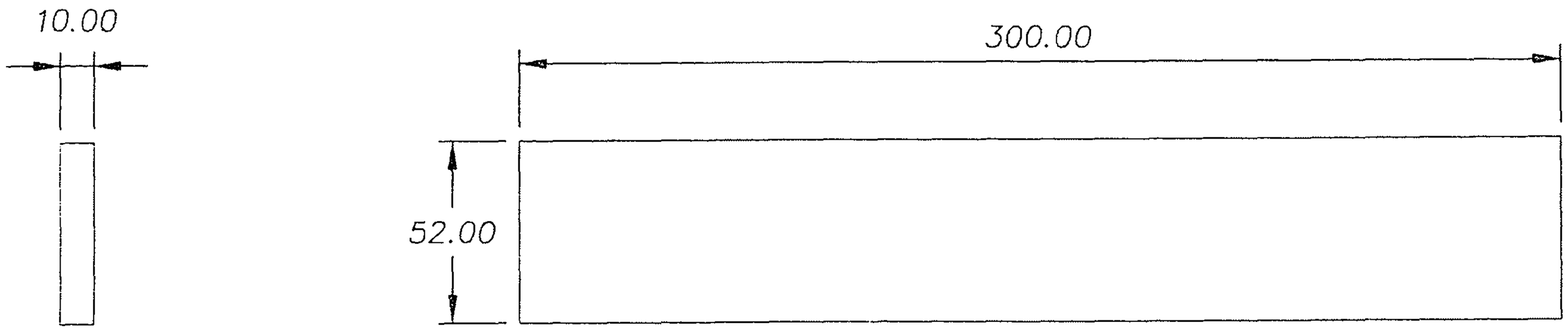

				CHANGE:	No.	DATE
TITLE: TOWER BACK PLATE				DRAWN: PDB	DATE: 15/04/05	APPROVED:
MATL: MILD STEEL PLATE			TOL: ±0.1 UNLESS STATED	SCALE : 1: 2	RMCS Cranfield UNIVERSITY	A4
DWG No. 011	ISSUE No. 2	ACAD FILE:	3.2 SURFACE FINISH IN μm UNLESS STATED	DIMS. IN: mm		

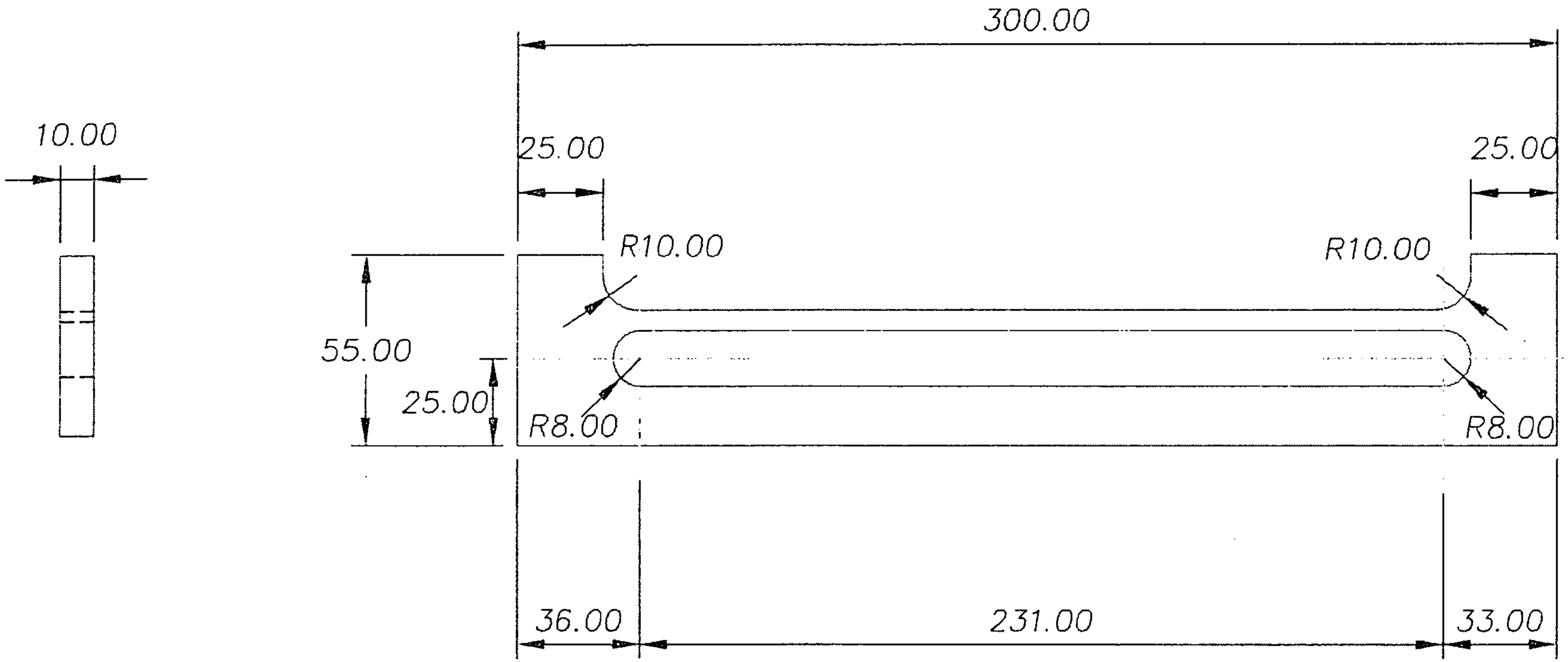

				Slot elongated to include upper mount hole	1	
				CHANGE:	No.	DATE
TITLE: TOWER SIDE PLATE (FRONT)				DRAWN: PDB	DATE: 15/04/05	APPROVED:
MATL: MILD STEEL PLATE			TOL: ±0.1 UNLESS STATED	SCALE : 1: 2	RMCS Cranfield UNIVERSITY	A4
DWG No. 012	ISSUE No. 2	ACAD FILE:	3.2 SURFACE FINISH IN μm UNLESS STATED	DIMS. IN: mm		

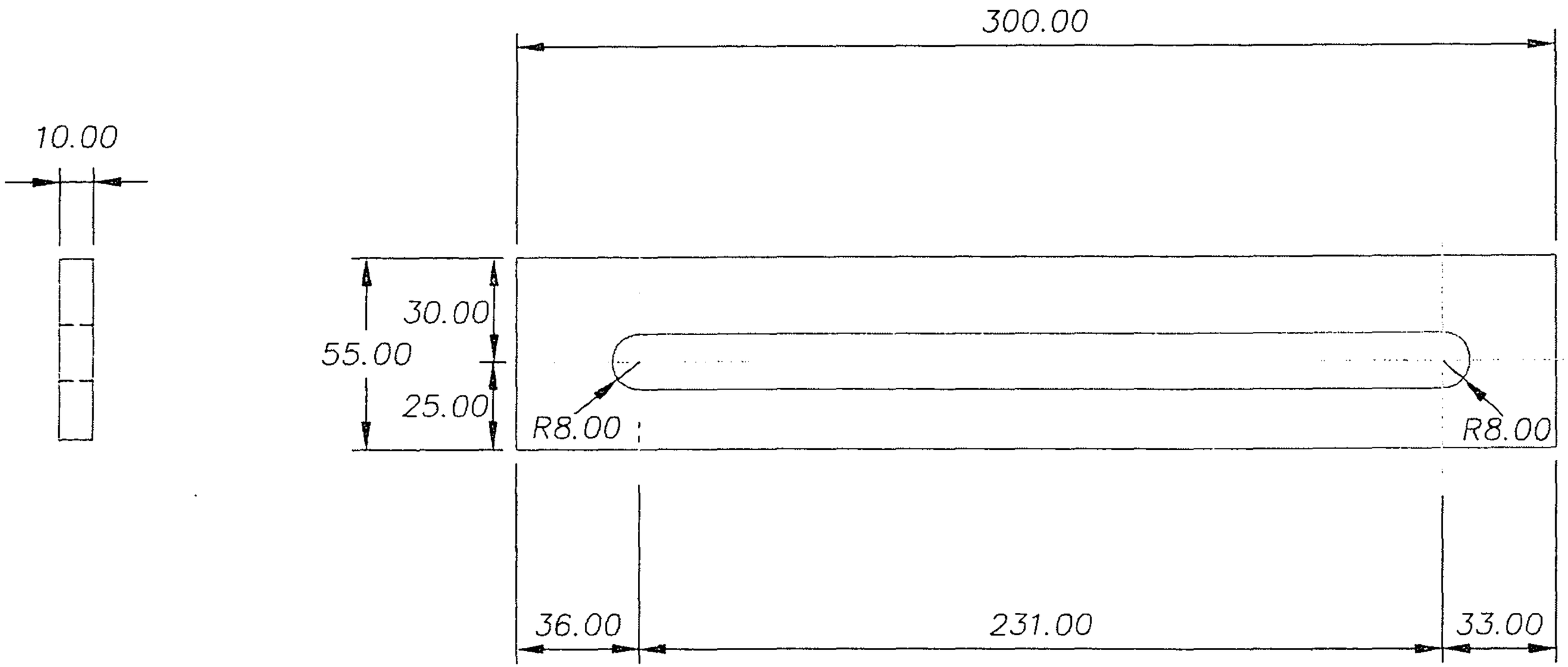

CHANGE:	No.	DATE
Slot elongated to include upper mount hole	1	
Dimensioning corrected	2	05/06/06

TITLE: TOWER SIDE PLATE (REAR)			DRAWN: PDB	DATE: 16/04/05	APPROVED:
MATL: MILD STEEL PLATE		TOL: ±0.1 UNLESS STATED	SCALE : 1: 2	RMCS Cranfield UNIVERSITY	A4
DWG No. 013	ISSUE No. 2	ACAD FILE:	3.2 SURFACE FINISH IN μm UNLESS STATED	DIMS. IN: mm	

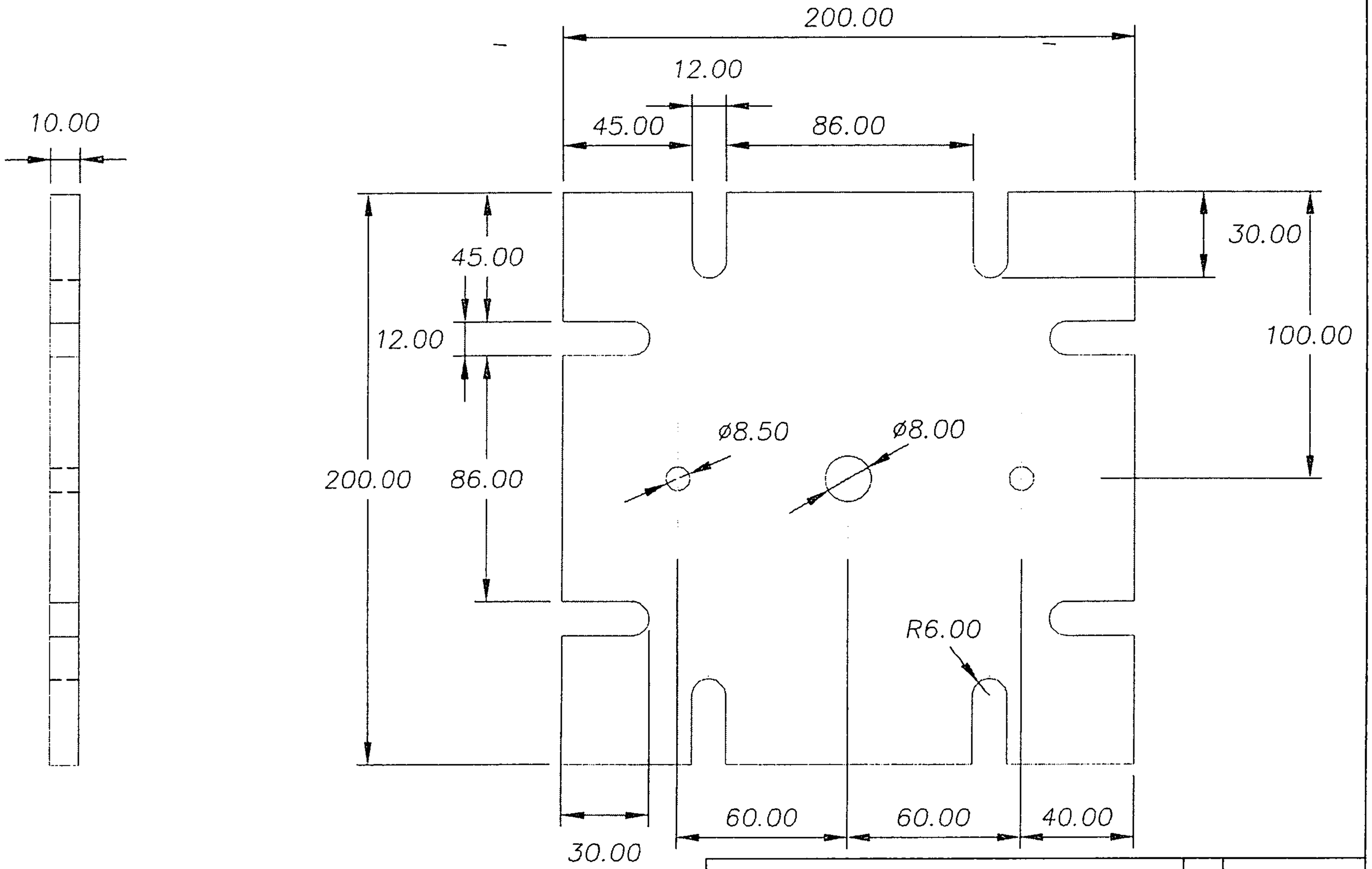

Access hole for calibration load added	2	
2nd Generation baseplate shape	1	
CHANGE:	No.	DATE

TITLE: TOWER BASE PLATE			DRAWN: PDB	DATE: 20/04/05	APPROVED:
MATL: MILD STEEL PLATE		TOL: ±0.1 UNLESS STATED	SCALE : 2:1	RMCS Cranfield UNIVERSITY	A4
DWG No. 015	ISSUE No. 4	ACAD FILE:	3.2 SURFACE FINISH IN μm UNLESS STATED	DIMS. IN: mm	

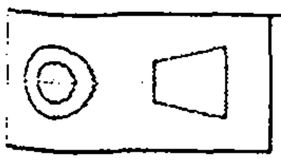

PART NUM	DWG NUM	PART NAME	NUM OF	MATERIAL
1	004	UPPER LOADBLOCK PIN	1	MILD STEEL
2	005	UPPER LOAD BLOCK	1	MILD STEEL
3	006	LOWER LOAD BLOCK	1	ALUMINIUM
4	007	UPPER MOUNT	1	MILD STEEL
5	008	LOWER STRIKE PIN	1	MILD STEEL
6	009	LOWER STRIKE PIN SLEEVE	1	MILD STEEL
7	010	STAND TOP PLATE	1	MILD STEEL SHEET
8	011	STAND BACK PLATE	1	MILD STEEL SHEET
9	012	STAND SIDE PLATE (FRONT)	1	MILD STEEL SHEET
10	013	STAND SIDE PLATE (REAR)	1	MILD STEEL SHEET
11	015	STAND BASE PLATE	1	MILD STEEL SHEET
12	N/A	M12x1.75 x 35 BOLT		12.8
a)		SAMPLE		
b)		LOAD CELL		

RMCS Cranfield UNIVERSITY

CHANGE:	No.	DATE

TITLE: DYNAMIC RIG PARTS LIST	DRAWN: PDB	DATE: 21/04/05	APPROVED:	
	MATL:	TOL: ±0.1 UNLESS STATED	SCALE:	
DWG No. 017 / ISSUE No.	ACAD FILE:	3.2 SURFACE FINISH IN μm UNLESS STATED	DIMS. IN: mm	A4

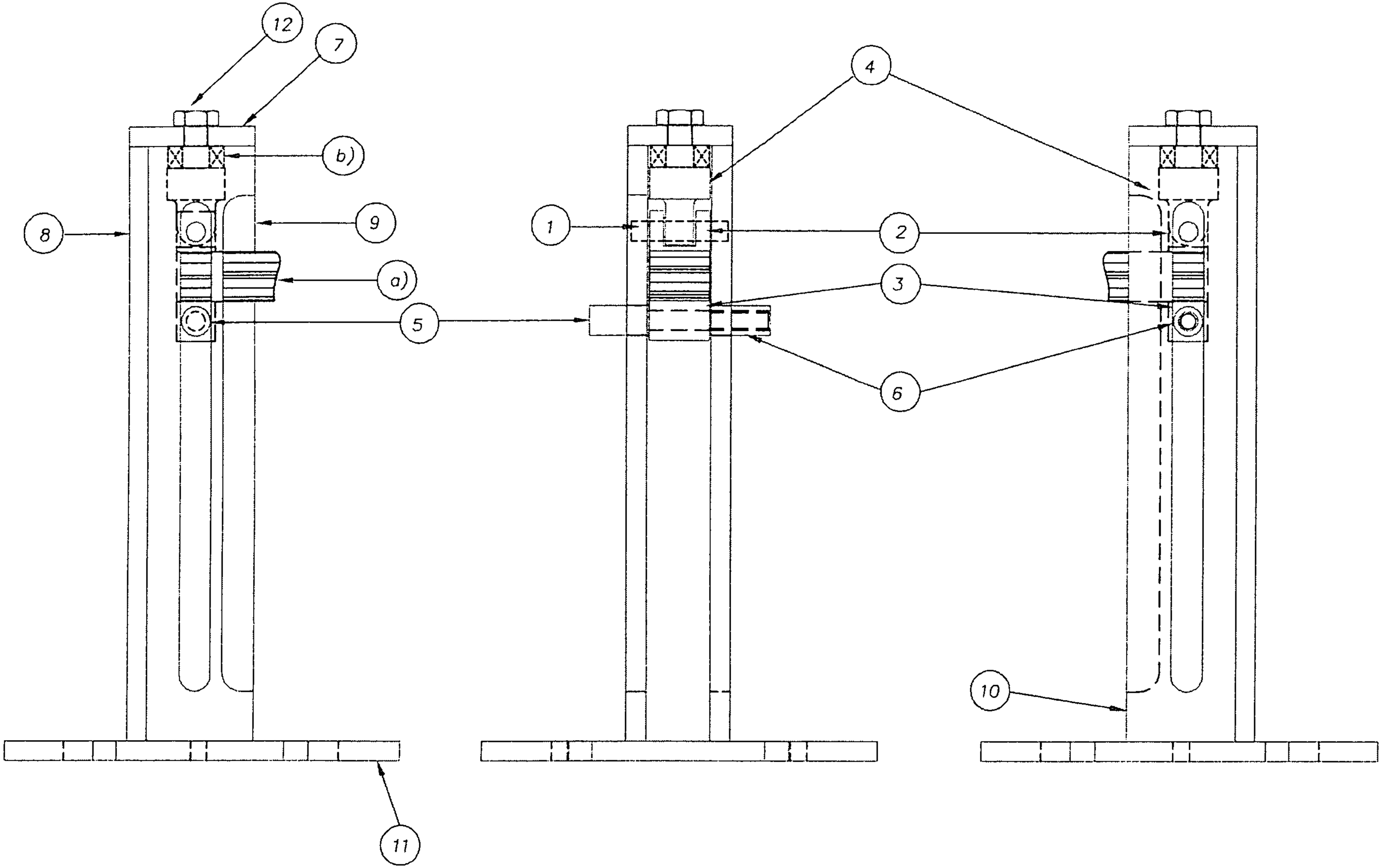

MATL:	DRAWN: PDB	DATE: 19/04/05 APPROVED:	SCALE 1:2	RMCS Cranfield UNIVERSITY	TITLE: DYNAMIC RIG – GENERAL ASSY	DWG. No. PHD 014 A3
	FINISH:	TOLERANCES: ±0.1 UNLESS STATED 3.2/ SURFACE FINISH IN µm UNLESS STATED	DIMNS. IN mm			ISSUE No. 4 ACAD FILE:

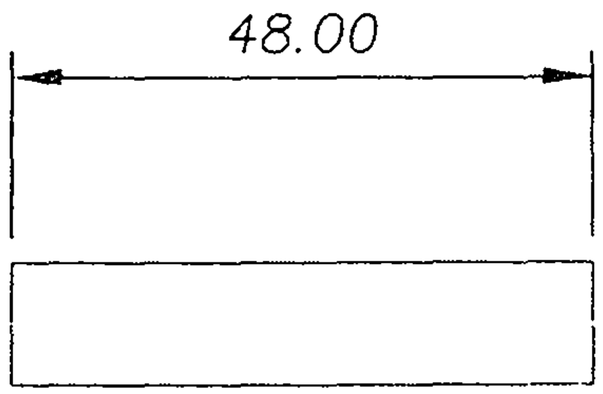

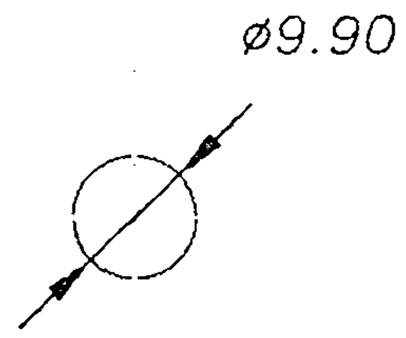

				CHANGE:	No.	DATE
TITLE: UPPER LOAD BLOCK PIN				DRAWN: PDB	DATE:14/04/05	APPROVED:
MATL: MILD STEEL			TOL: ±0.1 UNLESS STATED	SCALE : 1:1	RMCS Cranfield UNIVERSITY	A4
DWG No. 004	ISSUE No. 1	ACAD FILE:	3.2 SURFACE FINISH IN µm UNLESS STATED	DIMS. IN: mm		

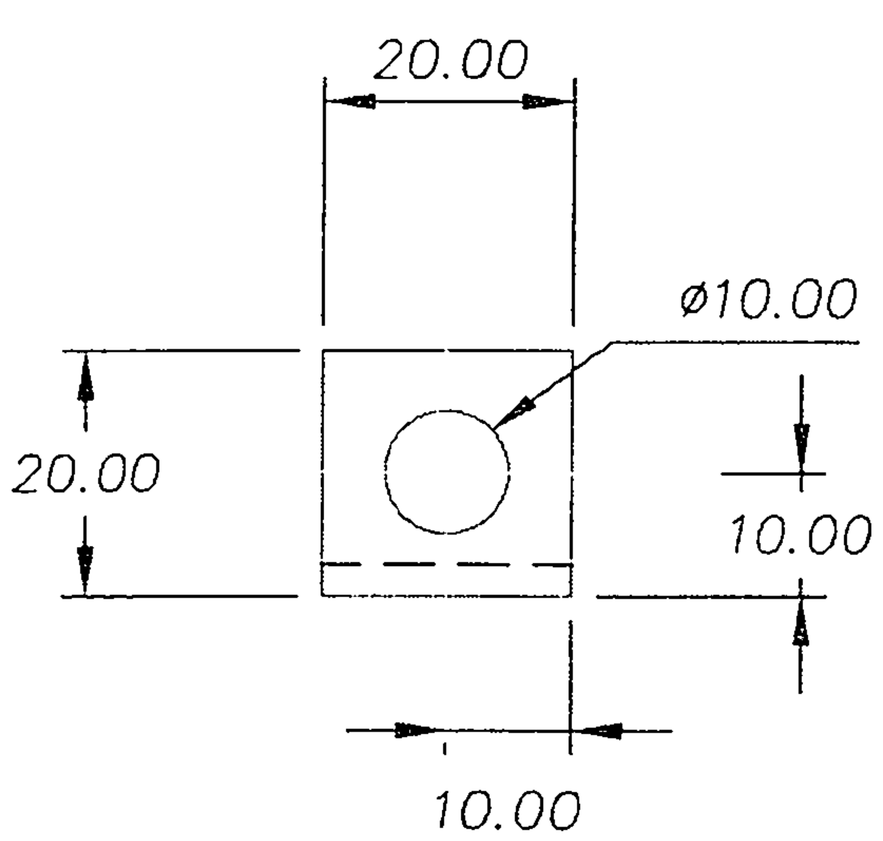

Dimensioning tidied	*1*	*5/6/06*
CHANGE:	No.	DATE

TITLE: *UPPER LOAD BLOCK – DYNAMIC*				DRAWN: *PDB*	DATE:*14/04/05* APPROVED:	
MATL: *MILD STEEL*			TOL: *±0.1 UNLESS STATED*	SCALE : *1: 1*	RMCS Cranfield UNIVERSITY	A 4
DWG No. *005*	ISSUE No. *2*	ACAD FILE:	3.2 SURFACE FINISH IN μm UNLESS STATED	DIMS. IN: mm		

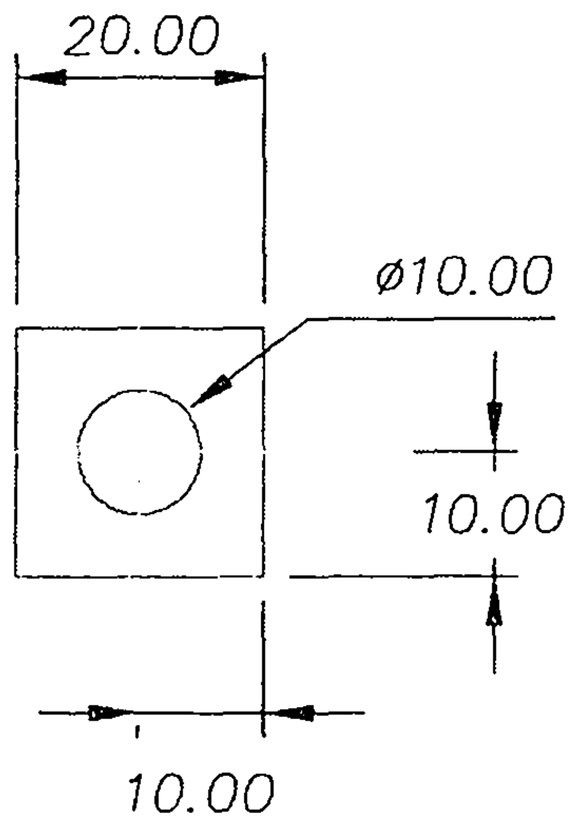

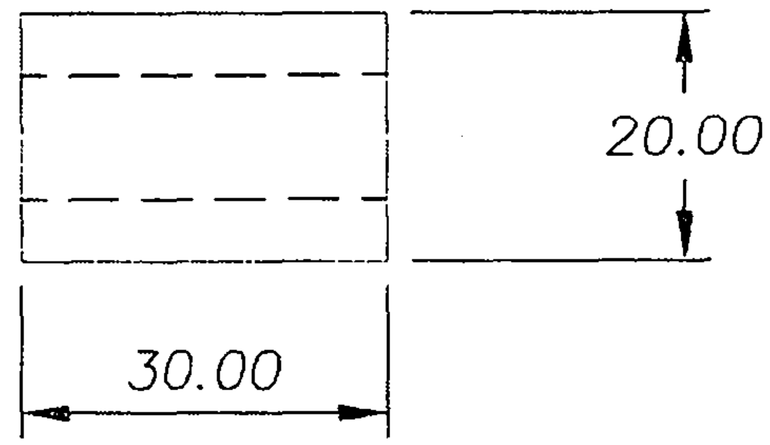

Dimensioning tidied	*1*	*5/6/06*
CHANGE:	No.	DATE

TITLE: *LOWER LOAD BLOCK – DYNAMIC*				DRAWN: *PDB*	DATE:*14/04/05*	APPROVED:
MATL: *ALUMINIUM*			TOL: *±0.1 UNLESS STATED*	SCALE :*1:1*	RMCS Cranfield UNIVERSITY	A4
DWG No. *006*	ISSUE No. *2*	ACAD FILE:	3.2 SURFACE FINISH IN μm UNLESS STATED	DIMS. IN: mm		

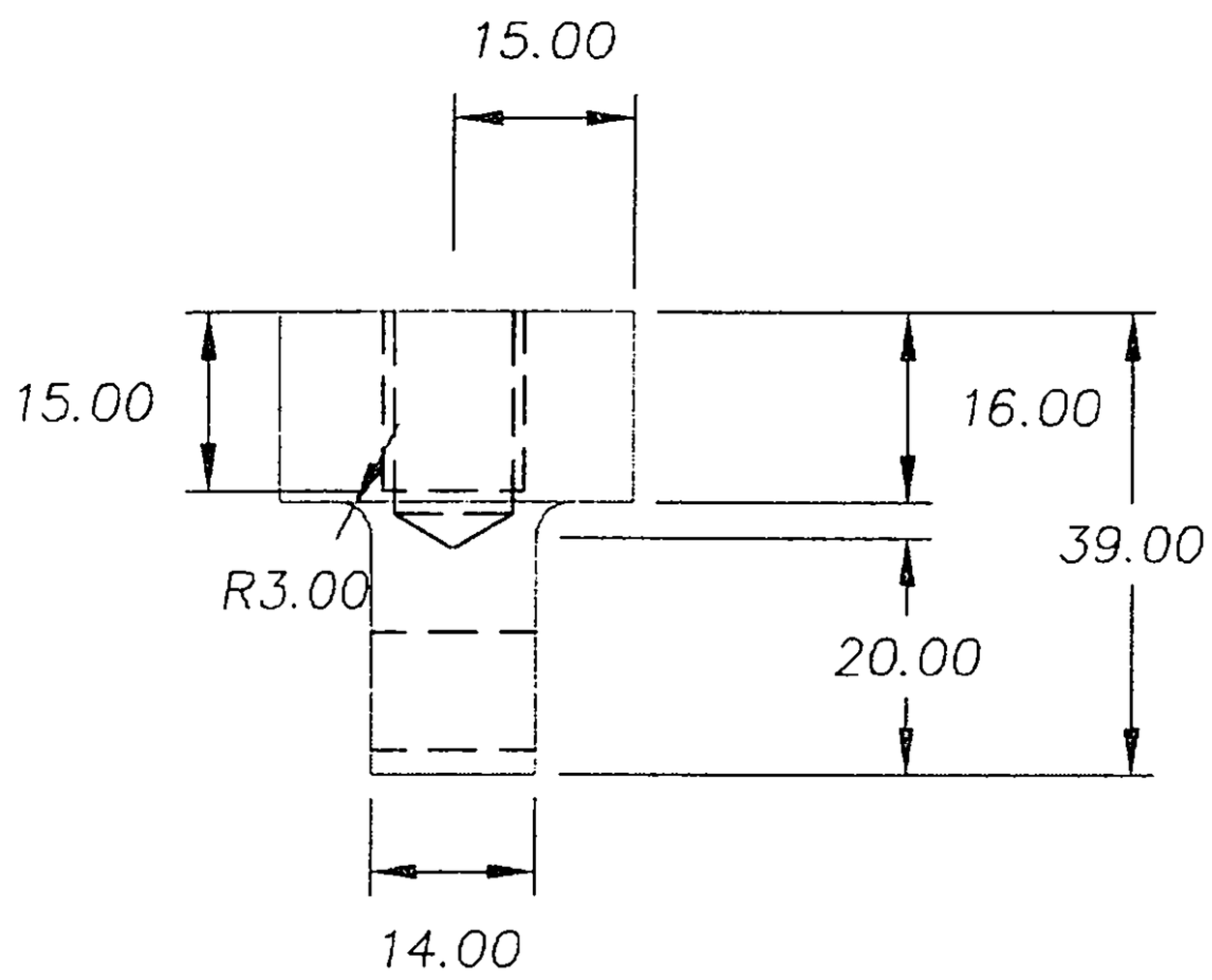

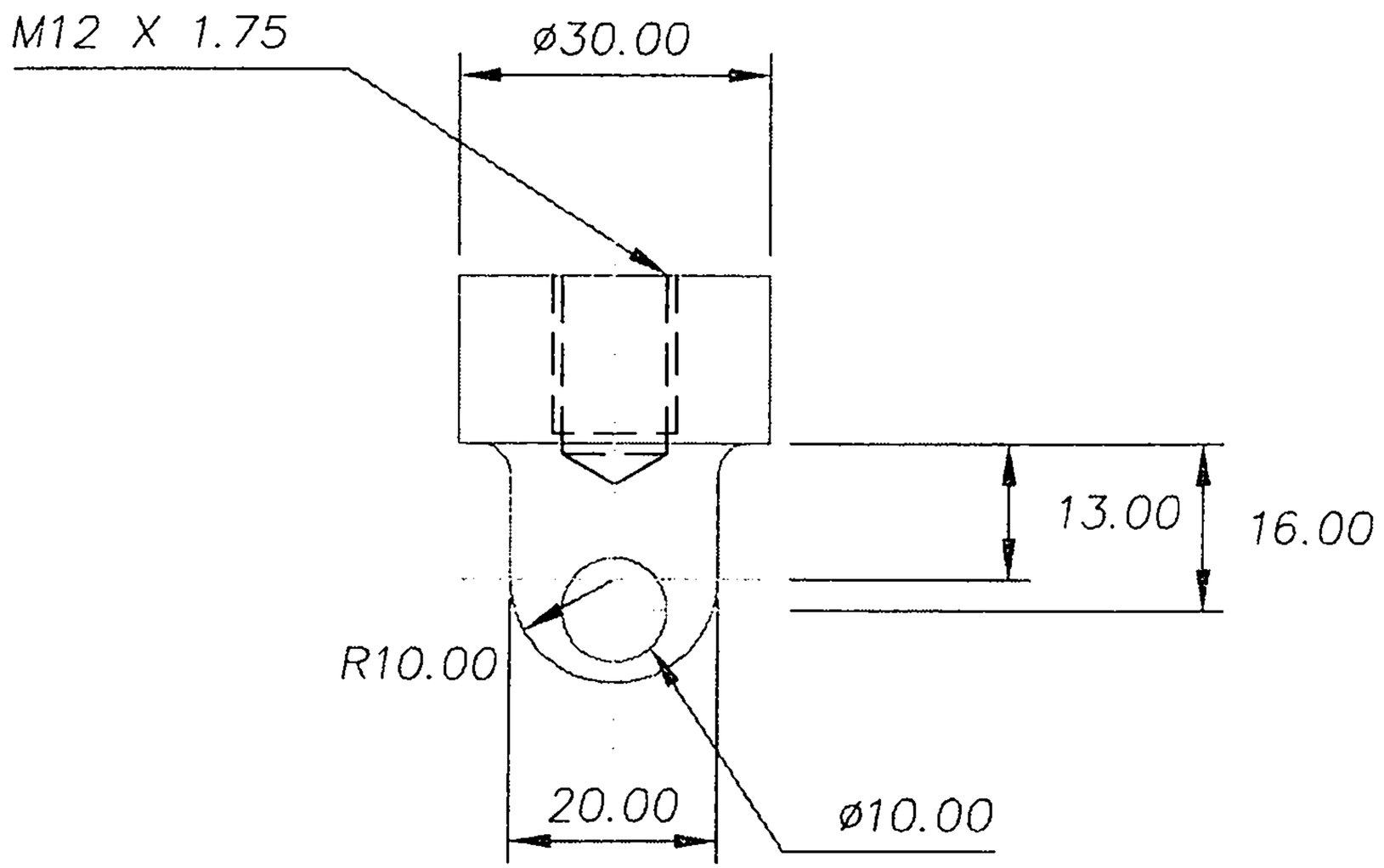

Dimensioning corrected	2	5/06/06
Mount base shape changed to cylider	1	
CHANGE:	No.	DATE

TITLE: UPPER MOUNT DYNAMIC				DRAWN: PDB	DATE: 14/04/05 APPROVED:
MATL: MILD STEEL			TOL: ±0.1 UNLESS STATED	SCALE : 1:1	RMCS Cranfield UNIVERSITY A4
DWG No. 007	ISSUE No. 3	ACAD FILE:	3.2 SURFACE FINISH IN µm UNLESS STATED	DIMS. IN: mm	

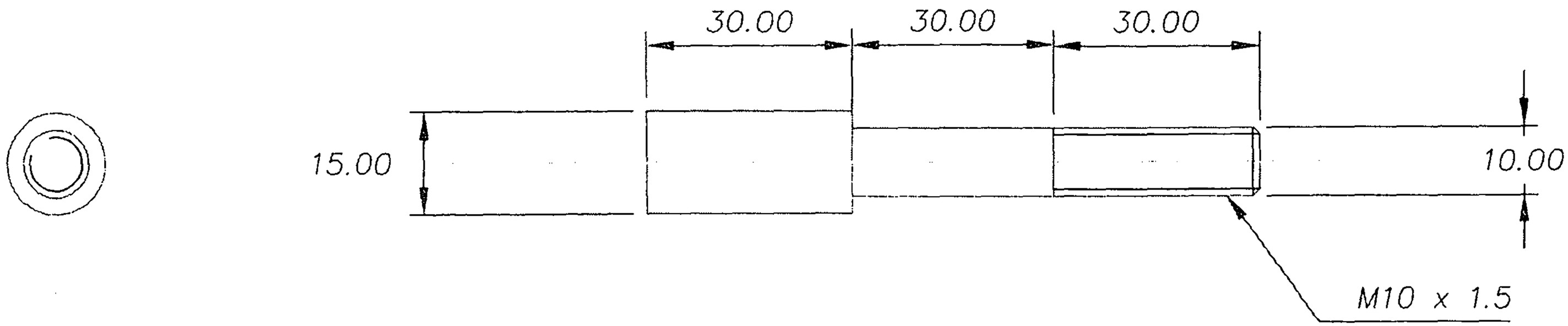

Dimensioning tidied	1	05/06/06
CHANGE:	No.	DATE

TITLE: LOWER STRIKE PIN				DRAWN: PDB	DATE: 14/04/05 APPROVED:	
MATL: MILD STEEL			TOL: ±0.1 UNLESS STATED	SCALE : 1: 1	RMCS Cranfield UNIVERSITY	A4
DWG No. 008	ISSUE No. 2	ACAD FILE:	3.2 SURFACE FINISH IN μm UNLESS STATED	DIMS. IN: mm		

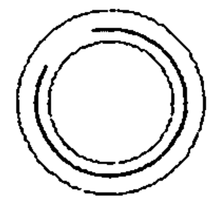

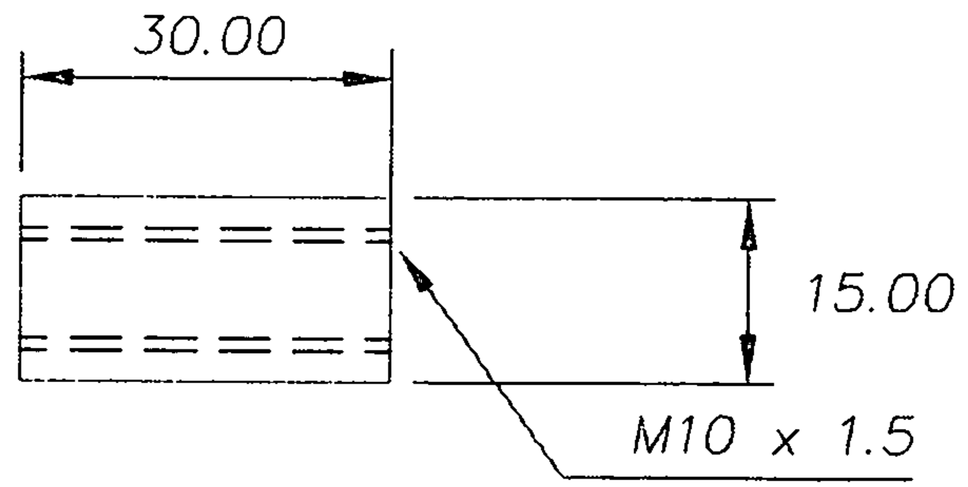

				CHANGE:	No. DATE
TITLE: LOWER STRIKE PIN SLEEVE				DRAWN: PDB	DATE: 15/04/05 APPROVED:
MATL: MILD STEEL			TOL: ±0.1 UNLESS STATED	SCALE : 1: 1	RMCS Cranfield UNIVERSITY A4
DWG No. 009	ISSUE No.	ACAD FILE:	3.2 SURFACE FINISH IN μm UNLESS STATED	DIMS. IN: mm	

Dynamic Mode I rig:

Striker Forks

ReadMe - Striker Forks Assembly Notes

Cranfield Dynamic Rig Assembly Notes - Striker Forks

Drawings 019 - 024
Author PDB

Construction:

Forks are to be assembled by suitable welds of sufficient strength - arc welding recommended

Considerations:

Striker forks MUST remain perpendicular to base plate and parrallel along their length (within 0.5mm), this should be checked after welding process to assess any heat induced distortion.

Ultimate distance between base plate and fork tips MUST be identical (less than 0.2mm) to ensure striker loads both sides of the sample simultainiously, finish machining may be peformed to achieve this.

Mounting to machine:

Drawing 020 shows mounting blocks used to fix striker forks to Cranfield (DCMT's) droptower. Different machines will require different fixtures.

It is suggested that a 10mm thick steel plate of the same overall dimensions as the striker baseplate (019) is attached to the test machine with countersunk fasteners. The baseplate should be bolted to this adaptor using existing mounting holes.

PART NUM	DWG NUM	PART NAME	NUM OF	MATERIAL
1	021	STRIKER FORKS	2	MILD STEEL PLATE
2	022	STRIKER FORK GUSSET	2	MILD STEEL PLATE
3	019	STRIKER MOUNT PLATE	1	MILD STEEL PLATE
4	020	STRIKER MOUNT BLOCKS	2	ALUMINIUM
5	N/A	M8x1.25 x 15 BOLTS	4	8.8

RMCS Cranfield UNIVERSITY

No.	DATE	CHANGE:
1	28/05/06	Fastner grade specified

TITLE: STRIKER FORK PARTS LIST

DRAWN: PDB | DATE: 24/04/05 | APPROVED:

MATL: | TOL: ±0.1 UNLESS STATED | SCALE:

DWG No. 024 | ISSUE No. 2 | ACAD FILE: | 3.2 SURFACE FINISH IN µm UNLESS STATED | DIMS. IN: mm | A4

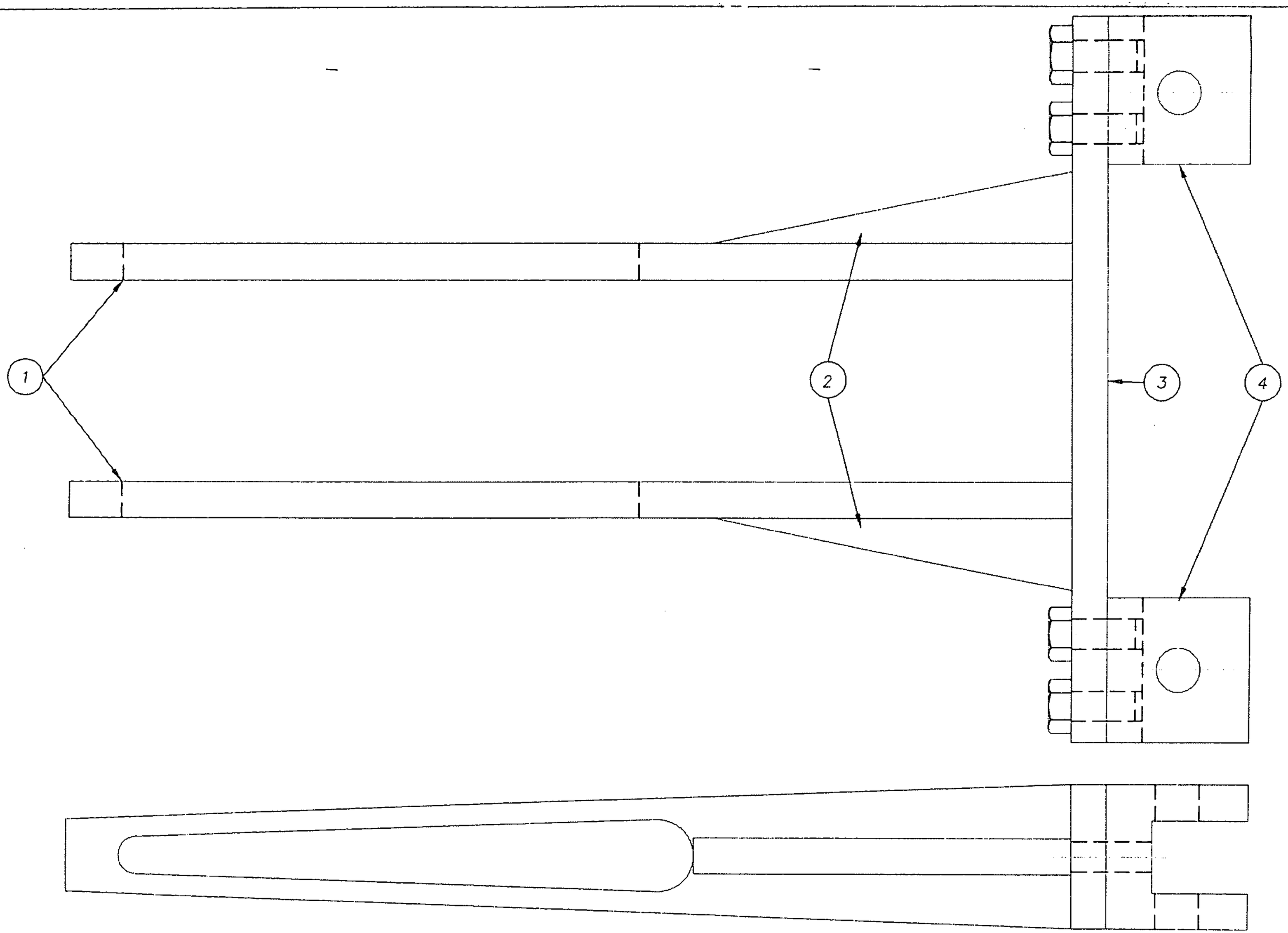

MATL:	DRAWN: PDB	DATE: 24/04/05	APPROVED:	SCALE 1:1	RMCS Cranfield UNIVERSITY	TITLE: STRIKER GENERAL ASSY	DWG. No. 023 / A3
	FINISH:	TOLERANCES: ±0.1 UNLESS STATED	3.2 SURFACE FINISH IN µm UNLESS STATED	DIMNS. IN mm			ISSUE No. 2 / ACAD FILE:

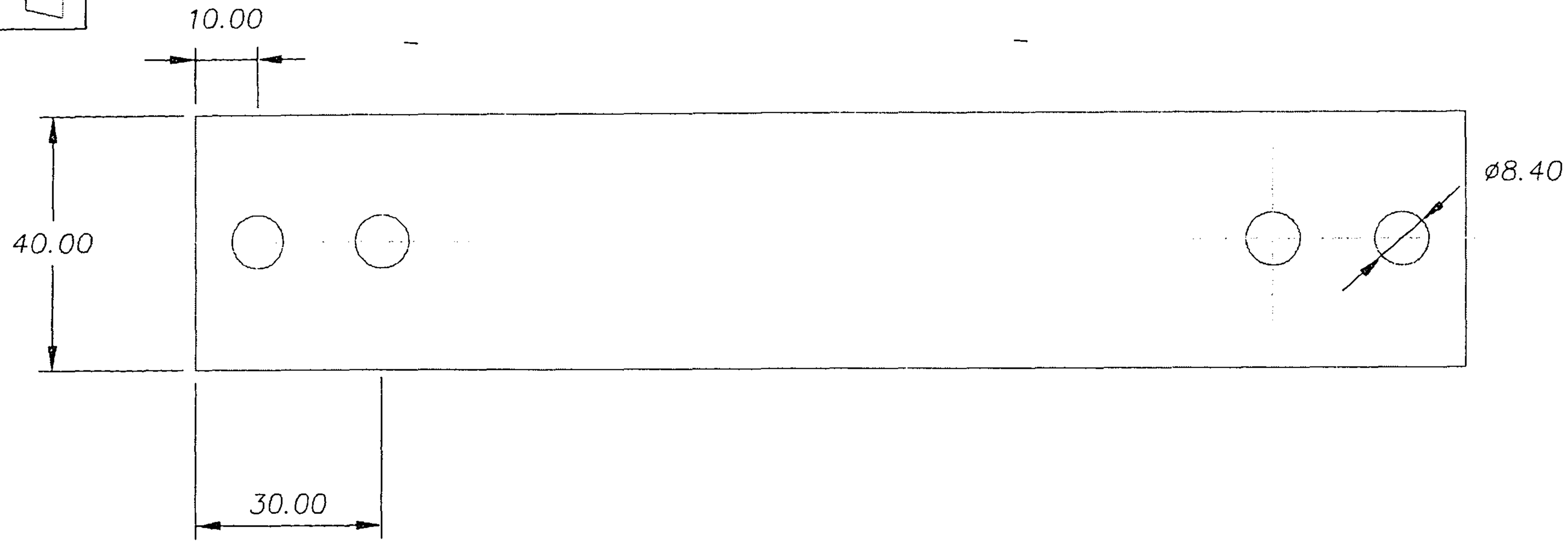

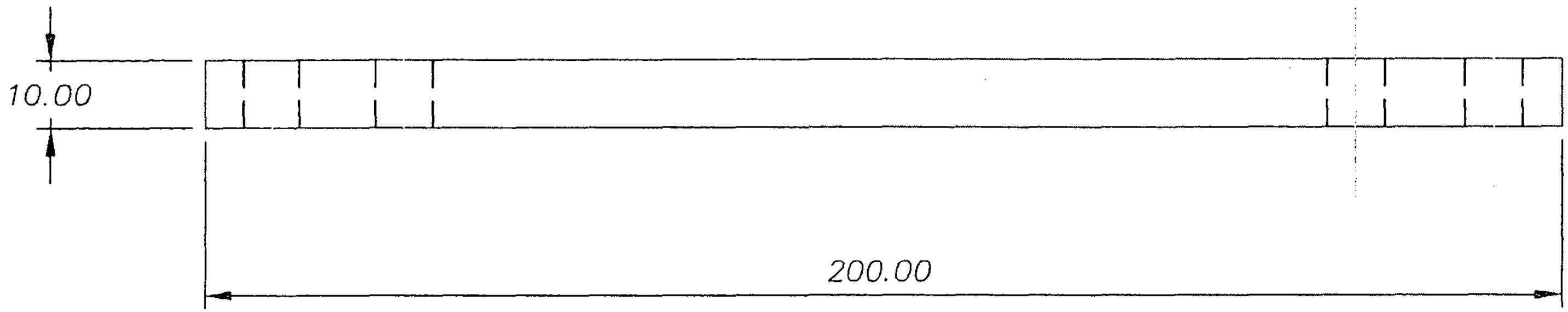

CHANGE:	No.	DATE
Mounting hole diameter	1	28/05/06
Dimensions tidied	2	05/06/06

TITLE: STRIKER MOUNT PLATE			DRAWN: PDB	DATE: 23/04/05 APPROVED:
MATL: MILD STEEL PLATE		TOL: ±0.1 UNLESS STATED	SCALE : 1:1	RMCS Cranfield UNIVERSITY — A4
DWG No. 019	ISSUE No. 3	ACAD FILE:	3.2 SURFACE FINISH IN µm UNLESS STATED	DIMS. IN: mm

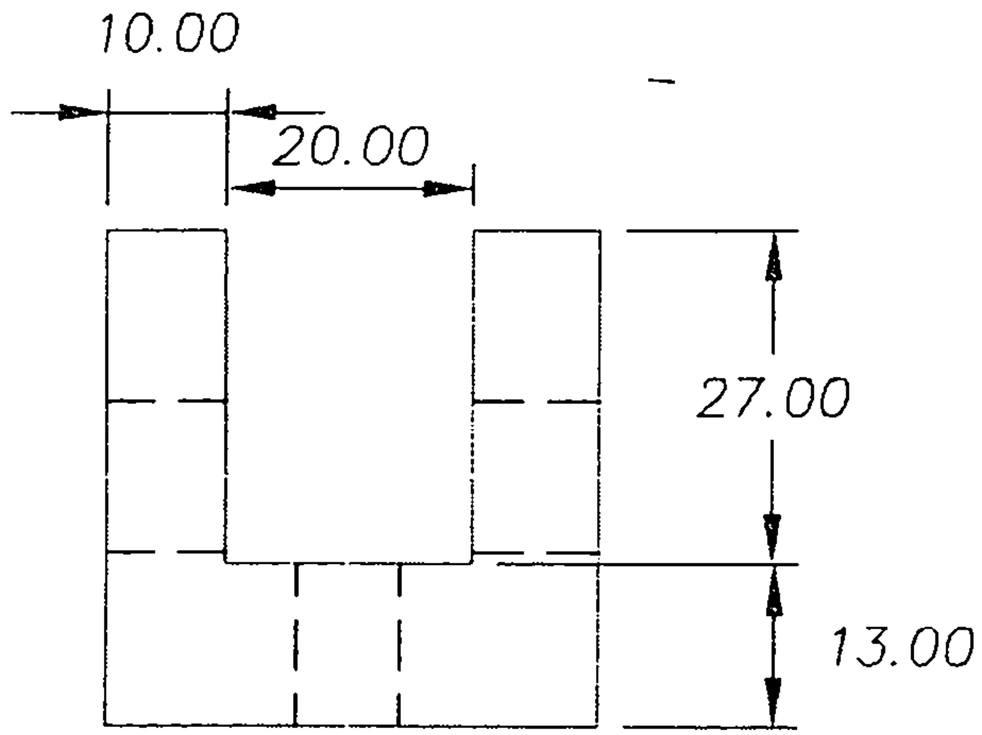

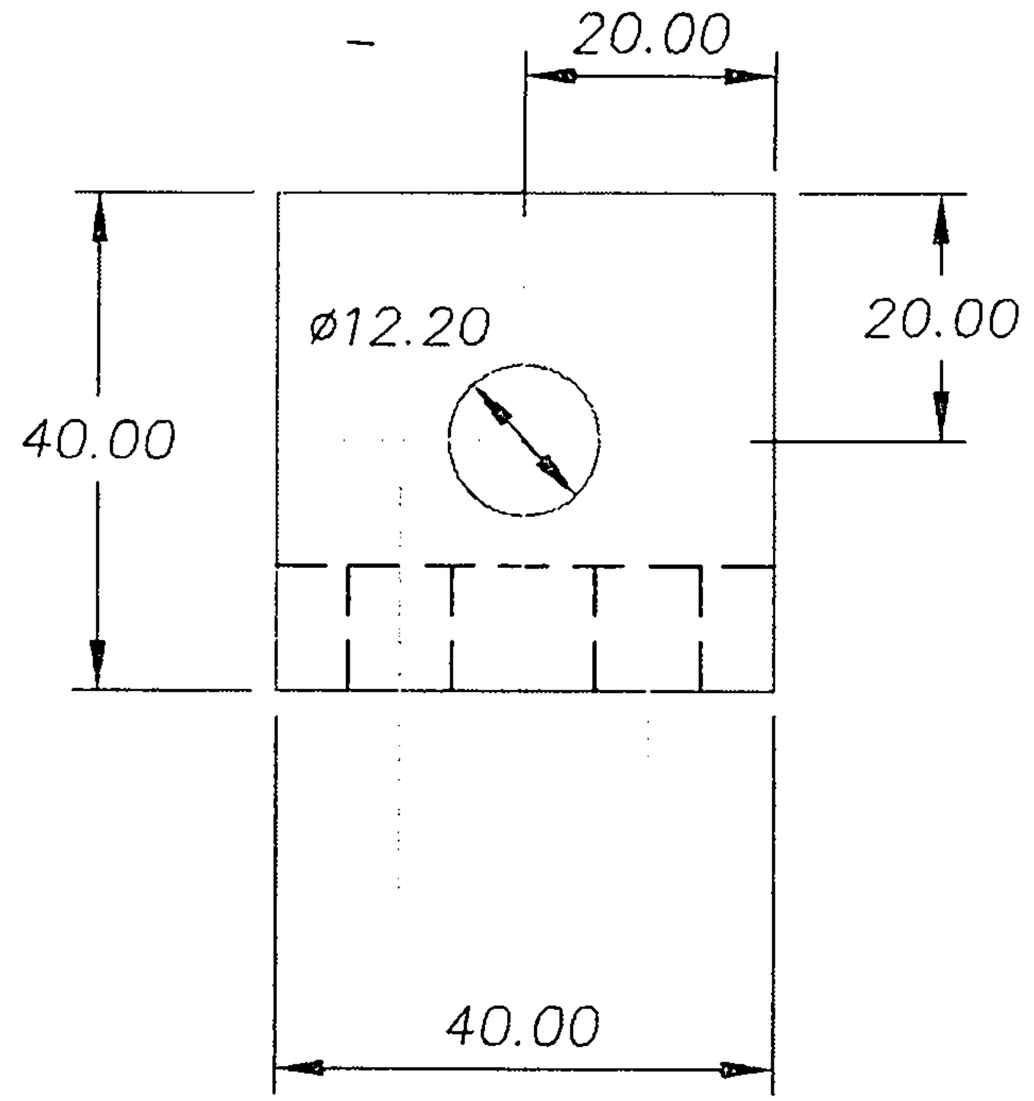

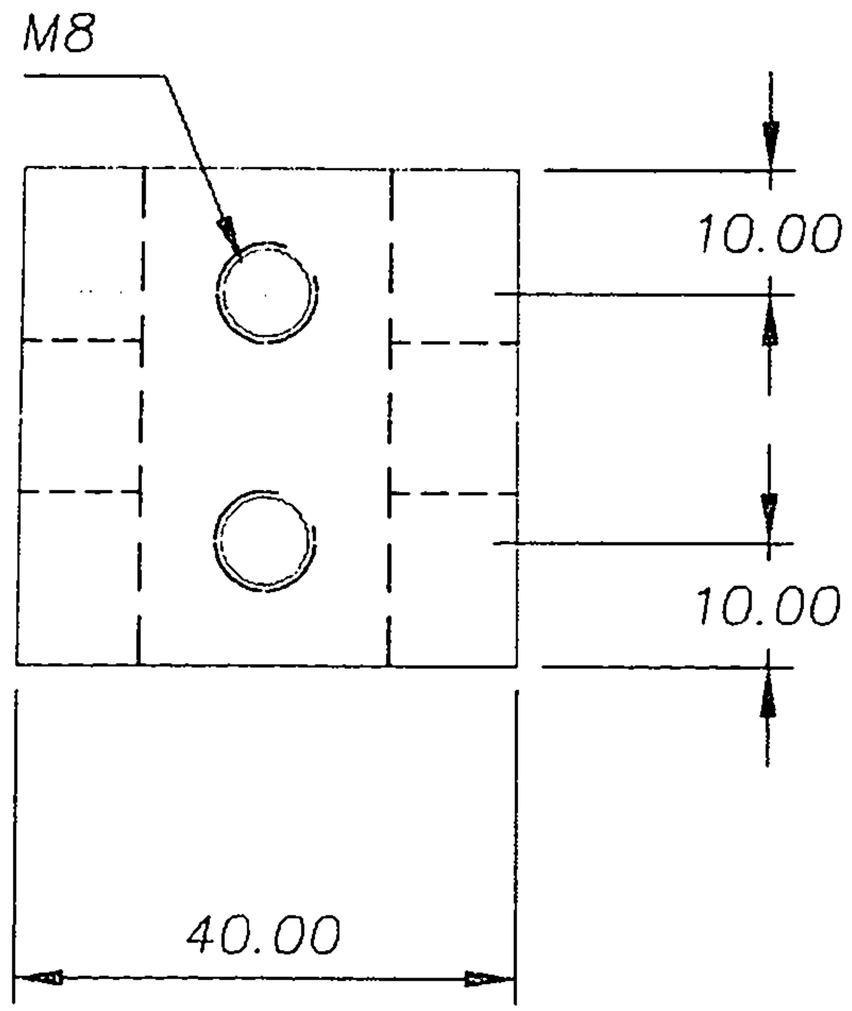

Mounting hole diameter				1	28/5/06
CHANGE:				No.	DATE
TITLE: STRIKER MOUNT BLOCKS			DRAWN: PDB	DATE: 23/04/05	APPROVED:
MATL: ALUMINIUM		TOL: ±0.1 UNLESS STATED	SCALE : 1: 1	RMCS Cranfield UNIVERSITY	A4
DWG No. 020	ISSUE No. 3	ACAD FILE:	3.2 SURFACE FINISH IN µm UNLESS STATED	DIMS. IN: mm	

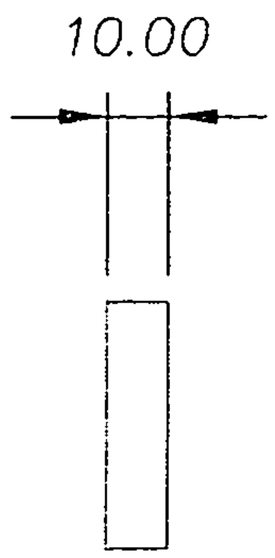

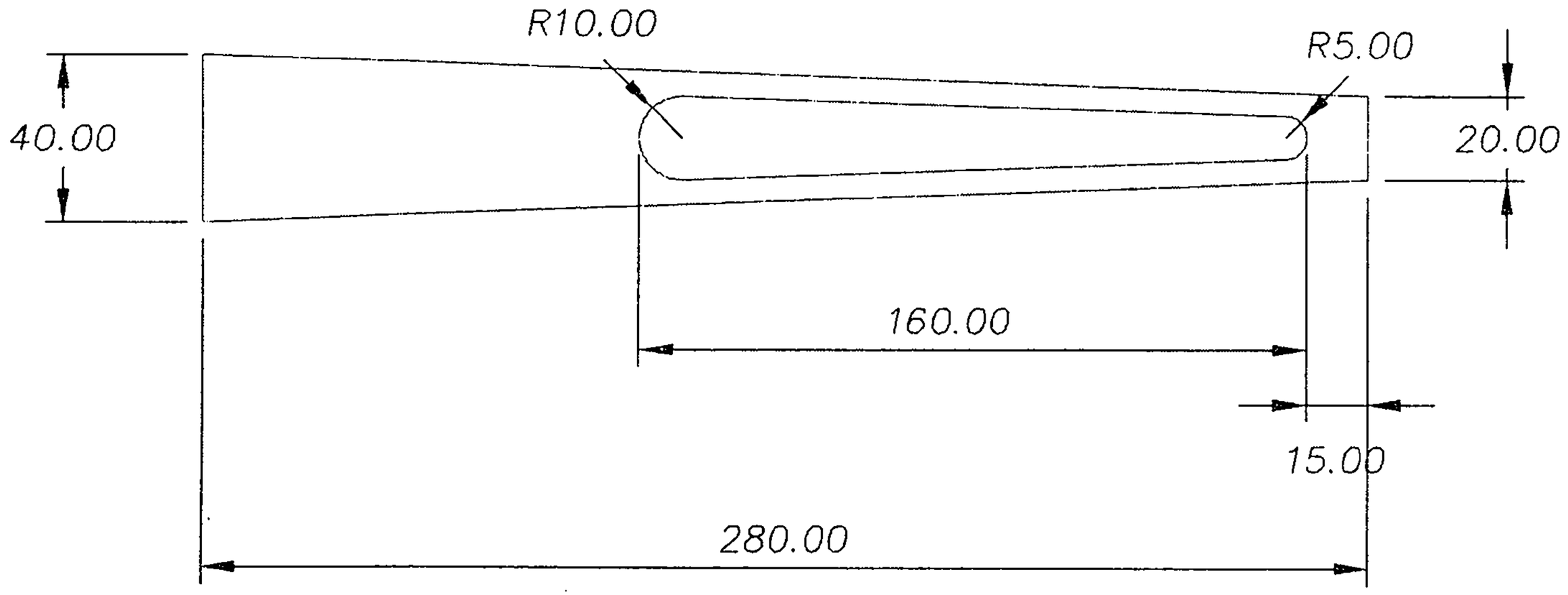

			CHANGE:	No.	DATE
TITLE: STRIKER FORKS (L & R)			DRAWN: PDB	DATE: 23/04/05	APPROVED:
MATL: MILD STEEL PLATE		TOL: ±0.1 UNLESS STATED	SCALE : 2:1	RMCS Cranfield UNIVERSITY	A4
DWG No. 021	ISSUE No. 2	ACAD FILE:	3.2 SURFACE FINISH IN μm UNLESS STATED	DIMS. IN: mm	

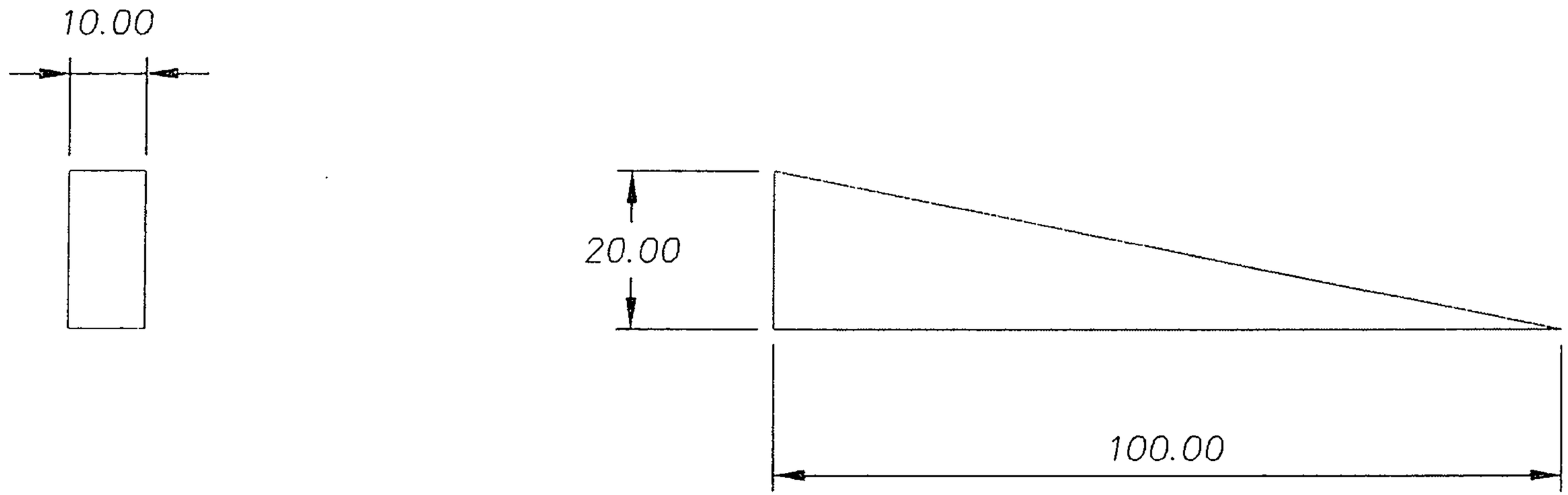

				CHANGE:	No.	DATE
TITLE: STRIKER FORK GUSSET				DRAWN: PDB	DATE: 23/04/05	APPROVED:
MATL: MILD STEEL PLATE			TOL: ±0.1 UNLESS STATED	SCALE : 1:1	RMCS Cranfield UNIVERSITY	A4
DWG No. 022	ISSUE No. 2	ACAD FILE:	3.2 SURFACE FINISH IN μm UNLESS STATED	DIMS. IN: mm		

Dynamic Mode I rig:

Sample Jig

PART NUM	DWG NUM	PART NAME	NUM OF	MATERIAL
1	PHD 025	SIDE PLATES	2	ALUMINIUM
2	PHD 026	BASE PLATE	1	ALUMIMIUM
3	PHD 027	MOUNTING PIN	2	MILD STEEL
4	PHD 028	SUPPORT PIN	1	MILD STEEL
5	PHD 029	SUPPORT ADJUSTER	1	ALUMINIUM
6		M6 NUT	4	
7		M6X15 BOLT	4	

RMCS Cranfield UNIVERSITY

CHANGE:	No.	DATE

TITLE: LOAD BLOCK JIG PARTS LIST	DRAWN: PDB	DATE: 24/07/05	APPROVED:
	MATL:	TOL: ±0.1 UNLESS STATED	SCALE:
DWG No. PHD 031 / ISSUE No.	ACAD FILE:	3.2 SURFACE FINISH IN μm UNLESS STATED	DIMS. IN: mm / A4

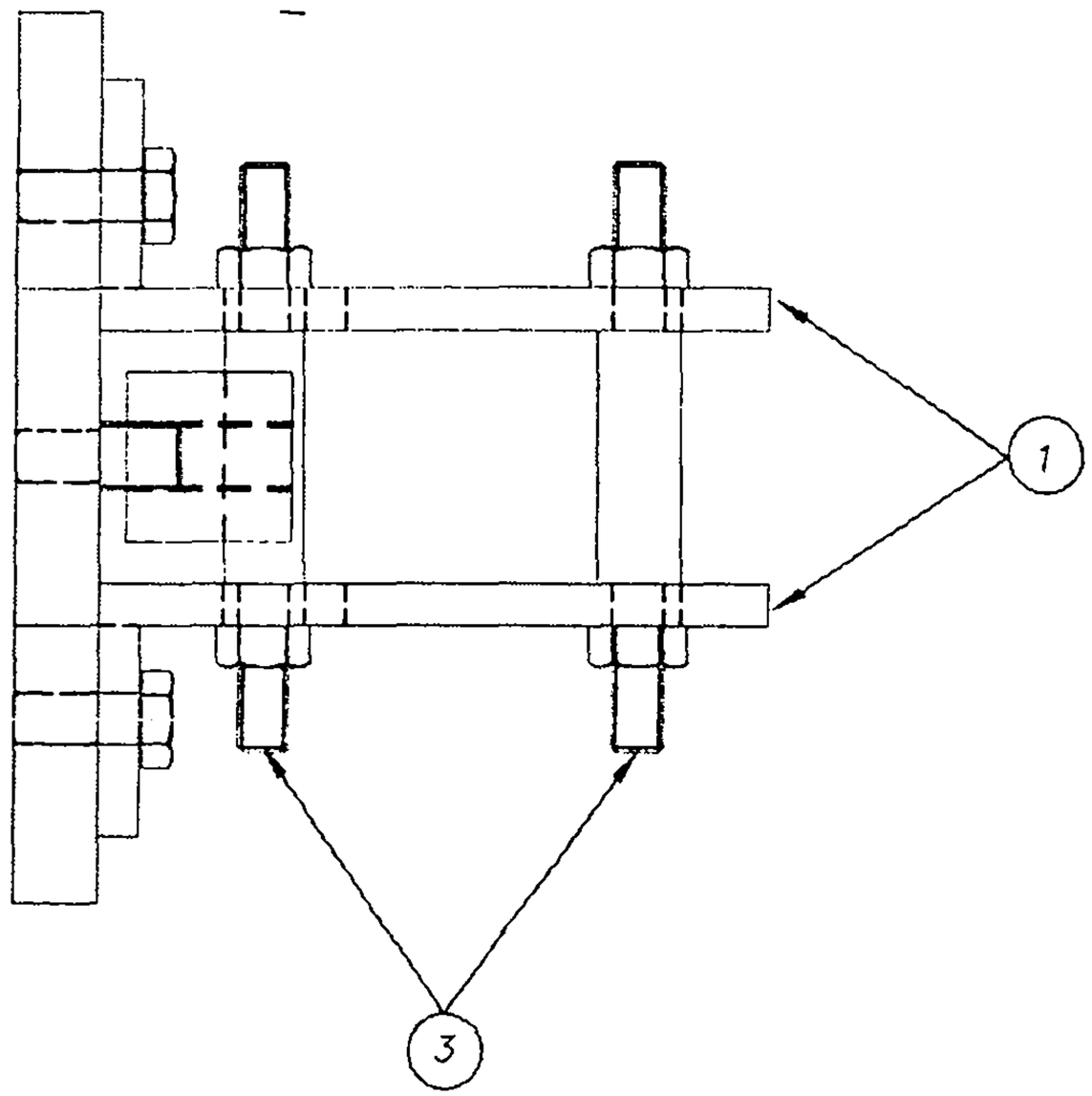

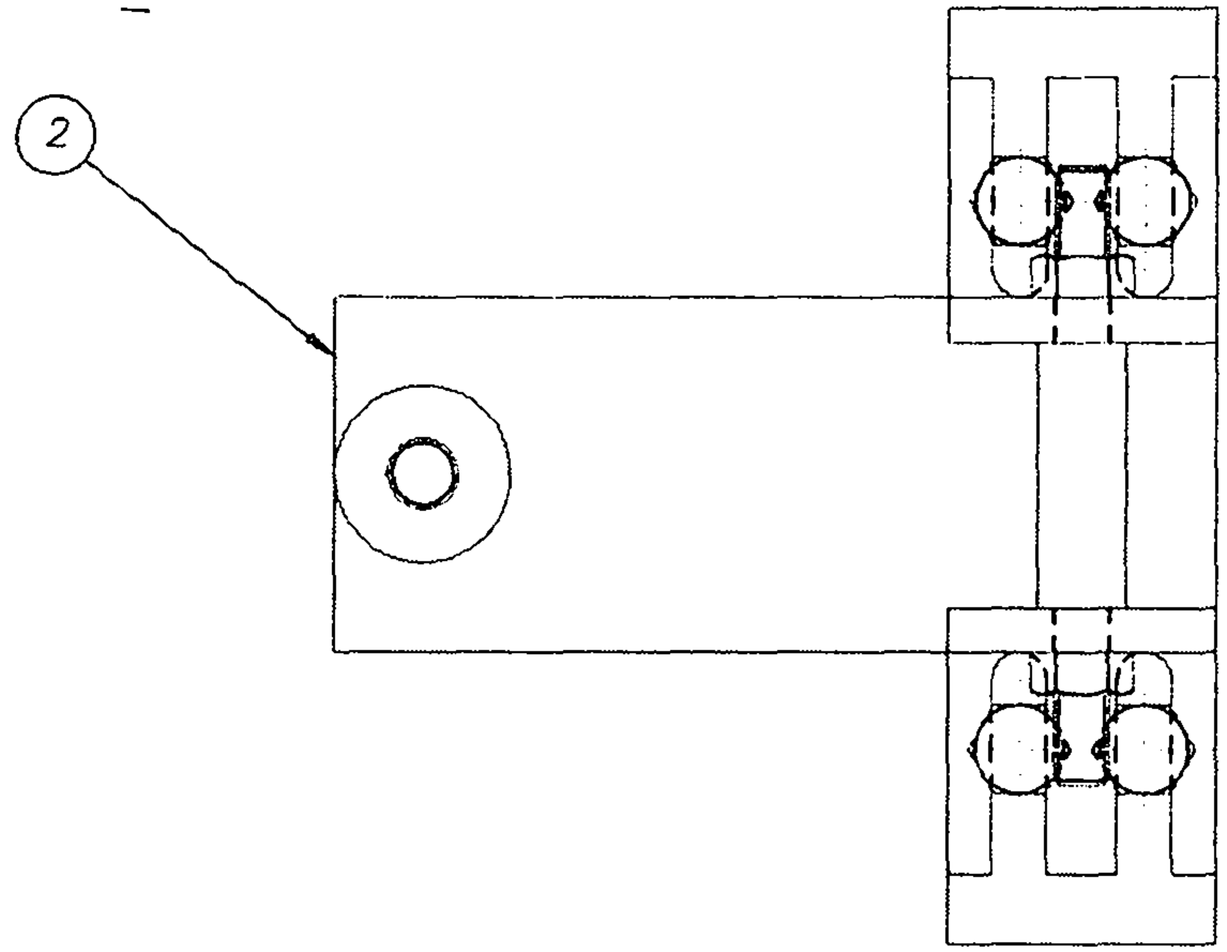

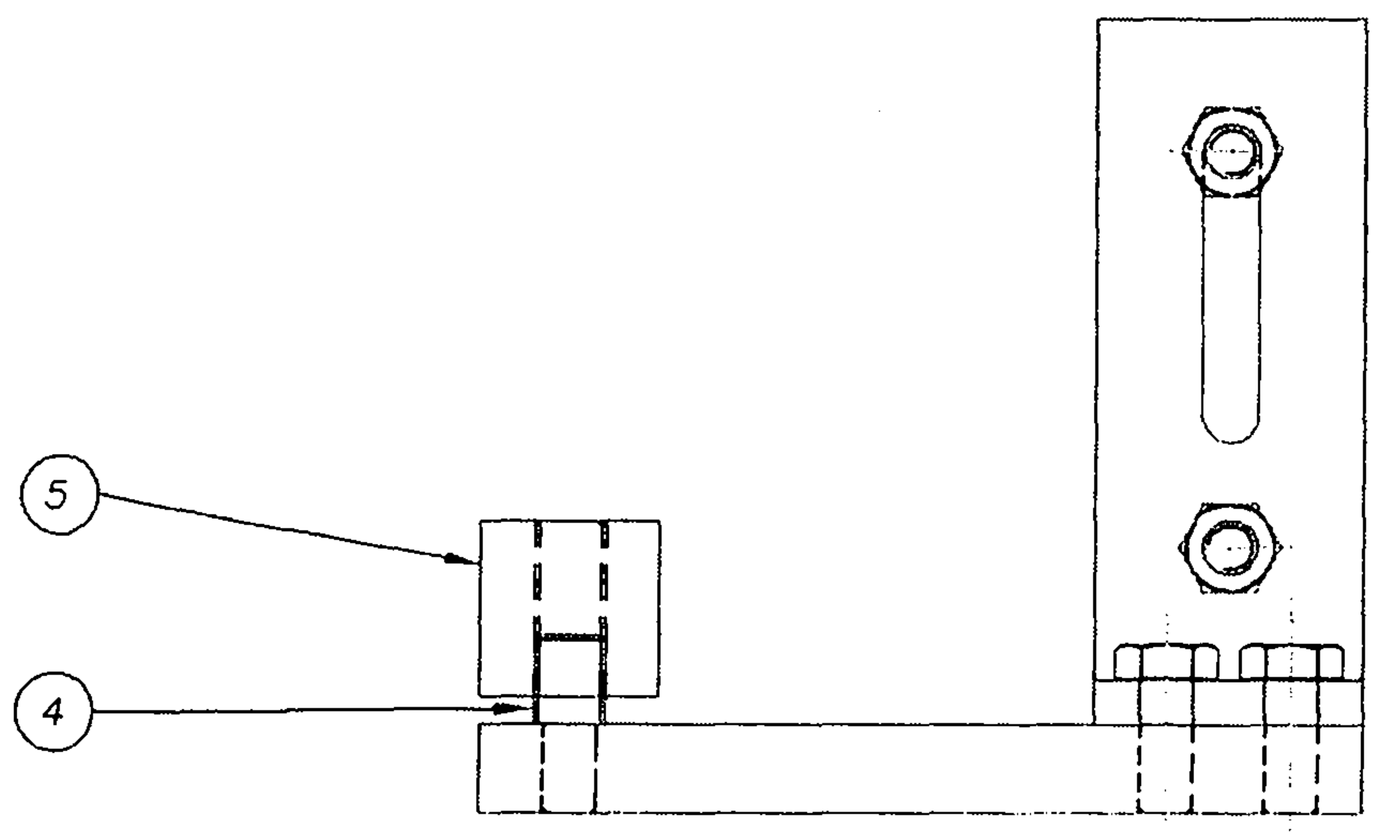

CHANGE			No.	DATE			
MATL:	DRAWN: PDB	DATE: 24/7/05	APPROVED:	SCALE 1:1	RMCS Cranfield UNIVERSITY	TITLE: LOAD BLOCK JIG GENERAL ASSY	DWG. No. PHD 030 A3
	FINISH:	TOLERANCES: ±0.1 UNLESS STATED	3.2/ SURFACE FINISH IN µm UNLESS STATED	DIMNS. IN mm			ISSUE No. 1 ACAD FILE:

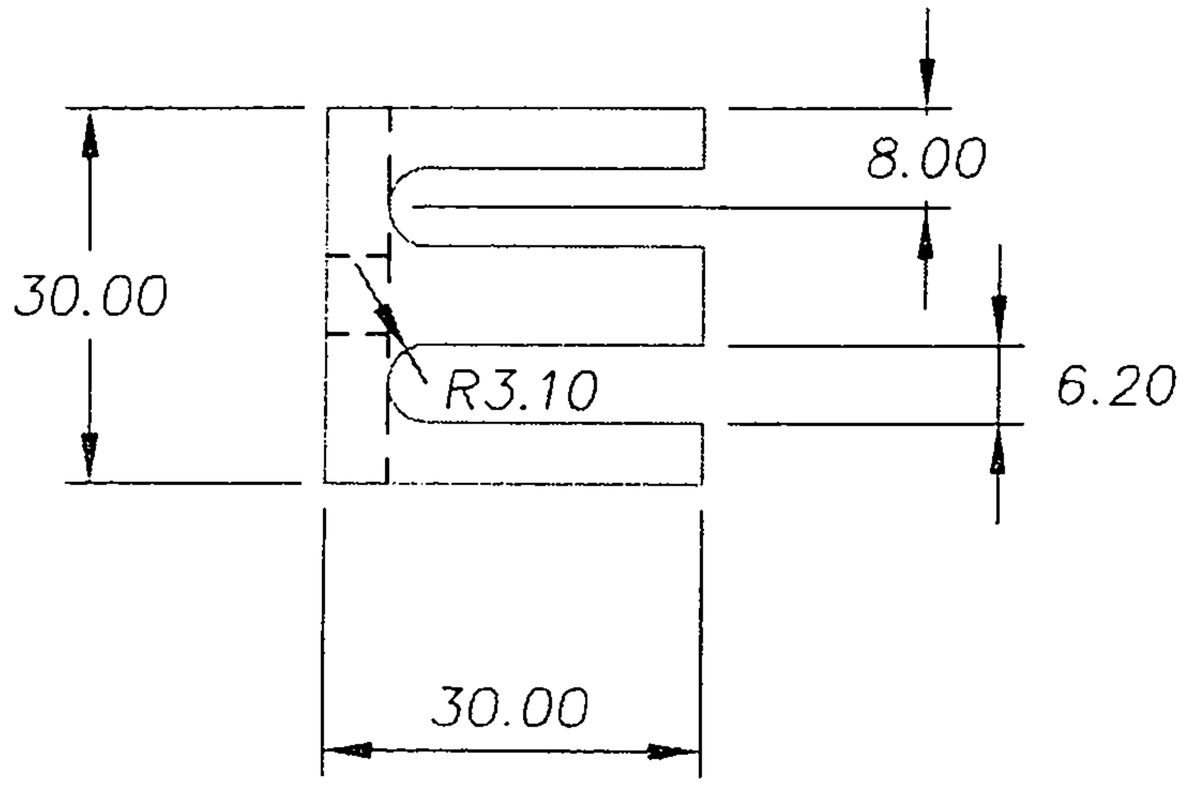

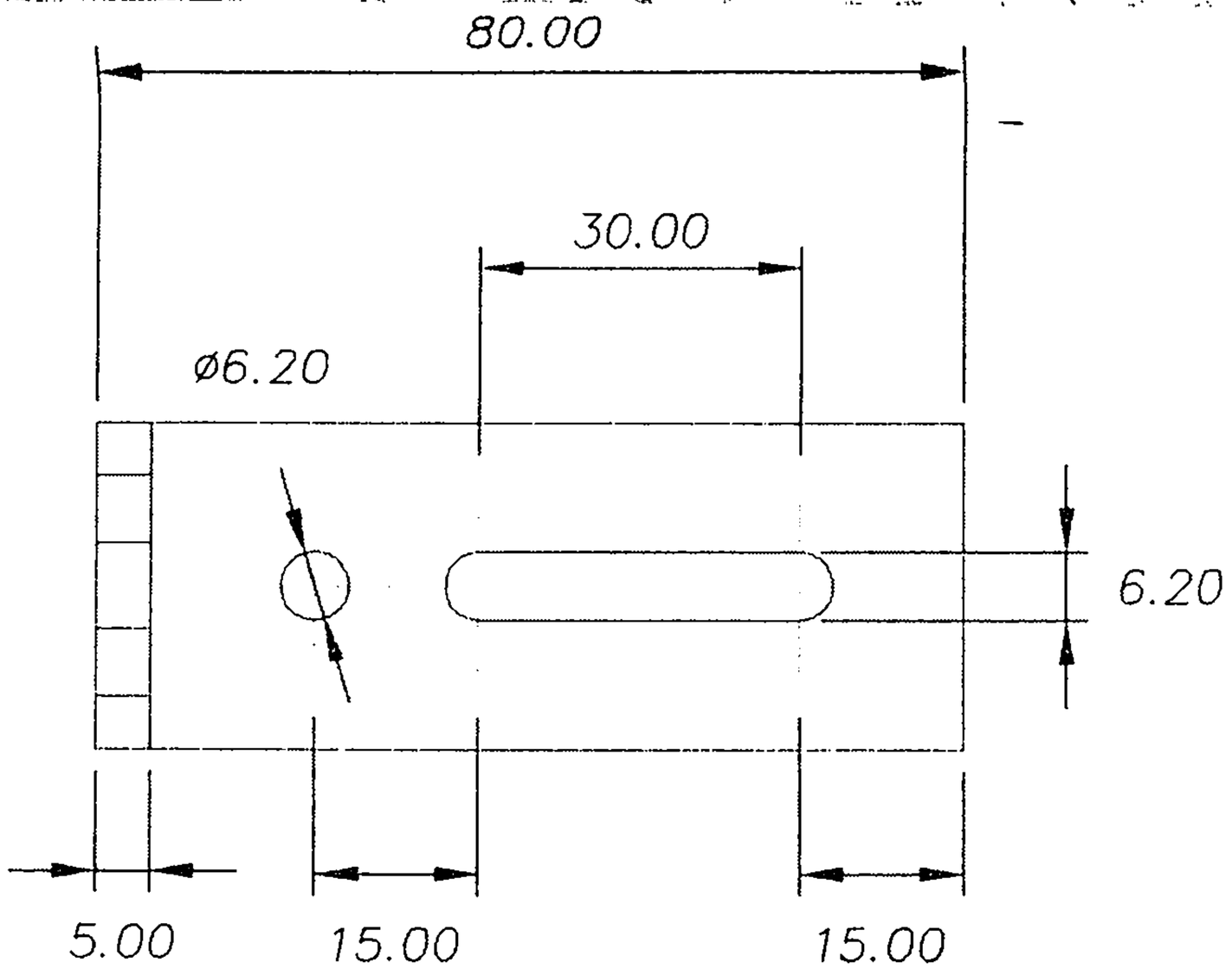

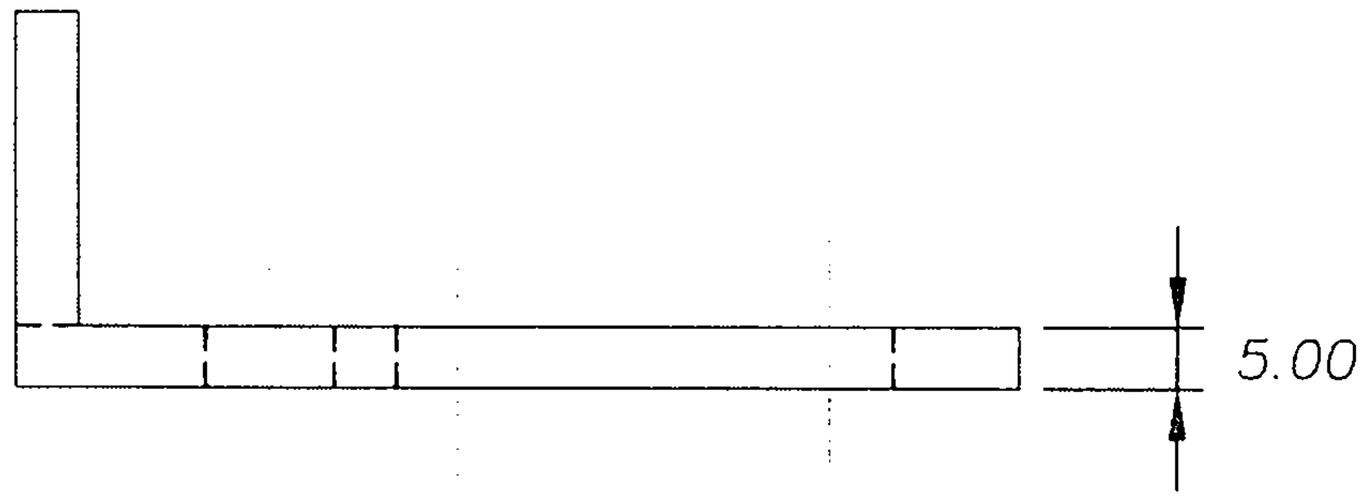

				CHANGE:	No.	DATE
TITLE: SIDE PLATE				DRAWN: PDB	DATE: 06/07/05	APPROVED:
MATL: ALUMINIUM			TOL: ±0.1 UNLESS STATED	SCALE : 1: 1	RMCS Cranfield UNIVERSITY	A4
DWG No. PHD 025	ISSUE No. 1	ACAD FILE:	3.2 SURFACE FINISH IN μm UNLESS STATED	DIMS. IN: mm		

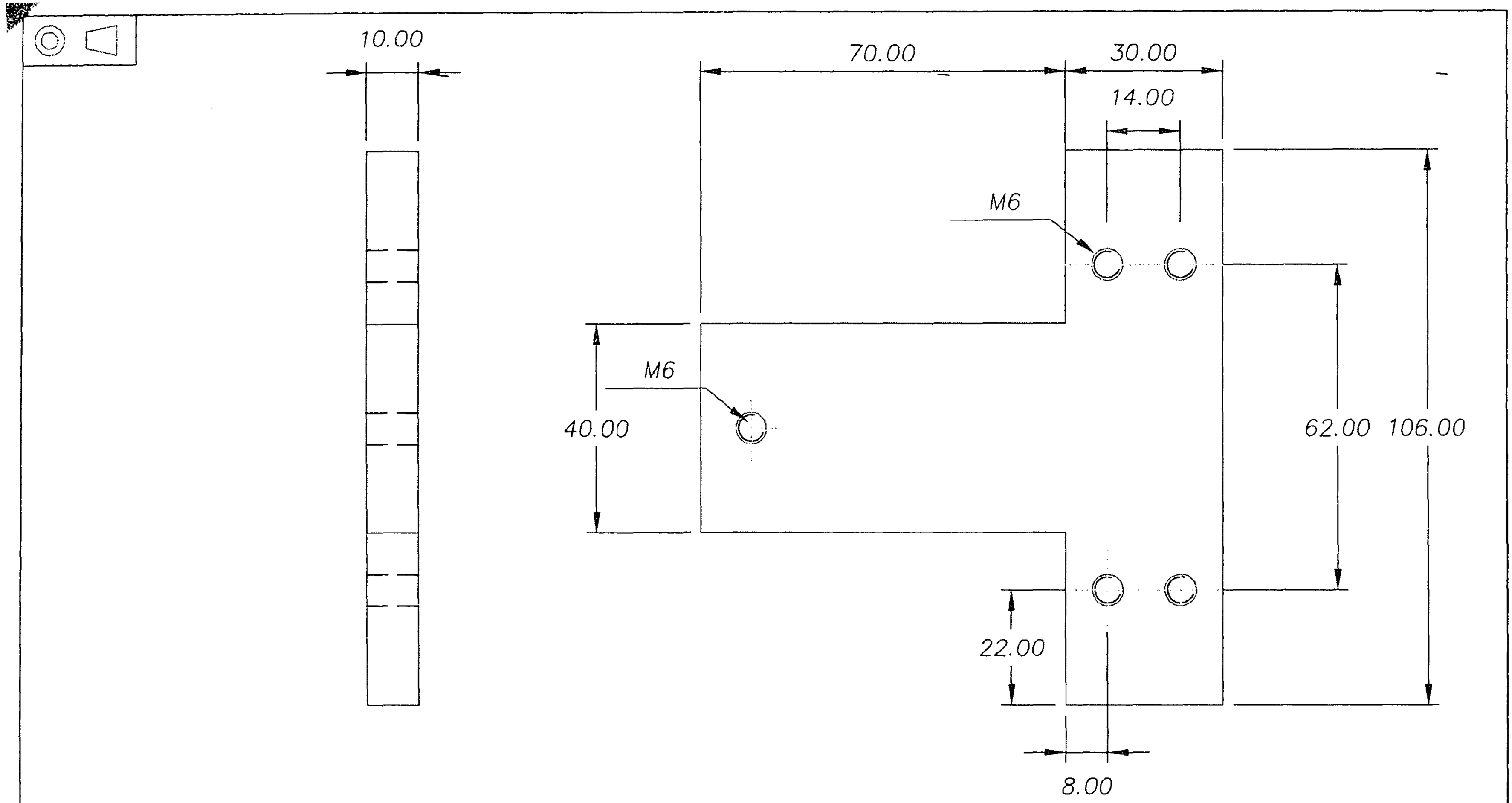

CHANGE:	No.	DATE

TITLE: BASE PLATE				DRAWN: PDB	DATE: 06/07/05 APPROVED:
MATL: ALUMINIUM			TOL: ±0.1 UNLESS STATED	SCALE : 1: 1	RMCS Cranfield UNIVERSITY A4
DWG No. PHD 026	ISSUE No. 1	ACAD FILE:	3.2 SURFACE FINISH IN μm UNLESS STATED	DIMS. IN: mm	

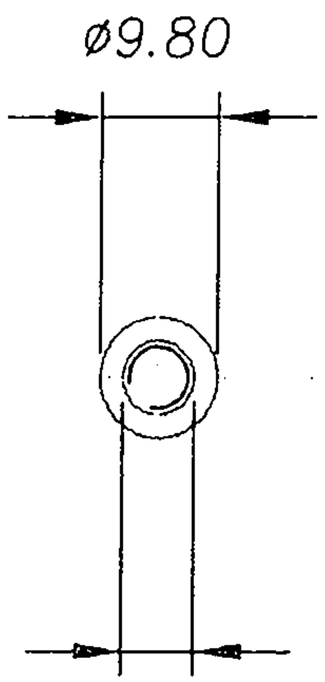

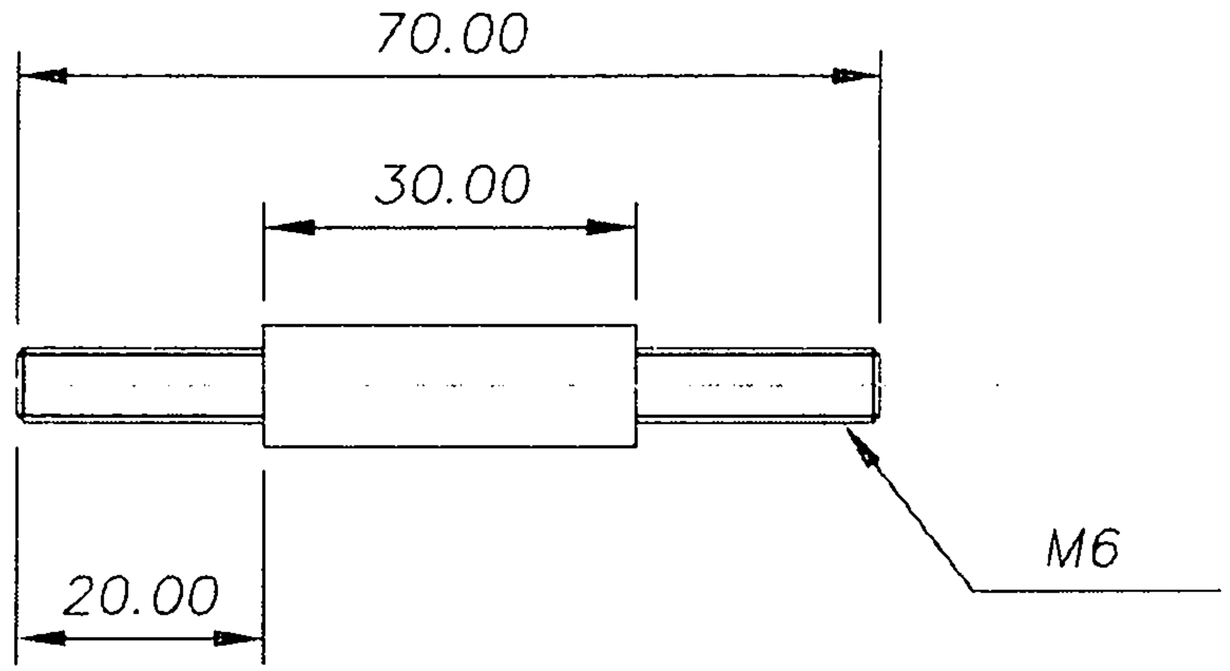

				CHANGE:	No.	DATE
TITLE: MOUNTING PIN				DRAWN: PDB	DATE: 12/07/05	APPROVED:
MATL: MILD STEEL			TOL: ±0.1 UNLESS STATED	SCALE : 1: 1	RMCS Cranfield UNIVERSITY	A4
DWG No. PHD 027	ISSUE No. 1	ACAD FILE:	3.2 SURFACE FINISH IN µm UNLESS STATED	DIMS. IN: mm		

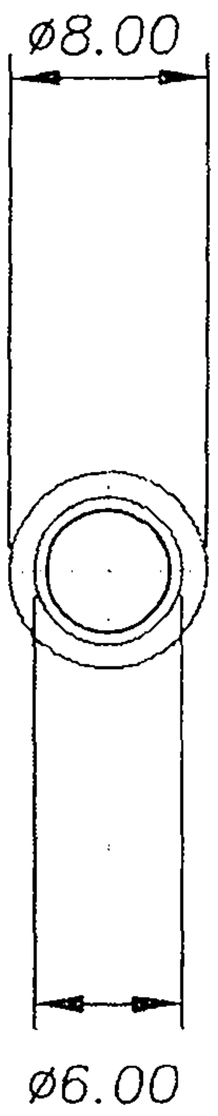

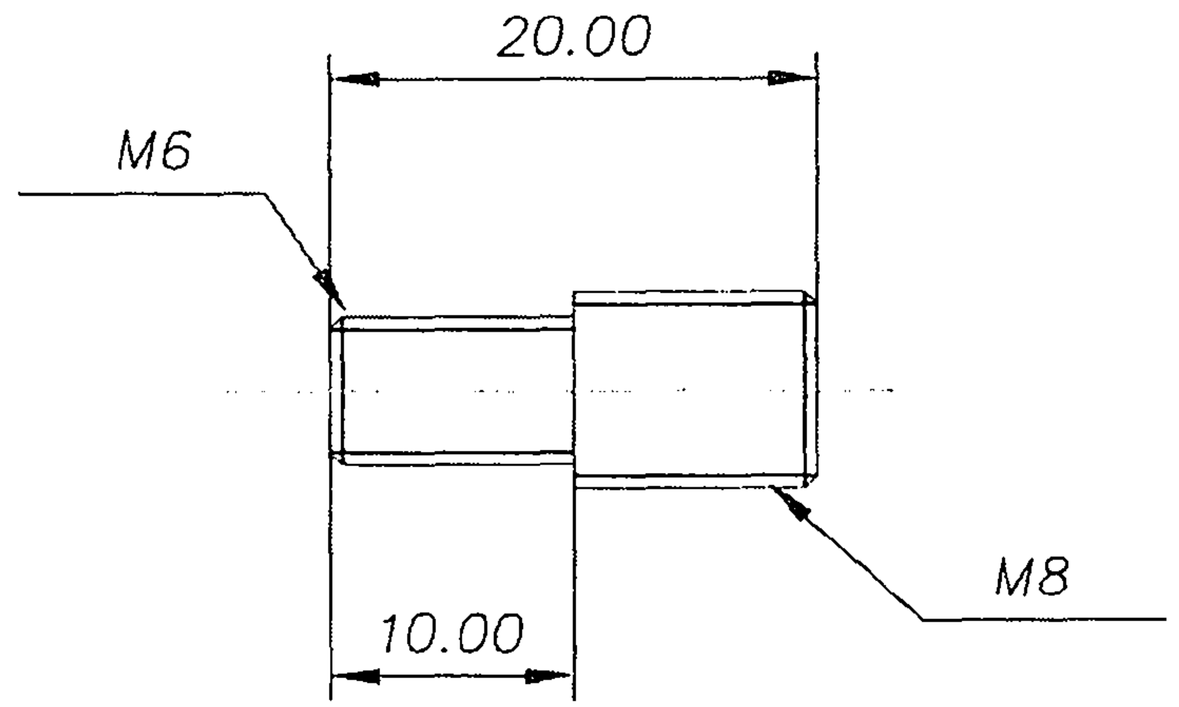

					CHANGE:	No. DATE
TITLE: SUPPORT PIN				DRAWN: PDB	DATE: 12/07/05	APPROVED:
MATL: MILD STEEL			TOL: ±0.1 UNLESS STATED	SCALE : 2:1	RMCS Cranfield UNIVERSITY	A4
DWG No. PHD 028	ISSUE No. 1	ACAD FILE:	3.2 SURFACE FINISH IN µm UNLESS STATED	DIMS. IN: mm		

Conical Indenters:

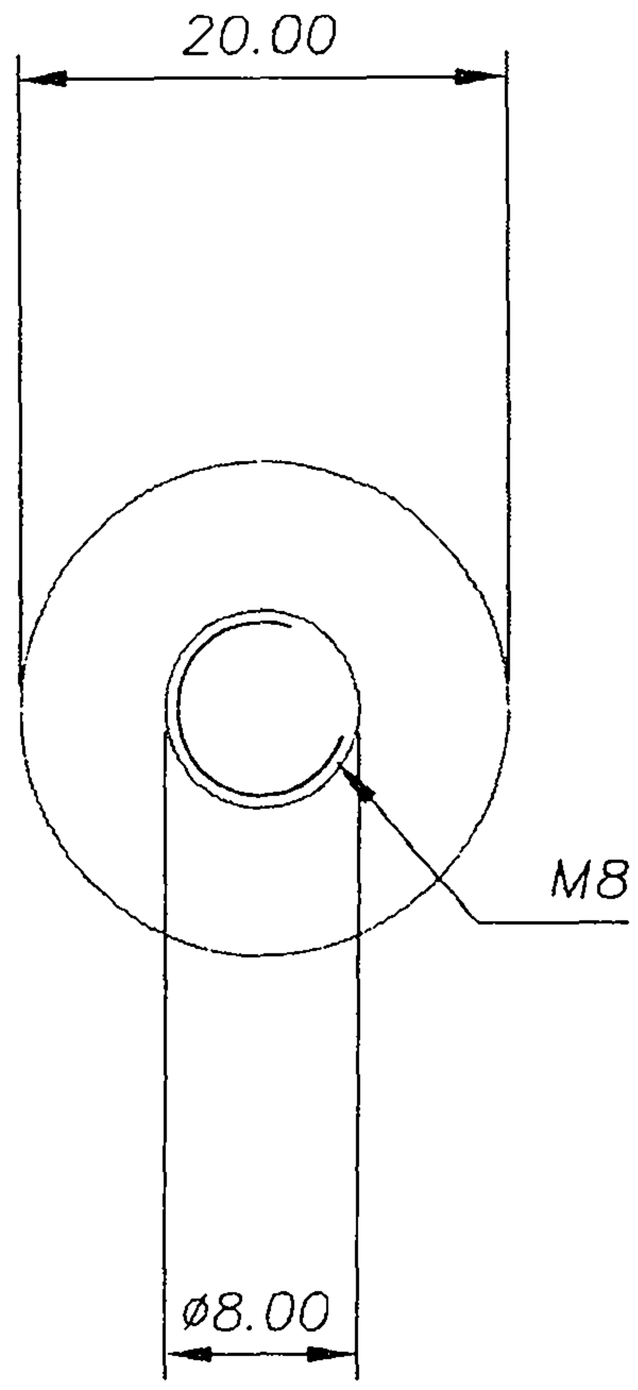

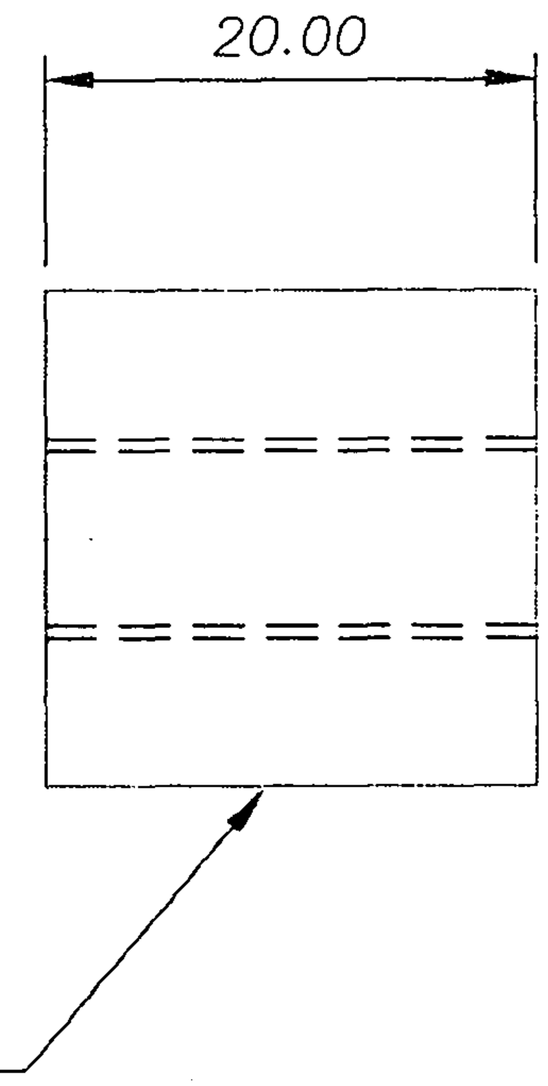

				CHANGE:	No.	DATE
TITLE: SUPPORT ADJUSTER				DRAWN: PDB	DATE: 12/07/05	APPROVED:
MATL: ALUMINIUM			TOL: ±0.1 UNLESS STATED	SCALE : 2:1	RMCS Cranfield UNIVERSITY	A4
DWG No. PHD 029	ISSUE No. 1	ACAD FILE:	3.2 SURFACE FINISH IN µm UNLESS STATED	DIMS. IN: mm		

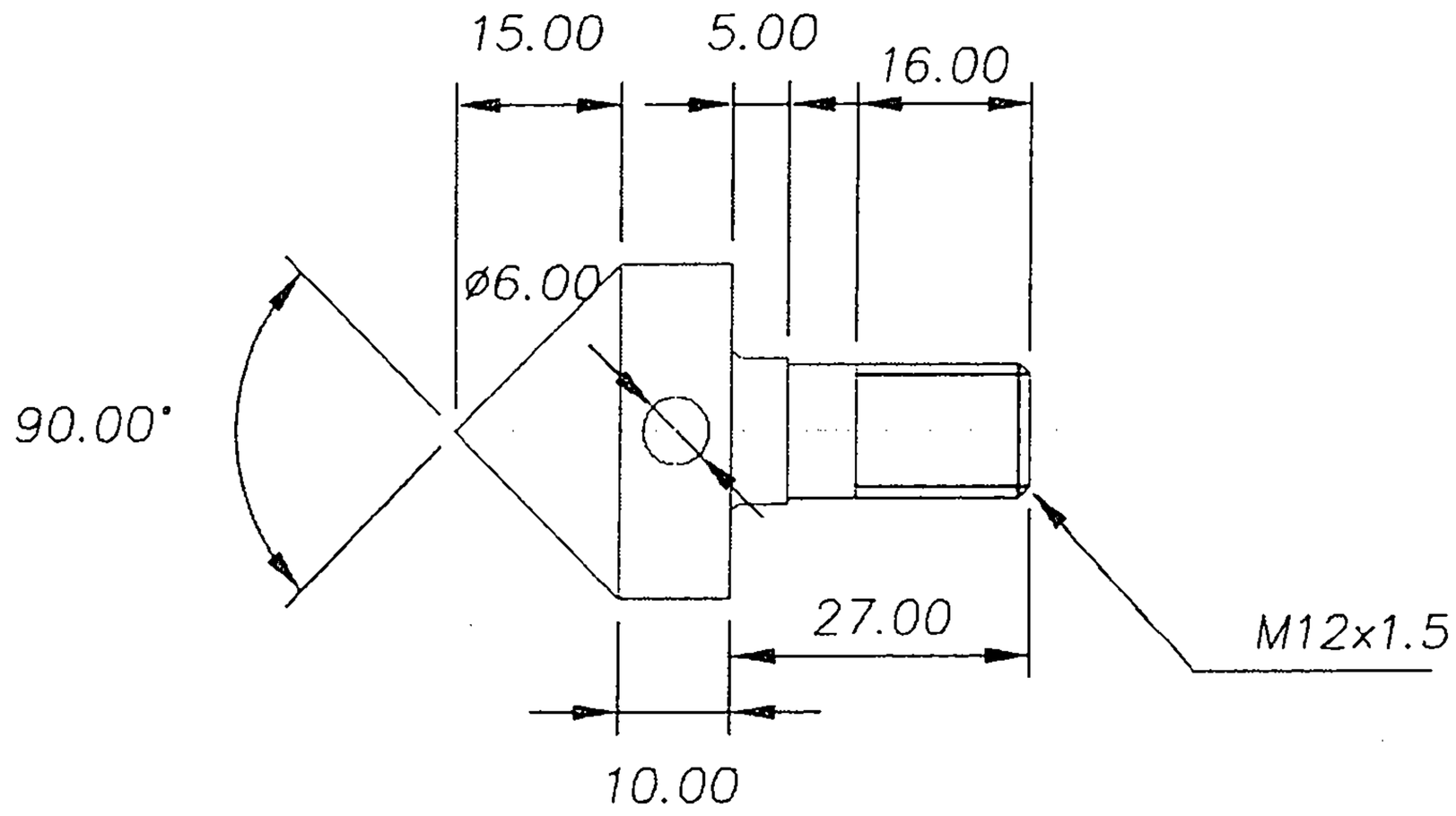

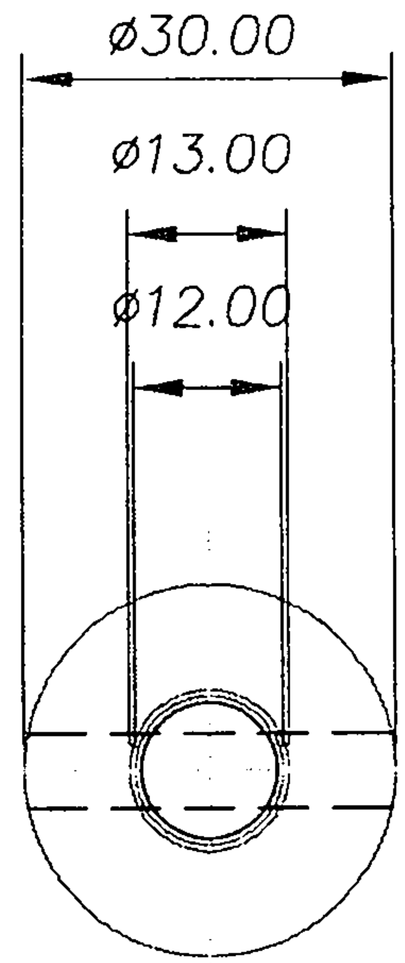

				CHANGE:	No.	DATE
TITLE: 90° INDENTOR				DRAWN: PDB	DATE: 1/11/05	APPROVED:
MATL: EN24			TOL: ±0.1 UNLESS STATED	SCALE : 1:1	RMCS Cranfield UNIVERSITY	A4
DWG No. PHD 032	ISSUE No. 1	ACAD FILE:	3.2 SURFACE FINISH IN µm UNLESS STATED	DIMS. IN: mm		

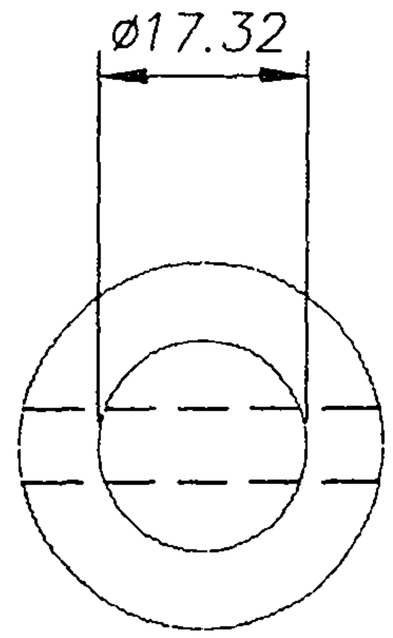

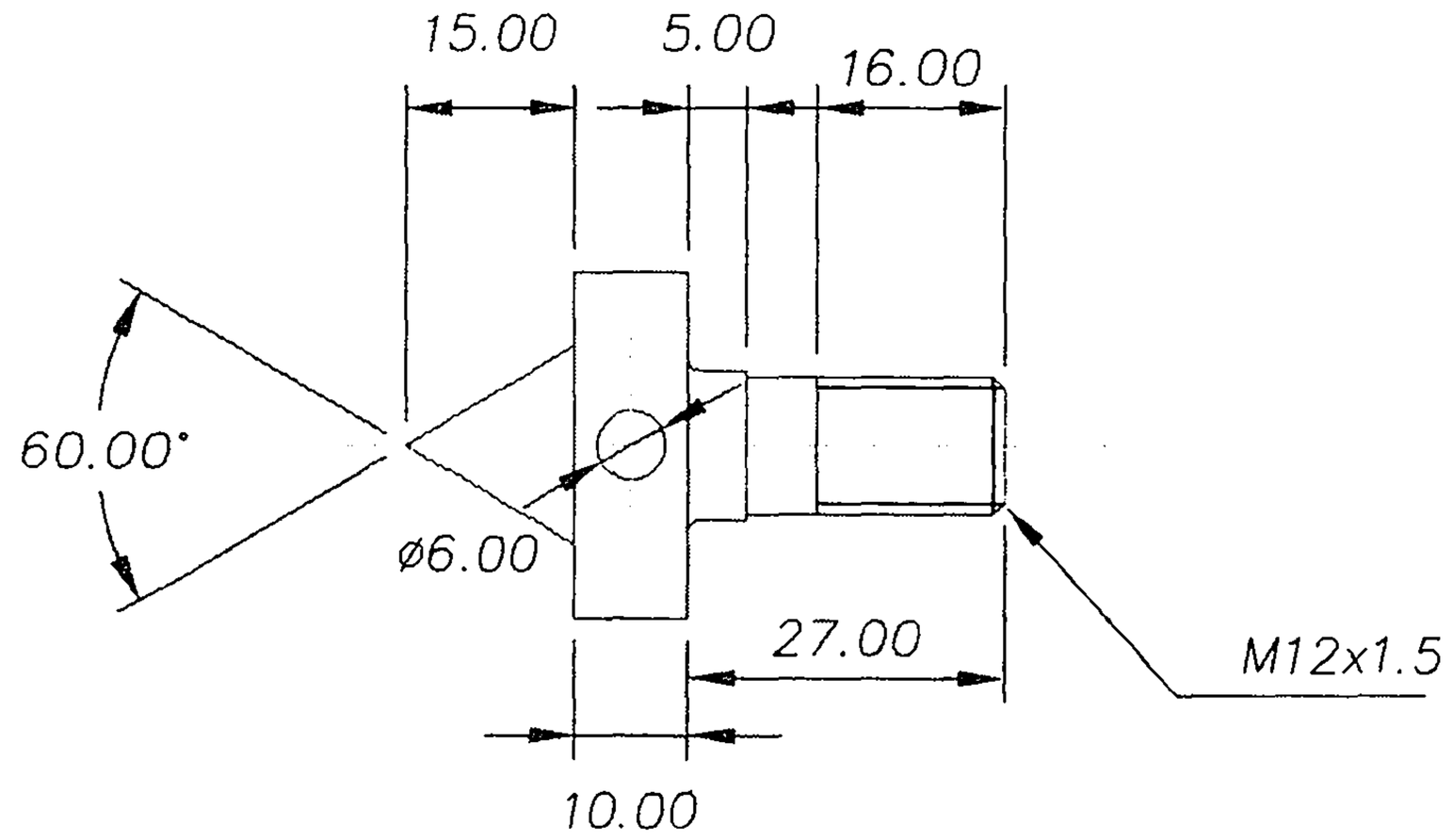

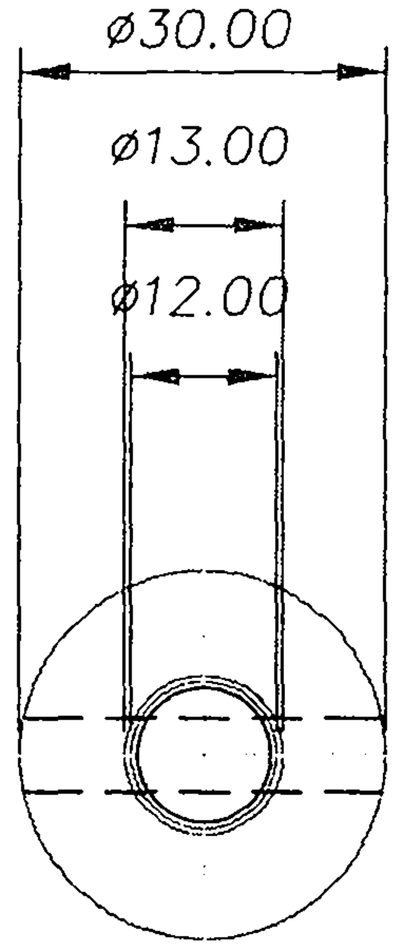

				CHANGE:	No.	DATE
TITLE: 60° INDENTOR				DRAWN: PDB	DATE: 1/11/05	APPROVED:
MATL: EN24			TOL: ±0.1 UNLESS STATED	SCALE : 1:1	RMCS Cranfield UNIVERSITY	A4
DWG No. PHD 033	ISSUE No. 1	ACAD FILE:	3.2 SURFACE FINISH IN µm UNLESS STATED	DIMS. IN: mm		

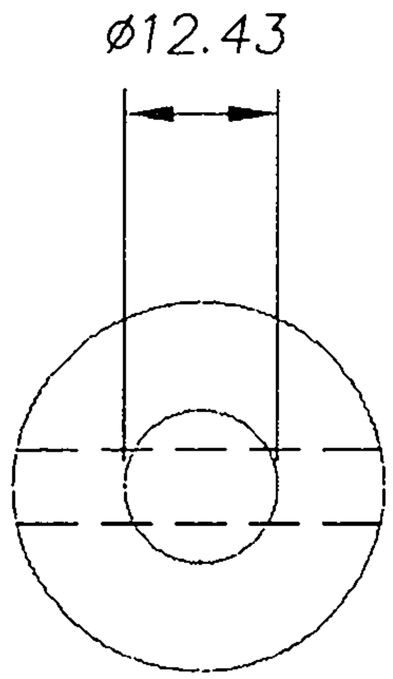

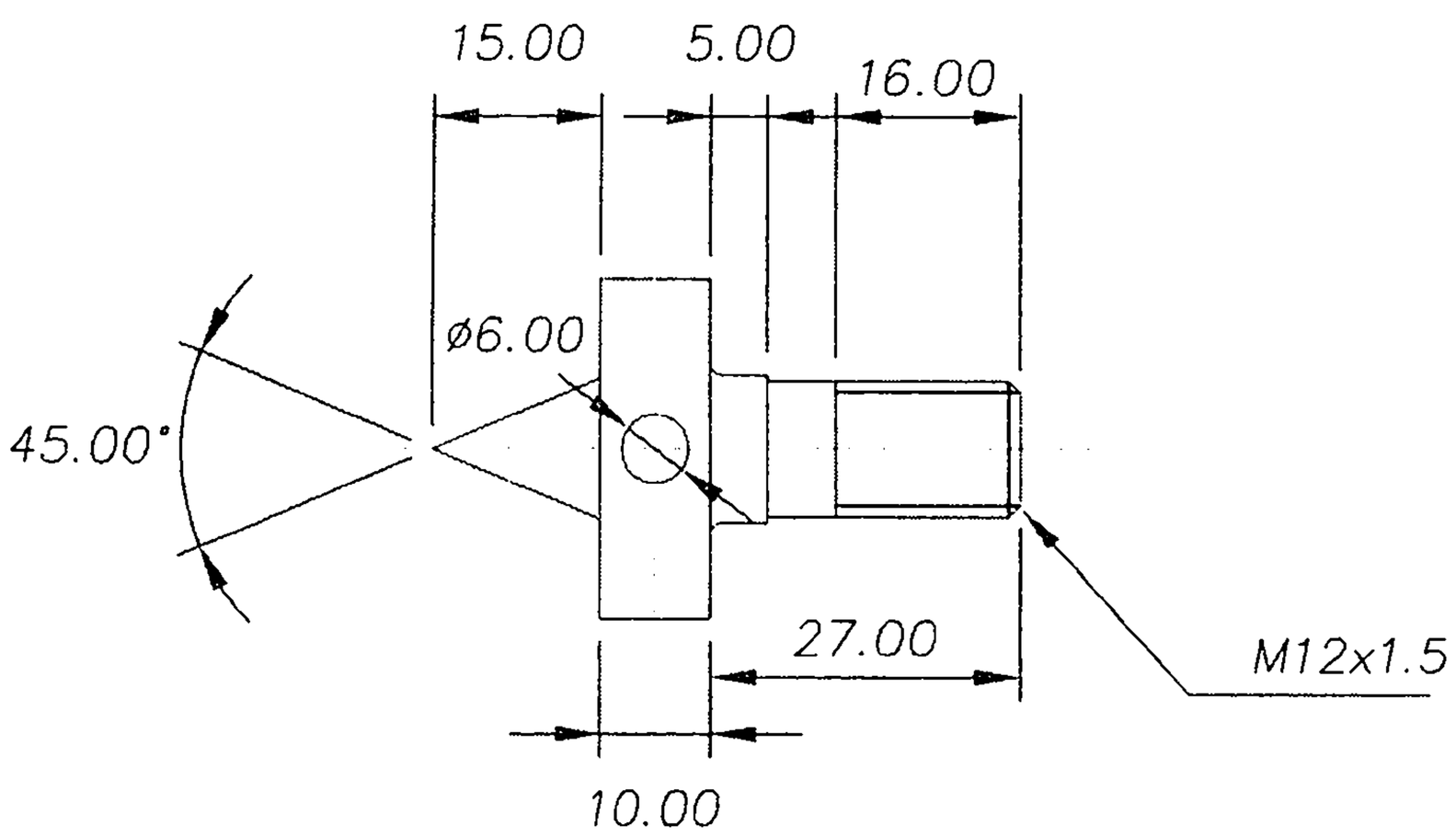

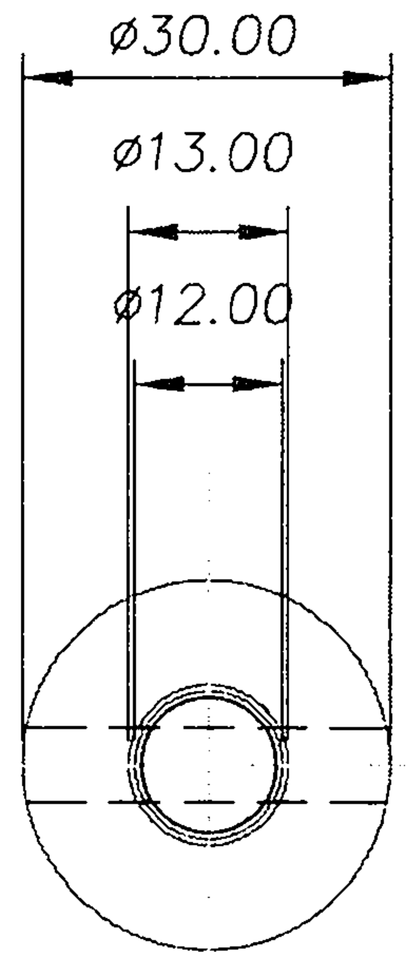

				CHANGE:	No.	DATE
TITLE: 45° INDENTOR				DRAWN: PDB	DATE: 1/11/05	APPROVED:
MATL: EN24			TOL: ±0.1 UNLESS STATED	SCALE : 1:1	RMCS Cranfield UNIVERSITY	A4
DWG No. PHD 034	ISSUE No. 1	ACAD FILE:	3.2 SURFACE FINISH IN µm UNLESS STATED	DIMS. IN: mm		

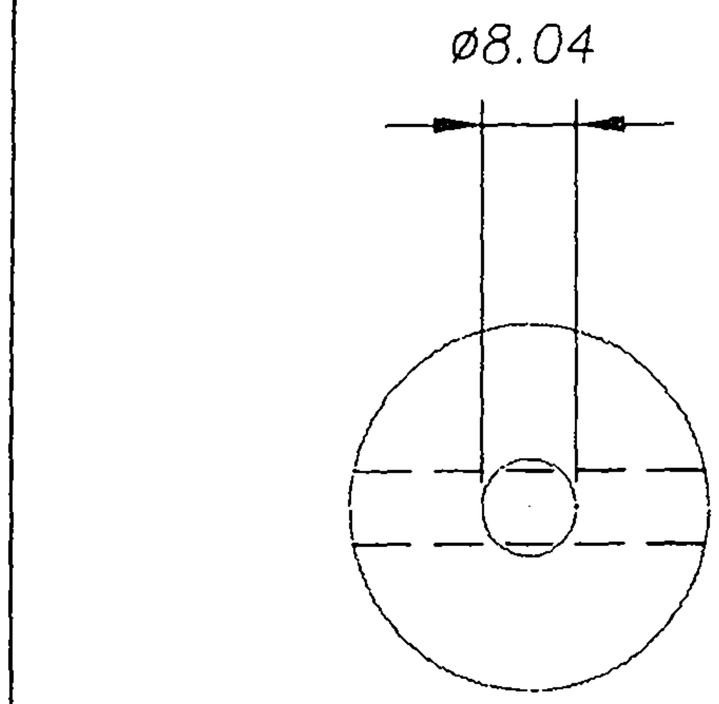

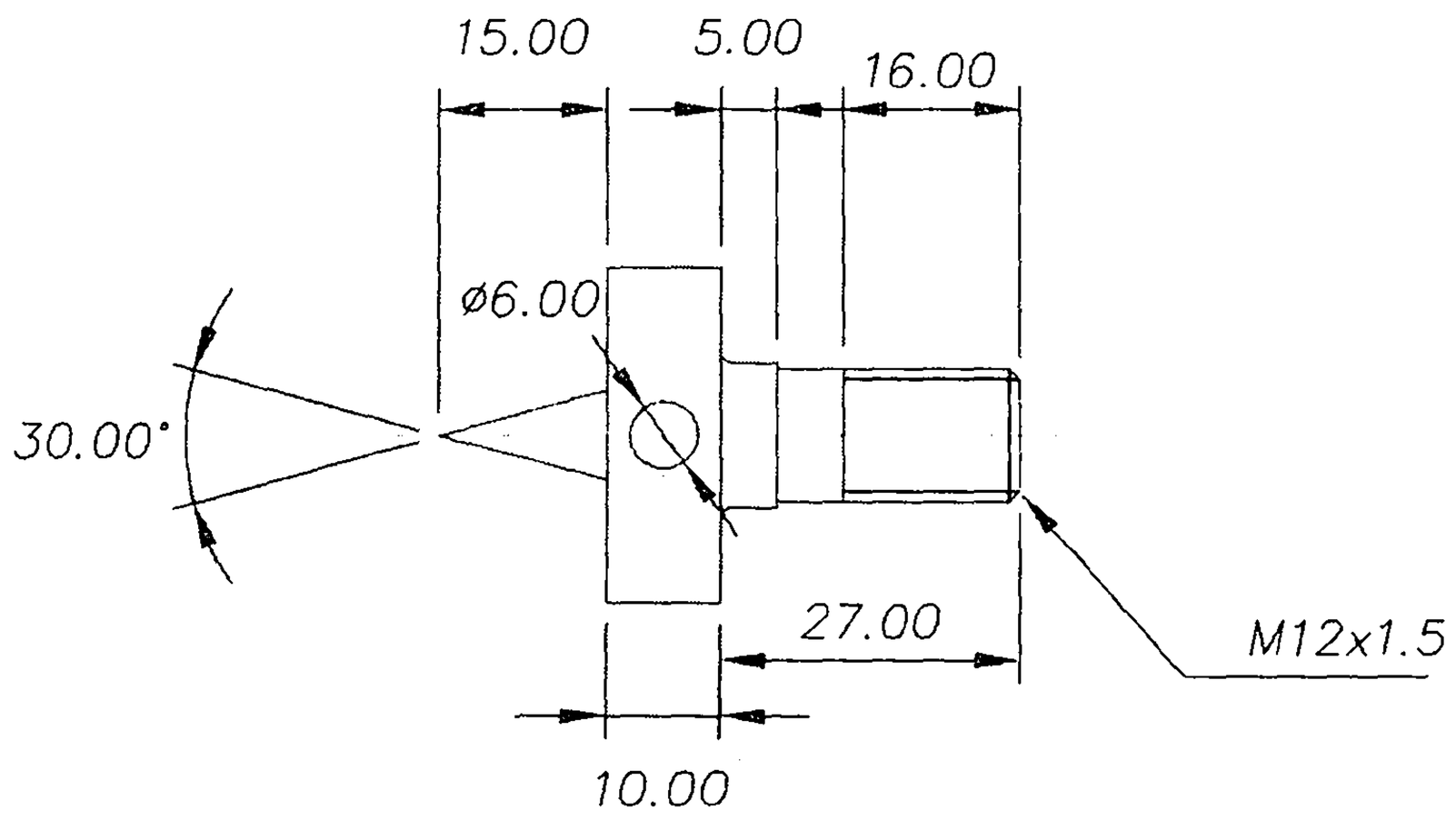

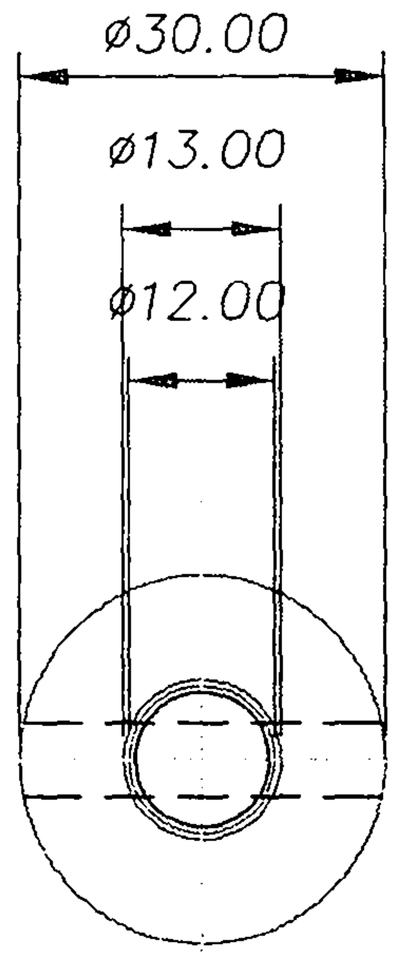

				CHANGE:	No. DATE
TITLE: 30° INDENTOR				DRAWN: PDB	DATE: 1/11/05 APPROVED:
MATL: EN24			TOL: ±0.1 UNLESS STATED	SCALE : 1:1	RMCS Cranfield UNIVERSITY A4
DWG No. PHD 035	ISSUE No. 1	ACAD FILE:	3.2 SURFACE FINISH IN µm UNLESS STATED	DIMS. IN: mm	

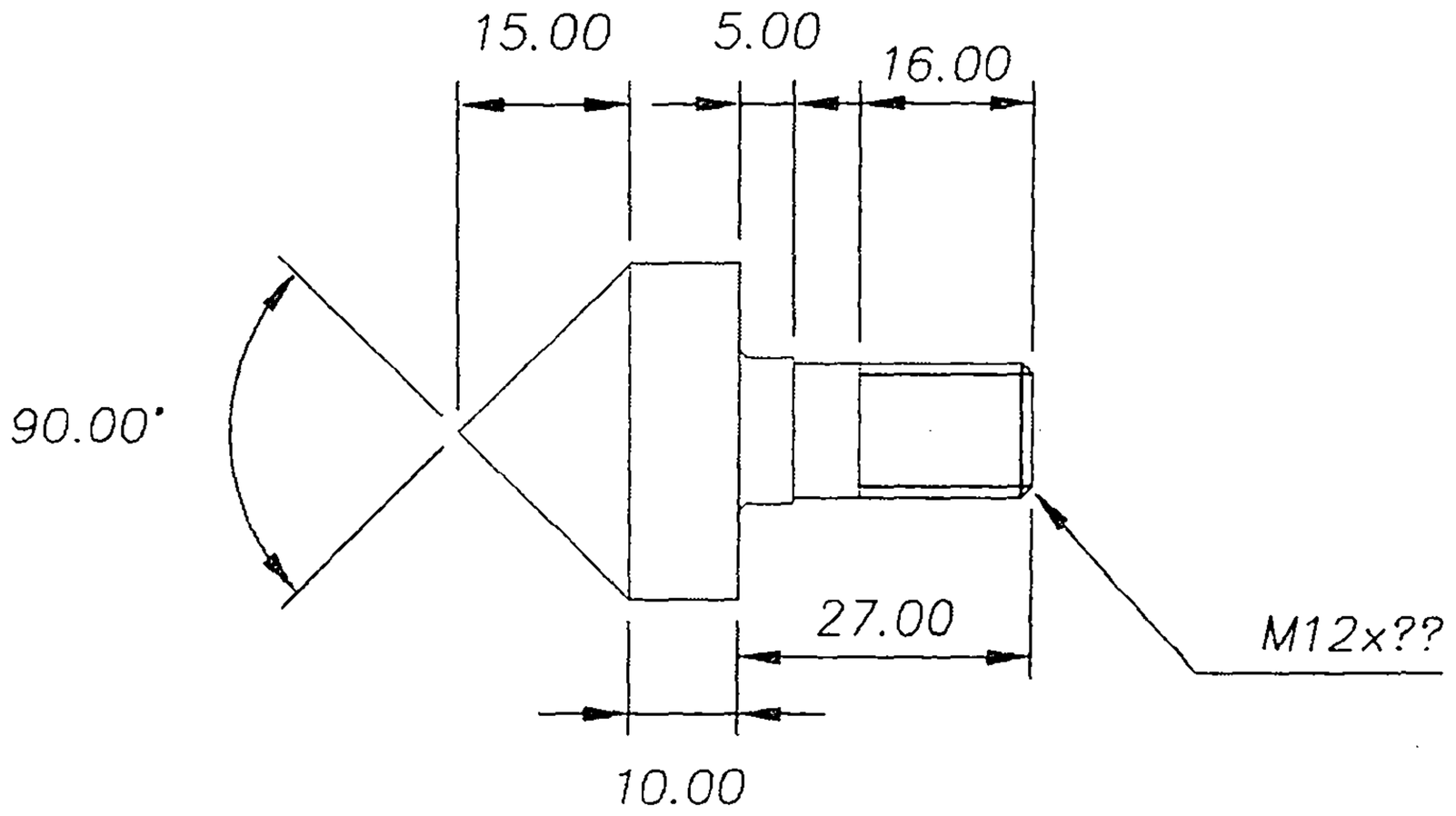

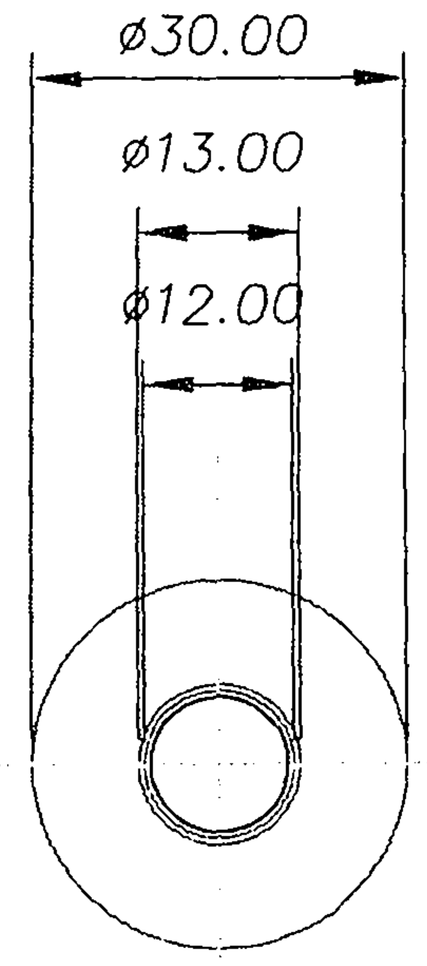

				CHANGE:	No.	DATE
TITLE: 90° INDENTOR				DRAWN: PDB	DATE: 1/11/05	APPROVED:
MATL: EN24			TOL: ±0.1 UNLESS STATED	SCALE : 1:1	RMCS Cranfield UNIVERSITY	A4
DWG No. 1	ISSUE No.	ACAD FILE:	3.2 SURFACE FINISH IN µm UNLESS STATED	DIMS. IN: mm		